



Terms and Conditions of Use of Digitised Theses from Trinity College Library Dublin

Copyright statement

All material supplied by Trinity College Library is protected by copyright (under the Copyright and Related Rights Act, 2000 as amended) and other relevant Intellectual Property Rights. By accessing and using a Digitised Thesis from Trinity College Library you acknowledge that all Intellectual Property Rights in any Works supplied are the sole and exclusive property of the copyright and/or other IPR holder. Specific copyright holders may not be explicitly identified. Use of materials from other sources within a thesis should not be construed as a claim over them.

A non-exclusive, non-transferable licence is hereby granted to those using or reproducing, in whole or in part, the material for valid purposes, providing the copyright owners are acknowledged using the normal conventions. Where specific permission to use material is required, this is identified and such permission must be sought from the copyright holder or agency cited.

Liability statement

By using a Digitised Thesis, I accept that Trinity College Dublin bears no legal responsibility for the accuracy, legality or comprehensiveness of materials contained within the thesis, and that Trinity College Dublin accepts no liability for indirect, consequential, or incidental, damages or losses arising from use of the thesis for whatever reason. Information located in a thesis may be subject to specific use constraints, details of which may not be explicitly described. It is the responsibility of potential and actual users to be aware of such constraints and to abide by them. By making use of material from a digitised thesis, you accept these copyright and disclaimer provisions. Where it is brought to the attention of Trinity College Library that there may be a breach of copyright or other restraint, it is the policy to withdraw or take down access to a thesis while the issue is being resolved.

Access Agreement

By using a Digitised Thesis from Trinity College Library you are bound by the following Terms & Conditions. Please read them carefully.

I have read and I understand the following statement: All material supplied via a Digitised Thesis from Trinity College Library is protected by copyright and other intellectual property rights, and duplication or sale of all or part of any of a thesis is not permitted, except that material may be duplicated by you for your research use or for educational purposes in electronic or print form providing the copyright owners are acknowledged using the normal conventions. You must obtain permission for any other use. Electronic or print copies may not be offered, whether for sale or otherwise to anyone. This copy has been supplied on the understanding that it is copyright material and that no quotation from the thesis may be published without proper acknowledgement.

**Dynamic Topography of Central and
Southern Africa**

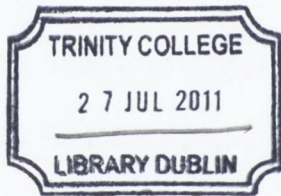
Eloise Peppard Rogers

A dissertation submitted for the degree of

Doctor of Philosophy

at the Trinity College Dublin

July 2009

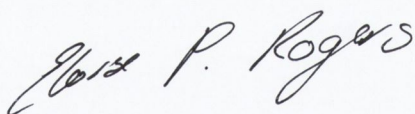


7405.8
9244

a) it has not been submitted as an exercise for a degree at this or any other University,

b) it is entirely the candidate's own work (in the case of a thesis for which the work has been carried out jointly; there must be a statement that it includes the unpublished and/or published work of others, duly acknowledged in the text wherever included) and

c) the candidate agrees that the Library may lend or copy the thesis upon request. This permission covers only single copies made for study purposes, subject to normal conditions of acknowledgement.

A handwritten signature in black ink that reads "Eloise P. Rogers". The signature is written in a cursive style with a large initial 'E'.

Eloise P. Rogers

Department of Geology, Trinity College Dublin

July 2009

Summary

Africa's basin and swell topography is thought to be dynamically supported by mantle convection because it correlates closely with long wavelength free-air gravity anomalies, which can be regarded as a proxy for the convective pattern. Seismic tomographic studies reveal a region of slow seismic velocity beneath sub-equatorial Africa. This region broadly correlates with a zone of anomalously high elevation, known as the African Superswell, that stretches from the South Atlantic Ocean across Africa to Afar. More recently temporal parameters such as uplift rate have been considered in dynamic topography modeling. However, theoretical predictions of dynamic topography have not been carefully tested against observations.

Chapter 2 begins by looking in detail at the geomorphology of the Congo River Catchment. The Congo River Catchment is of particular interest as it drains from areas of both negative and positive long wavelength free air gravity. The recent availability of global high-resolution topographic data (e.g. SRTM 90 meter) allows for detailed studies of geomorphological features of inaccessible areas such as the Congo Basin. DEMs show that drainage along the southern edge of the Congo River Catchment incises into a smooth, low relief surface. The low-relief surface represents the top of a group of fluvial sediments, known as the Sable Ocres believed to be deposited during the Neogene. This surface slopes northwards from elevations of 1500 m to 700m and the topography of the correlates with long wavelength free-air gravity anomalies. Plotting the elevation of the surface against long wavelength free-air gravity measures admittance in the spatial domain. A best fit line to the data points yields an admittance value of 40 mgals km^{-1} , consistent with dynamically supported topography. The morphology of profiles of rivers draining the southern edge of the Congo River catchment and the Angolan coastal margin indicate that the upper sections of the rivers have been recently captured. The capture of streams draining the flanks of the Bie Plateau is likely to have been result of vertical motions generated by mantle convection, tilting the region. Uplift rates for the region are estimated to be as high as 40 m Myr^{-1} , slightly greater than previously published estimates of uplift for southern Africa derived from tomographic velocity models.

The Congo low-relief surface is one of a number of ancient land surfaces (palaeosur-

faces) that have been recognized in classical geomorphological studies of Africa. Previous estimates of uplift and tilting of these surfaces have been used to constrain dynamic topography estimates for southern Africa. Chapter 3 tests if the topography of the palaeosurfaces can be used to predict dynamic topography, this study applied the gravity/topography correlation technique developed in the Congo Basin to all the palaeosurfaces defined by King (1962) and Partridge and Maud (2000). Many of these surfaces do not display the linear gravity/topography relationship expected for dynamic support and displayed so clearly in the southern Congo basin. However, the topography of smaller sections of the surfaces in the Bie plateau and Namibian highlands may be dynamically supported. One possible reason that evidence for dynamic support of palaeosurfaces is not more widespread could be that rates of palaeosurface erosion, incision and sedimentation can be more rapid than rates of dynamically supported vertical motions in some cases.

Chapter 4 examines the possibility that the unusual topography of Africa is not unique within Earth's continents. However, observations of oceanic plates and theoretical considerations suggest that dynamically supported topography is widespread and is likely to be present on other continents. This study reviews the large-scale geomorphology of worldwide continental areas bounded by passive margins in terms of both swaths of topographic profiles normal to the margins, and hypsometry of large regions. Comparison of the topographic swath profiles with dynamic support profiles estimated from the free-air gravity field suggests that edge-driven convection in the upper mantle may contribute to the topography of high elevation passive margins. However, the presence of dynamic support along the margin is not a sufficient condition for development of escarpments. A positive linear correlation between hypsometric integral and the average free-air gravity anomaly of continents may reflect a widespread influence of dynamic support in regional scale topography.

Chapter 5 summarises the conclusions of this study and suggests further work. In conclusion, it appears that dynamic topography can sometimes be identified by careful examination of the geomorphology of a region.

Acknowledgements

Most importantly, I would thank Stephen Jones for his support and encouragement for the past 4 years and Nicky White for inspiring the project and his supervision.

I am very grateful from the support of so many people here at the Department of Geology. In particular I would like to thank John Graham, Geoff Clayton, Ian Sanders, George Sevastopulo, Dave Chew, Declan Burke and Mags Duncan. I owe allot to Rob Hardy for rescuing me from many computer and data problems. During my time at Bullard Labs in Cambridge University, I benefited greatly from the knowledge of Max Shaw-Champion and Alistair Crosby, who patiently helped me with code and GMT scripts. Dave Lyness was very generous for letting me stay in his house.

There is many fellow postgraduates I would like to thank. I have been lucky to have had some great office mates in the URL, in particular Eoughan, Brian, Catherine and Aoife. I have made some fantastic friends along the way. I have enjoyed many curries and laughs with Jo, Sarah and Stuart and I am especially grateful to my to Jane and Aileen for all their encouragement and for having so much faith in me. Outside of college, there are those who provided a welcome distraction. I enjoyed many weekends at the with Hanna and Rui and hiking the wrong way up mountains with Lucy, Mark and Jo.

I wouldn't have made it without my family: my grandmother whose generosity knows no bounds, my wonderful sister who provided me with plenty of laughs whenever I was down and Aidan for being a friend, but most of all my absolutely fantastic parents who have always been there for me and encouraged me along the way. And finally Ian, thank you for putting up with me through the more difficult times and all your support over the past few years. I am so grateful to you all.

Contents

List of Figures	xii
Chapter 1 Introduction	1
1.1 Dynamic topography and Mantle Convection	1
1.2 Aims of this thesis	2
1.3 Measuring dynamic topography	3
1.3.1 Residual Topography	4
1.3.2 Long wavelength free-air gravity	6
1.3.3 Tomography	13
1.3.4 Slab models	17
1.4 Why study Africa?	17
1.5 Geological evidence for vertical motions	21

1.5.1	Geomorphic analyses and drainage patterns	22
1.5.2	Denudation rates	23
1.5.3	Sediment Flux in deltas	25
1.5.4	Magmatic events	26
1.5.5	Onshore record of marine sediments	27
1.6	Geomorphological terminology	27
1.7	Datasets	29
1.7.1	GRACE gravity field	29
1.7.2	SRTM topographic data	30
1.8	Thesis structure	31
 Chapter 2 Geomorphology and dynamic topography of Central Africa		33
2.1	Introduction	33
2.2	Regional setting	36
2.2.1	Climate and vegetation	37
2.2.2	Geology and Structure of Congo River Catchment	38
2.3	Evolution of the central Africa	41

2.3.1	Congo Basin	42
2.3.2	Drainage system	43
2.3.3	Denudation estimates along the Angolan coast	46
2.3.4	Offshore	47
2.4	River profiles	49
2.4.1	River profiles in equilibrium	50
2.4.2	Stream power law and migration of knickpoints	51
2.5	Methodology	53
2.5.1	Longitudinal River Profile Extraction	53
2.6	River profiles: results and interpretation	54
2.7	Low relief surface	63
2.8	Discussion	69
2.9	Conclusions	72

Chapter 3 Palaeo-Surfaces in southern Africa **75**

3.1	Introduction	75
3.2	Previous research of African surfaces	77

3.2.1	Lester C. King	79
3.2.2	Partridge and Maud	84
3.2.3	Denudational Surfaces	88
3.2.4	African Surface	91
3.2.5	Post-African Surface	92
3.2.6	Aggradational or depositional surfaces	96
3.3	Theoretical admittance relationships for warped surfaces	100
3.4	Methodology of Constructing Gravity - Elevation Plots	105
3.4.1	Georeferencing and digitising maps	108
3.4.2	Correcting for errors	110
3.4.3	Correcting for erosion by modern day drainage systems	112
3.5	Results and interpretation	133
3.5.1	Topography-Gravity relationship for King's surfaces	134
3.5.2	Topographic-Gravity relationships for Partridge and Maud's surfaces	140
3.6	Discussion	142
3.6.1	Constraints on the antiquity of surfaces in Africa	142

3.6.2	King's surface elevation-gravity plots	146
3.6.3	Partridge and Maud's surface elevation-gravity plots	147
3.6.4	Depositional surface elevation-gravity plots	147
3.7	Conclusions	148
Chapter 4 Is Africa unique?		161
4.1	Introduction	161
4.2	High-elevation passive margins	163
4.2.1	The Great Escarpment	172
4.3	Dynamic topography and mantle edge convection	175
4.4	Swath topographic profiles of passive margins	178
4.4.1	Methodology	180
4.4.2	Results	181
4.4.3	Discussion	187
4.5	Hypsography of the World	205
4.5.1	Background	205
4.5.2	Methodology	207

4.5.3	Results	211
4.5.4	Discussion	216
4.5.5	High elevation margins	216
4.5.6	Hypsometry of the continents	217
4.6	Conclusions	218
Chapter 5 Discussion and Conclusions		219
5.1	Introduction	219
5.2	Implications of findings on wider issues	220
5.3	Implications for southern Africa	221
5.4	Problems	223
5.5	Further work	224

List of Figures

1.1	Residual topography over Africa	4
1.2	Contributions to the gravity anomaly over a hot region in the upper mantle	6
1.3	A. Map showing the free-air gravity field across Africa	11
1.4	Admittance calculated for Central Africa	12
1.5	Maps of Africa illustrating dynamic topography and uplift rates	13
1.6	S-wave global tomography model S20RTS	14
1.7	Predictions of uplift rate on the African continent	15
1.8	Shaded relief map of Africa with gravity contours superimposed	19
1.9	A elevation map highlighting major geomorphological features in Africa	20
1.10	Summary of published uplift and denudation estimates	24
1.11	Summary of sediment flux to African rivers.	26

2.1	Map of the Central Africa	36
2.2	Geological map of the Central Africa	39
2.3	A north-south section illustrating the plantation surfaces and associated deposits of the Kalahari system.	40
2.4	Hypsometric curves of the Congo River tributaries	45
2.5	Tectonic uplift estimates of the West African margin	48
2.6	The timing of changes in sedimentation rate and flux along the margin of west equatorial Africa.	49
2.7	Congo River Catchment and selected river profiles	56
2.8	Geological boundaries along river profiles	57
2.9	Geological boundaries along river profiles	58
2.10	Incision of rivers measured relative to the surface of the Kalahari sediments	59
2.11	Profiles of rivers that drain the western Angola	60
2.12	Profile of the Kwanza River	61
2.13	Shaded relief and slope maps of the southern Congo Basin margin . . .	65
2.14	Cross sections taken through the DEM	66
2.15	Reconstruction of low relief surface	67

2.16	Elevation of surface plotted against long wavelength free air gravity . . .	68
3.1	Scanned section of the map published by King (1962)	78
3.2	Simplified map of the distribution of erosional land surfaces in southern Africa taken from Partridge and Maud, 2000.	84
3.3	Sections drawn inland from the coast across the south eastern hinterland of southern Africa taken from Partridge and Maud (1987)	86
3.4	Generalized contours on the Post-African I (Miocene) erosion surface taken from Partridge and Maud (2000).	87
3.5	Maximum depths of denudation for Namibia determined from apatite fission track data of the region taken from Cockburn et al. (2000).	93
3.6	Location of the cosmogenic sample sites taken from Bierman and Caffee (2000).	94
3.7	The effects the long wavelength uplift may have had on different land-surfaces and topographic features.	102
3.8	Denudational and aggradational surfaces of Africa digitised from King (1962).	106
3.9	Denudational and aggradational surfaces of Africa, reinterpreted from the map published by King (1962).	107
3.10	Correcting for localised incision in the Angolan region	113
3.11	Correcting for localised incision in the Namibian region	114

3.12	Correcting for localised incision in the Karoo region	115
3.13	Plot of elevation and long wavelength free-air gravity for the Congo surface	117
3.14	Correcting for localised incision in the South Congo region	119
3.15	Plot of elevation and long wavelength free-air gravity for King's Gond- wana surface in the Angolan	120
3.16	Plot of elevation and long wavelength free-air gravity for King's Gond- wana surface in the Namibian region	121
3.17	Plot of elevation and long wavelength free-air gravity for King's Gond- wana surface in the Karoo region	122
3.18	Plot of elevation and long wavelength free-air gravity for King's African surface in the Angolan region	123
3.19	Plot of elevation and long wavelength free-air gravity for King's African surface in the Namibian region	124
3.20	Plot of elevation and long wavelength free-air gravity for King's African surface in the Karoo region	125
3.21	Plot of elevation and long wavelength free-air gravity for King's Post African surface in the Angolan region	126
3.22	Plot of elevation and long wavelength free-air gravity for King's Post African surface in the Namibian region	127

3.23	Plot of elevation and long wavelength free-air gravity for King's Post African surface in the Karoo region	128
3.24	Plot of elevation and long wavelength free-air gravity for King's Post African aggradational surface in the Angolan region	129
3.25	Plot of elevation and long wavelength free-air gravity for King's Post African aggradational surface in the Karoo region	130
3.26	Plot of elevation and long wavelength free-air gravity for King's modern aggradational surface in the Namibian region	131
3.27	Plot of elevation and long wavelength free-air gravity for King's modern aggradational surface in the Karoo region	132
3.28	Elevation-gravity plots of King's surfaces that displayed high density of points in one area of the graph. A colour chart illustrates how many data points are displayed in each pixel. The ranges of the plots vary as they are determined by the extent of the datasets. The graphs highlight internal trends within the dense data clouds.	139
3.29	Plot of elevation and long wavelength free-air gravity for Partridge and Maud's above African surface in the Namibian region	150
3.30	Plot of elevation and long wavelength free-air gravity for Partridge and Maud's above African surface in the Karoo region	151
3.31	Plot of elevation and long wavelength free-air gravity for Partridge and Maud's African surface in the Namibian region	152

3.32	Plot of elevation and long wavelength free-air gravity for Partridge and Maud's African surface in the Karoo region	153
3.33	Plot of elevation and long wavelength free-air gravity for Partridge and Maud's Post African surface i in the Namibian region	154
3.34	Plot of elevation and long wavelength free-air gravity for Partridge and Maud's Post African surface i in the Karoo region	155
3.35	Plot of elevation and long wavelength free-air gravity for Partridge and Maud's Post African surface i in the Karoo region	156
3.36	Plot of elevation and long wavelength free-air gravity for Partridge and Maud's Kalahari surface in the Namibian region	157
3.37	Plot of elevation and long wavelength free-air gravity for Partridge and Maud's Kalahari surface in the Namibian region	158
3.38	Map of the Angolan region highlighting the location of the data trends	159
3.39	160
4.1	Map of the world, showing escarpments parallel to passive margins . . .	165
4.2	Shaded relief map of the world, showing escarpments along parallel to passive margins	166
4.3	Geological ages of the continental and oceanic crust	167
4.4	Shoulder-type and arch-type continental margins	168

4.5	Post-breakup evolution of passive continental margins	169
4.6	Cross sections through the topography southern Africa, before and after dynamic topography corrections	174
4.7	Numerical models of edge driven convection	175
4.8	Topographic map of escarpments in West Africa, Greenland, southern Africa and Norway	188
4.9	Topographic map of escarpments in Antarctica, Madagacar, South Amer- ica and East Australia	189
4.10	Cross sections through S20RTS tomography model (Ritsema et al., 1999) across central Africa	190
4.11	Cross section through S20RTS tomography model (Ritsema et al., 1999) across southern Africa	191
4.12	Swaths along the south west coast of Africa, north	192
4.13	Swaths along the south west coast of Africa, south	193
4.14	Swaths of southern Africa in a East-West direction and South-North direction	194
4.15	Swaths of West Africa in a West-East direction, north	195
4.16	Swaths of West Africa in a West-East direction, south and in a South- North direction, west	196

4.17 Swaths of West Africa in a South-North direction	197
4.18 Swaths of Madagascar in a East-West direction	198
4.19 Swaths of Greenland in a East-West direction and of Norway in a West- East direction	199
4.20 Swaths of Australia in a East-West direction, south	200
4.21 Swaths of Antarctica in a North-South direction, west	201
4.22 Swaths of Antarctica in a North-South direction, east	202
4.23 Swaths of South America in a East-West direction, west	203
4.24 Swaths of South America in a East-West direction, east	204
4.25 The evolution of hypsometric curves in glacial and fluvial landscapes	207
4.26 Hypsometric curves of continents	210
4.27 Hypsometric curves of regions with different crustal ages for each of the landmasses	212
4.28 Hypsometric integrals comparing regions of different gravity anomalies	213
4.29 Hypsometric integrals of regions with varying gravity anomalies	214
4.30 Hypsometric integrals of regions with different crustal ages for each of the landmasses	215
5.1 Component of dynamic topography on the African continent	222

Chapter 1

Introduction

1.1 Dynamic topography and Mantle Convection

Dynamic topography is topography on Earth's surface that is supported by mantle convection at the base of the lithosphere (Lithgow-Bertelloni and Silver, 1998; Steinberger et al., 2001). Mantle upwelling is thought to cause the Earth's surface to uplift and deform into broad swells. The converse is suggested to be true for mantle downwellings (Hartley and Allen, 1994; King and Ritsema, 2000). Vertical displacement of the Earth's surface caused by active circulation of the mantle is transient. The rate at which the resultant uplift or subsidence occurs is poorly constrained. Numerical models predicting time-scales of mantle flow range from years to hundreds of millions of years (e.g. Tackley et al., 1994; Larsen and Yuen 1997; Gurnis et al., 2000). Therefore measuring the rate at which dynamic topography develops has important implications for constraining the rate at which the mantle circulates.

The Rayleigh number, a measure of the ratio between the thermal driving force (buoy-

ancy of hot material) and viscous dissipative forces, can be used to predict if a fluid will convect. The Earth's mantle has a Raleigh number of 10^6 – 10^8 , which is well above the critical value for the onset of convection (e.g. McKenzie and Weiss, 1975).

Such supercritical convection is time dependent. The time dependence takes two main forms: (1) Horizontal movement of the upwelling/downwelling limbs and (2) advection of bodies of hotter and colder mantle around individual cells (White and McKenzie, 1995). We wish to constrain the time-scale for these changes.

1.2 Aims of this thesis

The main aims of this thesis are:

- To utilise available high-resolution topographic data of Africa to study the geomorphology of the Congo River Catchment region and locate areas that have been recently uplifted.
- To reassess uplift predictions from previous geomorphological studies of Africa and compare these estimates against dynamic topography predictions in southern Africa.
- To test the hypothesis put forward by Burke, 1996 that the dynamically supported swells in the topography of Africa are unique among the continents on Earth.

1.3 Measuring dynamic topography

There are a number of methods to predict the magnitude of the dynamic component of topography. The four main methods are briefly described below:

1. Residual topography methods

Topography due to the isostatic compensation of crustal and lithospheric thickness and density is estimated and subtracted from the actual topography to identify the dynamic part (e.g. Nyblade and Robinson, 1994; Lithgow-Bertelloni and Silver, 1998).

2. Gravity methods

The long wavelength component of the free-air gravity field is extracted and used as a proxy for the pattern of mantle convection. If the characteristic gravity/topography ratio (the admittance) is known then the dynamic topography can be estimated (McKenzie, 1994).

3. Tomography-based models

Density anomalies within the mantle are estimated from tomography models and are used to predict dynamic topography (e.g. Lithgow-Bertelloni and Silver, 1998; Gurnis et al., 2000).

4. Slab models

Mantle density heterogeneity is derived from the subduction history and used to generate dynamic topography models (e.g. Lithgow-Bertelloni and Silver, 1998).

Methods of measuring dynamic topography as outlined in 1.1 are described in detail. The applicability and predictions of these resultant models for predicting dynamic

topography across the African continent are also discussed.

1.3.1 Residual Topography

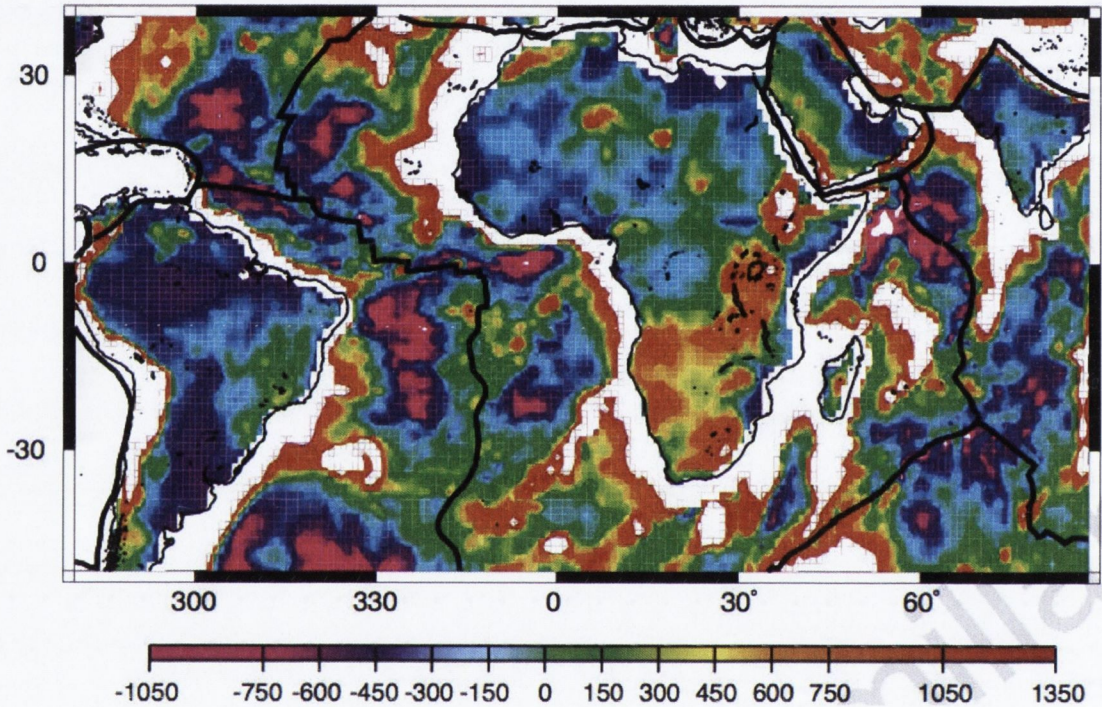


Fig. 1.1: Residual topography (in metres) over the African Continent and the surrounding oceans; after Lithgow-Bertelloni and Silver (1998). The residual topography for the continents was obtained by subtracting 565 m, the mean elevation of continents, from observed elevations. The residual bathymetry was calculated by subtracting a cooling half-space model from the observed values. Continental shelves and regions with residual topography of over 1,350m are represented in white.

Residual topography is the observed topography corrected for the average topography for crust of that age in the absence of dynamic topography and crustal thickening (Crosby et al., 2006). In the oceans residual topography is usually calculated by subtracting the normal subsidence due to the cooling of the oceanic lithosphere. Age-related subsidence in oceanic plates can be calculated using the half-space cooling

equation:

$$h_r = h_0 - (2600 + 220a^{1/2}) \quad (1.1)$$

where h_r is residual depth (in meters), h_0 is observed bathymetry and a is the age of the oceanic lithosphere. The half-space cooling model is only applicable to plates younger than 70 Ma.

A technique for isolating the residual topography of continents is more poorly constrained as there is not as simple a relationship between the topography and age of continents. Workers (e.g. Nyblade and Robinson, 1994; Lithgow-Bertelloni and Silver, 1998; Gurnis et al., 2000) commonly estimate the residual topography by subtracting the mean elevation of all the continents which estimated to be 565 m (Harrison et al., 1983). Large portions of southern and eastern Africa and the surrounding oceans display residual topography estimates in excess of 750 m (Figure 1.1).

Nyblade and Robinson (1994) produced a map of residual topography of Africa that highlighted a broad region of high elevation and shallow bathymetry comprising the East African rift system, the southern African plateau and the south-eastern Atlantic Ocean, which was described as the African Superswell. Gurnis et al. (2000) later published a global residual topography map and extended the African superswell to include an anomalously shallow bathymetry of the south-western Indian Ocean (Figure 1.8). Studies of tomographic models show that the African Superswell appears to be dynamically supported by hot upwelling mantle (Lithgow-Bertelloni and Silver, 1998; Grand et al., 1997; Ritsema et al., 1999; Ni et al., 1999; Gurnis et al., 2000).

1.3.2 Long wavelength free-air gravity

The long wavelength component of the free-air gravity field is commonly used as a proxy for the convective pattern (McKenzie, 1994). This has been successfully applied to Venus and Mars, as well as on Earth. Free-air gravity fields can be used to constrain the density structure of the mantle calculated from tomographic models (Ishii et al., 1999).

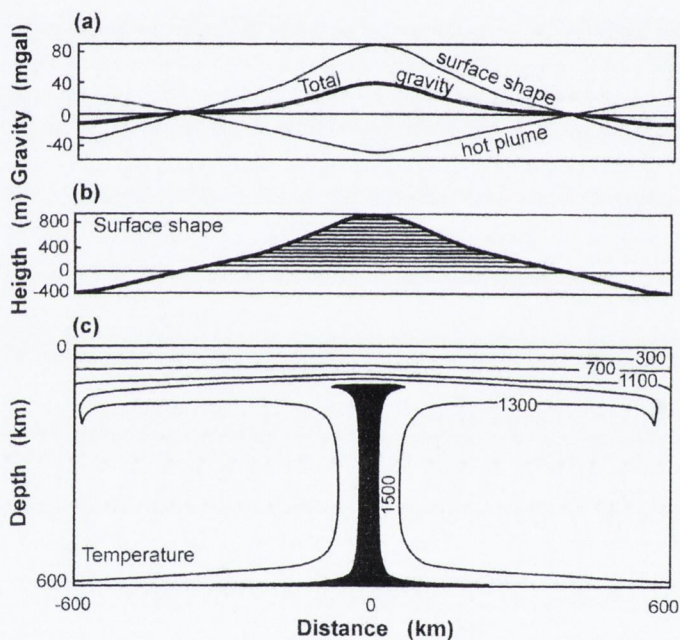


Fig. 1.2: Contributions to the gravity anomaly over a hot region in the upper mantle: (a) gravity anomaly, (b) surface shape, (c) mantle temperature ($^{\circ}$ C) after McKenzie 1998

Density heterogeneities in the crust and mantle and loading or flexure of the plate all contribute to free-air gravity anomalies. In general, shallow variation in density causes short wavelength, high amplitude free-air gravity anomalies, while deeper variations in density cause long wavelength, low amplitude free-air gravity anomalies. Short wavelength features are either partially or wholly supported by the strength of the plate and will have an associated gravity anomaly. Complete isostatic (Airy) compensation

occurs as the elastic strength of the lithosphere tends to zero. The effective elastic thickness, T_e , is defined transitional wavelength between uncompensated short-wavelength and isostatically compensated longer wavelength topographic relief (Turcotte & Schubert 1982).

Edge effects are another class of short wavelength gravity anomaly that are associated with the abrupt lateral density changes e.g. across a tectonic plate boundary. Edge effects arise because the gravity anomaly at any point is affected by the density structure over a wide area and not only the structure directly beneath the point. Filtering out shorter wavelengths of the gravity field removes the effects of shallow heterogeneities and edge effects associated with flexure of the plate.

The relationship between gravity and topography has been well understood in the oceans since the early 1970s (Anderson et al., 1973; Watts and Daly, 1981). There are two main reasons why this relationship are better established for the oceans than the continents. First, the oceans have a relatively simple thermal and mechanical evolution and it is possible to quantify how the cooling oceanic lithosphere contributes to observed gravity and topography anomalies. Secondly, orbiting satellites, beginning with SKYLAB in 1973, enabled the long wavelength gravity field over the oceans to be determined with great precision (Watts and Daly, 1981). Until recently, the gravity field over continents relied on modelled field measurements (e.g. EGM96 model). The availability of GRACE gravity field data since 2005 has improved the accuracy of long wavelength gravity field over the continents (Tapley et al., 2004). However the complex crustal and lithospheric structure of the continents is still problematic when understanding gravity and topographic relationships of continents. Recent research has improved structural models of the continental plates (e.g. Artemieva et al., 2006; Priestley et al., 2006).

Anomalous elevated regions such as hotspots have been found to correlate with positive long wavelength free-air gravity. The positive free-air gravity anomaly arises from the joint contribution of a topographic bulge in the surface, which gives a positive gravity anomaly, and the anomalously low density of the hot asthenosphere material beneath, which gives a negative, but smaller, anomaly (Figure 1.2).

The relationship between the topographic swells associated with hotspots and free-air gravity is well established in the oceans. Free-air gravity fields across known hotspots such as the Hawaiian and Icelandic Swells are consistent with regions that are dynamically supported (Jones et al., 2002; Crosby et al., 2006).

A number of long-wavelength topographic swells on the surface of Earth and other planets correlate with long wavelength free-air gravity and are thought to be a result of upwelling of the mantle. There is a close relationship between gravity and topography in the Apennines in central Italy and the topographic bulge in this region has been interpreted as an effect of upwelling of the mantle. The widespread surface uplift of the Apennines related to the upwelling of the mantle most likely occurred in the Quaternary as suggested by geological and geomorphological data (D'Ágostino et al., 2001). Free-air gravity anomalies on Mars and Venus are often associated with topographic swells and volcanism (Anderson et al., 1997; Crough, 1983; McKenzie 1994).

The relationship between gravity and topography is referred to as the admittance, Z . The component of convectively supported topography, $h_{convective}$, can be predicted using the long wavelength free-air gravity, g , if the admittance, Z , is known (McKenzie, 1994) using the following equation:

$$h_{convective} = g/Z \tag{1.2}$$

The admittance is constant at long wavelengths of ~ 400 to 1000 km (Tiley et al., 2003). Numerical studies of mantle convection show that admittance values of 50 mgals km^{-1} over the continents and 30 mgals km^{-1} over the oceans are typical for convection at high Rayleigh numbers (McKenzie 1994). Across areas of the ocean that are thought to be dynamically supported, the admittance has been measured as between 20 – 35 mgal km^{-1} (e.g. Anderson et al., 1973; Parsons and Daly 1983; McKenzie, 1994). More recent values, further constrained by correcting for the isostatic effect of sediments, are closer to 30 mgal km^{-1} (Crosby et al., 2006). Calculating admittance for the continents has proved more elusive, and most published values for admittance have been estimated through elastic thickness calculations. The decay of the admittance function at transitional wavelengths can be modelled by the theoretical admittance of an elastic plate and used to derive an estimate of T_e . Air-loaded continents are thought to have a greater admittance than the oceans where the plate is loaded by water. As discussed before continental lithosphere has a more complex evolution than oceanic lithosphere. In addition erosion or infill of dynamic topography can affect calculations of admittance. The current estimate of air-loaded continental regions using free-air gravity about 50 mgal km^{-1} (McKenzie, 1994; Tiley et al., 2003). Similar studies reveal Mars and Venus have a similar admittance value at wavelengths longer than 700 km (McKenzie et al., 2002).

Coherence measures the phase relationship between gravity and topography at a particular wavelength. A coherence of 1 indicates that the topography and density contrasts are compensated locally while a coherence of 0 indicates that the topography and density are entirely supported by the strength of the plate (Hartley and Allen, 1994). In general, coherence increases with wavelength.

Admittance can be either calculated using Bouguer gravity or free-air gravity. The most commonly used admittance calculations across continents are those based on the

Forsyth method, which uses coherence between Fourier transforms of the Bouguer gravity and the topography to calculate admittance and T_e (e.g. Forsyth, 1985; Hartley and Allen, 1994; Hartley et al., 1996; Watts, 2001). There are two main reasons that traditionally Bouguer gravity was used in admittance studies of the continents. Firstly, the Bouguer correction accounts for mass of topography both above and below sea level and therefore the Bouguer anomaly represents the mass anomaly within the crust. Secondly, the Bouguer correction reduces the free-air gravity to a value close to the geoid, which at the coast corresponds to mean sea level (Watts, 2001). However, McKenzie and Fairhead (1997) argued that the large T_e values estimated by the Forsyth method are not compatible with pressure and temperature estimates from the mineralogy of mantle nodules. McKenzie (2003) states that erosion and sedimentation can produce loads that are not associated with any topography and in such cases where these loads are important T_e and admittance values will be overestimated by the Forsyth method. McKenzie and Fairhead (1997) instead maintained that the free-air anomaly provided the best estimate of the coherence between gravity and topography that has been corrected for sediment infill (McKenzie & Fairhead, 1997; McKenzie, 2003; D'Agostino et al., 2001; Crosby et al., 2006).

This study uses the McKenzie method as outlined in McKenzie & Fairhead, (1997). There are limitations to the analytical method applied in this study to calculate admittance. The model used is clearly too simple to represent the complicated density structure within the continental crust. Recent research has improved structural models of the African plate (e.g. Artemieva et al., 2006; Priestley et al., 2006), however it is beyond the scope of this study to assess how the impact of the crustal and lithospheric structure contributes to the free-air gravity field. The method relies on accurate long wavelength gravity measurement over the African continent, which until recently were limited to EGM96. This study takes advantage of the recently available GRACE gravity datasets which displays a significant improvement for wavelengths greater than 300

km compared to EGM96 (Tapley et al., 2004).

Free-air gravity field and admittance across Africa

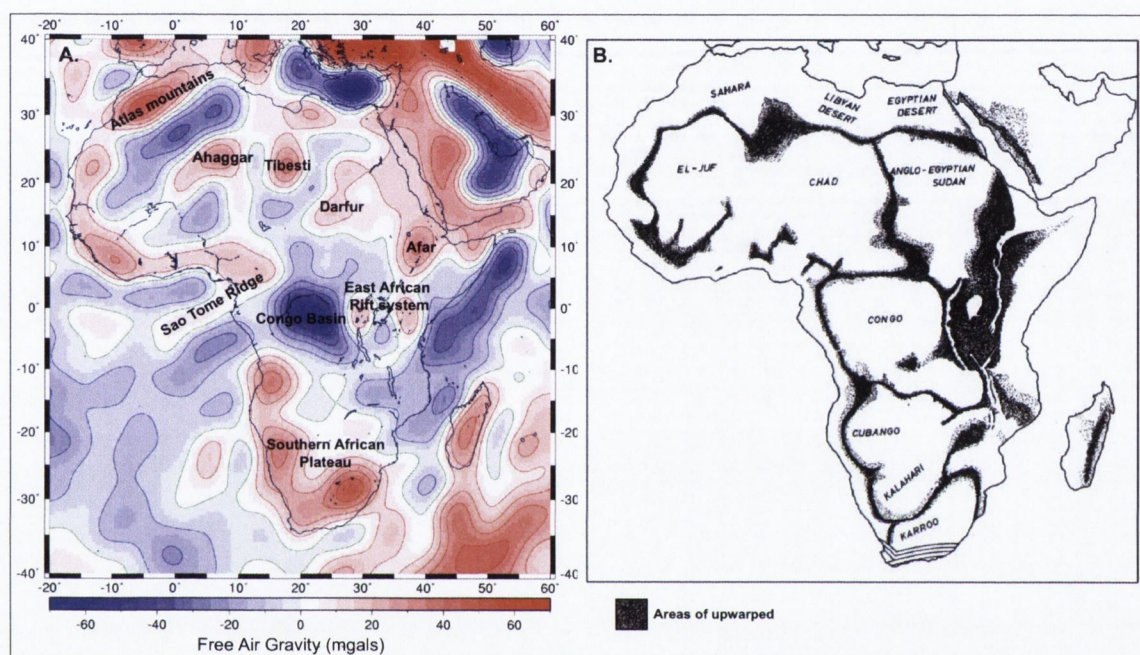


Fig. 1.3: Map showing the free-air gravity field across Africa and the surrounding oceans, calculated using the GRACE spherical harmonic model GGM02C, which was low-pass filtered at 800 km with a cosine taper. A number of geological features associated with gravity anomalies are labelled. **B.** Map displaying 'basin and swell' topography of Africa after Holmes, 1944

There is a strong correlation in Africa between positive free-air gravity anomalies and large scale topographic swells such as Tibesti, Afar, Darfur and Ahaggar (Figure 1.3 and 1.4 A). A large negative long wavelength free-air gravity anomaly is associated with the Congo Basin, a large intra-continental sedimentary basin.

McKenzie (1994), estimated admittance across Africa to be between 40–80 mgals km⁻¹ and a coherence of less than 0.5. He concluded that this was consistent with dynamically supported topography. However, the dominant gravity anomaly in Central Africa,

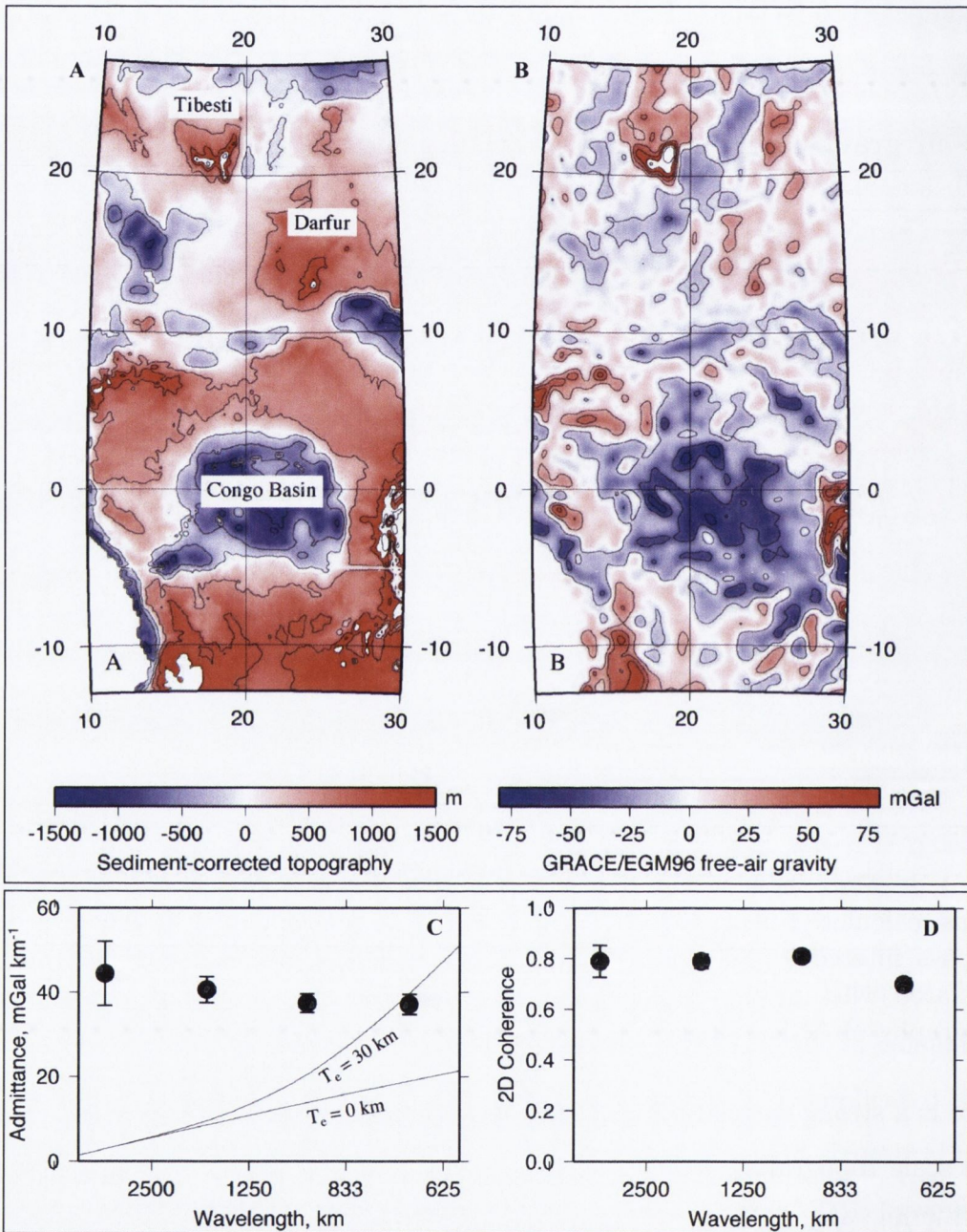


Fig. 1.4: Admittance calculated for Central Africa after Crosby (2006). **A.** Topography after sediment isostatic correction is applied. Sediment thickness estimates used for correction were taken from the first two layers of the model produced by Laske and Masters (1997) **B.** Free-air gravity map created using the extended GGM02C model from Texas (www.csr.utexas.edu/grace). At wavelengths shorter than 400 km, GGM02C uses GRACE satellite-only model GGM02S and is reliable. At shorter wavelengths down to 110 km, it blends EGM96 model, which is based on field data over land and maybe less reliable. **C.** Admittance between sediment-corrected topography and gravity (as described before). Errors are assumed to be limited to the topography. **D.** 2D coherence for the same dataset.

occurs over the Congo Basin, which is infilled with sediments to an elevation of 500 to 600 m. A simple hypothesis is that basin is a result of mantle dynamic processes and that the sediments deposited in the basin will cause further isostatic subsidence. Sediments have a density between that of normal crust and air; therefore the infill of sediments increases the regional admittance while decreasing coherence. Crosby (2006) used global sediment thickness model published by Laske and Masters (1997) to correct the topography to correct for the isostatic loading of sediments (Figure 1.4 A and B). Coherence between topography and free-air gravity for wavelengths over 800 km is ~ 0.8 (Figure 1.4 C). Admittance is ~ 40 mgals km^{-1} for all wavelengths measured and is consistent with dynamic support of the topography in Central Africa (Figure 1.4 B).

1.3.3 Tomography

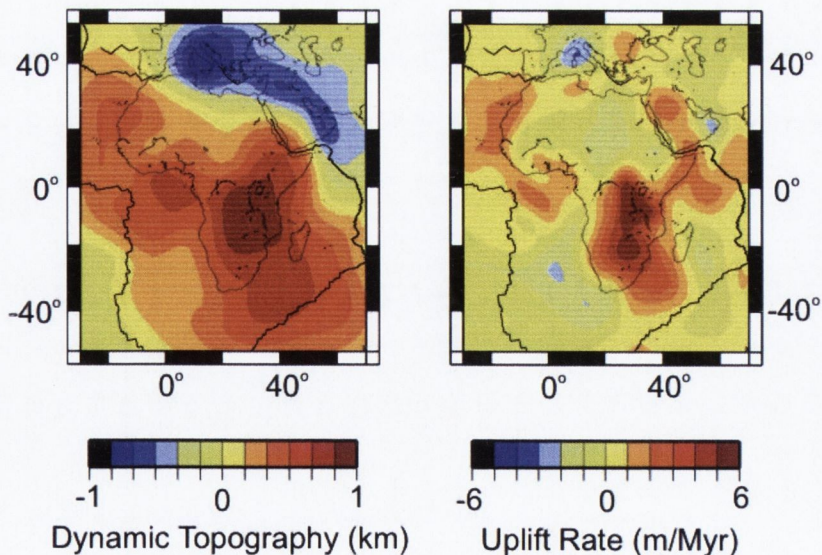


Fig. 1.5: Maps of Africa illustrating dynamic topography (left) and uplift rates (right) predicted for the Cenozoic after Gurnis et al. (2000).

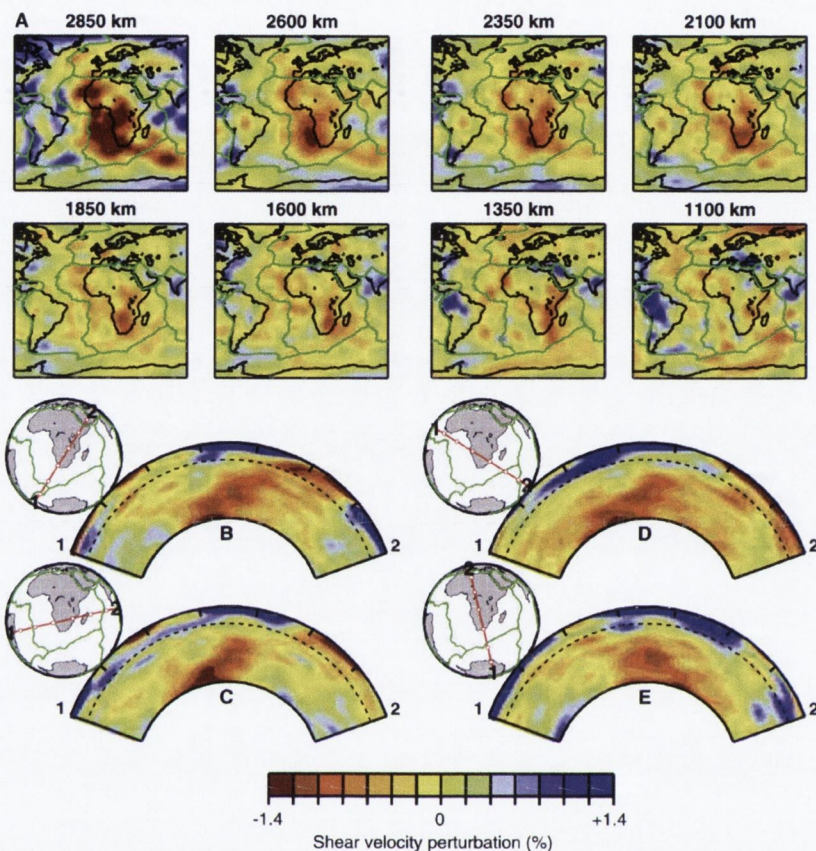


Fig. 1.6: S-wave global tomography model S20RTS, taken from Ritsema et al. (1999). The cross sections B to E show a region of low velocity that appears to originate from the core mantle boundary. This low velocity anomaly is interpreted to be the African Superplume.

Seismic tomography is a technique that resolves the velocity structure of Earth by modelling seismic waves travel-time travel through earth. Most seismic tomography models are derived with respect to Preliminary Reference Earth Model (PREM), using large databases of shear (S) or compressional (P) wave arrivals (e.g. Dziewonski, 1984; Grand et al., 1997; Ritsema et al., 1999; Zhao, 2001). Whole-mantle density models can be predicted by scaling S-wave velocity models (Gurnis et al., 2000). Cold subducting slabs, with a higher density than the surrounding mantle, are imaged by tomographic models as regions of high velocity (Ricard et al., 1993). Conversely, regions of low

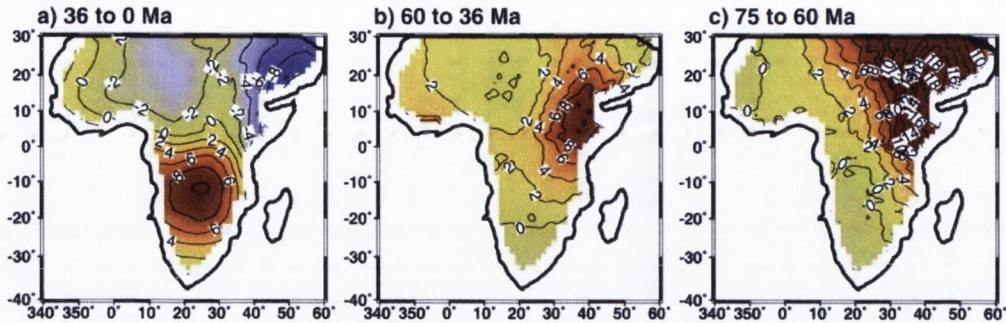


Fig. 1.7: Predictions of uplift rate on the African continent, shown in meters per million years after Conrad and Gurnis (2003). Uplift rate is calculated by differencing snapshots of predicted dynamic topography while taking into account the motion of the African plate between these snapshots.

seismic velocities are thought to be areas of warm, low-density material. However, S-wave velocity models can only be used to calculate whole-mantle density if it is assumed that the heterogeneity has a single cause that affects both the density and velocity of the mantle. Normal modes are more sensitive than body waves to density heterogeneity and have been used to further constrain the density structure of the mantle i.e. they potentially can be used to separate the effects of temperature and composition of the mantle (Ishii and Tromp, 2004). Normal modes are free oscillations of the Earth excited by very large earthquakes and therefore are more rare to observe than body waves (Ishii and Tromp, 2004).

Density models of the mantle can be used to compute dynamic topography (Lithgow-Bertelloni and Silver, 1998; Gurnis et al., 2000). The amplitude of the dynamic topography calculated is sensitive to the mantle viscosity structure used (Gurnis et al., 2000). More recently, tomographic modelling has been used to estimate uplift rates due to dynamic support at the surface the Earth (Gurnis et al., 2000; Conrad and Gurnis, 2003). Dynamic topography as a function of time can be derived by using the tomographic model of the mantle as an initial condition while reversing the direction of

flow and incorporating advection of the density field (e.g. Conrad and Gurnis, 2003).

Tomography models of the mantle beneath the African plate reveal a region of low velocity that appears to originate from the core mantle boundary (Figure 1.6). This low velocity anomaly is interpreted as large-scale thermal up-welling referred to as the African Superplume (Gurnis et al., 2000). Dynamic topography and uplift rates have been estimated from tomographic models for Africa (Figure 1.7). Studies of dynamic topography using different tomographic models predicts that the large seismically-slow (and presumably hot) upwelling structure beneath southern Africa supports between 300 – 700 m of dynamic topography (Lithgow-Bertelloni and Silver, 1998; Gurnis et al., 2000; Conrad and Gurnis, 2003). The best fit between observed topographic highs and modelled dynamic topography suggests that the high topography of Africa is maintained by density heterogeneity within the lower half of lower mantle (Lithgow-Bertelloni and Silver, 1998; Gurnis et al., 2000). Gurnis et al. (2000) estimated uplift rates for Southern Africa to between 5 to 30 m Myr⁻¹ during the Cenozoic (Figure 1.5). Conrad and Gurnis (2003), predicted that since 30 Ma, the region of active uplift has moved from eastern to southern Africa, where uplift rates are ~ 10 m Myr⁻¹ (Figure 1.7).

More recently, improved resolution of tomographic models suggests that the boundary between the regions of fast and slow velocity of the African superplume is sharp. Dynamic models that fit the seismic constraints imply the low velocity structure is the result of a dense chemical layer within an upwardly flowing thermal structure (Ni et al., 2002). Inversion of normal modes appears to support the theory that the low velocity region near the CMB is a high density anomaly (Ishii and Tromp, 2004). However, Gurnis et al. (2000) concluded that their models of dynamic topography and uplift rate are compatible with a region of high density in the lowermost part of the mantle beneath Africa, provided that the region above this has lower density.

1.3.4 Slab models

Cold slabs subducting into the mantle can cause large density anomalies within the asthenosphere. Dense slabs produce an upper mantle flow that deflects the surface of the Earth downward above them (Husson, 2006). However, Africa has not experienced significant subduction since Mesozoic times and therefore we can assume the mantle beneath Africa contains no significant amount of dense, cold slab material. Hence, we consider that slab models of dynamic topography are not relevant to Africa.

1.4 Why study Africa?

Nyblade and Robinson (1994) defined the African superswell as a broad region of anomalously shallow bathymetry and high topography, encompassing parts of the southern and eastern Africa continent, as well as the South Atlantic and Southwest Indian Ocean (Figure 1.8). Many tomographic studies now support the hypothesis that the Superswell is maintained by hot upwelling in the mantle (Lithgow-Bertelloni and Silver, 1998; Grand et al., 1997; Ritsema et al., 1999; Ni et al., 1999; Gurnis et al., 2000).

There are a number of reasons that Africa is an ideal continent to identify dynamic topography:

The African continent is almost entirely surrounded by passive margins. Therefore the mantle convection pattern under African plate has not been extensively modified by cold subducting slabs. The African topography has not been substantially altered by compressional tectonics. Africa has not undergone a major orogenic event for the past 500 Ma, with the exception of the Atlas Mountains in North Africa which formed

during the Cenozoic Alpine Orogeny. Variation in topography due to mantle convection is predicted to range up hundreds of meters (Gurnis et al., 2000) and therefore dynamic topography should be more easily identified in Africa than in a region with a more complicated tectonic regime.

In addition, Africa is moving slowly in a hot-spot reference frame over 6 Ma (Gripp and Gordon, 1990) and therefore susceptible to motions in the underlying mantle (Burke and Wilson, 1972). Therefore Africa's large surface area, has only moved slightly relative to the mantle beneath, allowing the surface expression of mantle convection to develop.

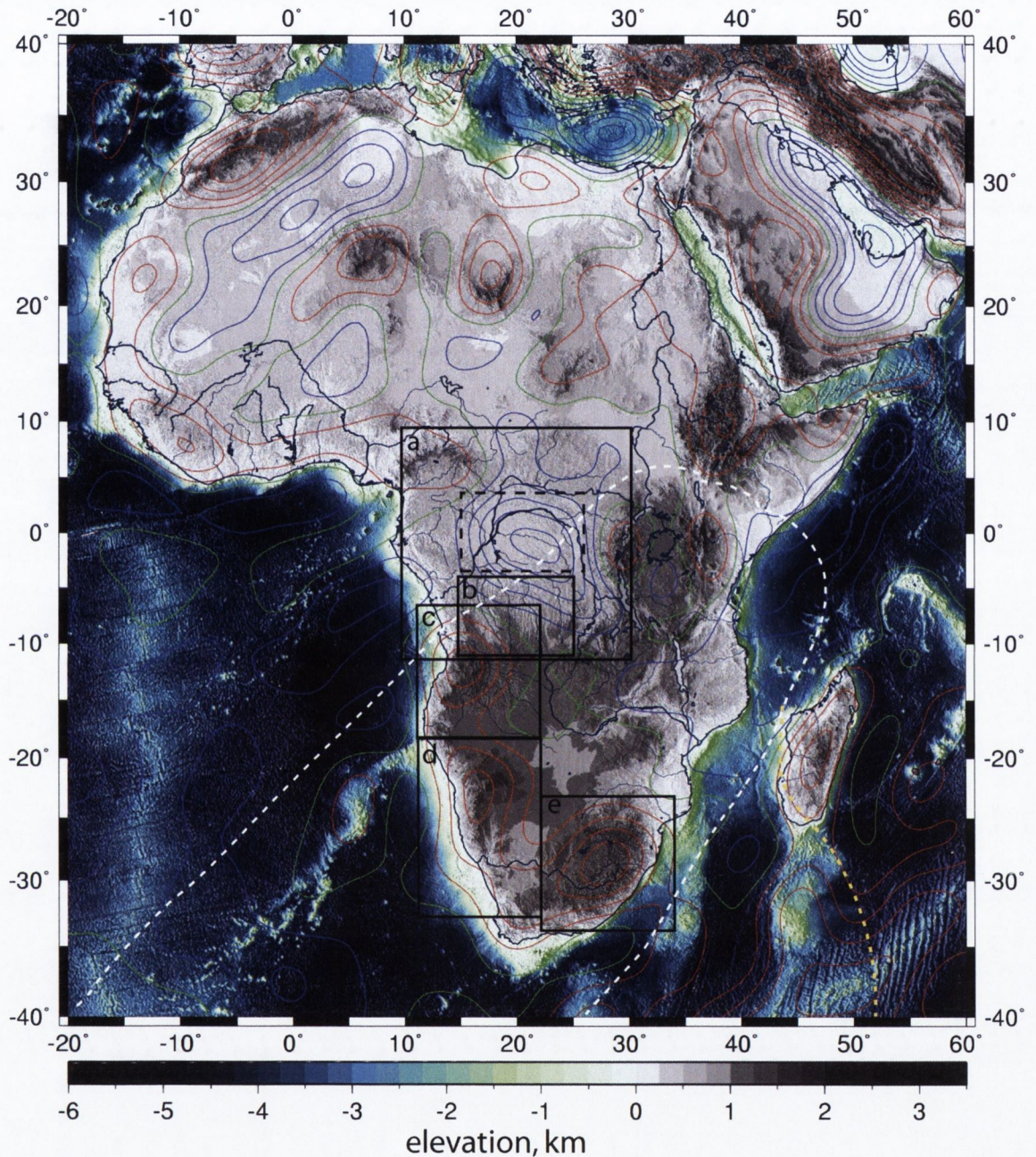


Fig. 1.8: Shaded relief map of Africa generated using SRTM 30 data. Free-air gravity contours (10 mgals intervals), which was low-pass filtered at 800 km are superimposed on top. White dashed line represents the extent of the African Superswell, identified from Nyblade and Robinson (1994). Yellow dashed line shows extent of anomalous shallow bathymetry calculated by Gurnis et al. (2000). Regions outlined are areas of interest within this study; a = the Congo River catchment, b = the southern edge of the Congo River catchment, c = the Angolan region, d = the Namibian region, e = the Karoo region.

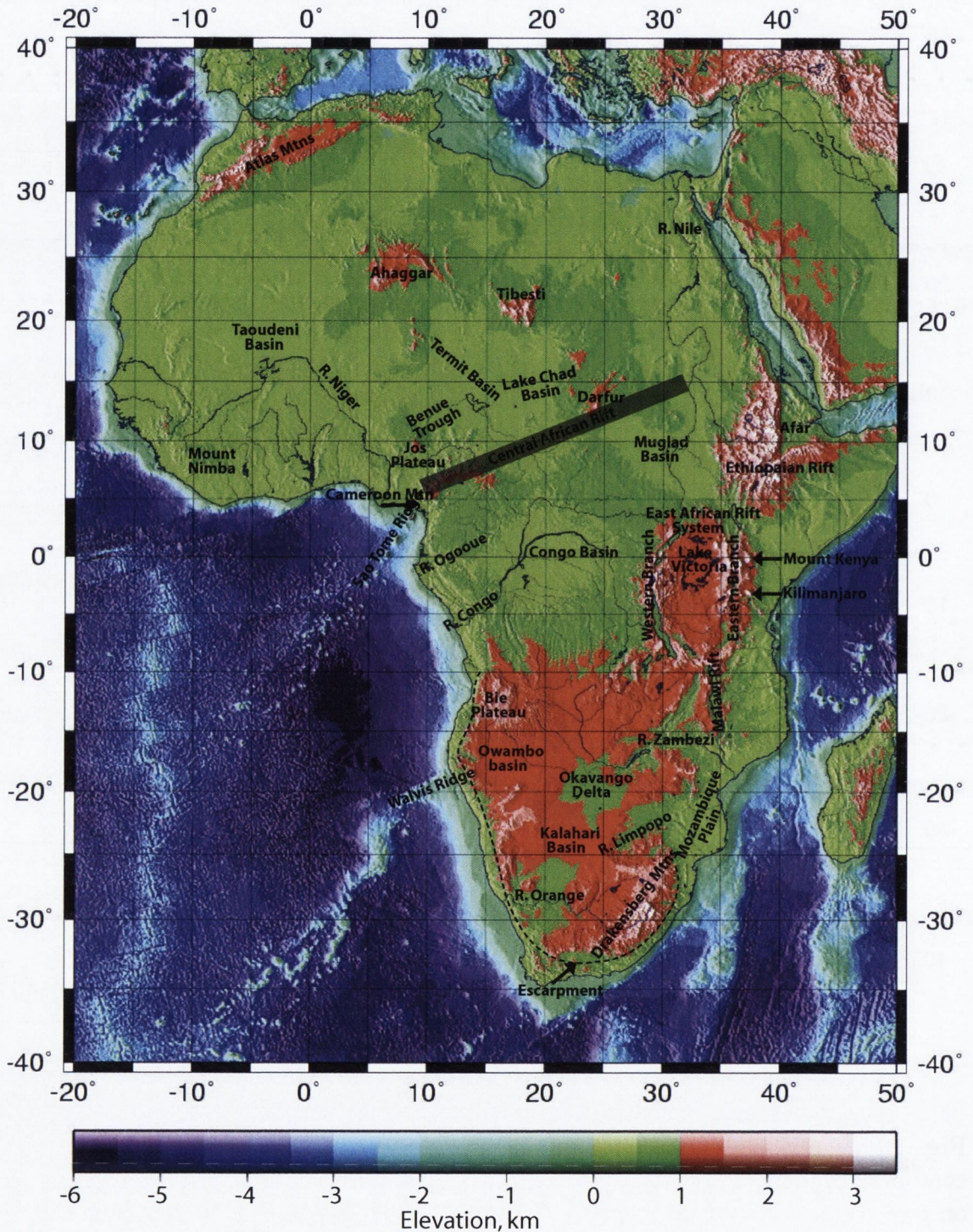


Fig. 1.9: A elevation map of Africa and its surrounding oceans. Elevations over 1000 m are highlighted in red to white colours. Major physiographical features are labelled.

1.5 Geological evidence for vertical motions

Africa has an unusual elevated topography (Burke, 1996). The elevation of the African continent is higher than any other continents that have not undergone recent compressive tectonics (Gurnis et al., 2000). In addition, the characteristic hypsometry of the continent indicates recent widespread uplift (Bond, 1978; Cogley, 1985). The southern half of the African continent is dominated by an extensive plateau with an elevation in excess of 1 km and surrounded by a steep escarpment. Most researchers agree that the escarpment is an ancient feature which originated after the break-up of Gondwana (e.g. Partridge and Maud, 1987; Partridge, 1998; Gallagher and Brown, 1999a; Brown et al., 2002). However, Burke (1996) maintains the escarpment is a young feature and has formed since the initiation of uplift in southern Africa at ~ 30 Ma. The East African Rift Valley has resulted in mountain ranges which reach elevations of over 3 km. The distinctive topography of Africa has attracted much research, however the precise timing, duration and magnitude of uplift in Africa has remained enigmatic. Evidence from different sources suggest the topography of Africa formed as result of a number of pulses of uplift and subsidence since the Cretaceous (Partridge and Maud, 1987; Hartley and Allen, 1994; Partridge, 1998; Gallagher and Brown, 1999; Brown et al., 2002; de Wit 2003). However, Burke (1996) argued that the African continent was largely flat lying until uplift, coinciding with volcanism, began at ~ 30 Ma (figure 1.10)

Sedimentary-fill in a basin preserves a record of the subsidence history. The thickness, age and geometry of sedimentary deposits can provide a direct measurement of subsidence rates, assuming that the rate of sedimentation is equal to subsidence. (e.g. Hartley and Allen, 1994). Quantifying the uplift rate is more complex and is usually estimated indirectly. There are a number of methods to infer spatial and temporal variations in the vertical motions of the Earth's surface, which will be briefly explained.

1.5.1 Geomorphic analyses and drainage patterns

Geomorphic analyses of palaeosurfaces have been used to estimate uplift rates (e.g. King, 1962; Partridge and Maud, 1987). Partridge and Maud (1987) hypothesised that the African erosional surface developed at two levels above and below the escarpment during the Cretaceous, and were unmodified until the Miocene. During the middle Miocene, asymmetrical uplift and tilting of the African surface occurred with an amplitude of 150 ± 300 m. As a result of the uplift a new cycle of erosion was initiated. A further, more significant period of uplift occurred during the late Miocene. Uplift as estimated from the tilting of the African and Post African surface, to range from 100 to 900 m (Partridge, 1998; Partridge and Maud, 2000). This method will be discussed in more detail in Chapter 3.

Drainage systems are sensitive to vertical motions of the surface they flow across. Uplift or subsidence of tens to hundreds of meters can result in a drainage system being diverted and changing course. For example regional uplift along the western branch of the East African rift system caused tilting and drainage reversal that resulted in the formation of Lake Kyoga and Lake Victoria (Doornkamp and Temple, 1966; Giresse, 2005). Dating changes in river patterns can provide a constraint on the timing of an uplift event. Cox (1989) argued that drainage patterns which indicate topographic doming associated with Tristan and Karoo plume activity are still preserved.

Migration of depot centres during the Upper Cretaceous to Tertiary along the gulf of Guinea are thought to be related to a major change in drainage organization between the Ogooe River, Kwanza River and Congo River catchments (Ishii and Tromp, 2004my et al., 2002). Studies of the depot-centres of these rivers, abandoned river courses and even the introduction of new fish species to a river all indicate that the catchments of the major river systems in southern Africa have changed many times since the break-

up of Gondwana. Many of the changes are thought to have been the direct result of subsidence or uplift within or adjacent to the rivers catchment area. The Zambezi River drains a substantial part of southern Africa. The catchment area of the modern Zambezi river is thought to have evolved as two separate fluvial systems on either side of the Victoria Falls, until the capture of the Upper Zambezi during Pleistocene times (Thomas and Shaw, 1988; Walford, 2003). The river can be divided into two distinct double concave profile, above and below Victoria falls, indicating that the two catchments have only recently been joined together. Studies of the independent evolution of fish faunas in the palaeo-catchment areas also help constrain the timing of the capture of the upper Zambezi river (Thomas and Shaw, 1988). According to the high Similarity Index between fish populations in the Okvango and the Cunene points to a former link between the two rivers, that was disturbed in the Early Cretaceous (Moore, 2001).

The longitudinal profiles of bedrock rivers are more sensitive indicators of uplift rate than other morphological properties (Whipple, 2004). Convex upward river profiles are commonly associated with regions that are actively uplifting or have recently been uplifted (Hack 1973; Howard, 1994; Kirby and Whipple, 2001). Partridge (1998) noted that the profiles of major river systems of the east coast of southern Africa are convex upward, consistent with uplift and warping. This will be discussed in more detail in Chapter 2.

1.5.2 Denudation rates

Denudation is defined as the amount of rock stripped away and measurements of denudation rates can indirectly infer uplift events in terms of magnitude and age. In areas where significant unconformities are present, apatite fission track analysis (AFTA) can

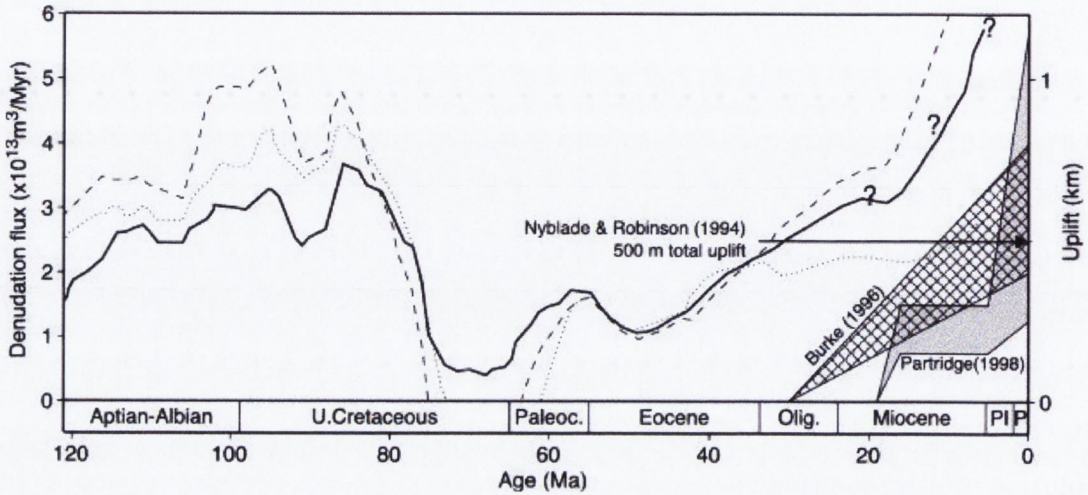


Fig. 1.10: Summary of published uplift and denudation estimates plotted as a function of time after Walford (2003). Left-hand scale: solid line = denudation flux determined from apatite fission track thermochronology in South Africa and Namibia using maximum likelihood temperature history estimate, from Gallagher and Brown (1999); dashed and dotted lines = upper and lower 95 % confidence limit on temperature history. Increasing denudation flux from 20 Ma is an artefact resulting from under prediction of fission track annealing at low temperatures (Gallagher and Brown, 1999). Right-hand scale: polygons = estimates of African uplift taken from Burke (1996) and Partridge (1998).

be used measure rate of denudation. Fission track analysis yield high erosion rate estimates during the late Cretaceous (between 100–80 Ma) across southern Africa which has been interpreted as a pulse of uplift (Gallagher and Brown, 1999; Brown et al., 2002; Tinker et al., 2008). Up to 5 km denudation since 140 Ma has occurred along the west coast of southern Africa, with as little as 1 km of denudation predicted to have occurred inland of the escarpment (Gallagher and Brown, 1999; Brown et al., 2002). Denudation fluxes are predicted to peak between 90 and 80 Ma, ~ 40 Ma after continental break-up (Figure 1.10). Gallagher and Brown (1999) calculated the palaeotopography of Africa by loading the present-day topography with the estimated denudation and adjusting for isostasy. They concluded that the African topography has been elevated to present day values since the break-up of Gondwana.

1.5.3 Sediment Flux in deltas

The stratigraphic record of fan deposits from a large river can be exploited to constrain the temporal variation of vertical motions within a catchment (Walford, 2005). Most research agrees that the maximum elevation of a catchment area is a primary control on the sediment supply of rivers. Analysis of 280 rivers revealed that the primary controlling factors of both sediment load and sediment yield are the basin area and maximum basin elevation (Milliman and Syvitski, 1992). Therefore, variation in vertical motions affecting the catchment area of a river should be reflected in its sediment load and yield (i.e. sediment load per unit area of catchment). Milliman and Syvitski (1992) concluded that climatic variables such as run-off are of secondary importance. More recently, analysis of a global dataset of 97 rivers subdivided by tectonic setting showed rate of uplift and drainage areas provide first order controls on sediment yield (Hovius, 1998). Therefore the stratigraphic record of fan deposits from a large river can be exploited to constrain temporal variation of vertical motions within a catchment (Walford, 2005).

Accumulation rates in offshore basins along the southern Cape in South Africa were highest in the early Cretaceous, which coincides with increased onshore denudation rates as derived from AFTA (Tinker et al., 2008). Many Africa deltas show significant increase of sediment flux in Early Oligocene and Miocene times (Ishii and Tromp, 2004; et al., 2002; Walford, 2003). A dramatic increase is also seen in sediment accumulation since Pliocene times in most African deltas (Figure 1.11).

1.5.4 Magmatic events

The onset of volcanism is often used to infer either transient or permanent uplift events. Mantle plume models for volcanism predict regional, domal, kilometre-scale lithospheric uplift between 5 to 10 Ma prior to the onset of flood basalt volcanism (Richards et al., 1989; Campbell and Griffiths, 1990). Magmatic activity, can lead to the addition of large thicknesses of igneous material at the base of the crust (a process known as underplating) and the permanent uplift of the region (e.g. Brodie and White, 1994). Africa has experienced a number of major magmatic events which are thought to be the result of plume activity. The Karoo plume is thought to have been centred around the east coast of southern Africa. Magma activity associated with the Karoo plume generated extensive flood basalt and reached its volcanic peak at 183 Ma (Duncan et al., 1997). The Tristan plume erupted to create the basaltic

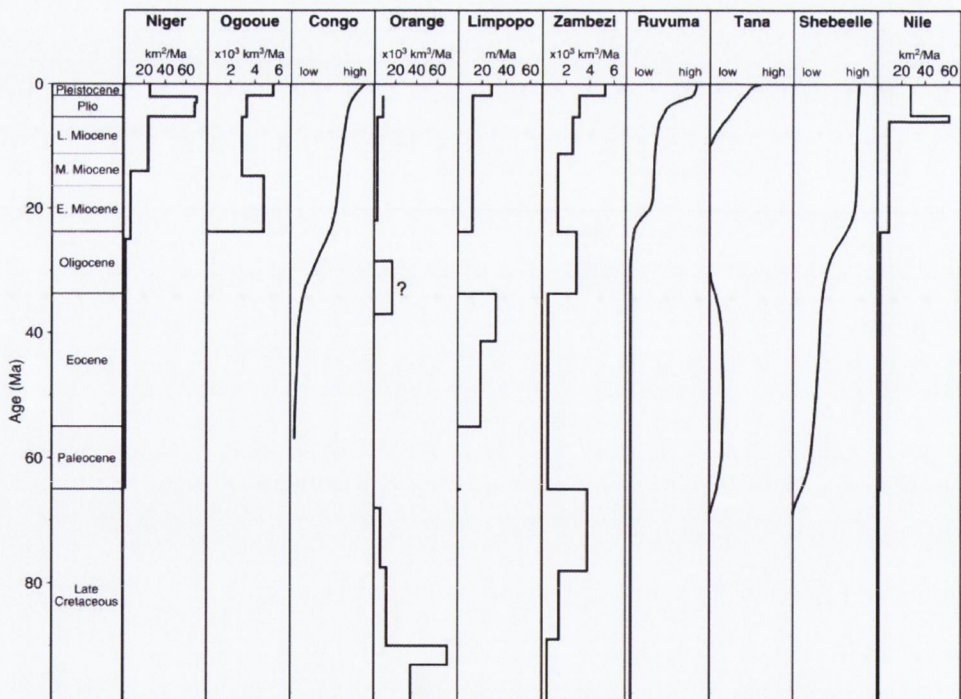


Fig. 1.11: Summary of sediment flux to major African rivers after Walford (2003).

plateaux of the Parana in South America and Etendeka in Namibia at 137–127 Ma (Stewart et al., 1996). Palaeocene and Eocene times were relatively quiet periods in Africa's magmatic history. The eruption of the Afar flood basalts is thought to mark the onset of East African rifting. $^{40}\text{Ar} - ^{39}\text{Ar}$ ages for the volcanic succession in southern Ethiopia confirm the presence of two distinct magmatic phases of the Afar eruption at 45–35 Ma and 19–12 Ma (George et al., 1998).

1.5.5 Onshore record of marine sediments

On land, elevated marine sediments and shoreline deposits provide markers to calculate uplift rate. For example, Sahagian (1988) inferred epeirogenic motions from Cretaceous shoreline deposits. Raised Cretaceous marine deposits were found on the coastal plain below the Great Escarpment, several hundred meters above sea-level (Partridge and Maud, 1987; Sahagian, 1988). However, no marine Cretaceous deposits are found on the southern African plateau (Sahagian, 1988). Burke (1996) argued that the absence of marine sediments from regions inland of the escarpment is a result of the sediments having been eroded away.

1.6 Geomorphological terminology

This study encompassed a wide area of geoscience, including geophysics, geomorphology and geology. Some terms used are may be unfamiliar to researchers in different fields. In addition, I have found that the definitions of some of the terms used in the geomorphological literature can differ. In this section, the way in which definitions for land-surfaces have evolved is discussed and the terminology employed in this study is

defined. Gunnell (1998) and Twidale (2003 b) have provided very useful summaries of definitions of geomorphic surfaces.

This study looked at two main types of palaeosurfaces: denudational surfaces formed by weathering and/or erosion; and aggradational/depositional surfaces formed by the accumulation of sediments. Palaeosurface is a very general term and implies that the surface is ancient and stagnant and has not been further eroded since its formation i.e. preserved (Gunnell, 1998). The term does not make the distinction between surfaces that have different initial morphologies or surfaces formed by different processes. In this study the term palaeosurface was applied to aggradational/depositional surfaces as well as denudational surfaces. In most cases aggradational surfaces can be defined by the depositional process that created them. However literature defines denudational surfaces by a number of different criteria including relief, formation and original elevation and some of these terms are discussed below.

A planation surface is a flat-lying, often low relief land surface that cuts across underlying geological structures (e.g. folding, bedding planes) regardless of the varying degrees of resistance the rock outcrops have to erosion. Twidale (2003 b) argues a planation surface is a low relief surface that can include both erosional and depositional elements. The fact that planation surfaces are widespread on many continents is a geomorphological 'anomaly', as most landscape evolution theory expects the surface of the land to erode at varying rates, which are often influenced by factors such as geological structures and contrasting lithologies (Gunnell, 1998). The main distinction between the different classification of planation types, is how they formed. Types of planation surfaces include peneplains, pediments, pediplains and etchplains.

A peneplain is a low-relief erosional plane worn down to near base-level i.e. the lowest level to which a land surface can be reduced by the action of running water (Philips,

2002). The formation of a peneplain is based on the Davis (1899) model of landscape evolution in which the down-wearing by fluvial erosion eventually reduces the topography to a plane near base-level. Lester King argued that landscape evolution was dominated by the fluvial back-wearing of escarpments and mountains, resulting in what he termed pediment surfaces. King, (1962) defines the pediplain as the sum of all the pediments forming a large low relief plain and the residual monadnocks or inselbergs, that forms after a extended period of erosion. Etchplain are formed where deep weathering occurs on a landscape and subsequent erosion removes the weathered regolith, forming a planation surface. The elevation of the newly formed etchplain is controlled by the depth of weathering (Twidale, 2002).

1.7 Datasets

Throughout this dissertation a number of datasets were used. A brief description of the two main datasets is included below.

1.7.1 GRACE gravity field

Throughout this dissertation, the gravity model used is calculated from the GRACE spherical harmonic model GGM02C and is low-pass filtered to retain only the long wavelength component. The filter function $F(f)$, is defined as the frequency domain ($f = 1/\lambda$), where wavelength = λ , for $f < f_c$ by

$$F(f) = \frac{1}{2} \left[\left(\frac{2}{\pi} \tan^{-1} \left(\frac{f_c - f}{\Delta f} \right) \right) + 1 \right] \quad (1.3)$$

For example $f_c = 1 \times 10^{-3} \text{ km}^{-1}$ (i.e. $\lambda = 1000 \text{ km}$) so that $F(f)$ drops off to half its maximum value at a wavelength of 1000 km, and $\Delta f = 1 \times 10^{-4} \text{ km}^{-1}$. For frequencies above f_c , the filter function is extrapolated linearly to zero;

$$F(f) = \frac{1}{2} + \left(\frac{f_c - f}{\pi \Delta f} \right) \quad (1.4)$$

This study used filter function $F(f)$ of 1/800 km which agrees with models for admittance where the highest coherence is seen at wavelengths of 800 to 900 km (Figure 1.4). GGM02C gravity field model was generated using data collected by the twin GRACE satellites between April 2002 to December 2003. The error estimates indicate a cumulative error less than 1 cm geoid height to spherical harmonic degree 70, with no discrimination between land and oceans (Tapley et al., 2004). In addition, GGM02C performs significantly better than EGM96 for wavelengths greater than 300 km (Tapley et al., 2004).

1.7.2 SRTM topographic data

SRTM 90 data is a satellite elevation model released by NASA and the US Geological Survey with near global coverage in 2004. DEMs created with SRTM have a horizontal resolution of 90 meters and a vertical error of less than 16 m over bare ground. The radar signal used to create the dataset does not penetrate thick forest canopies or man-made objects such as buildings. The resolution of SRTM 90 is over ten times better than GTOPO 30, which was the most commonly used global elevation dataset prior to 2004. The new release of high resolution topography data presents an opportunity to study the geomorphology of inaccessible regions of the world.

SRTM 90 is released as $1^\circ \times 1^\circ$ blocks which then have to be gridded together to cover larger areas. Regional scale elevation maps were produced using SRTM 30 data, which has horizontal resolution of approximately 1 km (e.g. Figure 1.8). The SRTM 30 model was generated by sampling SRTM 90 at a coarser resolution. Bathymetry estimates from ETOPO5 were used to infill regions below sea-level.

1.8 Thesis structure

Due to the geographically widespread region examined in this study, the main body of this thesis will be presented in three parts, starting with the most detailed studies and then applying the findings on a global scale.

Chapter 2 begins by looking in detail at the geomorphology of the Congo River Catchment. River profiles for the tributaries of the Congo river and adjacent coastal rivers are generated and analysed. In addition, the drainage patterns and palaeosurfaces in the southern region of the Congo River Catchment are studied.

Chapter 3 reviews the historical literature published on palaeosurfaces of Africa by King (1962) and Partridge and Maud (1987), in light of more recent analytical developments in dating surfaces such as AFTA and analysis of cosmogenic isotopes. This chapter exams the relationship between long wavelength free-air gravity and the elevation of these surfaces which have been warped by mantle convection.

Chapter 4 examines the possibility that the unusual topography of Africa is not unique as claimed by Burke (1996). Dynamic topography is thought to be a global phenomenon and therefore we look for evidence of this in the topography of other continents. This chapter begins by looking at the morphology of other passive margins around the world.

In addition Chapter 4 investigates how dynamic topography may effect the hypsometry of continents.

Chapter 5 summarises the conclusions of this study and suggests further work.

Chapter 2

Geomorphology and dynamic topography of Central Africa

2.1 Introduction

The drainage of central Africa is dominated by the Congo River. The Congo River Catchment is of particular interest as its large catchment area includes regions both of positive and negative long wavelength free-air gravity anomalies. In addition the southern margin of the Congo, situated at least 1 km above sea level, is considered part of the African Superswell. Therefore, the geomorphology of the Congo River Catchment is expected to record the influence of dynamic topography.

The tributaries of the Congo River drain into the Congo Basin, a circular intracontinental sedimentary basin associated with a large negative long wavelength free-air gravity anomaly. In addition, P-wave velocity through the mantle below the Congo region is anomalously fast (Fairhead and Reeves, 1977). Tomographic models suggest that

there is a high velocity region in the mantle extending beneath the Congo region that has been interpreted as a large mantle downwelling structure (King and Ritesma, 2000). Hartley and Allen (1994) suggested that a downward-acting dynamic force on the base of the lithosphere may have caused additional subsidence during the Cretaceous and Tertiary of the Congo basin. Mesozoic–Recent sedimentary fills of only ~ 1 km define the present-day physiographic basin (Hartley and Allen, 1994; Giresse, 2005). However, Giresse (2005) speculated that accumulation of sediment since the Mesozoic was not a result of noticeable subsidence, as Mesozoic and Cenozoic deposits within the Congo basin are characterised by a nearly horizontal structure. The negative free-air gravity anomaly, using an admittance estimate of $40 - 50$ mgals km^{-1} , suggests an amplitude of up to 1 km of dynamic subsidence within the Congo Basin.

The southern region of the Congo River catchment is situated at the edge of the African Superswell as defined by Gurnis et al. (1999) and lies between the relative topographic low of the Congo basin associated with a negative gravity anomaly and the topographic high of the Kalahari and Bie plateau associated with a positive gravity anomaly. Residual topography estimates for the southern margin indicate an average of 800 – 1000 m of excess topography (Lithgow-Bertelloni and Silver, 1998). Conrad and Gurnis (2003) predict that the large seismically-slow and presumably hot structure beneath southern Africa produced 500 – 700 m of dynamic topography throughout the Cenozoic. Using an admittance of $40 - 50$ mgals km^{-1} , free-air gravity gives estimates of dynamic topography with an amplitude of up to 750 m, centred over the Bie Plateau (Figure 2.1).

Difficult terrain and political instability in Angola and the Democratic Republic of the Congo has restricted field work in this region for the last forty years. This study has utilised newly available satellite topographic and gravity data to study this region.

This chapter aims to analyse the drainage and topography of central Africa to further understand how the geomorphology of this area has evolved during the Cenozoic. In addition, the relationship between geomorphology features and dynamic topography predicted by long wavelength free-air gravity is examined.

This chapter will be divided into the following sections:

- Description of the present day geomorphology, geology and climate of the Congo River catchment.
- Summarise evidence from previous research of how the drainage systems, geology and geomorphology evolved in Central Africa.
- Examine river profiles of the Congo River and coastal Angolan rivers to further our understanding of how the geomorphology of central Africa evolved. The majority of profiles calculated for rivers on the northern and eastern edge of the Congo basin display a mature concave upwards pattern. The morphology of profiles of rivers that drain the southern margin of the Congo River Catchment and the coastal margin of Angola suggest that the upper sections of the river were recently captured.
- Study the morphology and origin of a low-relief surface in the southern region of the Congo River Catchment. The surface appears to be tilted to the north and north-east. There is a positive linear relationship between long wavelength free-air gravity and the elevation of the surface suggesting that it is dynamically supported.

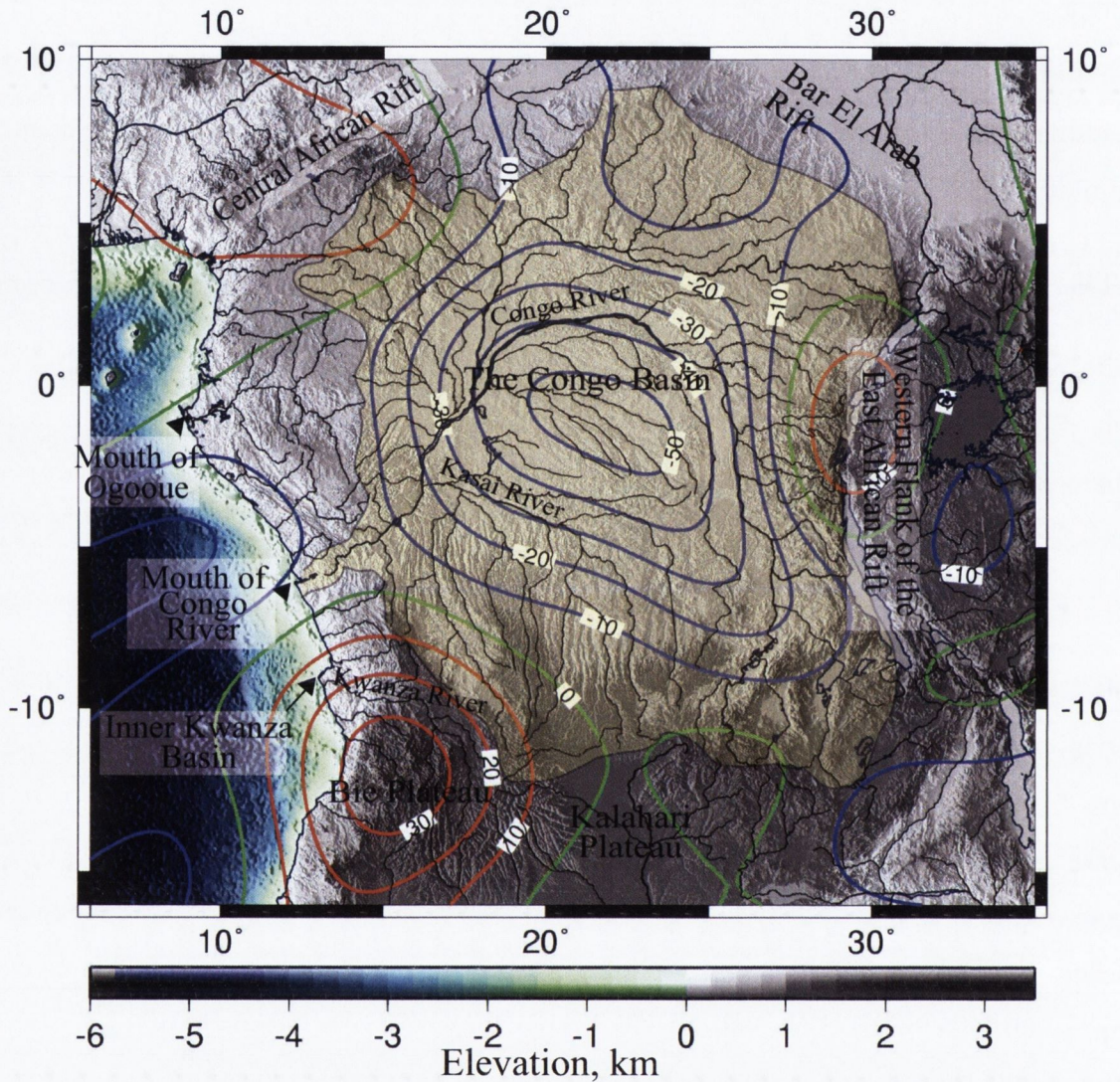


Fig. 2.1: Shaded relief map of the Central Africa with long wavelength free-air gravity contours superimposed on top. The Congo River catchment is highlighted in yellow.

2.2 Regional setting

The Congo River drains an area of 3,800,000 km², approximately one eighth of the surface area of Africa (Milliman and Syvitski, 1992). The Congo drainage system is centred around the Congo Basin, a large sedimentary basin that has been established

since the Palaeozoic (Figure 2.1).

The drainage divide of the Congo River catchment is defined by a number of topographic highs (Figure 1.9). The eastern tributaries of the Congo River drain from the western branch of the East African rift system, which presently reaches heights of up to 3400 m. The Central African Rift System forms the northern morphological boundary of the Congo Catchment, reaching elevations of 900 m. The Kalahari plateau forms the southern edge of the Congo drainage divide. Tributaries of the Kasai Branch of the Congo River flow from the Kalahari Plateau with a maximum elevation of 1400 m to the Congo Basin, with an elevation of 500 to 600 m.

The surface of the Kalahari is covered with Cenozoic sediments and the relief appears smooth. The Angolan highlands, also referred to as the Bie plateau, are located to the south west of the Congo Catchment. Basement rock outcrops in this region and the relief of the Bie plateau is high in contrast to the smooth surface of the Kalahari. Topographic peaks in the Bie plateau region reach elevations of up to 2 km. The antiquity of the topography of the Kalahari and the adjacent Bie Plateau is not constrained but forms part of the African Superswell. A large positive long wavelength free-air gravity anomaly is centred around the Bie plateau. The coastal edge of the Congo River catchment is bordered by a 500 to 800 m topographic bulge, thought to be the result of flexural upwarping due to sediment loading offshore (Lucazeau et al., 2003).

2.2.1 Climate and vegetation

The central and northern areas of the Congo Basin are covered in dense humid rainforest. The areas in the south are covered in wet savanna, with smaller areas of grassland. The Congo Basin experiences an average annual rainfall of 1000 to 2000 mm of rainfall

a year (Nicholson, 2000). Maximum rainfall of between 1600 and 2000 mm of rain occurs within 8 degrees latitude from the equator. The southern edge of Congo River catchment experiences less rainfall with an average of 1400 to 800 mm of precipitation per year (Nicholson, 2000). Very low amount of precipitation occur along coastal areas of Angola and a semi-arid climate persists in the region. The coastal rivers of Angola are mainly fed by precipitation falling in the Bie plateau.

The position of the Congo region has been within 20 degrees of latitude relative to the equator for at least the past 40 Ma (Reeves and De Wit, 2000). The Permo-Carboniferous glaciation is the most recent glacial event to affect southern Africa. The ice margin was located to the north of the Congo basin during the maximum extent of the ice sheets, before retreating in the Sakmarian (Visser, 1995). Therefore the main influence on landscape evolution for the past 200 Myr has been fluvial erosion and lacustrine and fluvial deposition. However there is also evidence for the periodic encroachment of the Kalahari desert in the past that may have caused aeolian processes to affect the areas in the southern of the Congo River Catchment (Thomas and Shaw, 1990).

2.2.2 Geology and Structure of Congo River Catchment

The geology of the region is characterised the Congo Basin, a circular intracontinental sedimentary basin surrounded by Precambrian rocks. The bedrock geology of the Congo region can be divided into four units, Archean and Proterozoic basement rock, the Jurassic and Triassic Karoo series, the Cretaceous Kwango series and the mainly Tertiary to Quaternary Kalahari Group (Figure 2.2). The Karoo series (sometimes referred to as the Lualaba series) in the Congo region consists mainly of fluvial, fluvial–glacial and lacustrine deposits (Giresse, 2005). Outcrops of the Karoo series

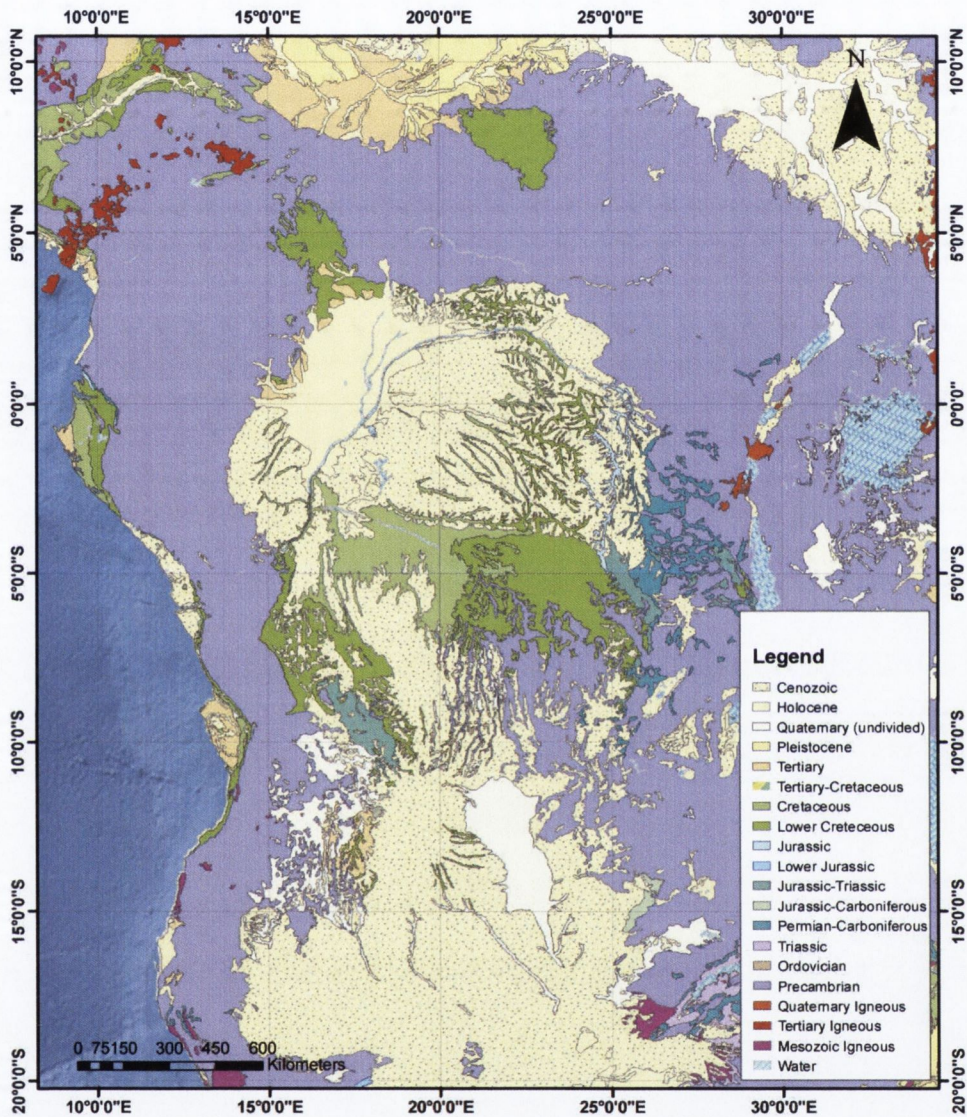


Fig. 2.2: Simplified geological map of the Central Africa based on UNESCO 1:5,000,000 geologic map. Several geologic age subdivisions on the original were combined into single unit. In general, outcrops of Quaternary and Tertiary age belong to the Kalahari Group sediments (yellow to cream); outcrops of Cretaceous age belong to the Kwango series (green); outcrops of age Jurassic and Triassic belong to the Karoo series (blue to greeny-blue) and undifferentiated basement.

are mainly limited to the east and south of the Congo region.

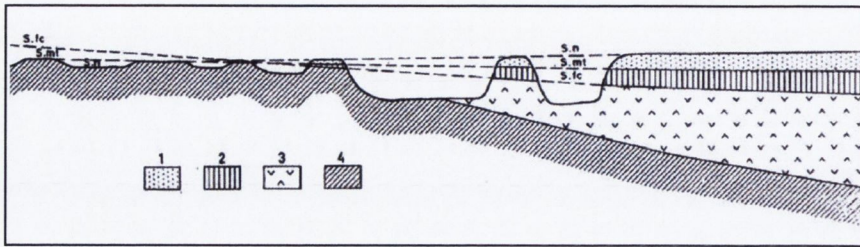


Fig. 2.3: A north-south section from the southern margin of the Congo Basin to the central Congo Basin illustrating the deposits and plantation surfaces after De Ploey et al. (1968). S.n = Neogene surface; S.mt = Mid-Tertiary surface; S.fc = Late Cretaceous surface. 1 = Sables Ogres Series; 2 = Gres Polymorphes Series; 3 = Mesozoic deposits; 4 = Precambrian basement

The main Kwango series outcrop is in the south where it overlies either the Karoo series or basement rock. The Kwango series consists mainly of soft sandstones, with conglomerates often found near its base. The surface between the Karoo series and the underlying rock is usually uneven and warped (Giresse, 2005). The upper Kwango series is cut by a Late Cretaceous planation surface (Cahen and Lepersonne, 1952). The late Cretaceous planation surface now gradually dips to the north at ~ 0.7 m per 1 km.

The youngest group of sediments is the Kalahari group which consists of the Sables Ogres Series and the Gres Polymorphes series. The Kalahari sediments were deposited across the interior of South Africa and stretch almost continuously for 2200 km from the south Kalahari Basin to the Congo basin (Haddon and McCarthy, 2005). All of the Mesozoic and Cenozoic deposits exposed in the Congo Basin and its circumference are composed primarily of clay, sands or soft sandstones characterised by a nearly horizontal structure (Giresse, 2005).

The lower unit of the Kalahari sediments, the Gres Polymorphes series, is up to 80

m thick in the Congo region and is dated by fossils to be Paleogene in age (Cahen and Lepersonne, 1952). An ostracod fauna found within the Gres Polymorphes series indicate the series is Eocene–Oligocene–Miocene in age (Grekoff, 1958). The Gres Polymorphes series is mainly composed of silicified sandstones with a basal conglomerate and its dominantly deposited by eolian processes (De Ploey et al., 1968). Cahen and Lepersonne (1952) define the Mid-Tertiary erosional surface between the upper Sables Ogres Series and the Gres Polymorphes series as a planation level (Figure 2.3).

The upper unit of the Kalahari sediments is the Sables Ogres Series. They are unconsolidated sands and have an average thickness of about 120 m in the Congo region. The sediments are believed to be deposited during the Neogene, however the age is not carefully constrained as fossils were absent in the sands (Cahen and Lepersonne, 1952).

Although the unconsolidated sands in the Kalahari Basin show evidence of aeolian reworking there is no evidence for this in the Congo region. The high portions of angular to rounded grains, scarcity of chatter marks and a poor sorting exclude an eolian origin for the sable ogres (De Ploey et al., 1968). Therefore the Sables Ocre sediments are thought to have been deposited in a slowly aggrading fluvial environment. The surface of the sable ogres is aggradational or depositional rather than erosional. De Ploey et al. (1968) compares it to some of the Quaternary deposits near Kinshasa near the centre of the Congo basin, which has a smooth, near-horizontal surface.

2.3 Evolution of the central Africa

The present day Congo River catchment dominates the drainage of central Africa. Offshore sediment accumulation indicates that other rivers, such as the Ogooué and

Kwanza, may have drained significant areas of central Africa in the past. Migration of depot centers during the Upper Cretaceous to Tertiary along the gulf of Guinea is thought to be related to a major change in drainage organization inland between the Ogooe River, Kwanza River and Congo River catchments (Leturmy et al., 2002). Therefore the drainage evolution of central Africa reflects an interplay between a number of river catchments.

The present day drainage divides of the Congo River catchment developed as a result of a number of pulses of uplift during the Cenozoic (Leturmy et al., 2003). The tributaries of the Congo River drain into the Congo Basin, which forms a topographic low relative to the surrounding area. The low elevation of the central Congo Basin is thought to be a very old feature as suggested by multiple marine incursions occurring since the Late Jurassic.

2.3.1 Congo Basin

Seismic reflection profiles taken along the Congo River continued with borehole data reveal the Congo Basin is filled with up to 9 km of sediment and suggest that the basin developed as a result of Late Proterozoic rifting and subsequent thermal relaxation (Daly et al., 1992). The earliest post-rift sediments were Infra-Cambrian carbonates and evaporites, and Cambrian marine clastics. Deformation of the basin due to the Pan African orogeny lead to uplift and subsequent erosion. Lying above the Pan-African unconformity are Ordovician-Devonian marine clastics and Carboniferous-Permian glacial deposits. A second unconformity cuts the top of the Permian sediments and was formed due to a Late Palaeozoic phase of compression (Daly et al., 1992). Late Jurassic, Cretaceous and Tertiary deposits are mainly fluvial, aeolian and lacustrine with two marine horizons. The lower marine horizon is thought to be Late Jurassic in age, while

the upper horizon represents a marine incursion during the Cenomanian to Turonian when sea level was about 150 m higher than today (Hartley and Allen, 1994). Mesozoic to Recent sediments account for 1 km thickness of the basin deposits, that cannot be directly linked to the earlier rifting process. It has been proposed that the additional subsidence may be due to a downward-acting dynamic force on the base of the lithosphere (Hartley and Allen, 1994).

2.3.2 Drainage system

Uplift along the East African Rift system began at 30 Ma as suggested by the basalt eruptions in Afar (Hofmann et al., 1997). By the middle Miocene at latest it had formed the east boundary of the Congo River (Leturmy et al., 2003). Stankiewicz and de Wit (2006) suggested that the Congo region drained eastward into the Indian Ocean until the uplift of East African Rift system in the Oligocene or Eocene (30–40 Ma). Central Africa then became a landlocked basin until it was captured by the coastal river system draining into the Atlantic during the Miocene (5–15 Ma). Prior to the Miocene the base-level of the Congo is assumed to correlate with the elevation of the lower Congo basin presently at 457 m (Stankiewicz and de Wit, 2006). Leturmy et al. (2002), suggested an alternative scenario in which the Ogooe and Kwanza depot centers migrated during the Upper Cretaceous and Tertiary along the gulf of Guinea to the present location of the Congo River mouth.

The northern morphological boundary of the Congo Catchment is formed by the Central African Rift System. It was active from late Jurassic to the Early Cretaceous and was later inverted during the Santonian (Guiraud and Bosworth, 1997). However Leturmy et al. (2002) proposed that the Central African rifts never reached heights of the East African Rift System based on the presence of Lower Cretaceous deposits

on its southern flank. The Cameroon Volcanic Line forms a chain of mountains to the north-west of the Congo River catchment boundary. The Cameroon Volcanic line is presently active and K-Ar dates of extrusive rocks indicate that it has been erupting since Latest Eocene times, ~ 37 Ma (Fitton, 1987).

The Kalahari plateau forms the southern edge of the Congo drainage divide. Tributaries of the Kasai Branch of the Congo River drain down the slope between the Kalahari plateau, with an average elevation of 1 km and the Congo Basin, with an elevation of 500 to 600 m. The sources of some of the southern tributaries are located in the Bie plateau, which reaches heights of up to 2 km. The Kwanza River (also referred to as the Cunene River) flows through the centre of the Bie plateau. It is thought that the Upper Kwanza river originally drained into what was a fresh-water lake, located over what now is the Etosha Pan, south of the Bie plateau (Goudie, 1995). The disappearance of the lake during the Late Pliocene indicates that the Kwanza changed course during the Pliocene and unified to form the present day Kwanza river (Hipondoka 2005; 2006).

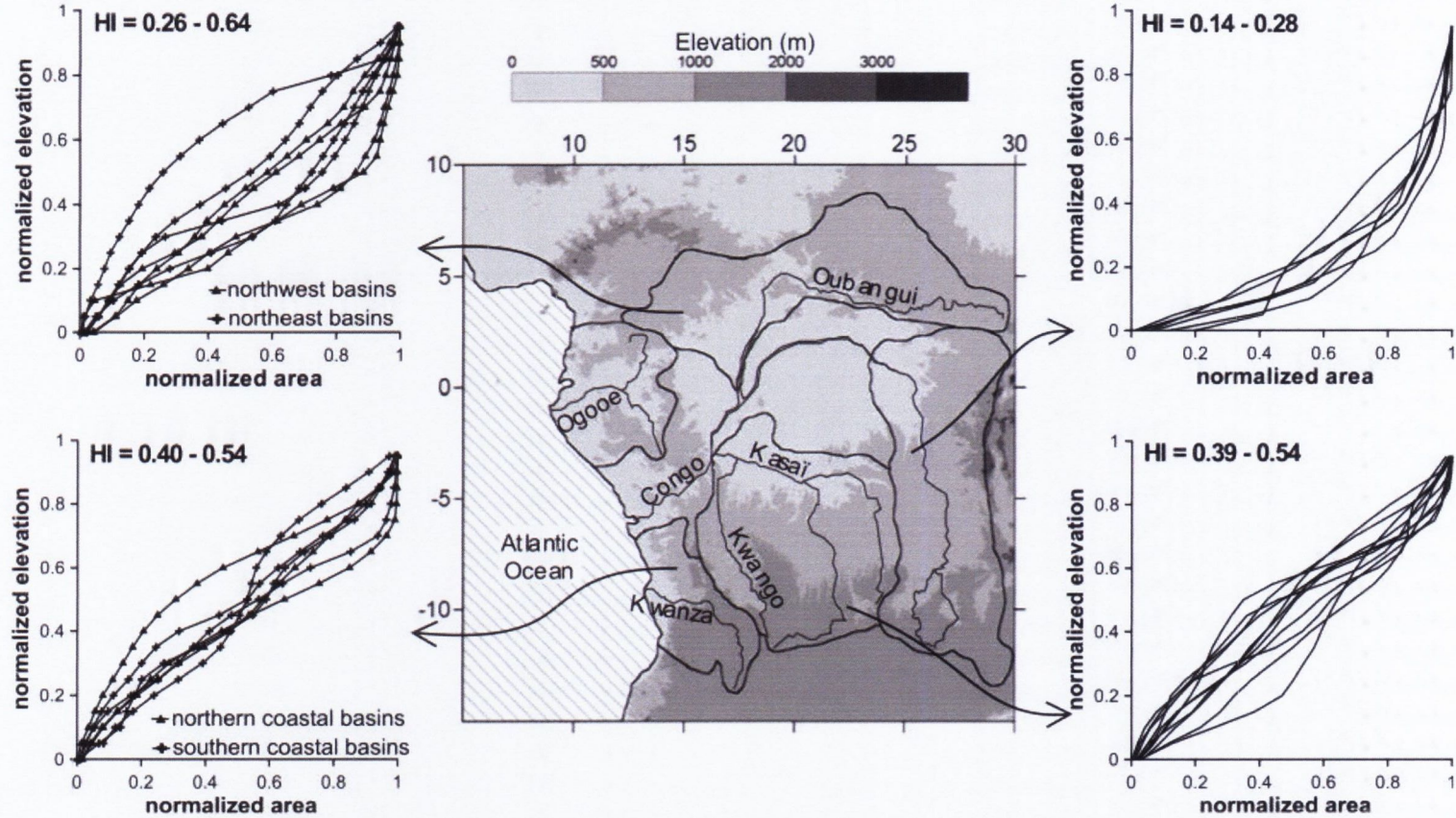


Fig. 2.4: Hypsometric curves of basins of the Congo River tributaries after Leturmy et al., (2003). Hypsometric curves show a regional distribution with both mature drainage basins (low HI and concave curves) along the East African Rift flank and immature drainage basins (high HI and convex curves) to the south. To the north, hypsometric parameters also show both immature drainage basins and mature drainage basins

The hypsometry of tributaries that drain into the Congo River show a regional distribution of immature drainage basins to the south and mature drainage basins along the East African Rift flank. Hypsometry in the northern drainage basins display both immature drainage basins and mature drainage basins (Figure 2.4). Leturmy et al. (2002) concluded the immaturity of the basins in the south when compared with the maturity of the East African Rift basins, as indicated from the hypsometry, suggest that uplift of the Kalahari plateau is not older than 10 Ma.

2.3.3 Denudation estimates along the Angolan coast

There is at present an absence of denudation rate estimates from Apatite Fission Track Analysis (AFTA) within the Congo region. Recently, Jackson et al. (2005) published fission track results for the Inner Kwanza basin in Angola. The Kwanza basin is located within the region that is associated with the long wavelength free-air gravity anomaly centred on the Bie plateau (Figure 2.1). The Kwanza Basin comprises of two sub-basins: the Inner Kwanza Basin which roughly equates to the present day onshore Kwanza basin and Outer Kwanza Basin which lies on the continental shelf offshore Angola. The Inner Kwanza Basin originally formed offshore and was exhumed during the Tertiary, as shown by the Pliocene marine terraces that rim the coastline (Jackson et al., 2005). The surface of the Inner Kwanza Basin is presently elevated at up 250 m. Apatite fission track analysis of samples taken from the Inner Kwanza Basin and Precambrian rim suggest the presence of three thermal events: 150 Ma, during rifting and volcanism; 100 – 70 Ma, during shortening and volcanism; and 20 – 10 Ma, during exhumation (Jackson et al., 2005).

Two major unconformities are present in the West African shelf stratigraphy. The first of these unconformities occurred in the Oligocene and was probably related to

changing ocean circulation (Walford, 2003). The more recent unconformity formed in Late Neogene times, causing truncation of strata at the seabed on the shelf. Denudation estimates were calculated using inversion of seismic velocity data of West African continental and suggests uplift of 400 m north of the Congo River, 300 m in the central part of the area investigated and up to 200 m in the south occurred since the Neogene along the West African margin (Figures 2.5).

2.3.4 Offshore

The West African continental margin was formed when South America rifted away from Africa in Early Cretaceous times, during which time many of the coastal sedimentary basins were formed. Rifting began south of the Walvis ridge at ~ 126.5 Ma and propagated northwards. Rifting ceased in Early Aptian times which is marked by marine transgression which generated thick salt deposits along the Gabon-Angolan margin. During Albian times, a shallow water carbonate platform formed along the Congo to Angolan margin. Further subsidence of the margins led to deltaic sedimentation along the coast. Sedimentation rates along the margin were high during this period and probably were a result of increased erosion rates along the uplifted rift flanks (Leturmy et al., 2002). Sedimentation rates remained low during the Late Cretaceous and Early Tertiary. During the Oligocene, sedimentation rates along the margin increased and high sedimentation rates/sediment flux persisted to the present-day (Figure 2.6).

Most of the stratigraphy of equatorial western Africa margin is deformed by salt tectonic structures. Three main periods of salt tectonics have been interpreted through analysis of growth structures (Seranne, 2005). The Albian carbonates and Aptian salts both were affected by early extensional deformation during the Cretaceous. A second phase of extension occurred on the slope during the Oligocene, resulting in the reac-

tivation of faults and the formation of salt rafts. A further phase of salt tectonics took place during the Late Miocene and Pliocene. Seranne (2005) suggested that high sedimentation rate during the Neogene reactivated gravitational tectonics along the equatorial western Africa margin. However it has also been suggested that the uplift centred on onshore Angola may have tilted the offshore shelf, which resulted in Tertiary deformation on the slope (Jackson et al., 2005).

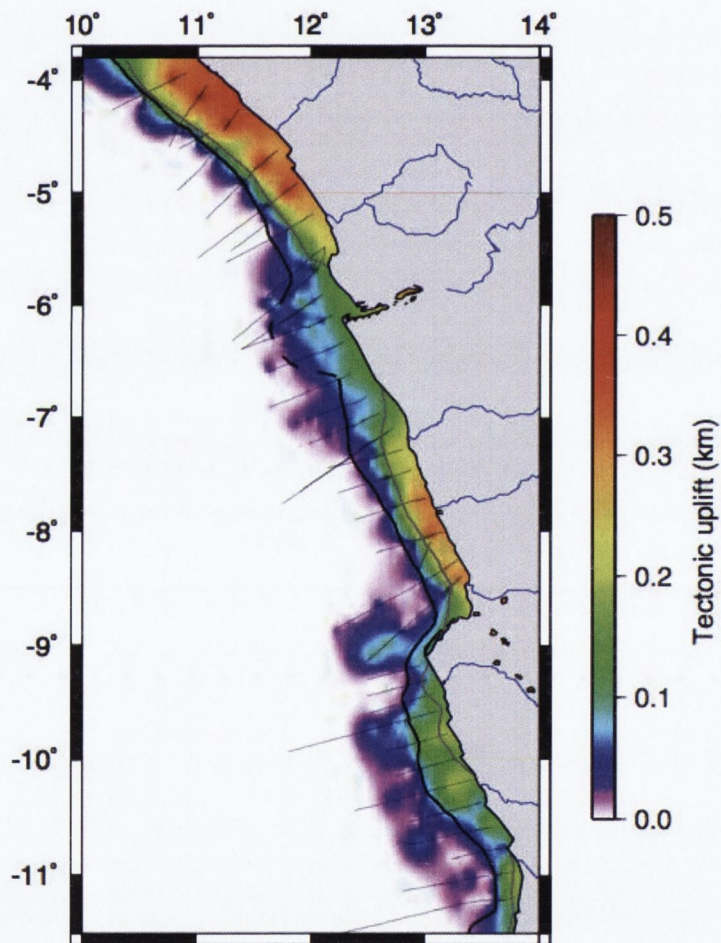


Fig. 2.5: Tectonic uplift calculated from denudation estimates using inversion of velocity data of West African continental shelf after Walford (2003). Thin lines show the location of the seismic profiles used in the denudation estimates.

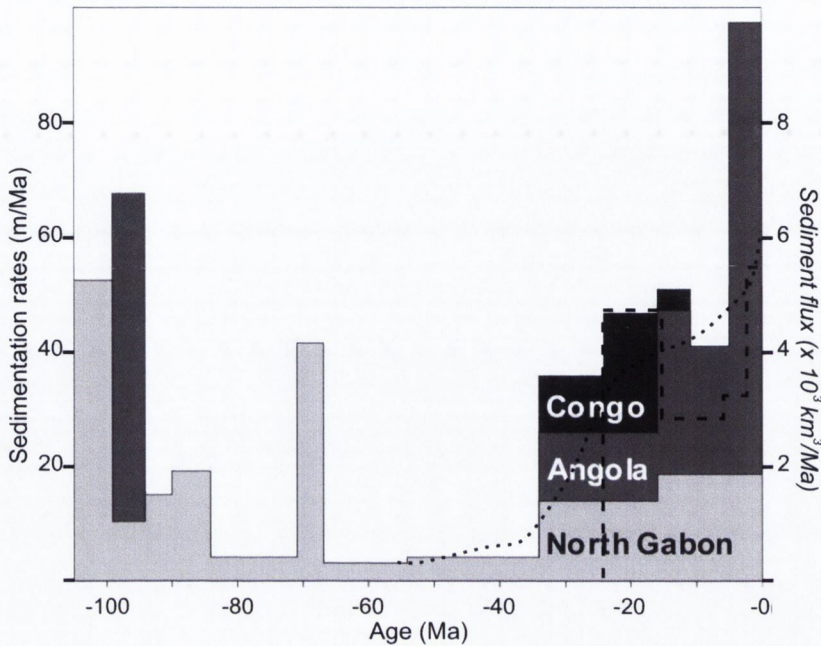


Fig. 2.6: The timing of changes in sedimentation rate and flux along the margin of west equatorial Africa. Bar chart redrawn from Leturmy et al., (2003) shows the average sedimentation rates across three seismic sections in the gulf of Guinea. Dashed line represent sediment flux into the Ogooué delta redrawn from Walford (2003). The lack of well data prevented the dating of the horizons in the Ogooué delta with any confidence prior to the major Oligocene unconformity. Therefore it was not possible to quantify the sediment flux prior to the beginning of the Miocene. The dotted line provides a qualitative estimate of the sediment flux history for the Congo delta based on examination of interpreted seismic reflection profiles and borehole data (redrawn from Walford (2003)).

2.4 River profiles

The longitudinal profiles of bedrock rivers are more sensitive indicators of uplift rate than other morphological properties (Whipple, 2004). Convex upward river profiles that are commonly associated with regions are actively uplifting or have recently been uplifted (Hack 1973; Howard et al., 1994; Kirby and Whipple, 2001). Partridge (1998) noted that the profiles of major river systems of the east coast of southern Africa are

convex upward, consistent with uplift and warping.

Knickpoint migration has long been recognised as a primary mechanism of river response to sudden base-level fall (Whipple, 2004). Base-level is the lowest level to which a land surface can be reduced by the action of running water and can be triggered by tectonic upheaval, climatic change, sea-level fall, or river capture. Knickpoints are represented in river profiles by a steepening of gradient. This can be a sharp change in gradient e.g. a waterfall or a more gentle steepening of the river profile, usually associated with rapids. Migration rates and the form of knickpoints may be dependent on the mechanical properties of substrate lithology (Sklar and Dietrich, 2001). Variations in the erodibility of rock a river flows across is also shown to cause knickpoints. Where knickpoint migration dominates, an analysis comparing incision rates to modern stream gradients can be rendered meaningless (Whipple, 2004).

2.4.1 River profiles in equilibrium

Hack (1957; 1973) stated that the geometry of a river profile that has reached equilibrium flowing over rocks of uniform resistance to erosion can be described by a simple logarithmic function. That is, elevation plotted versus the natural log of the distance from the source of the river should form a straight line. This relationship is described by the equation:

$$SL_n = \frac{(H_{n-1} - H_n)}{\ln L_n - \ln L_{n-1}} \quad (2.1)$$

where n = a point on a river profile, S = local slope, L = length from source (down stream distance) and H = elevation. SL is also referred to as the stream-gradient index

in Hack(1973).

Deviation from this straight line was used by Goldrick and Bishop (1995) to quantify disequilibrium in a river. D^* is the amount of deviation at any point downstream of the point of departure from the semi-log straight line.

$$D^* = (SL_x - SL_y) \ln \frac{ab}{ac} \quad (2.2)$$

SL_x equals the upstream stream-gradient index Hack(1973) and SL_y equals the downstream stream-gradient index. The value D^* at any point along the stream records the total height of the original knickpoints that have migrated upstream of the point (Goldrick and Bishop, 1995).

Hack (1957) also noted a relationship between between upstream drainage area and local slope in rivers that had reached equilibrium by comparing two different rivers. He measured the discharge along a river and found it proportionally increased with upstream drainage area. Therefore he took upstream drainage area as a proxy for discharge.

2.4.2 Stream power law and migration of knickpoints

Howard (1983) used channels in soft sediments (with very short erosional scales) as an analogue for channel erosion rate. He concludes that the erosion rate at any point in the river is proportional to $4/9^{th}$ the power of the drainage area, A , and $2/3^{rd}$ the power of the gradient, S .

Howard et al., (1994) reviewed the power law to have variable powers to become:

$$U(x, t) = KA^m S^n \quad (2.3)$$

and therefore:

$$\Delta h = U(x, t) - -KA^m S^n \quad (2.4)$$

Where $U(x,t)$ = erosion rate, Δh = the rate of change in river elevation, K = a constant affected by erodibility of the lithology. Howard (1994) used varying m and n values to test the upstream retreat of knickpoints following a fall in base-level. A period of slow constant uplift (in which the river has reached equilibrium) is interrupted by brief pulses of uplift. The simulation shows a steep gradient at the farthest downstream section of the stream. The model predicts that as the kickpoint retreats upstream it becomes less steep.

Most tests of river incision models assume steady-state conditions and channel gradient does not change with time (Lague, et al., 2000; Kirby and Whipple, 2001). If the incision is episodic and driven by knickpoint migration, as is the case for most rivers that drain the southern edge of the Congo Basin, these assumptions are not valid as channel gradient will change with time.

Van der Beek and Bishop (2003) used transient river profile evolution to compare and test several models. Early Miocene river channels in the Blue Mountains, Australia are preserved by basalt flows and used to test different incision rate models. K-Ar geochronological data indicate that most of the Blue Mountains basalts erupted in a relatively short time span (20.1–14.5 Ma). They estimate that major knickpoints along the river retreat upstream at a rate of $\sim 800\text{--}1200$ m Myrs⁻¹. The bedrock geology of study area comprised metamorphic rocks, granite and basalt tops, which are all relatively resistant rock (Sklar and Dietrich, 2001). The best fit predictions of the

tested models were the detachment-limited stream power model and the undercapacity model (in which river width varies as function of drainage area).

2.5 Methodology

SRTM 90m data was used to construct DEM (Digital Elevation Models) of the region. The approach taken to analyse the DEMs is summarised in Table 2.1.

2.5.1 Longitudinal River Profile Extraction

Detailed river profiles have been constructed by tracking the co-ordinates of the rivers along the SRTM 90 m data. The co-ordinates of the rivers were originally obtained from GIS data. However, when the co-ordinates of the river were plotted over the DEM the river co-ordinates did not always correspond to base of the river valleys. Horizontal errors in river coordinates tended to produce positive noise in the river profiles, as it tended to include elevations from the interfluves and sides of the river valleys. The positive noise was most evident along knickpoints in the river profiles where the river valleys were steep and vertical distance between the top of the interfluve and the base of the river valley were large.

Two methods were tested to solve this problem. The first method, assumed that since rivers flow downhill elevation should only decrease downstream. Although this method produced geologically believable results, profiles lost resolution that was contained in the original DEM. The second method obtained the river co-ordinates by digitising the base of the river valley from topographic maps. The co-ordinates acquired from the GIS data were used as a starting point and plotted on a topographic map which

Step	Procedure	output	Analysis and Interpretation
1.	Display DEM grey scale DEM 3D surface	Contour map	visual interpretation
2.	Relief	shaded relief map	geomorphological units
3.	Cross-section swath profiles	2D profile gradient, curvature, relief	identify peaks, river valleys,
4.	Slope	slope map	classification of degree of slope
5.	Aspect	aspect map	spatial distribution, shape
6.	Overlay DEM with	(a) drainage patterns (c) geology (c) Free Air Gravity	interpretation of geomorphology
7.	Extraction of river profiles	river profiles of catchment	concavity index, knickpoint identification

Table 2.1: Procedure for analysis of geomorphological features in DEMs (Digital Elevation Models).

illustrated 20 m changes in elevation as colour intervals. The river co-ordinates were then picked from the topographic map at a greater horizontal resolution and accuracy than the original river co-ordinates. The first method was applied to over 50 river profiles from the Congo River catchment and smaller catchments along the Angolan coast. The second method was used to obtain profiles of major rivers that were studied

in more detail, such the rivers that drain the southern region of the Congo basin and the Angolan coastal margin.

The second phase of the analysis was to determine if knickpoints could be explained by changes in lithology. Many river profiles that drained the southern margin of the Congo River catchment contain knickpoints or changes in gradient. The geology of this region is quite simple therefore the geological boundaries were plotted on the on the profiles. Geological information was obtained from two maps, a geological map of the Democratic Republic of Congo published in 1952 with a scale of 1: 2,000,000 and a geological map of Angola published in 1987 with a scale of 1:1,000,000.

2.6 River profiles: results and interpretation

This section describes the results for the river profiles obtained and interprets the morphology of the profiles. Over 40 elevation profiles of the tributaries of the Congo River were created. A sample of some of the major river profiles can be seen in Figure 2.7. In addition, river profiles of the smaller catchments that drain the Angolan coastal margin were also created. Analysis of river profiles indicates a correlation between convex upward river profiles and the elevated areas to the southern edge of the Congo Basin and along the Angolan coast. In contrast, the majority of profiles taken from rivers on the northern and eastern edge of the Congo basin show a concave upwards pattern. Rivers that drain the region south of the Cameroon Volcanic Line also appear convex upward in the upstream region of the profile. The Upper Sandgha Dja River drains the flanks of the Cameroon Volcanic Line. Two knickpoints can be identified in the profiles of the Sandgha Dja river at 80 km and 150 km from its source (Figure 2.7).

The majority profiles of the tributaries that drain onto the Kasai River contains an inflection point. Upstream the profile appears convex up upstream and downstream the profile appears concave down downstream. Downstream of the inflection point the river has incised through the thin Kalahari sediments and is currently eroding into the older Kwango sediments (Figure 2.8c and 2.8c). The Wambia river has incised through the Kwango sediments to expose the basement in areas (Figure 2.9(b)). The base river valleys downstream of the inflection point are up to 400 m lower than the interfluves (Figure 2.10). The river has not incised through the younger Kalahari cover in the immature, convex upward portion of the profile. The Luluia river can be divided into two distinct double concave profile. The Luluia river flows across PreCambrian outcrops with a complex geology. The inflection points on the river profiles usually

occurs at between 0.8 and 1 km of elevation.

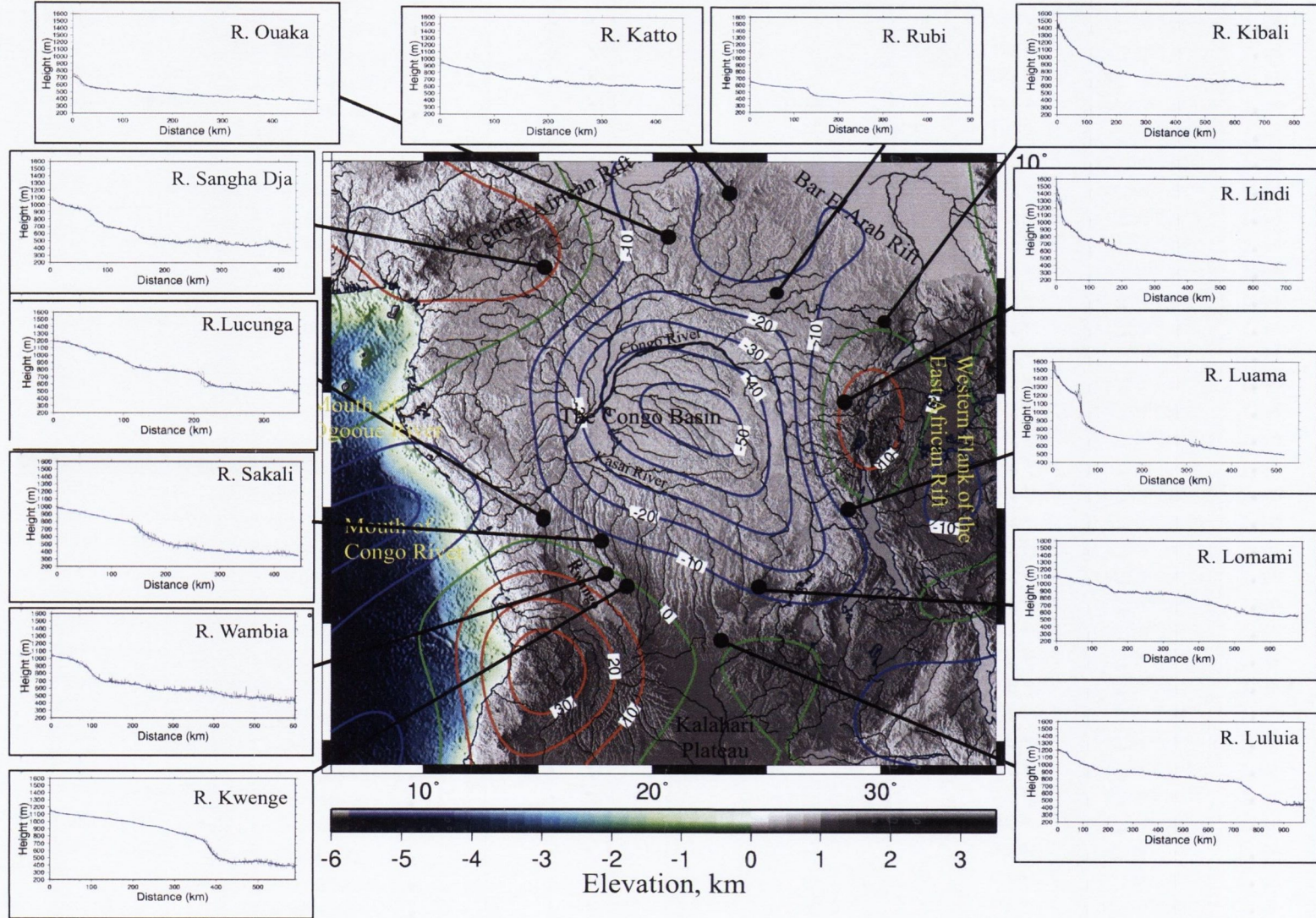


Fig. 2.7: River profiles of selected tributaries of the Congo River. The locations of the rivers are identified on a shaded relief map.

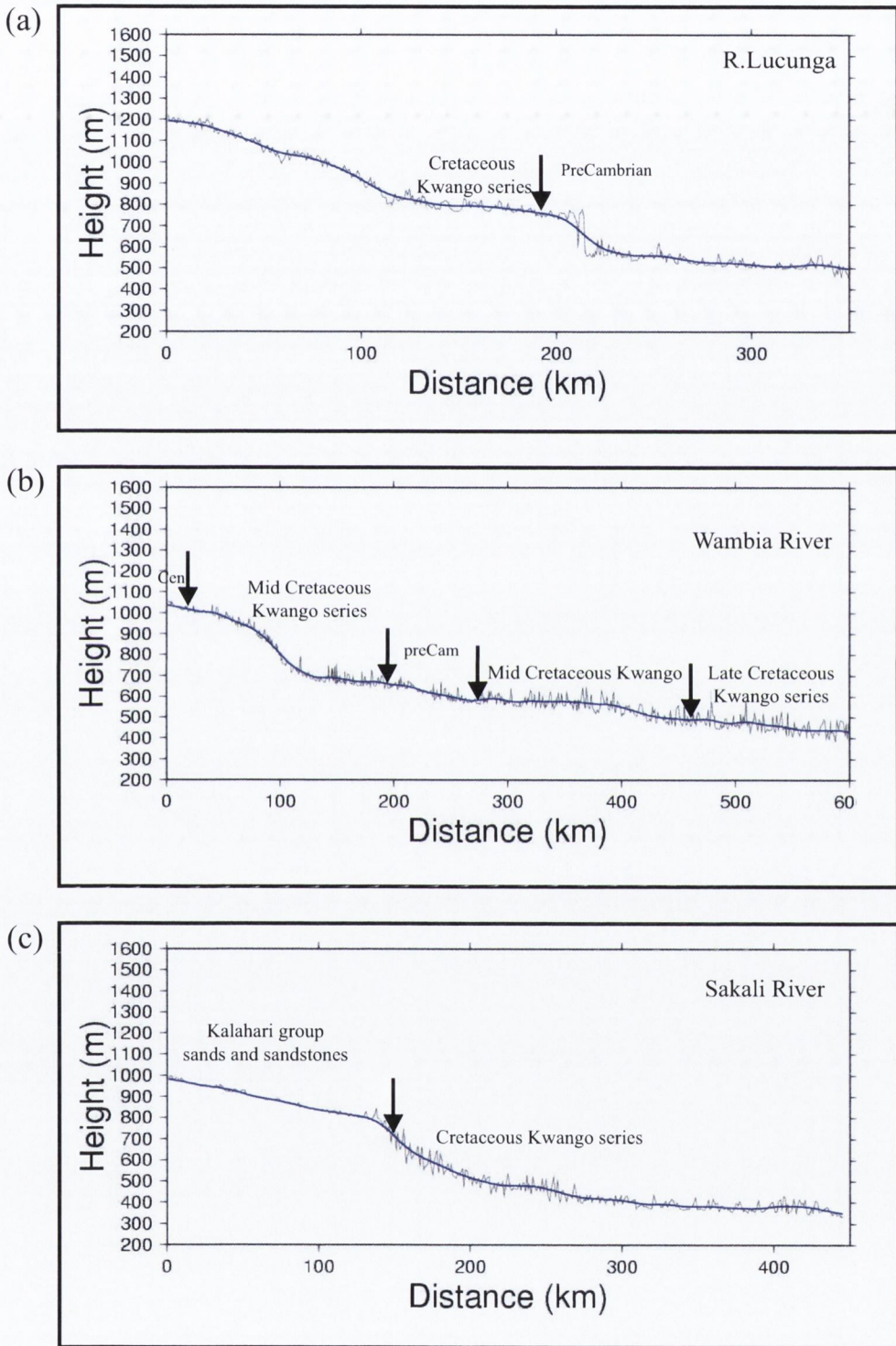


Fig. 2.8: Geological boundaries are highlighted along the Lucunga, Wambia and the Sakali river profiles. The thin black line plots the actual elevation values. The blue line represents the average elevation values. The location of the rivers are plotted on Figure 2.7.

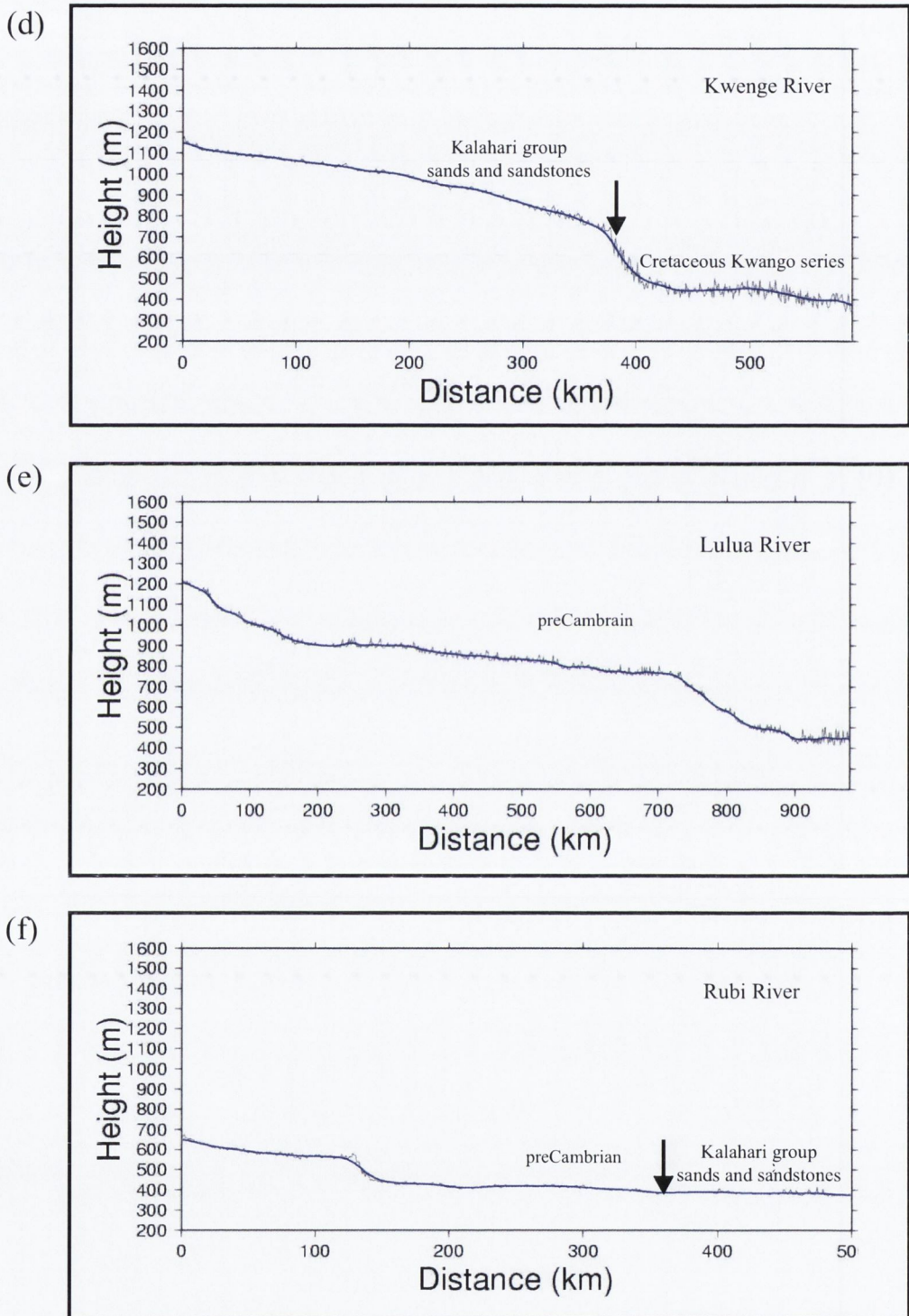


Fig. 2.9: Geological boundaries are highlighted along the Kwenge, Lulua and the Rubi river profiles. The thin black line plots the actual elevation values. The blue line represents the average elevation values. The location of the rivers are plotted on Figure 2.7.

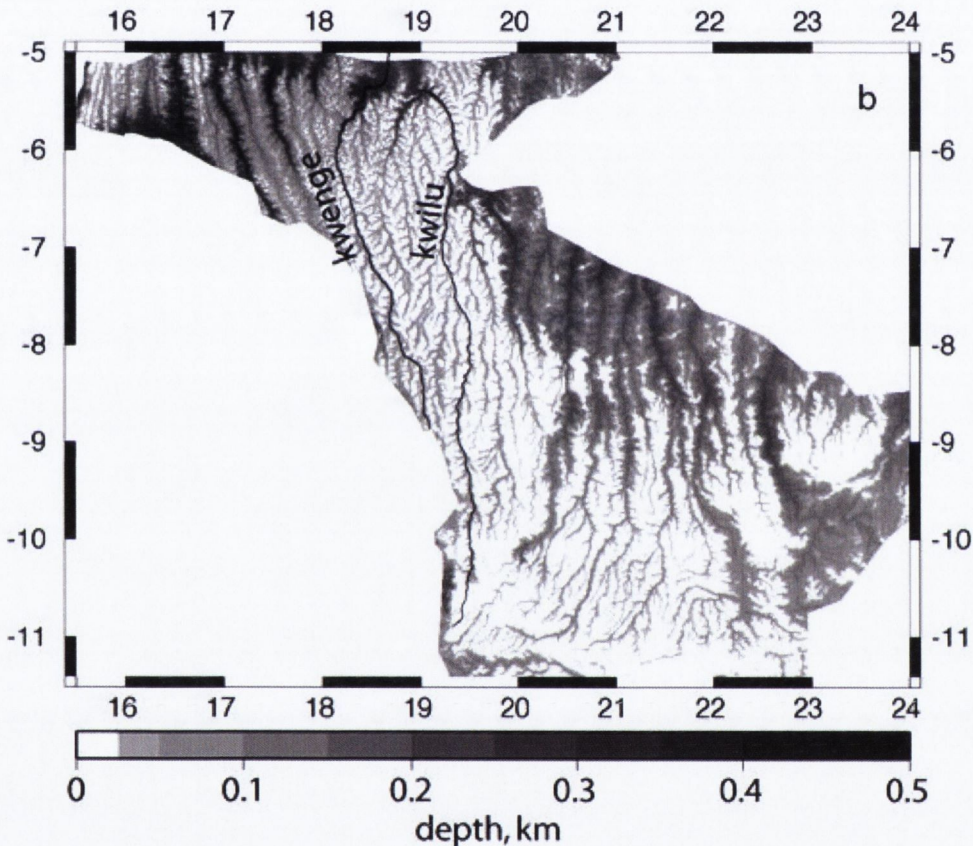


Fig. 2.10: Incision of rivers measured relative to the surface of the Kalahari sediments. Present day topography was subtracted from the reconstructed surface of low relief surface.

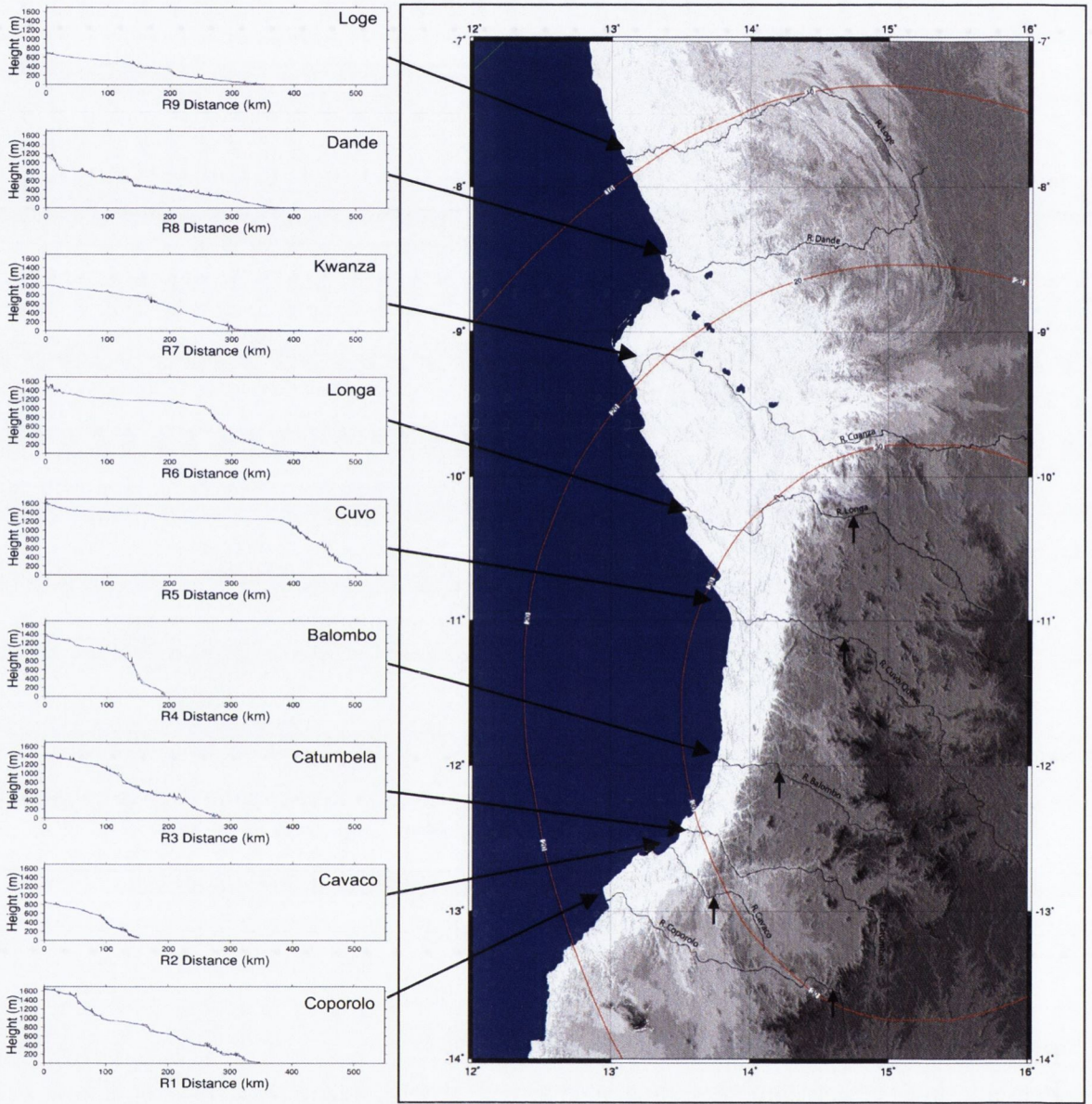


Fig. 2.11: Profiles of rivers that flow through western Angola and into the South Atlantic. The locations of the rivers are plotted on a shaded relief map. Black arrows on the map represent location of inflection points which can be seen in the river profiles. The thin black line plots the actual elevation values. The blue line represents the average elevation values. Long wavelength free-air gravity contours are superimposed on top of the relief map in 10 mgal intervals.

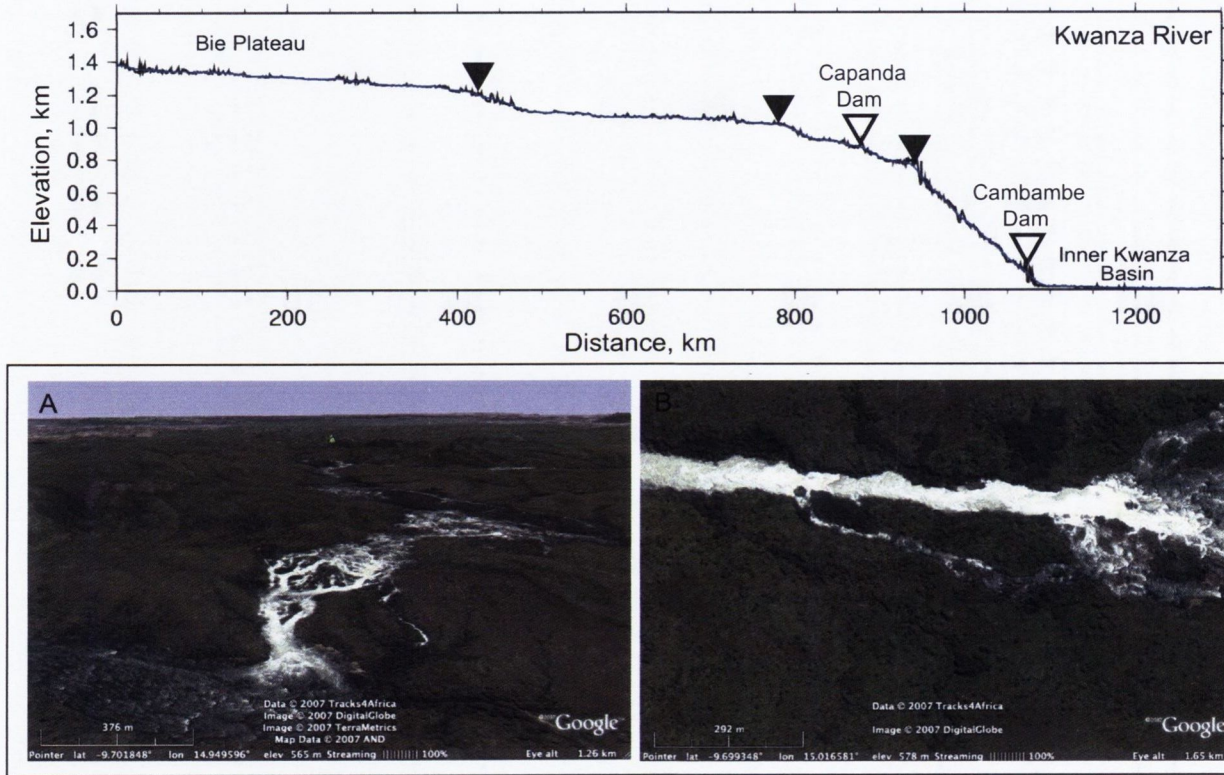


Fig. 2.12: Top: Profile of Kwanza river: Inflection points are marked as black triangles. Two dams have been built on the river; Capanda Dam (15.461709° E, 9.791575° S) and the Cambambe Dam (14.480591° E, 9.752594° S). **A** Elevated view looking northwards (upstream) and **B** a plan view of Google Earth satellite images displays rapids on the Kwanza river downstream of the Capanda Dam.

The profiles of rivers that drain the Angolan coastal margin display similar morphology to the southern Congo River profiles (Figure 2.11). The change in gradient of the profiles is most pronounced in the Longa, Cuvo and Balombo rivers, which all drain areas associated with a long wavelength free-air gravity anomaly of over 30 mgals. The inflection points on the river profiles usually occurs at between 0.8 and 1 km of elevation. Smaller knickpoints along the Loge and Dande rivers are probably controlled by the structure and lithology changes of Western Congolian fold belt which it flows across.

The morphology of the Kwanza river profile is more complex and contains a number of changes in gradient. The Kwanza river drains through the centre of the Bie Plateau and there is evidence that the Upper Kwanza was captured recently (Hipondoka 2005; 2006). The steepest gradient of the river profiles occurs between elevations 900 and 1000 m along which rapids and waterfalls are common (Figure 2.12). Downstream of Cambambe Dam the Kwanza river meanders and abraids as it flows across the exhumed Inner Kwanza basin.

2.7 Low relief surface

DEMs and profiles show that drainage along the southern edge of the Congo River Catchment incises into a smooth, low relief surface (Figure 2.13). The surface represents the top of the Kalahari sedimentary series. The upper unit of the Kalahari sediments are the Sables Ogres Series which are unconsolidated sands and are thought to be largely deposited in a slowly aggrading fluvial environment during the Neogene (De Ploey et al., 1968). The Sables Ogres Series lie unconformably on top of the older Gres Polymorphes series. Cahen and Lepersonne (1952) define the Mid-Tertiary sur-

face between the Sables Ogres series and the Gres Polymorphes series as a planation level that was later deformed.

2D vertical profiles through a DEM of this region reveal that the low relief surface is undulating (Figure 3.3). To remove the effects of modern drainage eroding into the low-relief surface over one hundred vertical profiles were created through the DEM, every 0.1° (~ 10 km) parallel to latitude. Co-ordinates of where the surface was visible were digitised from the profiles. The elevation for each co-ordinate was extracted from the DEM. The longitude, latitude, elevation points were then used to create a surface using an adjustable tension continuous curvature surface gridding tool (Figure 2.15). The grid of the surface created has a resolution of about 2 km. This is higher than the density of picked points, in order to retain features.

Long wavelength free-air gravity, low pass filtered at 800 km is plotted against the elevation of the surface. There is an obvious linear relationship between the elevation of the reconstructed surface and free-air gravity. A least-squares regression line was fitted to the data points and had a slope of ~ 40 mgals km^{-1} (Figure 2.16).

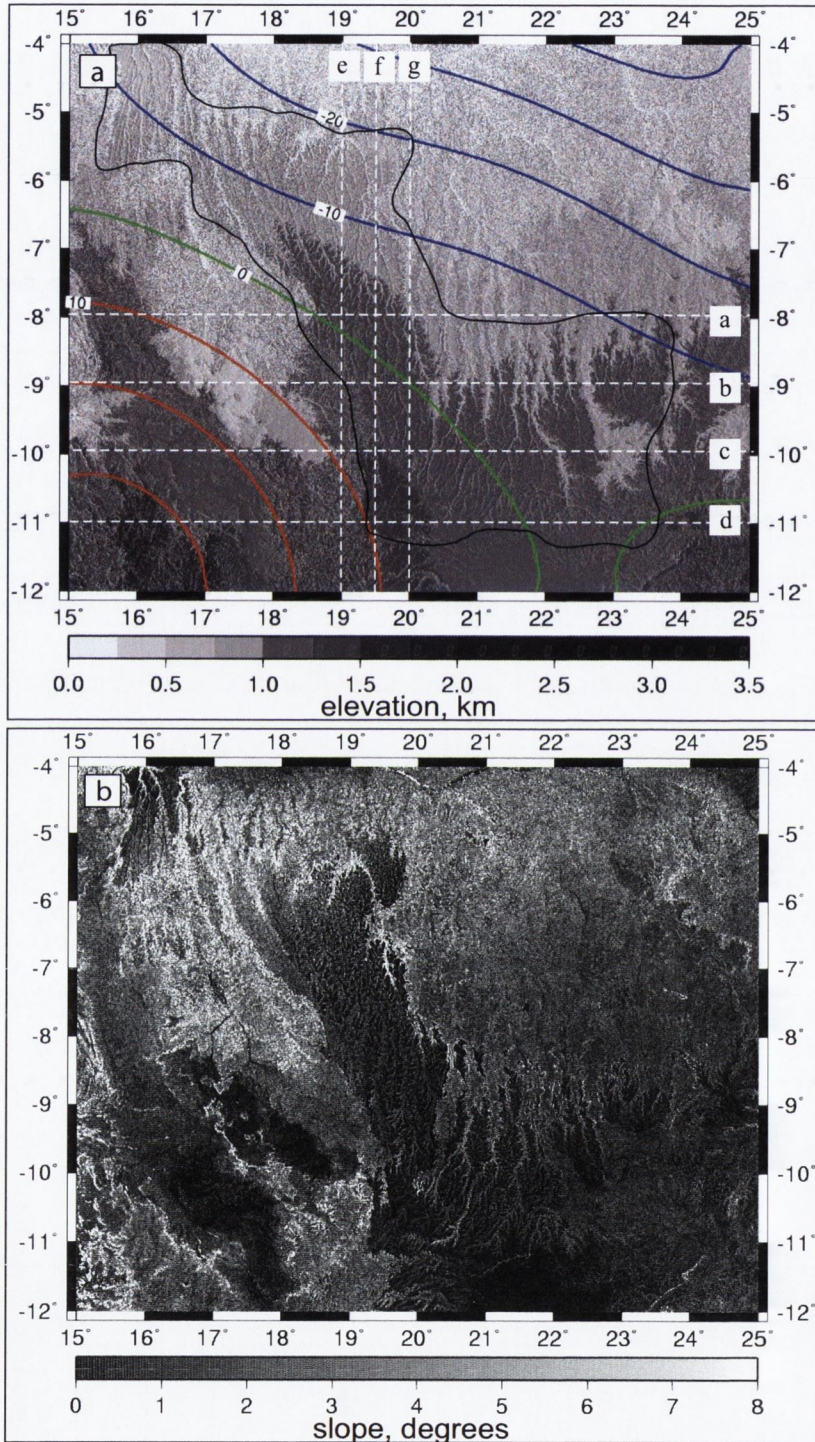


Fig. 2.13: (a) Long wavelength free-air gravity contours superimposed on a shaded relief map of the southern Congo Basin margin. Contours every 10mgals. Red contours equal positive gravity anomalies. Blue contours equal negative gravity anomalies. Green contour equals zero. White dashed lines show co-ordinates of cross-sections taken through the DEM. Black line shows extent of surface seen on cross-sections.(b) Slope map in degrees of the region. Dark areas are interpreted as regions of very low relief. Light areas are interpreted as regions of a high relief.

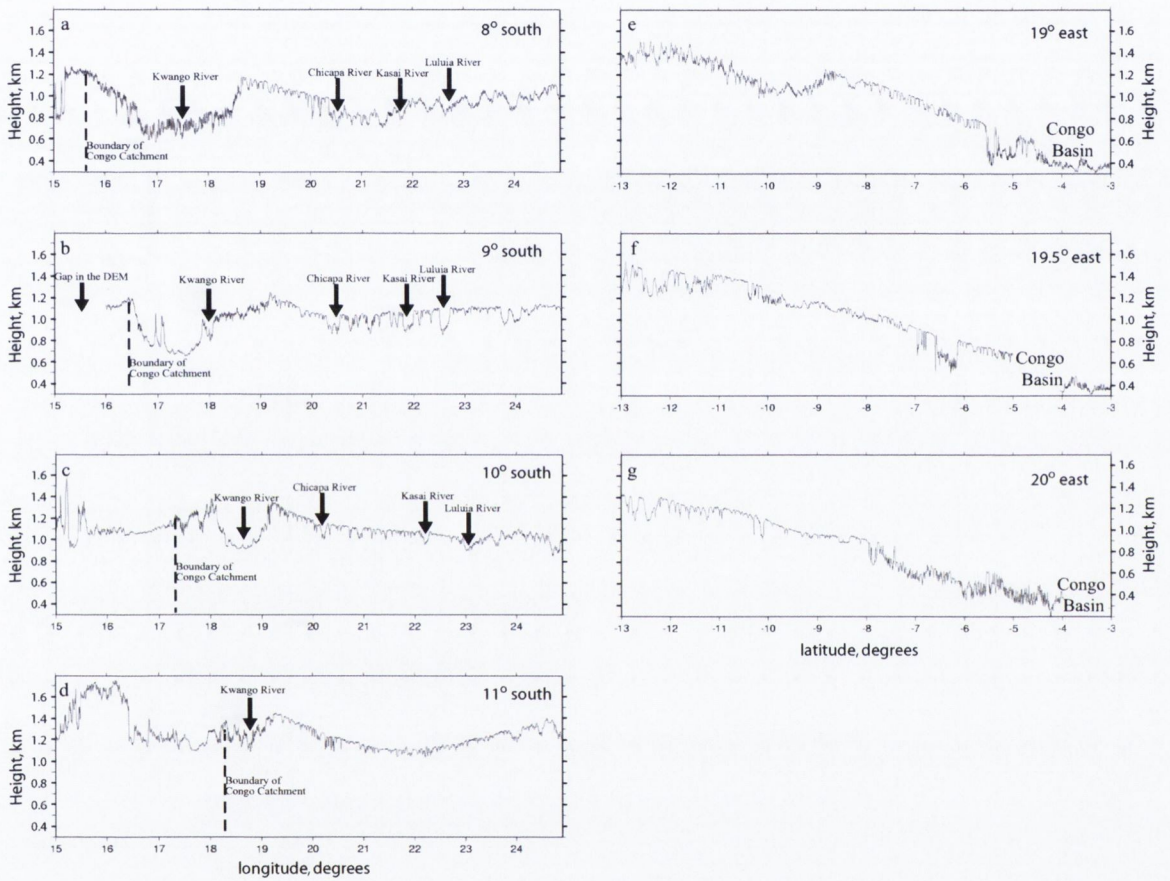


Fig. 2.14: (a), (b), (c), (d) Cross sections taken through the DEM of 90m resolution parallel to longitude at 8, 9, 10, and 11 degrees south of the equator. (e), (f), (g) Cross sections taken through the DEM parallel to longitude at 19, 19.5 and 20 degrees east of the Prime Meridian.

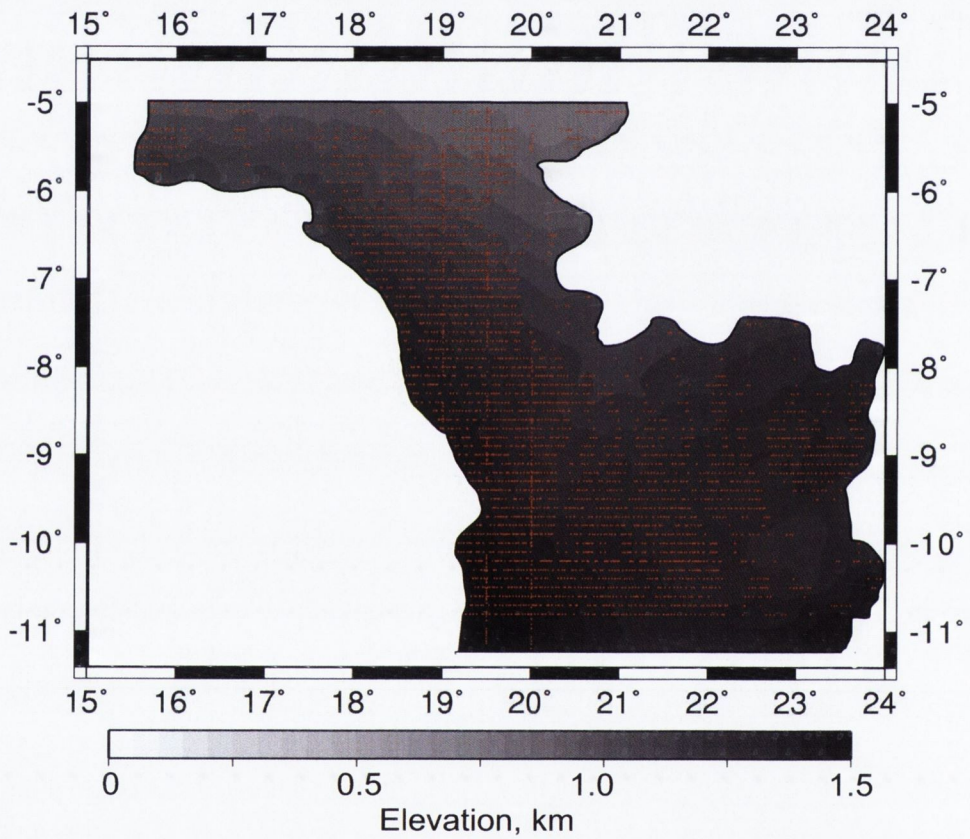


Fig. 2.15: A topographic map of the low relief surface with present-day fluvial incision removed. The points used to reconstruct the surface are plotted as red dots.

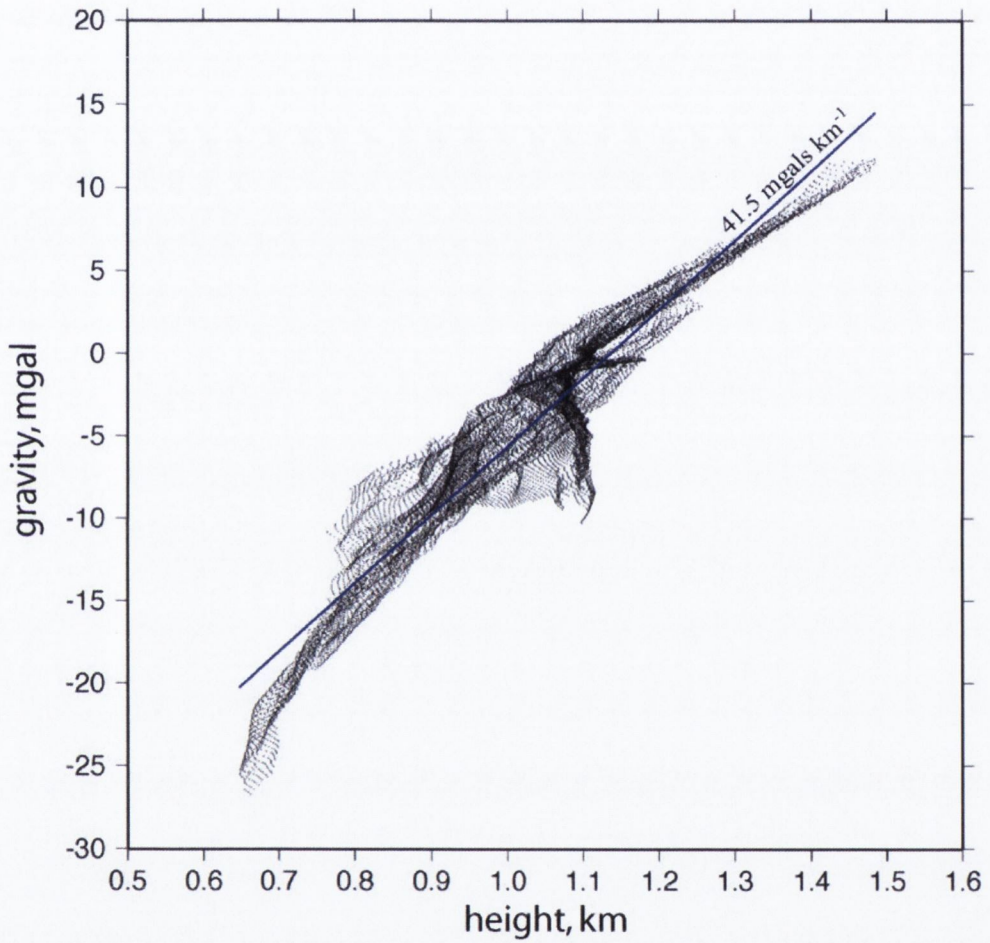


Fig. 2.16: The elevation of the reconstructed low relief surface is plotted against free-air gravity. GRACE Free-air gravity field low-pass filtered to remove wavelengths below 800 km as was described in Chapter 1. A least-squares regression line was fitted to the data points to calculate admittance in the spatial domain.

2.8 Discussion

Profiles of the rivers that drain the elevated areas along the southern edge of the Congo Basin and along the Angolan coastal margin display convex upward morphology in the upper sections of the river, which indicates the section of the river is immature. In the downstream regions, the profiles often display a more mature, concave upward shape that suggests a more mature river which has reached equilibrium as described by Hack (1957). The inflection point, marking the boundary between the immature and equilibrium parts of the river, usually occurs between elevations of 0.8 km and 1 km along the profile. The convex upward morphology in the upper reaches of the rivers implies that the lower river has recently captured the upstream catchment area. The southern edge of the Congo River catchment, prior to capture of upstream rivers, is estimated to be located near the inflection point of the river profiles i.e. between 0.8 and 1.0 km at the present-day elevation (Figure 2.7).

The Kwanza river has a number of inflection points along its profile which can be explained by the capture of the upper Kwanza by the lower Kwanza (Figure 2.12). A study of the original depot centre of the upper Kwanza suggests that capture occurred during the Pliocene (Hipondoka 2005, 2006).

In general, many knickpoints along profiles cannot easily be explained by lithological boundaries or the geological structure of the bedrock that the rivers flow across. Most rivers in the southern Congo margin flow across inter-bedded soft sandstones belonging to Kwango series. The change in lithology from younger, unconsolidated sands of the Kalahari series to the older Kwango series, often seen downstream of the inflection point on the profiles, is thought to be a result of the river incising through the thin covering of younger sediment (Figure 2.8c and 2.9c). It appears in this region that the geological outcrop pattern appears to be controlled by river incision.

In contrast to the southern region, the majority of profiles taken from rivers on the northern and eastern edge of the Congo basin show a mature concave upwards pattern (Figure 2.7). This analysis of river profiles broadly agrees with the results of a hypsometry study of catchments of tributaries that drain into the Congo River carried out by Leturmy et al. (2002).

The top of the Sable Ogres Series, which was deposited during the Neogene, forms a low-relief surface. This surface makes up part of regional surface called the Post African depositional surface that will be further discussed in Chapter 3. The low-relief surface displays a long wavelength topography which appears to correlate roughly with long wavelength free-air gravity. A strong positive linear relationship is seen between the elevation of the reconstructed low relief surface and long wavelength free-air gravity and the slope of best fit line displays an admittance value of $\sim 40 \text{ mgal km}^{-1}$ (Figure 2.16). The admittance estimate from the elevation–gravity plot is consistent with the admittance values calculated for Central Africa by Crosby (2006) and indicates that this low-relief surface is dynamically supported (Figure 1.4).

The Sables Ogres Series rests unconformably on a deformed planation level which is Mid-Tertiary in age (Cahen and Lepersonne, 1952). However it is likely that the long wavelength topography of the low-relief surface formed after deposition of the Sable Ogres for the following reasons: First, comparisons made with the depositional processes of modern fluvial aggrading environments such as Kinshasa the centre of the Congo Basin suggest that Sable Ogres formed in a near horizontal setting (De Ploey et al., 1968); Second, large river valleys incising through the Kalahari sediments show the region has changed from an aggrading to a denudational environment and indicates a change in base-level that may have been caused by tilting of the region.

Estimating Dynamic topography

Assuming an admittance of 40 mgal km^{-1} , long wavelength free-air gravity predicts a maximum of 750 to 850 m of dynamic topography in the centre of the Bie Plateau. The predicted dynamic topography varies by up to 1.8 km over the Congo River catchment and therefore we assume that the vertical motions associated with mantle convection cause warping and tilting of the region, rather than regional scale uniform uplift. The topography of the surface of Sable Ogres sediments appear representative of this warping event. The tilting of the region due to varying vertical motions probably resulted in the capture of upper streams of the southern Congo Rivers tributaries and the Angolan coastal rivers.

The elevation-gravity plot reveal that regions of the low relief surface associated with a low to near-zero gravity anomaly are elevated at $\sim 1.1 \text{ km}$ above present day sea-level. This elevation broadly correlates with a southern boundary of the palaeo-catchment for the Congo River as inferred from river profiles. The geomorphology and long wavelength free-air gravity suggests that the area the Bie Plateau was already elevated by up to 1 km or more prior to tilting.

Timing of vertical motions

This study suggests that uplift of the Bie plateau region in the order of hundreds of metres has occurred after the deposition of the Sable Ogres during the Neogene. The tilting of the southern region of the Congo River catchment resulted in the Congo River tributaries capturing the upstream catchment area. A similar event occurred in the Angolan rivers, including capture of the upper Kwanza river during the Pliocene (Hipondoka 2005, 2006). Increases in catchment area and maximum basin elevation

should be recorded in the sediment flux in the rivers. Estimates for sediment flux from the rivers along the Gulf of Guinea do indeed measure a dramatic increase during the Oligocene and again in the Pliocene ((Leturmy et al., 2002; Walford, 2003). However, the uplift of the western flank of the East African rift system probably also contributed to the increase in sedimentation rates from the Congo River.

Evidence from onshore and offshore Angola suggest uplift events occurred during the Neogene. Pliocene raised shorelines date the exhumation of the Inner Kwanza basin as 20 – 10 Ma (Jackson et al., 2005). Planation of the West African shelf during Late Neogene times attests to a further episode of continental uplift since 5 Ma. It has been suggested that this uplift event played a part in the reactivation of salt tectonics during the Pliocene (Jackson et al., 2005; Seranne, 2005).

Assuming uplift was initiated during the Neogene, at ~ 20 Ma, the uplift rate centred in the Bie Plateau is estimated as up to 40 m Myr^{-1} . It must be noted that uplift estimated in this study was spatially variable and is superimposed on a pre-existing topography. Previous numerical models of dynamic topography predict surface uplift rate of 5 to 30 m Myr^{-1} in southern and eastern Africa (Gurnis et. al., 2000). Similarly, Conrad and Gurnis (2003), estimated that since 30 Ma where uplift rates in southern Africa have been $\sim 10 \text{ m Myr}^{-1}$. Our model suggests an uplift rate in Bie Plateau due to mantle upwelling that is greater than what has been estimated by dynamic topography models. The spatial extent of the predicted uplift is not consistent with dynamic topography predicted from tomographic models (Figure 1.5 and 1.7)

2.9 Conclusions

- Profiles of the rivers which drain the southern region of the Congo River catch-

ment and the Angolan coastal margin indicate that the rivers have recently captured the upstream regions over 1 km in elevation. The tilting of the regions adjacent to the Bie plateau is probably responsible for increasing the catchment area of the Congo River and smaller coastal rivers that drain the Angola.

- A strong positive linear relationship is displayed between the topography of a low relief palaeo-surface and long wavelength free-air gravity and yields an admittance value of about 40 mgals km^{-1} , which agrees with calculations of admittance for Africa in the frequency domain.
- Measured uplift rate centred in the Bie Plateau is $\sim 40 \text{ m Myr}^{-1}$, slightly higher than those estimated by published dynamic topographic models
- Although many previous studies have proposed dynamic support for Africa's topography from indirect evidence (e.g. tomography, numerical modelling and gravity), this study of the low relief surface is the best direct quantification of dynamic support to date.

Chapter 3

Palaeo-Surfaces in southern Africa

3.1 Introduction

Chapter 2 examined a low relief surface that was identified at the edge of the Congo Basin. Sedimentary evidence suggested that the surface was originally sub-horizontal and was warped subsequent to deposition. The close correlation between the surface elevation and long wavelength free-air gravity indicated that the topography of the surface is supported by mantle convection. This surface was used to calculate admittance in the spatial domain.

Much of Africa's landscape can be described in terms of low relief plains and plateaus. Superimposed on Africa's present topography are structures including basins and topographic swells (Doucour and de Wit, 2003). These large scale topographic features often are associated with long wavelength free-air gravity anomalies. Previous geomorphological research observed that the surfaces of the African continent could be subdivided by their formation and age. The formation of these surfaces was described

in terms of erosional cycles (Dixey, 1942; King, 1962; Partridge, 1998; Partridge and Maud, 2000). It was recognised that these surfaces had been subjected to uplift and warping as late as the end of the Pliocene (King, 1962). Recent studies of Africa using low-temperature thermochronology and terrestrial nuclide cosmogenic analysis imply that the age of these surfaces do not correlate over wide regions as earlier geomorphological studies suggested. Prior to 2002, topographic data of Africa, such as SRTM30 and GTOPO30 produced DEMs with a maximum horizontal resolution of about 1 km. This limited these earlier studies of the geomorphology of Africa to larger scale structures. Newly released topographic data with a 90 m horizontal resolution has permitted the detailed study of low-relief surfaces identified in earlier studies.

Establishing if these surfaces have been warped by convection currents in the mantle has wider implications for our understanding of mantle evolution. The age of surfaces could help constrain when the warping occurred, and has implications for measuring the temporal variation in mantle currents. Measuring admittance of the continental lithosphere is difficult (as discussed in Chapter 1). The majority of published values for admittance at longer wavelengths in continents are calculated as a by-product of elastic thickness predictions. The direct comparison of a surface, warped by mantle convection, with long wavelength free-air gravity may provide an opportunity to estimate admittance in the spatial domain for continents.

The main aim of this chapter is to use palaeosurfaces identified by previous research of Africa's geomorphology and to test if there is any correlation between the topography of these surfaces and long wavelength free-air gravity. This chapter is organised as follows:

- A summary of the findings from previous research examining the formation and evolution of palaeosurfaces of Africa, paying particular attention to work by

Lester C. King and the more recent publications by Tim Partridge and Rodney Maud. Four main surfaces are recognised by both authors, the Gondwana, African, Post-African and aggradational surfaces in Africa and these are discussed in terms of ages and degree of planation/flatness.

- An examination of the hypothetical relationship between different types of surfaces that have been warped by mantle convection and long wavelength free-air gravity.
- The relationship between the elevation of different palaeosurfaces and long wavelength free-air gravity as established by plotting the elevation of surfaces outlined by King (1962) and Partridge (1998) against long wavelength free-air gravity.
- The results are used to assess the extent to which the palaeo-surfaces are supported by mantle convection

3.2 Previous research of African surfaces

The term 'Palaeosurface' suggests a land-surface that is ancient and has changed little since it has formed i.e. has not been further eroded (King, 1962; Hills, 1975). The term can be applied to described preserve land-surfaces that were formed by either denudation or aggradation. This chapter refers to two types of palaeosurface, denudational and aggradational surfaces. Aggradational surfaces mark the top of a depositional sequence onland. Denudational surfaces are formed from the erosion and the stripping away of rock. Particular attention in geomorphology is paid to a type of denudational



Fig. 3.1: Scanned section of the map published by King (1962) as a fold out A3 sized map showing the aggradational and denudational surfaces of the African landmass.

surface referred to as a planation surface. Planation surfaces are identified as low-relief plains cutting across varied lithologies and structures. Across Africa, planation surfaces are thought to be widespread and they have been interpreted as being caused by a number of denudational cycles that have affected Africa since before the breakup of Gondwana (Dixey, 1942; King, 1962; Partridge, 1998; Partridge and Maud, 2000). It was recognised that planation surfaces in Africa were deformed or warped subsequent to their formation due to vertical motions (King, 1962; Partridge, 1998; Partridge and Maud, 1987; 2000). Establishing the age and the initial elevation of planation surfaces has been used as a simple method for estimating the rate of vertical motions in southern Africa (Partridge, 1998). More recently, new techniques such as terrestrial cosmogenic nuclides can provide direct dating of a palaeo-surface. Fission track analysis can date increases in rates of erosion and therefore help date denudation events. However this technique is not particularly sensitive to temperatures colder than the top of the apatite partial annealing zone (≈ 60 C) and thus it is not suited to detecting recent exhumation pulses (i.e. late Cenozoic) of low magnitude (as discussed in Chapter 1). Results from cosmogenic nuclides and fission track analysis are inconsistent with earlier landscape models such as proposed by King and Partridge and Maud, which correlate large expanses of land surface based on age of the surfaces.

3.2.1 Lester C. King

Lester King was instrumental in the development of modern geomorphology in the twentieth century, and in particular his theories have had a lasting impact on our understanding of the formation of the African landscape. King rejected much of the Davisian theory of landscape evolution (Davis, 1899) which was widely accepted at the time. The Davisian theory asserted that downwearing erosion was the dominant process in forming landscapes. Instead, King emphasised the importance of scarp

<i>Denudational</i>	<i>Depositional</i>		Age
	<i>Continental</i>	<i>Marine</i>	
(a) pre-Karoo landscape of moderate relief, partly glacial.	Covered by Dwayka, Ecca and Beaufort series.	None.	Late Carboniferous and Permian.
<i>Mild Epeirogenesis</i>			
(b) intra-karoo landscape generally of low relief and desert form.	Stormberg series.	None.	Triassic.
<i>Mild Epeirogenesis</i>			
(c) Gondwana landscape of extreme planation.	Jurassic deposits known only in the Congo Basin.	None.	Jurassic (and late Triassic).
<i>Fragmentation of Gondwanaland</i>			
(d) post-Gondwana dissection usually in the vicinity of upwarps.	Série de Kwango ; dinosaur beds of Luangwa Valley and elsewhere.	Late- Jurassic to early-Cretaceous series of the west coast from Somaliland to Zululand.	Early Cretaceous.
<i>Mid-Cretaceous Disturbances</i>			
(e) African cyclic landscape of extreme planation forming the most perfectly planed surface of Africa, much dissected now by later cycles.	Late-Cretaceous dinosaur bed of Bushmanland ; early-Cainozoic Botletle beds , Kalahari marls, Grés polymorphe. Chief calcrete horizon	Littoral Senonian strata of east coast with succeeding Eocene in Moçambique. Late Cretaceous and Eocene strata of Angola.	Late Cretaceous to mid-Cainozoic.
<i>Widespread epeirogenic uplift of a few hundred feet</i>			
(f i) Broad valley-floor pediplains widespread into the early Cainozoic, African surface.	Plateau sands of the Kalahari-Congo region, Minor laterites and calcetes.	Burdigalian marine series.	Miocene.
<i>Slight uplift</i>			
(f ii) Second phase of late-Cainozoic valley planation. Coastal plains.	Pipe sandstone of the Zambezi valley.	Sands unconformably overlying Burdigalian and transected by coastal plain of the East Africa.	Pliocene.
<i>Strong Cymatogeny (crustal warping)</i>			
(g) Deep gorge-cutting in eastern and western coastal hinterlands. Locally multiphase	Widespread Kalahari sand (two phase). Cavern deposits.	Red Berea and other coastal sands.	Quaternary.
<i>Minor Differential movement</i>			
(h) Coastal drowning.	Recent alluvia.	Recent dune sands.	

Table 3.1: Cyclic episodes of Central and Southern African geomorphology, with tectonic interludes as defined by King (1962).

retreat over the downwearing of landscapes. Some of King's ideas have not stood the test of time. For example, he predicted much higher rates of escarpment retreat than is now accepted. Throughout his career King never shied away from the bigger picture. His vast knowledge of the geomorphology of the continents around the world allowed him a unique global perspective.

The majority of the following biographical information regarding Lester King is summarised from Twidale (1992):

Lester Charles King was born in London in 1907, and migrated to New Zealand as a young child with his parents. After receiving his Baccalaureate diploma at Victoria University College, Wellington, he obtained a M.Sc. in 1930. King was later offered a position lecturing geology in Victoria University College and he continued lecturing at the university until 1934. Earlier in his career, King's interests lay mainly in palaeontology, however Charles A. Cotton, the chair of geology in Victoria University College and a leading geomorphologist at the time had a strong influence on his research. Some of King's earliest papers examined researched the geomorphology of New Zealand such as raised beaches, the origin of the Motunau Plain and the topography of the fjordland of South Island. King never obtained tenure in Victoria University College and in 1934, due to the growing depression in New Zealand, he was told his contract would not be renewed. King wrote to various geologists letting them know of his availability, and in 1935 he was appointed Lecturer of Geology and Geography at University of Natal, Pietermaritzburg South Africa. His career in geology progressed quickly at the University of Natal. In 1936 he was awarded his Ph.D from the University of South Africa and in 1946 he was appointed Professor of Geology in the University of Natal. His first book, 'South African Scenery' (King, 1942) was a comprehensive study of African landscape and its formation.

The southern African landscape had a great influence on Lester King's understanding of geomorphology, and led him to recognise the importance of scarp retreat in the generation of planation surfaces. His theory of erosional cycles describes pulses of uplift that punctuate the erosion cycle by initiating renewed stream incision. King (1957; 1962; 1972) utilized the concept of parallel retreat of escarpments due to fluvial erosion (knickpoint upstream migration) to generate plains referred to as pediments. This theory questioned the earlier established Davisian theory (Davis, 1899) that called for the downwearing of plateaus to form peniplans. The concept that most erosion occurred in places of high slopes meant that on flatter regions such as plateaux older erosional surfaces could be preserved, thereby generating a stepped landscape. If there was no spatial variation in vertical motions over the region, this would mean that the oldest surfaces would be at the highest elevation.

Lester King published a book 'The Morphology of the Earth' (1962) in which he wrote a comprehensive chapter on the morphology of Africa, summing up 21 years of his research on Africa. He produced a map which summarises Africa's present-day surface into denudational cycles (figure 3.1). The following paragraphs outlines some of his conclusions on the development of Africa's landsurfaces. Various methods were used to date landsurfaces, including biostratigraphy of covering deposits, elevation above sealevel, correlation with adjacent surfaces that are already dated, correlation with episodes of erosion or deposition offshore and stage development in the cycle of erosion. He recognised that using elevation above sealevel in Africa was invalid due to spatially variable uplift and the warping of the palaeo-surfaces. He considered that the most valid method in establishing the age of the surface for comparison with other surfaces is "the oldest deposits known to exist upon a cyclic surface", i.e. the date of the planation surface can be constrained by assuming the it most be older then the oldest deposits sitting on top of the palaeo-surface.

Other works had also attempted to classify landforms in South and Central Africa in terms of erosional cycles, using sea-level as a datum and correlating the surfaces by elevation (e.g. Jessen, 1936; King, 1942). Dixey (1938) used fossiliferous evidence to constrain the dates of these surfaces. King (1962) recognised that over long distances, the planation surfaces in Africa are subject to vertical motions. He therefore accepted that it was incorrect to date surfaces by their elevation above sea-level and that the dates for palaeosurface planation published by Dixey (1938) were more accurate.

King (1962) summarised the formation of Africa's present-day surface into four important denudational land surfaces, the Gondwana/Post-Gondwana surface, the African surface, the Post-African surface and the Congo surface. The development of the surfaces is outlined in table 3.1 and a further synopsis of the character of each of the surfaces is included. The surfaces were dated relatively as Jurassic/Cretaceous, Early Cenozoic, Late Cenozoic and Quaternary. The Gondwana surface was created by a period of extreme planation during the Jurassic before Gondwana began to break up. Early Cretaceous periods of dissection of the Gondwana surface by between 300 to 500 m generated the Post-Gondwana surface. Continental uplift followed the fragmentation of Gondwana and initiated a new cycle of erosion. During this cycle, that lasted until the Miocene, most of Africa's relief was eroded to form the African Planation surface. The exceptions were the Kalahari and Congo basins, where sediments derived from the surrounding areas were deposited. The accumulation of sediments in these basins also contributed to the overall 'smoothness' of the African continent during this period.

Moderate epirogenic uplift at the end of the Oligocene and later at the end the Miocene brought the African Cycle to an end. Lowering of baselevels caused fresh fluvial erosion, and rivers soon cut down below the elevation of the African surface. This produced the gently rolling landscape that covers large regions of interior plateau of Africa referred

to as the Post-African surface. The uplift during this event is thought to be no more than a hundred metres. Towards the end of the Pliocene the continent was affected by major uplift and warping, that possibly may be ongoing to the present day. This uplift raised the interior plateau by approximately 4000 ft (about 1220 m) and deformed the older African and Post-African surfaces. Along the eastern and western margins of the southern African plateau, the older surfaces tilted outwards so that they now rise hundreds of meters over tens of kilometres.

3.2.2 Partridge and Maud

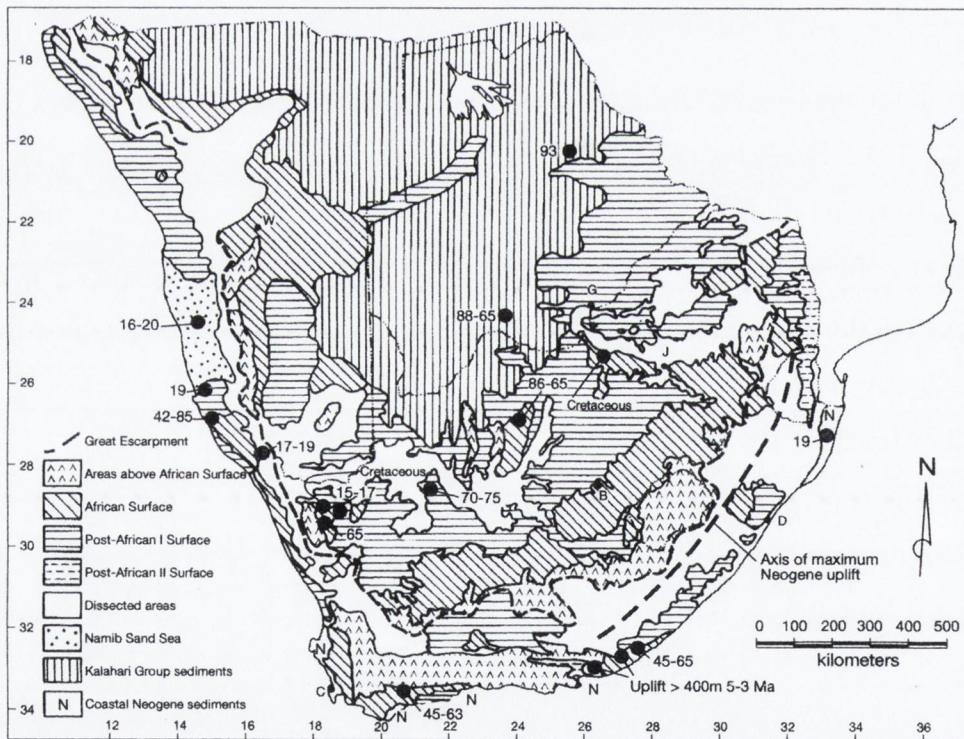


Fig. 3.2: Simplified map of the distribution of erosional land surfaces in southern Africa. Heavy dots show localities at which constraints on the age of the surfaces (in Ma) are available, taken from Partridge and Maud, 2000.

Tim Partridge and Rodney Maud were strongly influenced by the work of Lester King

and they agreed that the geomorphology of Africa could be explained in terms of a number of major erosional events as previously defined by King (1962) (Partridge and Maud, 1987). The timing of the erosional cycles differed from the results published King (1962), and this was partly due to data obtained by more recent geochronological techniques. The results of their research were summarised in a map showing the distribution of the preserved land surfaces in southern Africa (Figure 3.2). The present day elevation of the African and Post Africa was used to quantify the timing of uplift in South Africa (Figure 3.4). Partridge and Maud (1987) proposed that the Great Escarpment in southern Africa was formed following continental break-up and therefore was a much older feature in the African landscape than King (1962) maintained.

Partridge and Maud (1987; 2000) use a number of techniques to constrain the age of land surfaces in southern Africa such as fossil evidence, dating duricrusts and fission track analysis. Fission track evidence analysis (Brown et al., 1994) and the presence of a thick marine Cretaceous sequence offshore suggests that most of southern Africa had a high elevation prior to the break-up of Gondwana. The Great Escarpment was formed following continental rifting. The vertical separation of the plateau and the coastal plain resulted in distinct base-levels above and below the Great Escarpment. The formation of the African surface is considered a result of a widespread planation event caused by deep and intense weathering during humid conditions in Africa during the Early Cretaceous. By the middle Cretaceous, AFTA suggests that 1 to 3 km has been eroded from the African surface. The resulting erosional surface formed at different elevations both above and below the great escarpment but are coeval. Partridge and Maud (1987; 2000) see no evidence in southern Africa for preserved landsurfaces older than the African surface referred to by King (1962).

By the beginning of the Cenozoic, southern Africa was dominated by a widespread planation surface, cut at two levels above and below the Great Escarpment. A gentle

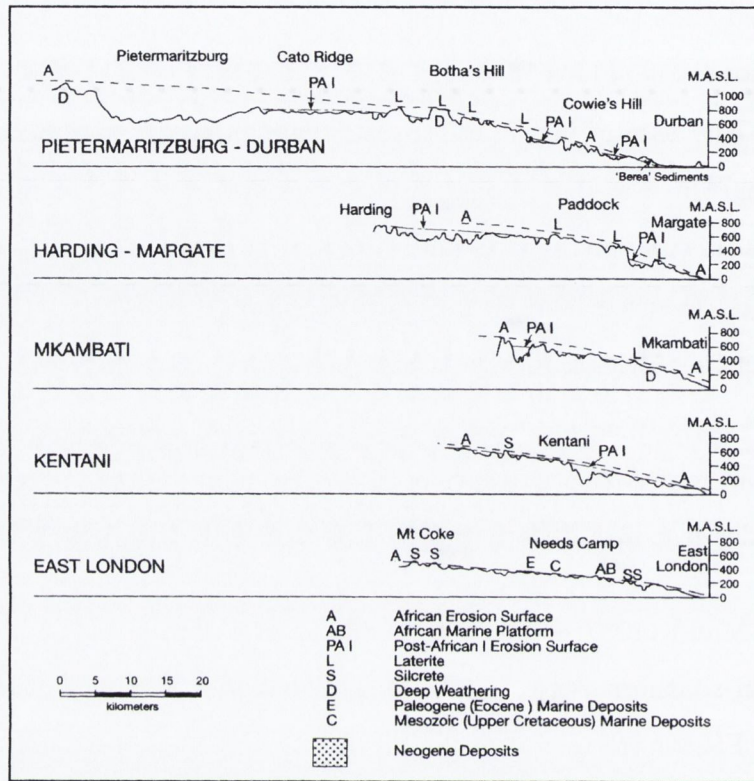


Fig. 3.3: Sections drawn inland from the coast across the south eastern hinterland of southern Africa showing erosional remnants, duricrusts associated with deep weathering and marine deposits from late Mesozoic and early Cenozoic transgressions. Taken from Partridge and Maud (1987)

pediplain (the African surface) extended across most of southern Africa, inland of the Great Escarpment, at elevations of 500m to 600m. Some high-standing mountain massifs that survived the planation event were elevated above the African surface (Figure 3.2). Throughout most of the Paleogene, offshore sedimentation rates remained slow and there is little evidence for regional uplift, although it is probable that early Cenozoic volcanism may have caused localised doming (e.g. McCarthy et al., 1985). During the African cycle, there was widespread development of duricrusts, which capped the African surface. The duricrusts consist of silcrete and calcrete in the west and laterite in the east of subequatorial Africa. A duricrust is a horizontal layer on the surface

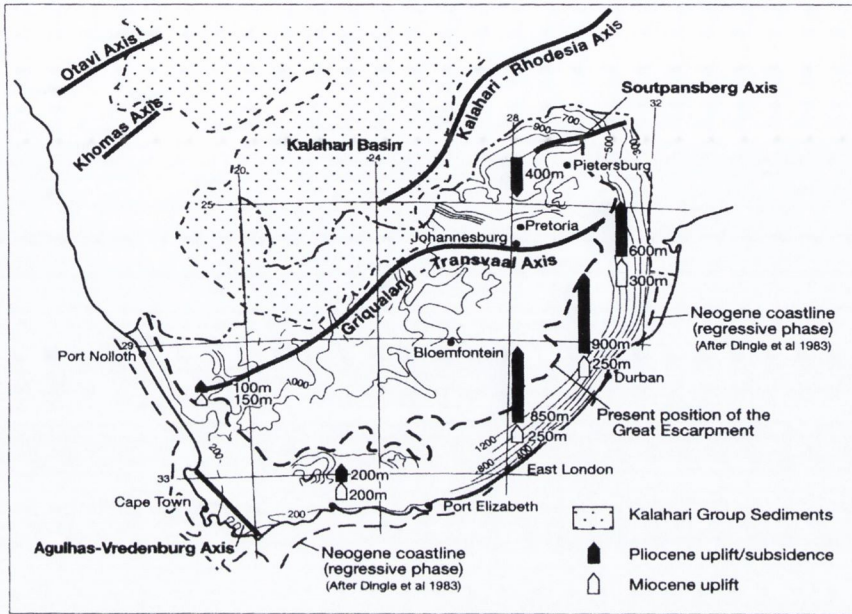


Fig. 3.4: Generalized contours on the Post-African I (Miocene) erosion surface taken from Partridge and Maud (2000). Open arrows indicate the amplitude of the early Miocene uplift; solid arrows show Pliocene uplift or subsidence. The present position of the Great Escarpment is shown by the broken line. Interior axes of uplift rate are after du Toit, 1933

or near the surface of the earth, hardened by the accumulation of calcite or silica. Palaeontological and radiometric ages confirm that the formation of duricrusts ceased by the early Paleocene.

The African cycle came to an end at the beginning of the Miocene with the onset of uplift. Terraces of rivers such as the Orange and the abandoned Koa valley indicate that the Africa pediplain was incised by 100–200 m, producing an imperfectly planed surface referred to as the Post African I surface.

A second phase of uplift began in the Pliocene and caused warping of the earlier African surface and Post-African I Surface (Figure 3.3). Partridge and Maud (1987; 2000) used the surfaces to measure the magnitude of the vertical motions (Figure 3.4).

This method of measuring vertical motions suggest that there has been as much as 900 m of uplift in southeastern Africa. Pliocene marine deposits are raised to elevations of up to 400 m above sea level between the axis of maximum uplift and the present day coastline (Figure 3.2). Some degree of planation was achieved during this event due to fluvial erosion in weaker lithologies. An undulating surface referred to as the Post-African surface II was formed, however the extent of this surface is limited when compared with the African surface and Post-African I Surface (Figure 3.2).

3.2.3 Denudational Surfaces

A series of great erosional events have affected the African continent since the break-up of Gondwana (King, 1962; Partridge, 1998; Partridge and Maud, 1987; 2000). Apatite fission track thermochronology (AFTT) predicts that up to 5 km of denudation has occurred in regions of Africa the last 140 Ma (Gallagher and Brown, 1999). The formation of widespread planation surfaces in southern Africa was the result of a number continental-scale erosional events or cycles (King, 1962; Partridge, 1998; Partridge and Maud, 1987; 2000). The preservation of the African and Post African surfaces in pristine condition over large areas is rare (Partridge and Maud, 1987). The following section discusses evidence for the age and existence of planation surfaces in southern Africa, particularly in light of more recent techniques for studying landscape evolution.

Gondwana surface

The oldest surface, known as the Gondwana surface, was recognised by King and was first proposed by Dixey (1938) as being Jurassic in age. Evidence for age of the Gondwana/Post-Gondwana surface is limited to the Congo Basin, where Jurassic de-

posits rest on top of the surface. The Gondwana surface is thought to have been a smooth planation surface when it first developed (King, 1962). The cycle of erosion during the early Cretaceous, brought on by the fragmentation of Gondwanaland is referred to as the Post-Gondwana cycle. The Post-Gondwana cycle of denudation caused the dissection of the Gondwana surface through river erosion and scarp retreat. In the Lesotho highlands (the Karoo region) the best preserved remnants of the Gondwana surface survive between 3050 to 3350 m along the crest of the Great Escarpment. However, in Angola and Namibia the Post-Gonwana surface is far more extensive than the Gondwana surface. The map of denudational and aggradational surfaces in Africa (King, 1962), does not differentiate between these two cycles of erosion (figure 3.8).

The antiquity of the Gondwana landscape has been called into question by a number of researchers. Studies of zeolite zonation in basalts of the Drakensberg Formation at the Sani Pass, on the Lesotho-Natal, border imply that 200 to 400 m of material has been removed from the top of the pile by erosion since the cessation of volcanic activity at 183 Ma (Dunlevey et al., 1993). However this observation does not indicate exactly when the erosion occurred. Cosmogenic ^{36}Cl concentrations in four basaltic samples taken from flat lying outcrops on the Drakensberg escarpment were analysed to provide denudation rates in the region for the past 10^4 to 10^5 years (Fleming et al., 1999). The results suggest that summit denudation rates (i.e. downwearing) range between 1.4 m Ma^{-1} and 10 m Ma^{-1} . Based on the assumption that the entire summit was subjected to this erosion rate, an "unmodified Gondwana erosion surface would not have survived" (Flemming et al., 1999). The samples were collected from near Sani Pass and Naudesnek on the south Drakensberg escarpment. However, on closer comparison between the sampling sites and the map produced by King (1962) (page 253 of *Morphology of the Earth*) of the extent of Gondwana surface in the Drakensberg mountains it is unclear if the samples were in fact taken from the Gondwana surface as outlined by King. Flemming et al. (1999) reference an earlier paper, King (1944) but

King (1962) corrects his earlier work in the Drakensberg saying “much of what was mapped here in 1946 as Gondwana is now known to be violently upwarped African surface”. Brown et al. (2002) carried out an apatite fission track study of samples taken from the the regions north-west and south-east of the Drakensberg highlands, including two boreholes. As no samples were taken from the Drakensberg highlands themselves, denudation rates were interpolated between the two boreholes using denudation estimates by Dunlevey et al. (1993) and Flemming et al. (1999). The boreholes showed a phase of accelerated denudation of 82 ± 43 m Ma from 78 to 64 Ma. Therefore, there appears to be no direct evidence to date from thermochronology and cosmogenic nuclide analysis, as of yet, that the planation surface that formed prior to the break-up of Gondwana has not survived in Africa. However, given the average denudation rates in Africa measured by AFTA and cosmogenic nuclide analysis, many researchers believe that the survival of a surface since the Jurassic is unlikely.

Partridge and Maud (1987, 2000) map the region above the Drakensberg escarpment as “areas above the African surface” (fig 3.2). The age of the Gondwana surface is questioned, as there is evidence that kimbelite pipe diameters have been reduced by some 300 m since approximately 90 Ma in this region (Partridge and Maud, 1987). It is also worth noting that elsewhere in the world extremely old peneplains at high elevations have been identified. For example, recent thermochronology and field data show that the plateau surfaces at elevations of 4000 m in Gobi Altay and Altay, Mongolia, represent uplifted parts of an ancient peneplain that formed during Jurassic time. The survival of these surfaces for the last 150 Ma is probably due to the generally dry climate and prolonged period of tectonic stability prior to the onset of recent deformation at 5 ± 3 Ma (Jolivet et al., 2007).

3.2.4 African Surface

The African cycle is a multi-phase erosional event that began as early as the Cretaceous and prevailed until the Miocene. The result of this cycle was to reduce much of the African surface to an immense, smooth planation surface. At the same time sediments being deposited in continental basins also helped level out the continent to flat plain (King, 1962). The little remaining topography that survived this event is now preserved as the Gondwana/Post-Gondwana surface (King, 1962) or the above African surface (Partridge and Maud 1987; 2000). King (1962) attributed the formation of the African surface to pedimentation i.e. the back-wear of a scarp to form a pediplain, which resulted in most of Africa being reduced to a minimum.

King (1962) limited the presently preserved regions of African surface to inland of the Great Escarpment. While Partridge and Maud located the African surface in similar positions to King above the escarpment, they also found evidence for its presence in regions below the Great Escarpment. Partridge and Maud (1987) and Partridge (1998) proposed the the African surface formed at two different levels, above and below the escarpment, due to localised difference of base-levels. Below the Great Escarpment the sea-level controlled the base-level, while inland of the Great Escarpment, major river systems such as the Orange and Limpopo provided the base-level for erosion. By the early Miocene, most of southern Africa was dominated by the African planation surface which lay at elevations of 500 to 600 m above sea-level inland of the escarpment ((Partridge and Maud 1987; 2000).

The African cycle was initiated during the Jurassic or Early Cretaceous and continued to the Early Miocene as the result of a change in oceanic base level set by the fragmentation of Gondwana (Partridge and Maud, 1987; Partridge, 1998). Fission track analysis indicates a period of accelerated denudation in the Middle to Late Cretaceous,

when one to three kilometres was eroded from southern Africa's surface as shown by Brown et al. (1994) and Gallagher and Brown (1999). Geochronological evidence, such as crater facies of diatremes of a known age (figure 3.2), indicate that the African surface formed no later than the end of the Cretaceous (Partridge and Maud, 1987; Partridge, 1998). Palaeontological and radiometric ages conform that the formation of duricrusts ceased by the early Paleocene (Partridge and Maud, 1987; Partridge, 1998). The present-day survival of the African surface in pristine condition over large areas is rare, and often the surface is preserved on interfluvies after erosion has removed deeply weathered material from the surrounding area (Partridge and Maud, 1987).

3.2.5 Post-African Surface

The African cycle (as described by King, 1962) came to an end at the beginning of the Miocene with the onset of uplift that initiated the Post-African I cycle. Terraces of rivers indicate that the African pediplain was incised by 100–200 m to produce an imperfectly planed surface (Partridge and Maud, 1987). The drainage system in southern Africa incised the landscape and created a rolling surface, referred to as the Post-African surface (King, 1962) or Post-African surface I (Partridge and Maud, 1987). Erosion during this phase was mainly limited to the removal of the deep weathering mantles on the African surface (Partridge and Maud, 1987). The final formation of this surface occurred in the Late Pliocene according to Partridge and Maud (1987) and Partridge (1998) or the late Cenozoic according to King (1962). Fauna taken from the terraces, believed to be part of the Post African surface, 40 – 50 m above the current channel of the Orange River indicates that the age of the terraces is basal Middle Miocene, about 17.5–17 Ma (Pickford et al., 1995b). The Tsondab Sandstone, which rests on the Post-African surface, contains eggshells of extinct giant avians that date back as far as 16 Ma (Pickford et al., 1995a; Partridge, 1998; Partridge and Maud,

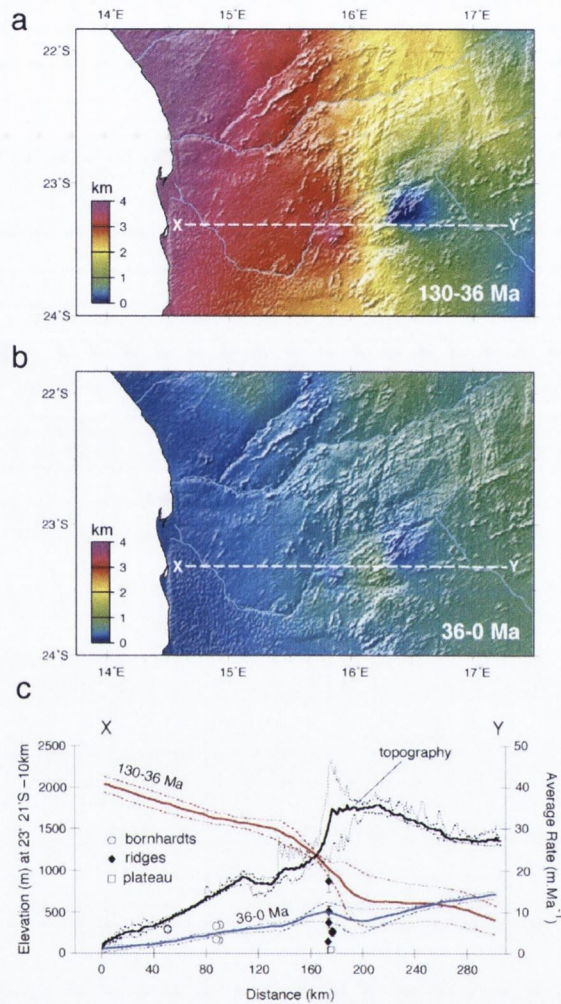


Fig. 3.5: Maximum depths of denudation calculated for two periods, (a) from the break up of Gondwana at approximately 130 Ma to the end of the Eocene (~ 36 Ma) and (b) post-Eocene to present determined from apatite fission track data of the region. Denudation in post-Eocene times is extremely low. (c) Variation in the mean denudation rate (solid lines) and standard deviation (dashed lines) modelled from cosmogenic isotope data, for the two time periods across the margin. Swath X–Y, 20 km wide, of the present day topography extracted from GTOPO 30 data. Taken from Cockburn et al. (2000).

2000). In addition, the $^{40}\text{Ar}/^{39}\text{Ar}$ technique has directly dated the timing of formation of a pedogenic manganese crust composed of potassium-bearing cryptomelane from immediately below the Post-African I surface of erosion at 12–15 Ma (van Nierkerk,

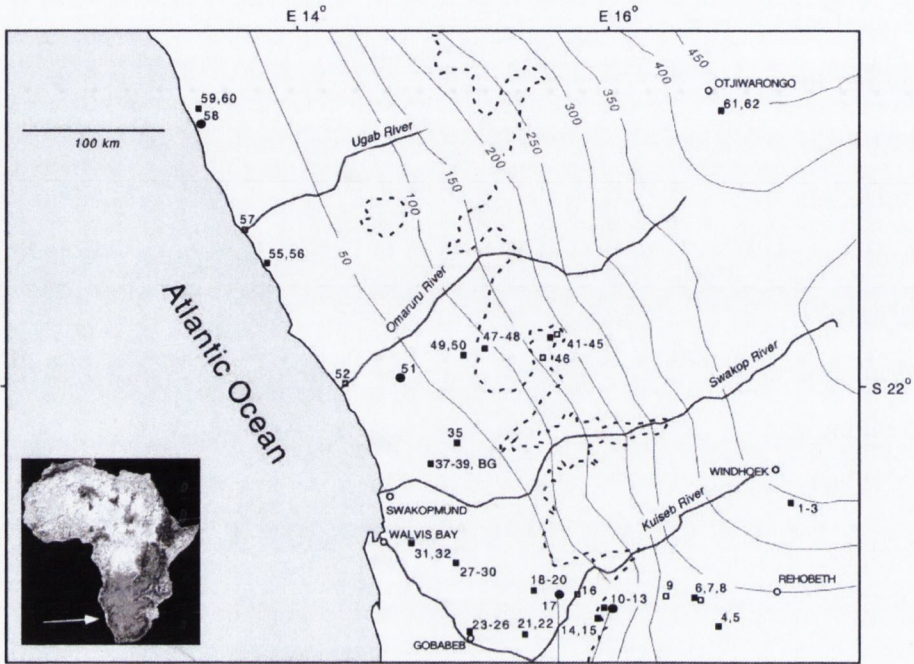


Fig. 3.6: Location of the cosmogenic sample sites. Filled squares are bedrock samples; filled circles are clast samples; open squares are sediment samples; open circles are cities. Dashed line is 1000 m contour (roughly escarpment–coastal plain junction). Thin grey lines are isohyets of mean annual precipitation in mm yr^{-1} adapted by Jacobsen et al., (1995). Taken from Bierman and Caffee (2000).

1999). The Post-African I Surface dominates many regions of the present day landscape in Africa (Figure 3.8 and 3.2).

A region of the Namib pediment and escarpment, north of the Namib Sea of Sand has been the subject of a number of landscape development studies using apatite fission-track thermochronology and cosmogenic isotope techniques to infer erosion rates (Cockburn et al., 1999; Cockburn et al., 2000; Bierman and Caffee, 2000; van der Wateren and Dunai, 2000). The surface of this region was defined as the Post-African I Surface and above the escarpment as a dissected area by Partridge and Maud (1987, 2000). King (1962) mapped the region between the escarpment and the coast as Post-African surface with most recent river valleys more recently eroding into it. Above the escarp-

ment the area is defined by King (1962) as the African surface with a small region above the Kuiseb River forming part of the Gondwana surface.

The in-situ-produced terrestrial cosmogenic nuclides of ^{10}Be and ^{26}Al have been used to date quartz-bearing samples of bedrock taken from inselbergs, of sediment from dry river and stream channels (all rivers and streams originating in Namibia are ephemeral), and of clasts from desert surfaces (Figure 3.6) indicates significant landscape stability over at least the past million years. Data from large rivers such as the Ugab, the Kahn, the Omaruru, and the Kuiseb, constrain erosion rates to between 3 and 9 m Ma^{-1} when averaged over 10^5 to 10^4 yrs (Bierman and Caffee, 2000). ^{10}Be abundances in small quartz clasts collected from the desert surface indicate a minimum exposure ages approaching 1.8 Ma, implying long near surface exposure. Erosion rates interpreted from the clast data reveal extremely low erosion rate of less than 0.1 m Ma^{-1} , which is consistent with the preservation of a Miocene surface (Bierman and Caffee, 2000). Measurements of ^{10}Be from granite inselbergs (steep-sided isolated hills on an otherwise featureless low relief landscape) in the coastal plain of Namibia and the summit of Gamsberg (the highest peak in the region) give denudation rate of approximately 5 m Ma^{-1} for the past 100 ka for the coastal plain, with as little as 0.4 m Ma^{-1} denudation occurring at the summit of Gamsberg (Cockburn et al., 1999; Cockburn et al., 2000). Apatite fission track thermochronology (AFTT) data support these results, showing low denudation rates of the coastal plain since the end of the Eocene (Figure 3.5). More recent cosmogenic isotope studies of the central Namib indicates denudation rates of 1 m Ma^{-1} or less may have persisted at least since the onset of hyper-arid conditions in the Namib desert (van der Wateren and Dunai, 2000). In addition, analysis of the terrestrial cosmogenic nuclide ^{21}Ne from a resistant quartz vein projecting above pediment, situated north of the Kuiseb River in the Namib desert, reveals a minimum exposure age of 5.18 ± 0.18 Ma (van der Wateren and Dunai, 2000).

The extreme aridity of the Namib desert is thought to have begun in the Middle Miocene when major upwelling of the Benguela current was established off the southwest Africa coast (Partridge, 1993; Siesser, 1980; Van Zinderen Bakker, 1984). Upwelling of the cold Benguela current offshore of Namibia ensures little precipitation reaches the coast. Present day average annual rainfall in the central Namib ranges from 10 mm near the coast to 100 – 200 mm at the foot of the Escarpment. Seranne and Anka (2005) suggest that the initiation of arid conditions in southwestern Africa may have been responsible for the slow erosion rates and the reduced sedimentation rates on the coastal margin. Cosmogenic isotope dating also indicates landscape rejuvenation in the Namib Desert in the Late Pliocene but is attributed it to an increase rainfall in the central Namib (van der Wateren and Dunai, 2000).

Partridge and Maud (1987) and Partridge (1998) also refer to a Post-African surface II, which was formed during Late Tertiary uplift of the continent. However the development of planation surfaces due to this erosion cycle is limited to small areas in the Algoa basin (northwest of Port Elizabeth in southern Africa) and the Lowveld of Swaziland.

3.2.6 Aggradational or depositional surfaces

Aggradation of terrestrial sediments leads to the formation of a depositional or aggradational surface. The very nature of sediment accumulation tends to infill depressions and create level plains. Depositional surfaces can form part of a planation surface (Twidale, 2003 b). A change in regime, such as base-level or sediment supply, can cause aggradation to cease and the depositional surface to become stagnant. The preserved depositional surface is considered as old as the last phase of aggradation that occurred. The surface will remain preserved until it is destroyed by erosion or buried

by further sedimentation.

Depositional surfaces are usually dated by the youngest materials incorporated in the accumulation (Twidale, 2003 b). Often dating aggradation surfaces is more straight forward than denudational surfaces, as it is possible to accurately date the sediments using fossiliferous evidence. However fossils are commonly absent from the Kalahari sands in southern Africa. Therefore the age of aggradational surfaces in southern Africa are sometimes estimated relative to other surfaces with known ages (Cahen and Lepage, 1952). This section discusses the formation and evolution of depositional surfaces in three regions of southern Africa, the Kalahari Basin, the northern rim of the Kalahari Basin and the Namibian sea of sand.

The surface of the Kalahari basin

Central southern Africa is dominated by a large sedimentary basin called the Kalahari basin. The surface of the Kalahari Basin is the largest continuous depositional surface in southern Africa. The Kalahari Group, the youngest sediments in the basin, are key in understanding the age and evolution of the surface of the Kalahari Basin. The stratigraphy of the Kalahari Group sediments is poorly understood and varies considerably throughout the Kalahari Basin (Haddon and McCarthy, 2005). The Kalahari Group sediments lies unconformably on Archaean to Cretaceous lithologies. A large portion of the base of the Kalahari Group consists of basalts belonging to the Karoo Supergroup (~180 Ma) (Haddon and McCarthy, 2005). The sediments that make up the Kalahari Group were predominantly deposited by rivers in the Late Cretaceous and early Cenozoic. The thickness of the Kalahari Group varies from a few metres to around 450 m. The thickest deposits are to the east of the Bie Plateau, the Owambo Basin in northern Namibia (in between the long wavelength free-air gravity highs of

Angola and Namibia) and the Okavango Basin (Haddon and McCarthy, 2005). Arid conditions prevailed from the late Pliocene to early Pleistocene (Partridge, 1993; Pickford et al., 1994). During this period of aridity, dunes formed in the Kalahari desert of Namibia and Botswana (Helgren and Brooks, 1983; Cooke, 1980; Strokes et al., 1997).

The topography of the central Kalahari Basin is predominately a flat, low relief surface elevated at approximately between 1 and 1.2 km. Sediments deposited around the flanks of the basin are at elevations of up to 1.5 km and are currently being eroded (Haddon and McCarthy, 2005). Studies of the thickness and nature of the Kalahari sediments show that depressions produced by vertical motions in central southern Africa often form internal drainage basins, such as the Okavango and Etosha basins. Accumulation of sediments in the Okavango and Etosha basins has the effect of levelling of the topography. The Okavango Delta has formed in the depression resulting from the uplift of the Ghanzi Ridge along its southern margin in the late Pliocene or early Pleistocene (Gumbricht and McCarthy, 2000). Drilling indicates that the sediment fill is up to about 300m thick (Gumbricht and McCarthy, 2000; Haddon and McCarthy, 2005). The difference in elevation of the surface of the delta varies by only 105m over an area of 72,500 km² (Gumbricht and McCarthy, 2000). The thickness of sediment and the low range of topography indicates that the sedimentation rate in the region is high enough to infill and level depressions in less than a few million years.

The Etosha pan is a large endorheic salt pan situated on top of the Owambo Basin in the Kalahari Desert between the Bie plateau in Angola and the Namibian plateau. The origin of the Owambo depression is poorly understood. It is assumed that the upper Kunene River once flowed into the Owambo Basin feeding a large lake (Wellington, 1938; Hipondoka et al., 2006). During the Pliocene uplift on the western side of the Etosha basin closed the outlet of the Hoanib River creating a saline lake about 45m deep with a surface area in excess of 82 000 km². Further uplift caused the of the

Kunene River to change course and flow westward towards the coast the Late Pliocene (Hipondoka, 2005). A semi-aquatic fossil fauna discovered on the Etosha Pan indicates that a lacustrine environment persisted into the Holocene (Hipondoka et al., 2006). The surface of the Etosha Pan has an extremely low relief and is elevated at approximately 1080 m. The topography above the Owambo Basin varies by less than 100 m. The thickness of the Kalahari group is thought to be up to 450 m in the Owambo Basin but the rate of sedimentation is unknown (Haddon and McCarthy, 2005).

King (1962) attributes most of the Kalahari Basin surface in southern Africa to a Modern depositional surface, with smaller regions of an African depositional surface mainly found near the Molopo River (figure 3.8). Partridge and Maud (1987) and Partridge (1998) do not differentiate the surface of the Kalahari Group sediments and instead only refer to the upper unit of Kalahari Group as being deposited during the Pliocene to Holocene.

The surface of the northern Kalahari basin

The evolution of the depositional surface of the northern rim of the Kalahari Basin is discussed in detail in section 2.7. The absence of dunes to the north of the Kalahari basin suggests that the surface was not reworked by aeolian processes during the Pliocene and Quaternary (De Ploey et al., 1968). The drainage evolution and depositional patterns discussed in Chapter 2, indicates northern Angola may have experienced variations in vertical motions since the Miocene. In the northern Kalahari region near the rim of the Congo basin the surface of the Kalahari sediments are thought to be co-eval with the Post-African denudational surface and therefore this aggradational surface formed during the late Cenozoic (King, 1962). The Kalahari sediments are represented by a thin group of sediments of about 200 m thickness known as the “sable

ocres” and the “gres polymorphes” that rest unconformably on top of Precambrian and Cretaceous rocks. They are respectively Neogene and Palogene in age (Cahen and Lepersonne, 1952) and their top forms the Post-African aggradational surface (King, 1962).

The surface of the Namibian sands

A large proportion of Namibia on the seaward side of the Great Escarpment is covered with aeolian sands and is referred to as the Namib sea of sand. The Namib sea of sand lies between 26° and 23° S and is bounded by the Kuiseb River to the north. The landscape is dominated by large dunes up to 383 m high. All rivers and streams originating in Namibia are ephemeral and therefore deposition in the present-day desert is controlled by aeolian accumulation. The surface of the Namib sands is recognised as a modern aggradational surface (King, 1962; Partridge and Maud (1987). The sands rest on top of the Post-African surface (King, 1962; Partridge and Maud 1987). Geological maps of the region reveal that bedrock is exposed in scattered patches suggesting that the dune structures are superimposed on top of an erosional surface.

3.3 Theoretical admittance relationships for warped surfaces

In order to detect the signature of mantle convection using admittance calculations, the warping of the Earth’s surface in response to convection must be preserved. In other words, a surface must not be filled in or eroded faster than it is warped by mantle convection processes. It is also important to be able to establish the initial shape

of the surface before it was warped by mantle convection. In practice this usually means using geological evidence to determine the topography of the surface before it was warped. Africa's topography is dominated by a number of planation surfaces. Many of the planation surfaces are believed to have formed as smooth flat surfaces and later uplifted. For example at the beginning of the Cenozoic, the African surface extended across most of southern Africa inland of the Great Escarpment, at elevations between 500 – 600m (Partridge and Maud, 1987). Aggradational surfaces also form large flat plains in central southern Africa and therefore may also provide a good estimate for initial shape. If the area did however have a constant slope that was later tilted or warped by mantle convection there should be a linear relationship between the height and the associated gravity anomaly. Without adjusting for the initial slope, the admittance calculation would probably be under- or over-estimated. The topography of the deformed surface must be preserved and the effects of present day erosion such as fluvial erosion removed. A coherence between gravity and topography of 1 indicates that topography and density contrasts are compensated locally, while a coherence of 0 indicates the topography and density contrasts are entirely supported by the strength of the plate (Hartley and Allen, 1994). Coherence between gravity and topography is highest when the African topography is corrected for recent sediments thickness (chapter 2). The surface of deep sedimentary basins in Africa are therefore not ideal representations of dynamically supported topography in southern Africa.

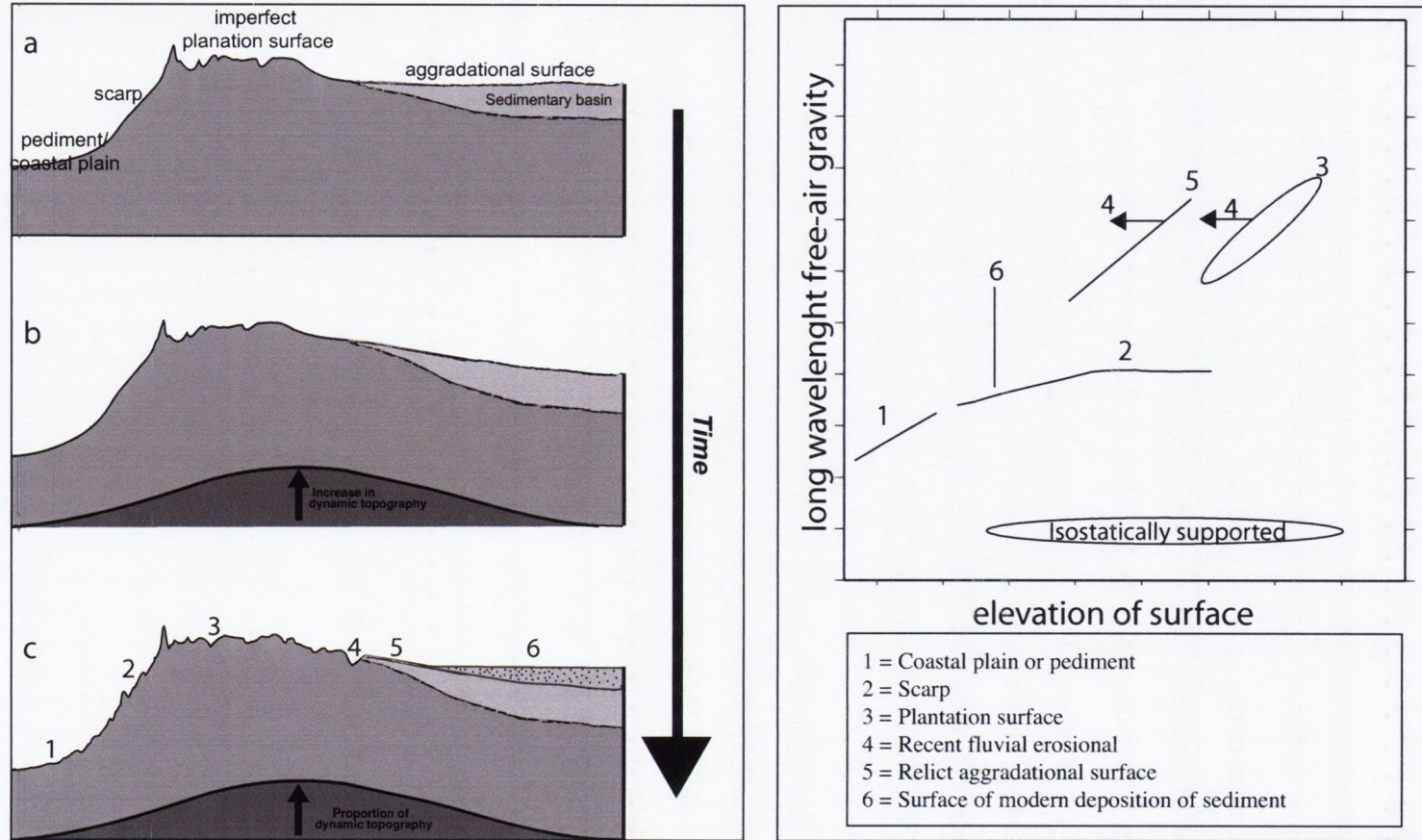


Fig. 3.7: Right: The effects the long wavelength uplift may have had on different landsurfaces and topographic features. (a) A cross-section of the topography of a passive margin with a coastal plain, escarpment and inland elevated plateau and sedimentary basins. (b) Uplift due to mantle convection causes the surfaces to warp (b) Further erosion and deposition occurring after uplift. Resultant surfaces are classified into 6 types. Left: Hypothetical relationship between the topography and long wavelength free-air gravity for the six hypothetical surfaces.

Summary of the working hypothesis

Here we examine the relationship between the topography and long wavelength free-air gravity for six hypothetical surfaces in a region that has been tilted due to mantle convection and dynamic uplift (Figure 3.7). The initial landscape was assumed to be similar to the African topography at the beginning of the Cenozoic as described by Partridge and Maud (1987) (Figure 3.7a). A gentle planation surface existed at two levels, above and below the Great Escarpment. The planation surface inland of the escarpment was between elevations of 500 – 600 m above sea level. Deposition of sediments in the Kalahari Basin has been ongoing since the Late Cretaceous (Haddon and McCarthy, 2005).

Mantle convection is then assumed to cause uplift in the region and results in warping of the surface of the landscape (Figure 3.7b). The emplacement of dynamic support results in a long wavelength free-air gravity anomaly. During and subsequent to the establishment of mantle support, further erosion and deposition occurs (Figure 3.7c). Dissection of the uplifted regions of the plateau begins. Deposition resumes in regions with a lower elevation relative to the surrounding basin (e.g. the Owambo and Okvango Basins). It is unlikely that sedimentation would occur on depositional surfaces which have been uplifted relative to the rest of the region. The following section describes the nature of each surface identified on a cross-section through our hypothetical model of the resultant topography. It also looks at the probable relationship between topography and long wavelength free-air gravity of each for the surfaces when plotted on a graph (Figure 3.7 (right)).

Surface 1 : A pediment or coastal plain that has been tilted by inland uplift. The topography of the surface may not have originally been horizontal. As a result there is a positive, near linear correlation of data points but they may underestimate admittance.

Surface 2: A scarp that has been tilted by inland uplift. The relationship between the topography and long wavelength free-air gravity in the scarp region will probably be a positive non-linear correlation that will under estimate admittance. Regions that are very steep or near vertical (e.g. parts of the Great Escarpment) will show increases in elevation (X-axis) but no increase in gravity (Y-axis) (plot in a horizontal trend on graph). Long wavelength vertical motions will have little effect on short wavelength features except to change the overall elevation of the feature.

Surface 3: A imperfect planation surface that have been warped by dynamic uplift. Provided the surface of the peneplain was originally near horizontal there should be a linear relationship between long wavelength free-air gravity and the topography of the surface that represents true admittance. However small-scale erosion (e.g. fluvial) before and after the unset of uplift may cause systematic negative error. The planation surface often survives on interfluves between river valleys.

Surface 4: Modern day fluvial erosion such as V-shaped valleys. There should be no clear relationship between long wavelength free-air gravity and the elevation of the surface. Steep sides of fluvial valleys may plot as changing elevation (X-axis) with no changes in long wavelength free-air gravity (Y-axis) and therefore the points should plot in a horizontal trend on graph.

Surface 5: Preserved aggradational surfaces that have been warped. Provided the surface of the aggradational was originally horizontal there should be a linear relationship between long wavelength free-air gravity and the topography of the surface that represents true admittance.

Surface 6: A depositional or aggradational surface that formed after uplift or subsidence. Evidence in the Kalahari Basin shows that deposition often infills subsided areas causing the topography to be levelled off. As a result even if there is variation

in long wavelength free-air gravity in the region, there should be little topographic expression of dynamic support. Therefore changes in long wavelength free-air gravity on the Y-axis are not reflected changes in elevation of the X-axis and the points should plot in a vertical trend on the graph.

3.4 Methodology of Constructing Gravity - Elevation Plots

Both King (1962) and Partridge and Maud (2000) published maps outlining the surfaces they identified in Africa (Figure 3.1 and 3.2). The object of this chapter was to use these maps to produce plots of elevation versus gravity plots of each of these surfaces. A number of steps were necessary to extract the elevation from DEMs and gravity signal for each of the surfaces:

1. Georeferencing and digitising maps
 - (a) Obtain geographic co-ordinates of the surface boundaries by digitising the scanned map. The map projection and origin must be known to complete the this step. (b) If this is not known, it is found by trial and error by overlaying the scanned original map with a series of basemaps of known projection.

2. Correcting for errors

At this stage, the position of the surface boundaries can be inaccurate because of (a) remaining uncertainties in finding the true map projection and origin (b) problems in distinguishing surfaces on maps because of blurred ornament on 1960s maps (c) differences between modern DEM data and older topography datasets. This step attempted to correct for these errors by refining surface boundaries,

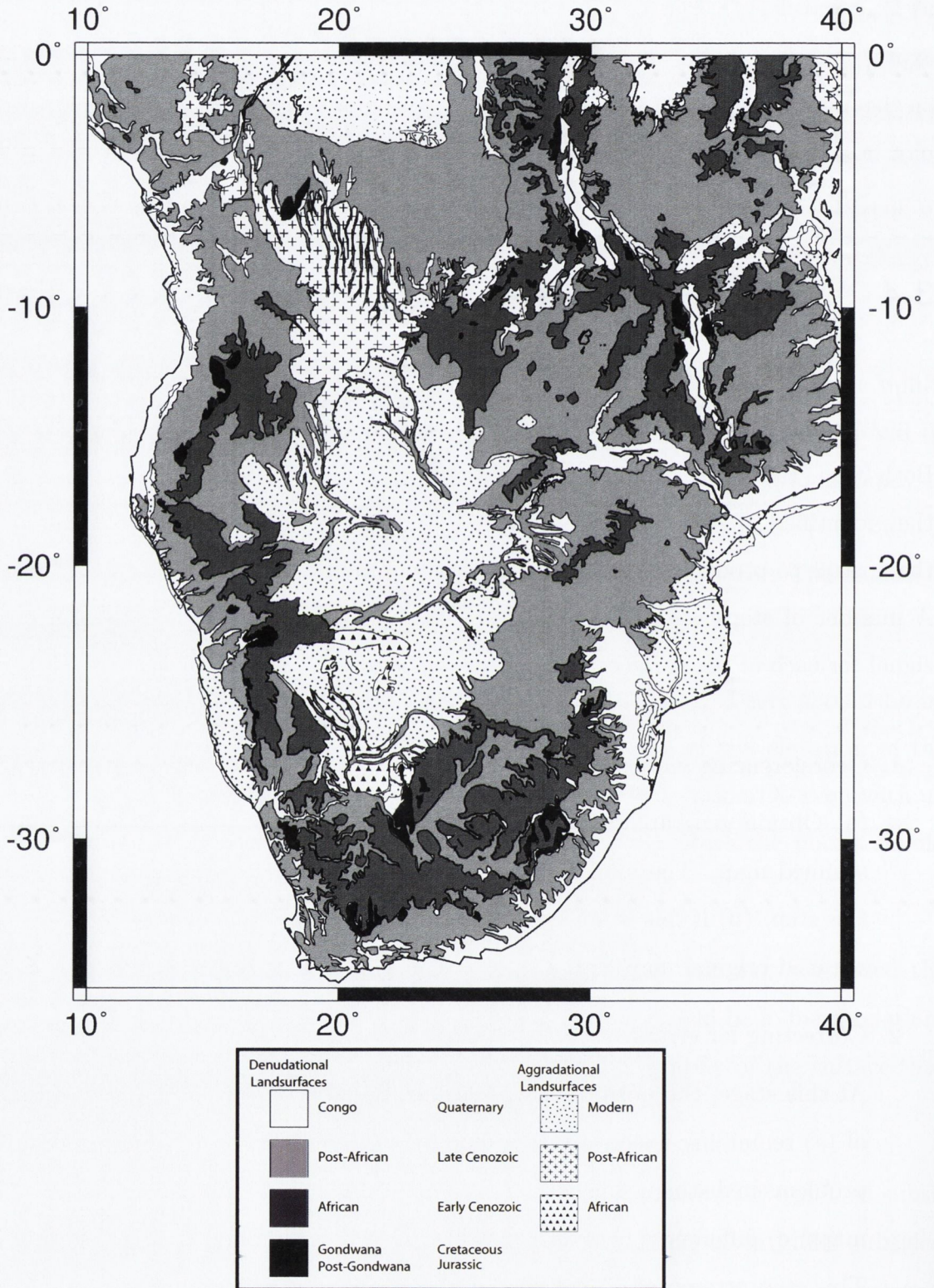


Fig. 3.8: Denudational and aggradational surfaces of Africa digitised from King (1962).

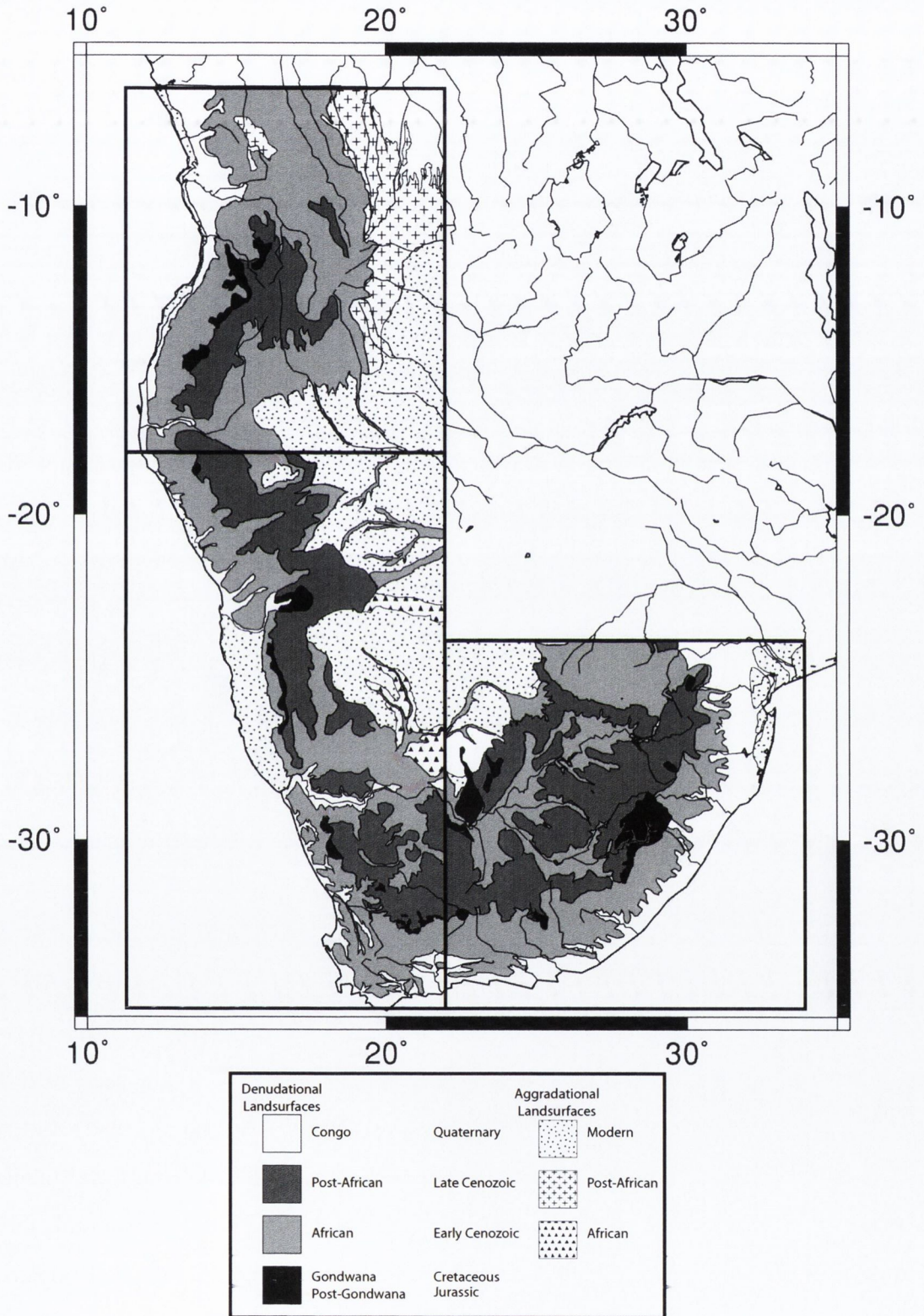


Fig. 3.9: Denudational and aggradational surfaces of Africa, reinterpreted from the map published by King (1962).

to make them consistent with modern topographic data. Outlines of the coast and drainage systems also provided useful reference points when correcting the surface.

3. Removing fluvial incision

These are corrected for localised incision caused by fluvial erosion within the surface boundary.

Step 1 was applied to both maps. Step 2 was only applied to King's map as the projection of the Partridge and Maud map was already known. Step 2 was not applied to the Partridge and Maud map as they had access to modern topography maps when they mapped the surfaces. In addition, when the coordinates of the digitised surfaces taken from the Partridge and Maud map were plotted, they were consistent with the outline of the coast and drainage systems, indicating that there was little error when projecting the surface boundaries. Step 3 applies to both maps.

3.4.1 Georeferencing and digitising maps

In order to compare the surfaces mapped by King (1962) and Partridge and Maud (2000) with recently released DEMs and long wavelength free-air gravity, the original surface boundaries had to be digitised from the original maps. The first step in digitising the surface boundaries is to correct for the map projection used in order to find the geographical coordinates. The map produced by Partridge (1998) and reproduced in Partridge and Maud (2000) was projected using Gauss Conformal projection (confirmed with personal communication with Tim Partridge). Gauss Conformal is a common projection applied to southern African maps. To test the information provided by Partridge, a map of coastlines, political boundaries and river systems was produced

using a Gauss Conformal with longitude of origin of 24° E, which gave a very close fit with original map. No further corrections were needed after the Partridge (1998) map was digitised.

There were a number of difficulties in digitising the map produced by King (1962). The original map does not contain any (longitude, latitude) reference points or map projection information, both of which are needed for digitising coordinates of the surface boundaries. Therefore, it was necessary to find the projection and origin information by trial and error, by comparing the published maps with a series of maps of known projection. Other maps by King indicated that he often used azimuth projection with a point of origin near the centre of the map. Two other maps published in the *Morphology of the World* (1962) had a point of origin, where a longitude of multiple of 10° and a latitude of 0° and this provided a good starting point. Overlaying the original map with coast lines, national boundaries and drainage were plotted in various known projections provided points of reference. An azimuth projection with an origin of longitude 20 degrees, latitude 0 degrees appeared to be the closest fit with the coastlines and political boundaries. However there appeared to be more deviation with the large lakes such as Lake Victoria and some rivers. However even small misalignment of coordinates on a map of this scale could cause significant shifts in boundaries of the surface, and will have to be accounted for when looking at the surfaces in more detail.

A further difficulty in digitising surface boundaries from King's map was differentiating the Gondwana and African surface. The Gondwana surface is represented by a black filled polygon and the African surface is represented as closely spaced vertical lines. The Gondwana surface is often surrounded by the African surface. In areas it is difficult to pick out the Gondwana surface from the African surface, where the African surface appears to be smeared.

As there were some problems fitting the original map to a projection there is some latitude and longitude shift of the surfaces that has to be corrected for. More detailed DEMs were used to correct errors in the boundaries of the different surfaces as defined by King (1962). The use of geological maps may also be useful especially in establishing the position of modern sedimentary cover indicating aggradational surfaces or exposed basement rock indicating an erosional surface.

3.4.2 Correcting for errors

Southern Africa was subdivided into three regions which broadly correlate with Angola, Namibia and the geological region referred to as the Karoo (figure 1.8). The main reason to look at smaller scale regions was to fully utilise the high resolution topographic data both as relief maps and 2D cross-sections. Examining the whole of southern Africa at one time would limit the resolution of the topographic data. The regions were chosen as they centre on a positive long wavelength free-air gravity anomaly and show large variations on long wavelength free-air gravity .

The first step involves being able to recognise the surfaces on the DEM through relief, texture and elevation. Slope maps and geological maps were also used to identify surfaces. Errors introduced by difficulties with the chosen projection were corrected using co-ordinates of major river systems and coastlines as reference points. Aggradational surfaces tend to have a very smooth relief and were straightforward to identify on relief and slope-maps. The boundaries of aggradational surfaces were also checked against geological maps. A smooth, low relief surface is typical of the top of the Kalahari sediments, where it can be easily traced for thousands of kilometres. The exception to this is in the Namibian Desert, also referred to as the sea of sand. The surface in this region is dominated by large sand dunes. The dunes can be seen as linear features on

the DEMs created from SRTM30. The same area on more detailed DEMs generated using SRTM 90m data show a large loss of information.

The oldest Gondwana surface on the map appears as small areas of high relief peaks usually elevated above the Great Escarpment. The African and Post-African surfaces are the most difficult to differentiate on the DEMs. Both can appear to be smooth to higher relief. The Post-African surface occurs at two levels, both below the escarpment and above the Great Escarpment. The African surface occurs inland of the Great Escarpment and is often rimmed by Gondwana surface to its seaward side. Therefore little adjustment is made to these surfaces apart for corrections for projection of the co-ordinates.

Alterations made to the King's surface boundaries

In the Angolan region, the boundary of the Post-African aggradational surface that forms the top of the Kalahari Group sediments in this region could be more accurately defined by its characteristic smooth surface on the DEM. The western boundary of the Post-African aggradational surface was altered in accordance with the DEM and the limit of Kalahari sediments as defined on geological maps. Most other adjustments appeared to be a result of longitude and latitude shift of the boundaries due to misalignment of boundaries with the topographic map. Some of the smaller tributaries of the Okavango river below 1000 m showed no topographic expression on the DEMs and therefore were not included on the Post-African surface.

In the Namibian region, adjustments to the original surface boundaries were made to correct for misalignments with rivers and coastlines plotted on the map. For example the Congo/modern erosional surface of the central Namibian desert was realigned with

modern major river systems (figure 3.9). Regions of the Gondwana surface to the south of the Namibia region show a strong north-south trend that is not reflected in the DEMs. The trend may be an artifact as a result of poor differentiation between the African and Gondwana surface when digitising from the original map (as discussed before).

In the Karoo region, adjustments were made to conform with modern day drainage patterns. In addition small adjustments to the Post-African and African surface were based on to evidence suggested by the relief and drainage of the region. The reinterpreted map can is plotted in Figure 3.9.

3.4.3 Correcting for erosion by modern day drainage systems

Fluvial erosion by modern drainage systems incises all the topographic surfaces. Failure to account for the effect of rivers or streams cutting into a surface will produce a systematic negative error to the overall elevation of the surface. It will also cause unwanted scatter in a topographic-gravity plot, making it more difficult to interpret whether the surface was warped by mantle convection. Erosion by larger rivers has been identified on the original map and marked in as surfaces of Quaternary or Congo erosion and can be mostly seen around the coast (figure 3.8). However the scale of the original map did not allow for the removal of smaller scale modern erosion features.

Removing the effects of modern erosion by digitising river valleys by eye, as was applied to the Congo surface in Chapter 2, is difficult and time consuming. Instead a surface or envelope of the topography is created by taking the highest points in a window of predefined size. In this case the size of the window chosen was 10km by 10km as it removed most smaller scale erosion from the DEM without losing detail. Enveloped

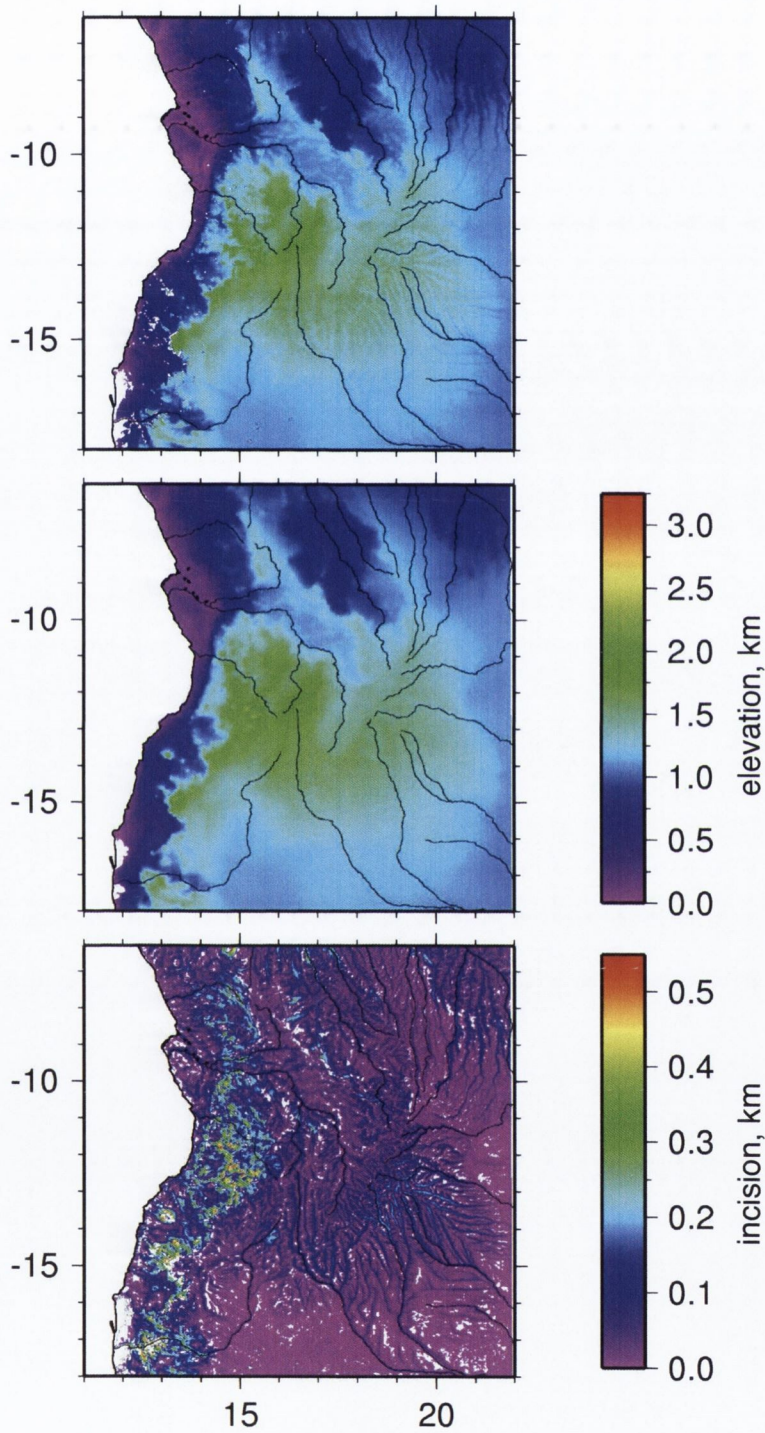


Fig. 3.10: The Angolan Region. a. the original DEM generated with SRTM 90m data sampled every 30 arc seconds, b. envelope of the topography is created by taking the highest points within a window of 10km by 10km, c. incision measured by subtracting the original DEM away from the envelope of topography

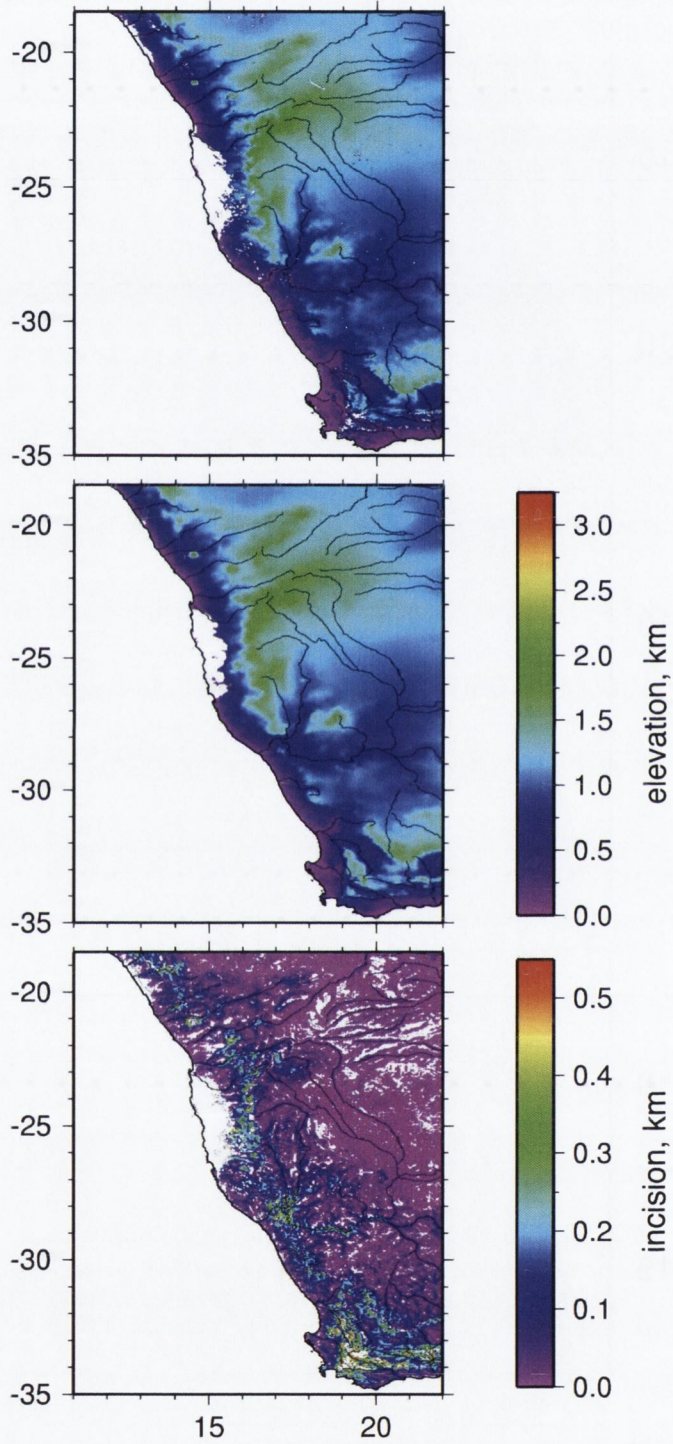


Fig. 3.11: The Namibian Region. a. the original DEM generated with SRTM 90m data sampled every 30 arc seconds, b. envelope of the topography is created by taking the highest points within a window of 10km by 10km, c. incision measured by subtracting the original DEM away from the envelope of topography

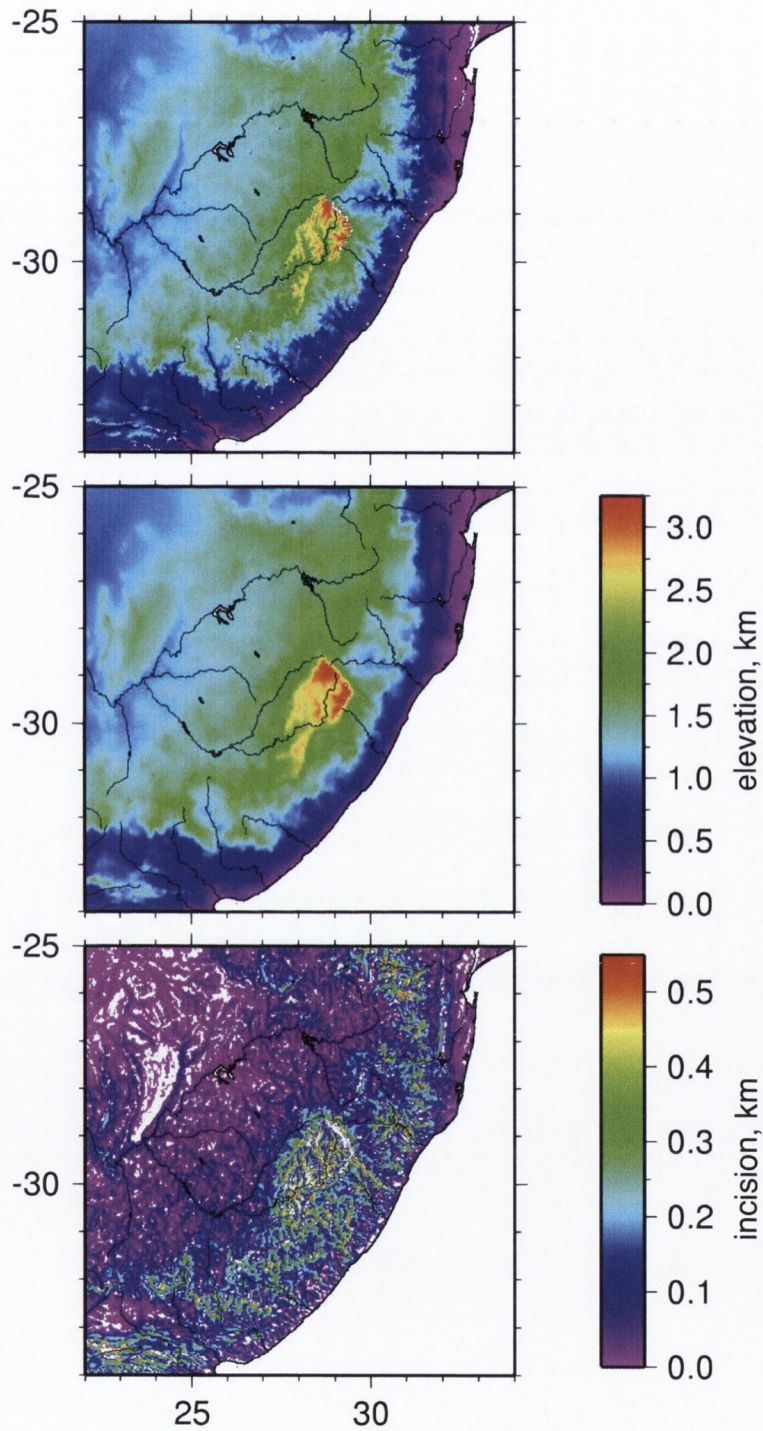


Fig. 3.12: The Karoo Region. a. the original DEM generated with SRTM 90m data sampled every 30 arc seconds, b. envelope of the topography created by taking the highest points within a window of 10km by 10km, c. incision measured by subtracting the original DEM away from the envelope of topography

surfaces of the Angolan, Namibian and Karoo regions were produced (figure 3.10, 3.11 and 3.12). River valleys wider than these are common in Africa (e.g. the Orange River) however it was assumed that these were identified as surfaces of Quaternary erosion on the original map. Removing the original DEM from the enveloped DEM indicated the areas that have been filled in by the enveloped surface. The match between the areas that have been filled in and modern drainage system is close, and therefore the technique of creating an envelope of the topography to remove modern erosion appears to work well (figure 3.10).

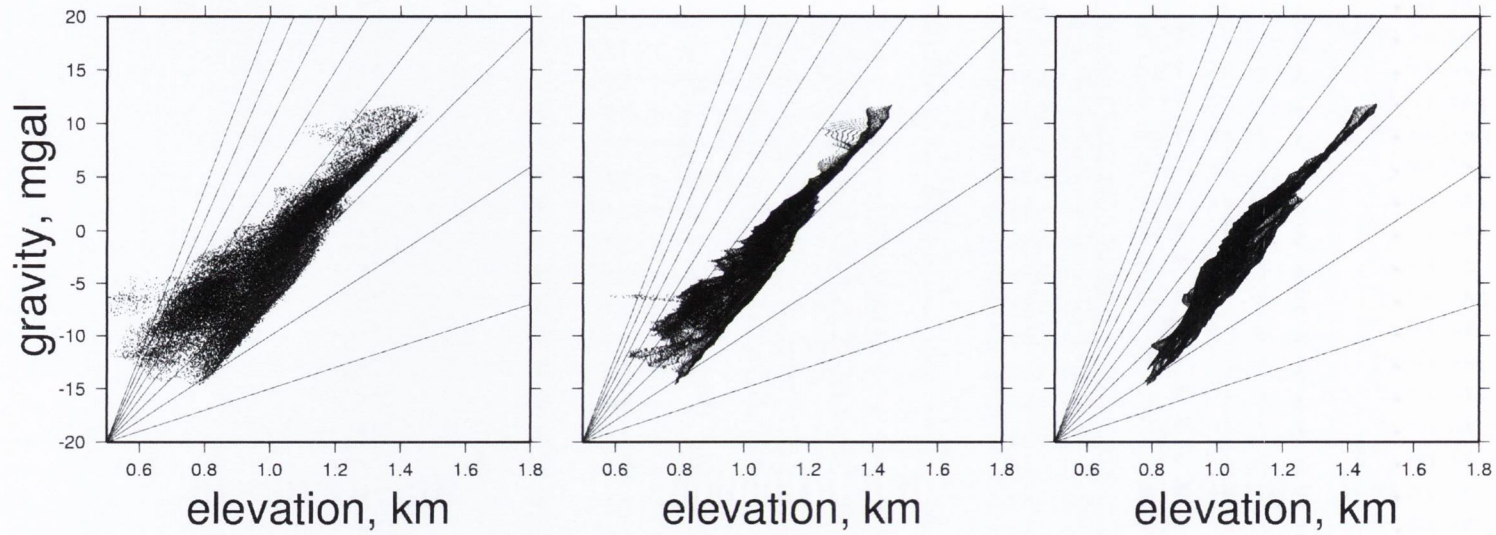


Fig. 3.13: Plot of elevation and long wavelength free-air gravity for the Congo surface (from Chapter 2) to show a comparison between different methods to remove the effects of fluvial incision; (a) modern topography of region containing surface (b) envelope of topography of the region containing the surface (c) elevation of the surface reconstructed by digitising profiles through topography.

In Chapter 2 a surface was reconstructed from digitised profiles of the topography and plotted against long wavelength free-air gravity. The resultant plot was compared with a similar plot based on a reconstruction of the surface using an envelope of the topography of the same region (figure 3.13). The plot using the enveloped topography is effective at removing some of the scatter produced by the erosion of the surface. However at lower elevations where the river valleys are wider the method of creating an envelope of the topography is less effective. It should also be noted that the upper limit of the surface elevation varies little in all topography-gravity plots and the upper limit of the surface elevation shows a strong positive correlation in all three plots (figure 3.13). Overall, producing an envelope of the topography of a surface is quite effective at filtering out small scale modern erosion. Larger scale erosional features were identified on the original maps and marked as the Congo denudational surface (King,1962) or dissected areas (Partridge and Maud, 1998). This maybe a useful observation when describing plots of other surfaces.

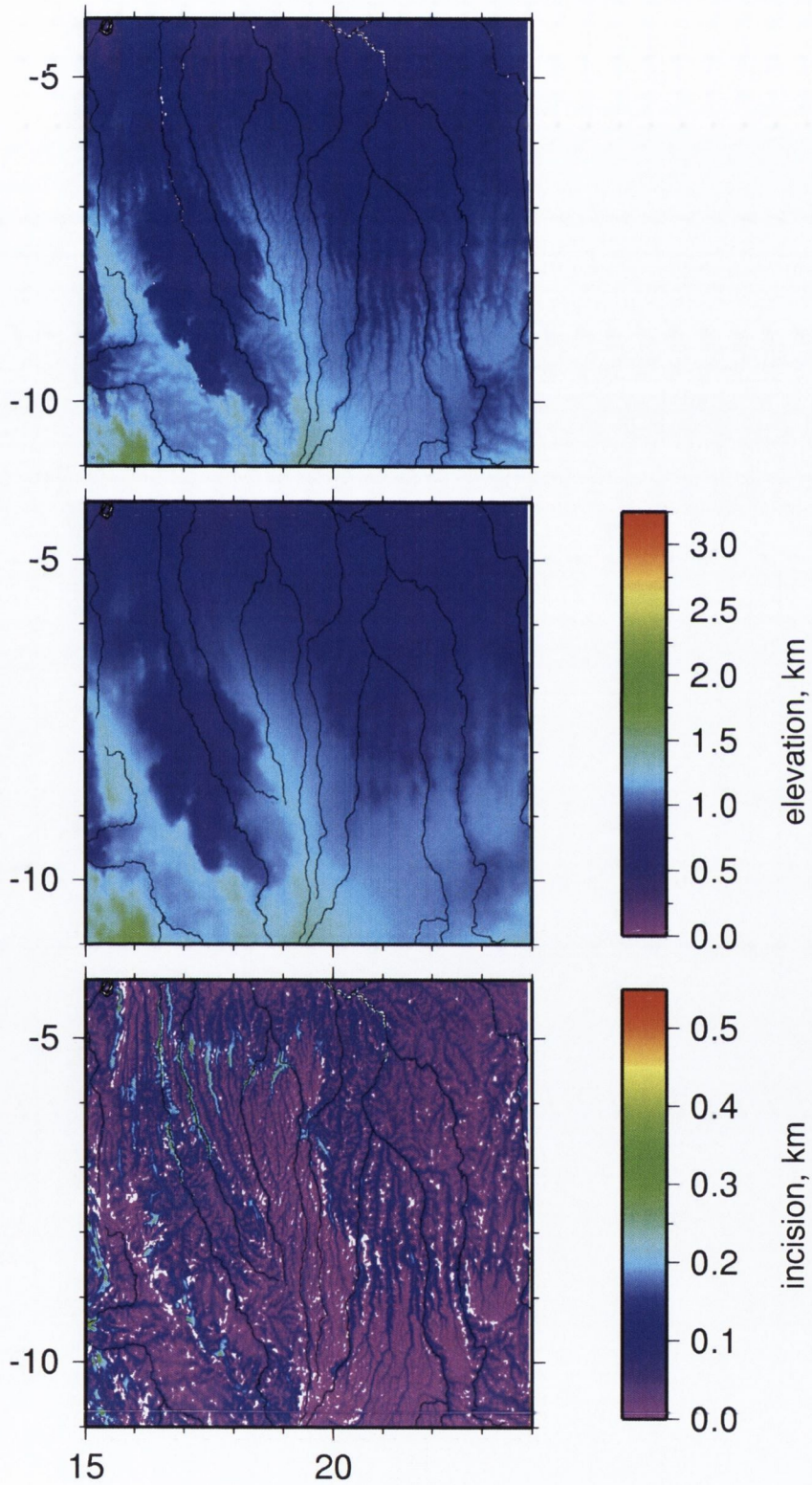


Fig. 3.14: The South Congo Region a. the original DEM generated with SRTM 90m data sampled every 30 arc seconds, b. envelope of the topography is created by highest points within a window of 10km by 10km, c. incision measured by subtracting the original DEM away from the envelope of topography

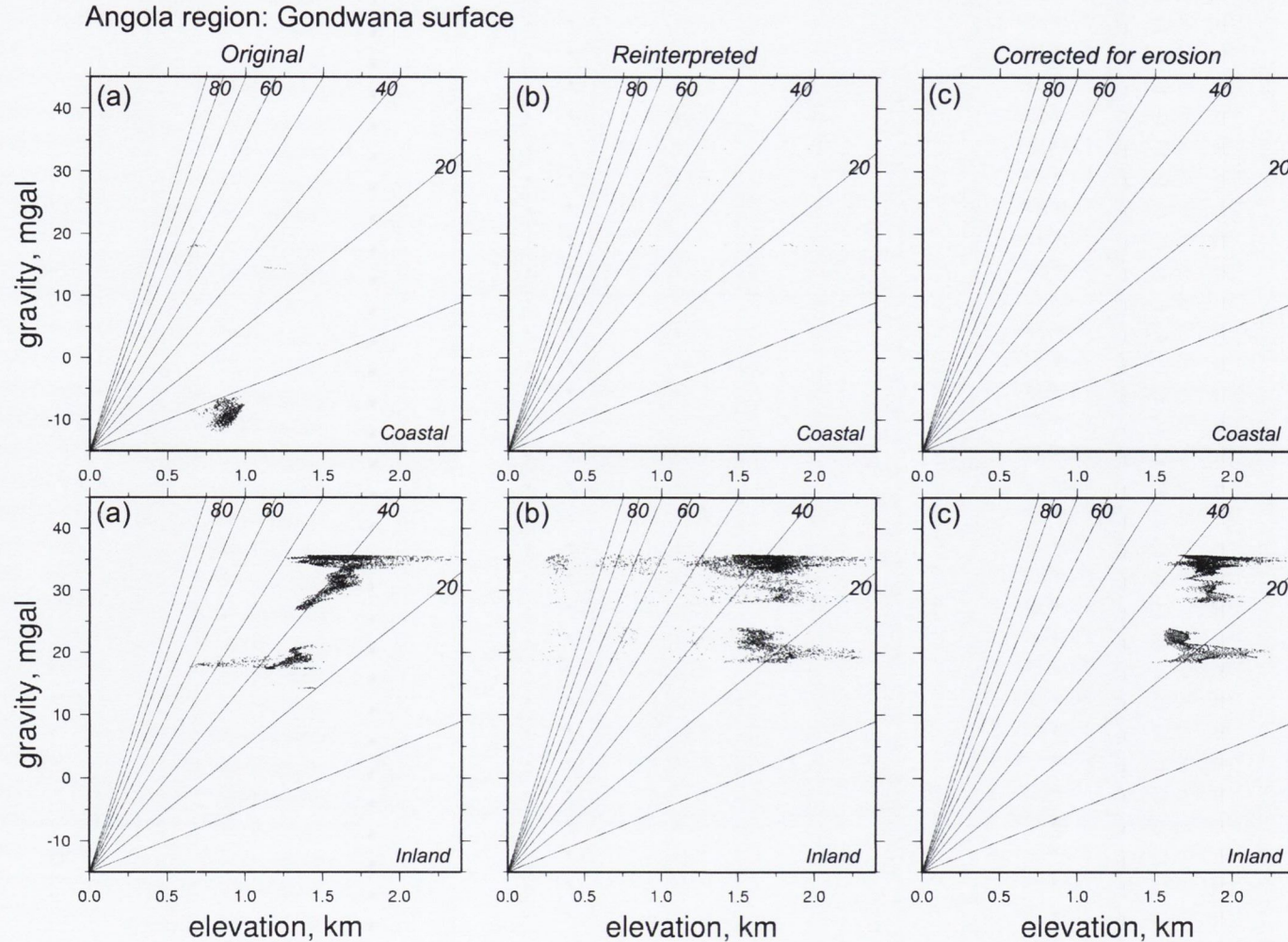


Fig. 3.15: a. The topography of the Gondwana surface digitised from King, 1962 b. The topography of the reinterpreted Gondwana surface c. The enveloped topography of the reinterpreted Gondwana surface plotted against long wavelength free-air gravity in the Angolan region. Regions inland of the escarpment are plotted on the bottom, regions on the coastal side of the escarpment are plotted on the top row. Lines on the graph represent admittance slopes in intervals of 10 mgals km^{-1} . Lines on the graph represent admittance slopes in intervals of 10 mgals km^{-1}

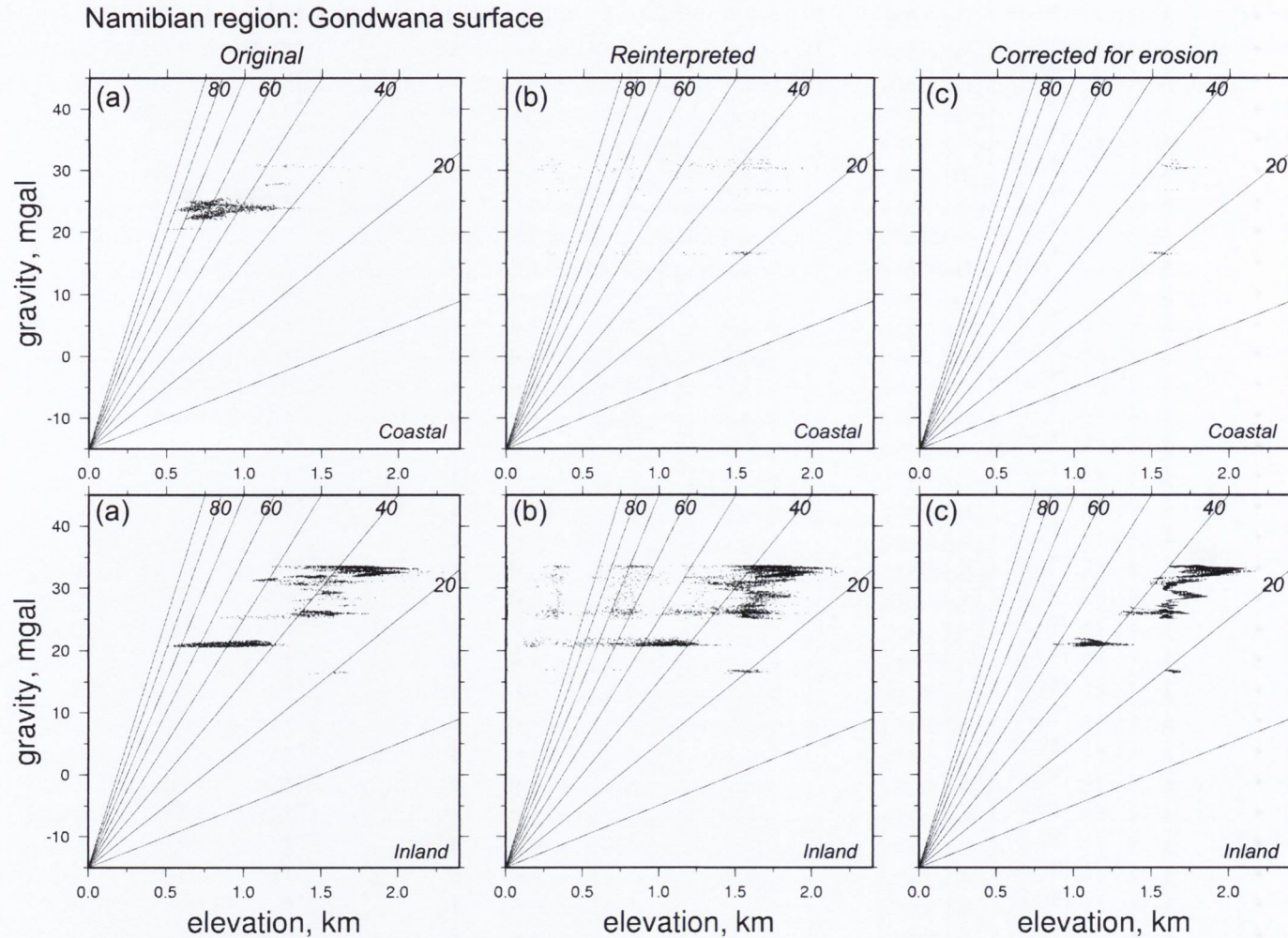


Fig. 3.16: a. The topography of the Gondwana surface digitised from King, 1962 b. The topography of the reinterpreted Gondwana surface c. The enveloped topography of the reinterpreted Gondwana surface plotted against long wavelength free-air gravity in the Namibian region. Regions inland of the escarpment are plotted on the bottom, regions on the coastal side of the escarpment are plotted on the top row. Lines on the graph represent admittance slopes in intervals of 10 mgals km⁻¹.

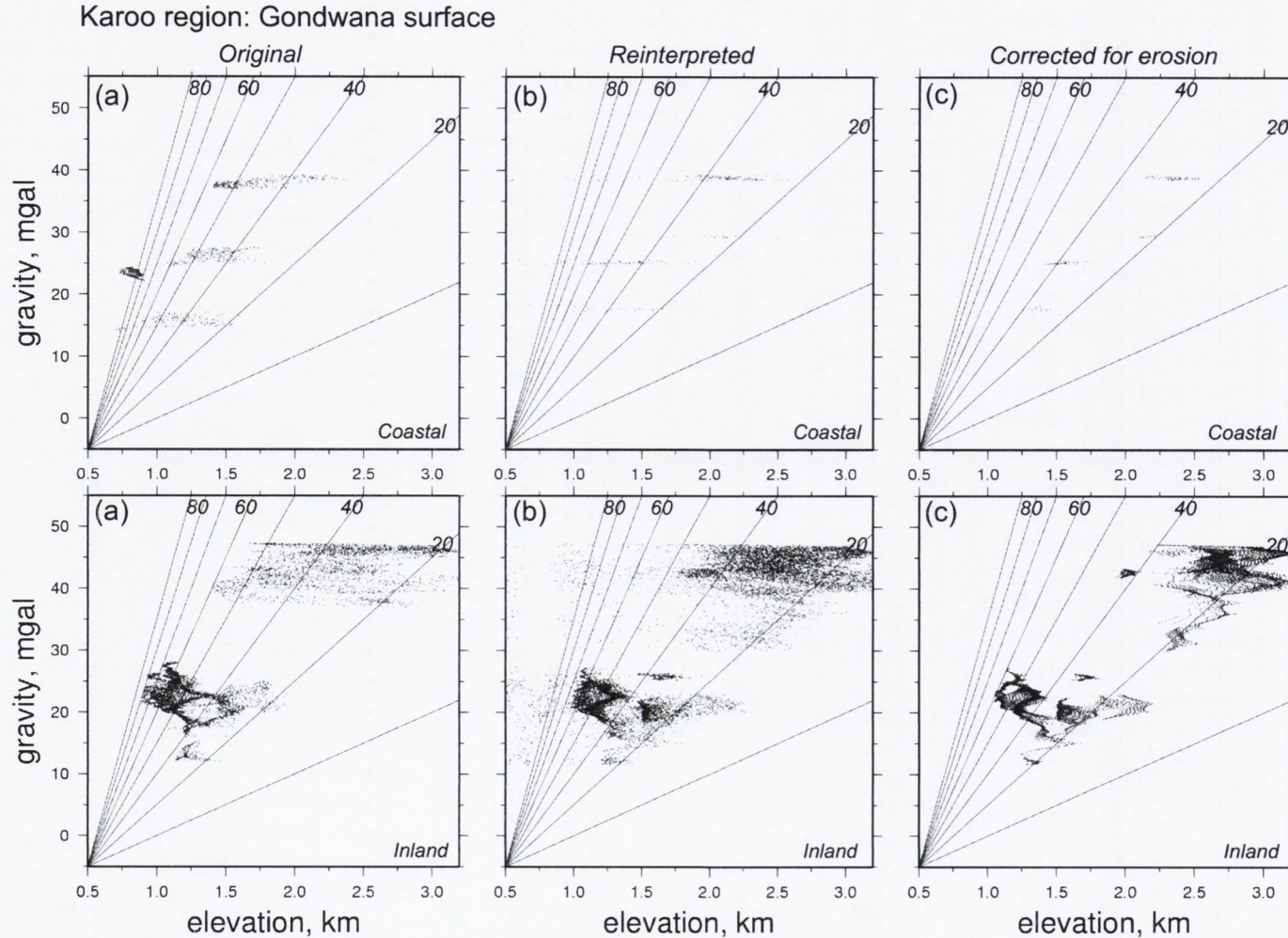


Fig. 3.17: a. The topography of the Gondwana surface digitised from King, 1962 b. The topography of the reinterpreted Gondwana surface c. The enveloped topography of the reinterpreted Gondwana surface plotted against long wavelength free-air gravity in the Karoo region. Regions inland of the escarpment are plotted on the bottom, regions on the coastal side of the escarpment are plotted on the top row. Lines on the graph represent admittance slopes in intervals of 10 mgals km^{-1} .

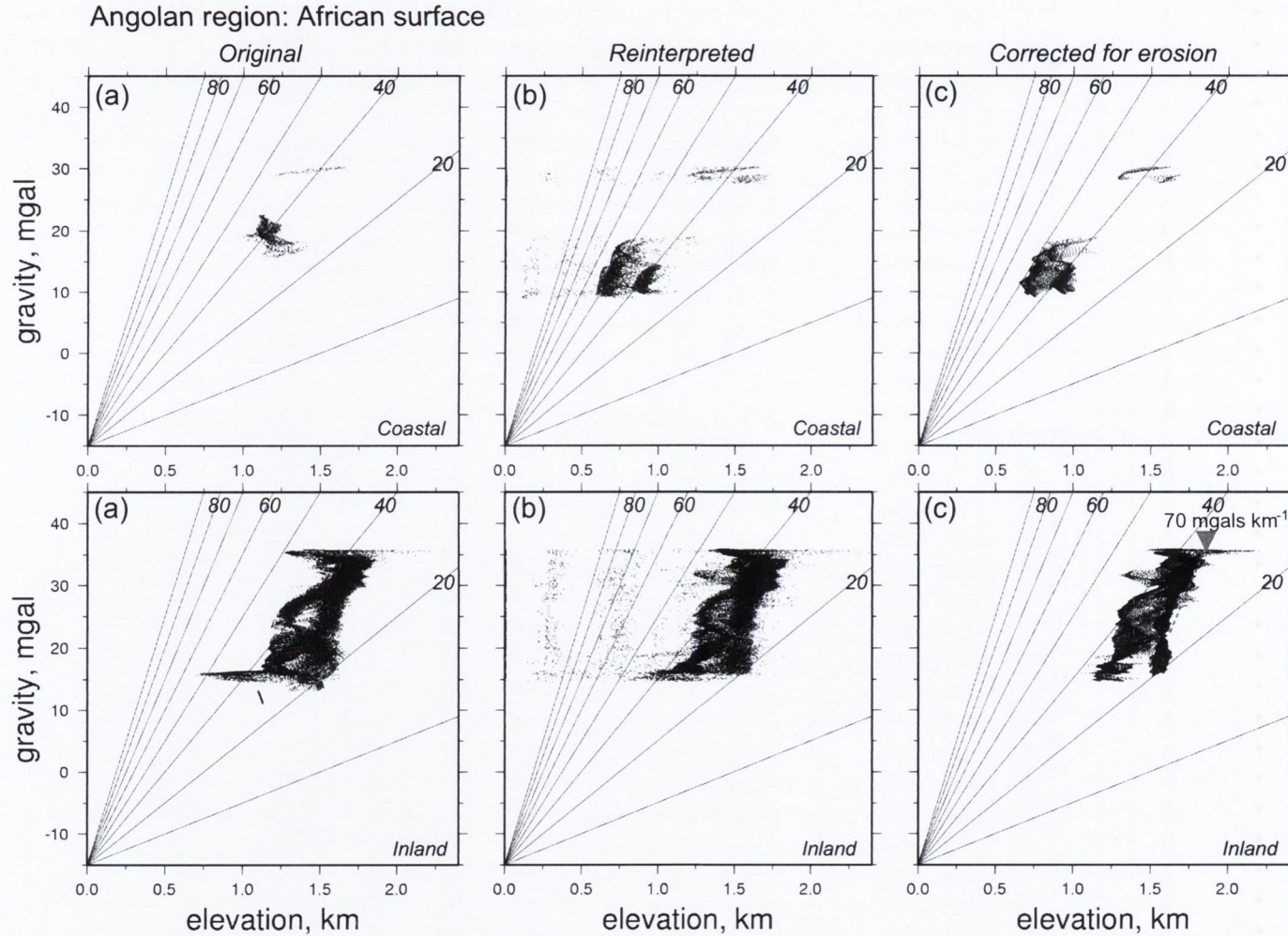


Fig. 3.18: a. The topography of the African surface digitised from King, 1962 b. The topography of the reinterpreted African surface c. The enveloped topography of the reinterpreted African surface plotted against long wavelength free-air gravity in the Angolan region. Regions inland of the escarpment are plotted on the bottom, regions on the coastal side of the escarpment are plotted on the top row. Lines on the graph represent admittance slopes in intervals of 10 mgals km^{-1} .

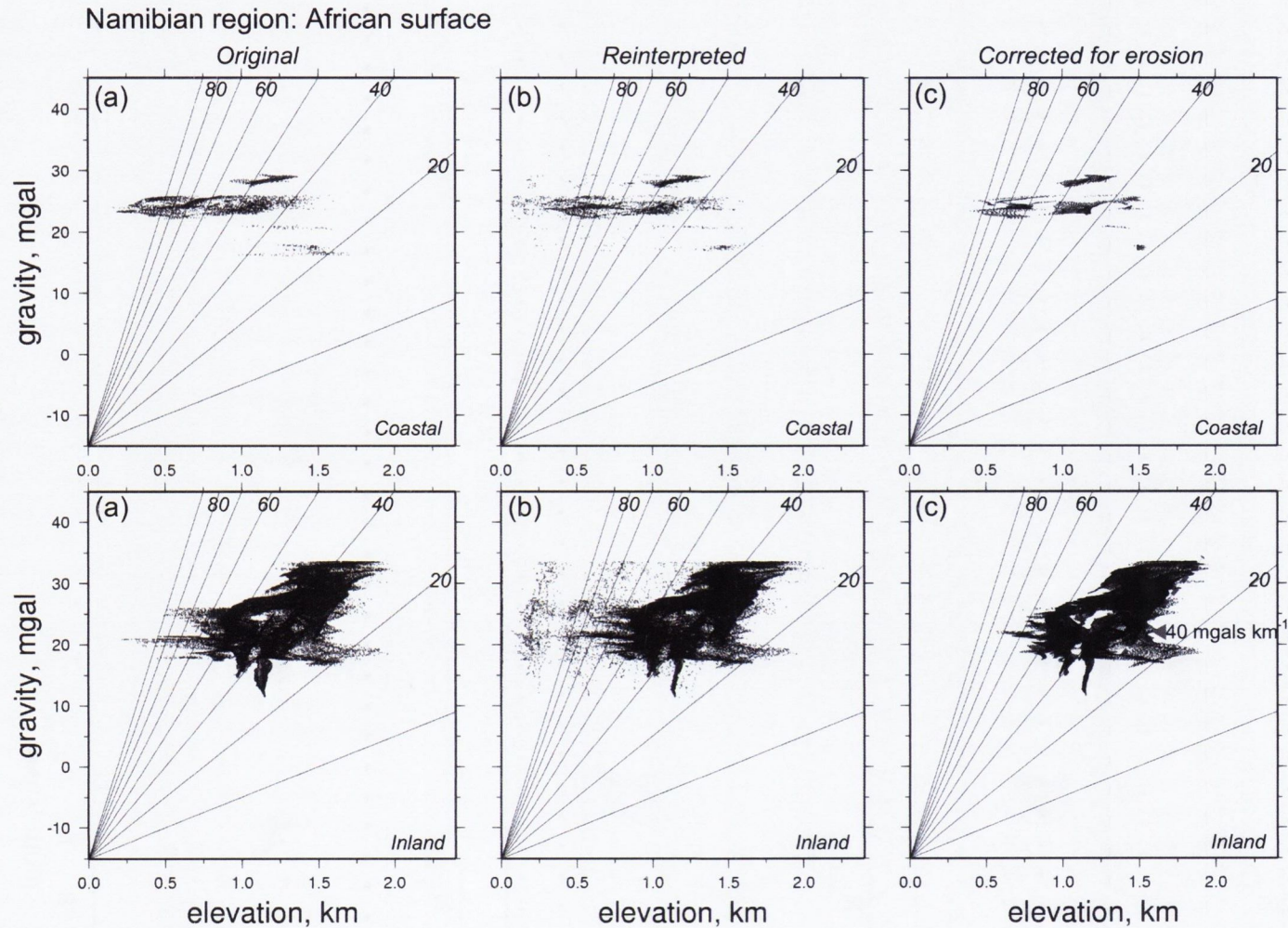


Fig. 3.19: a. The topography of the African surface digitised from King, 1962 b. The topography of the reinterpreted African surface c. The enveloped topography of the reinterpreted African surface plotted against long wavelength free-air gravity in the Namibian region. Regions inland of the escarpment are plotted on the bottom, regions on the coastal side of the escarpment are plotted on the top row. Lines on the graph represent admittance slopes in intervals of 10 mgals km^{-1} .

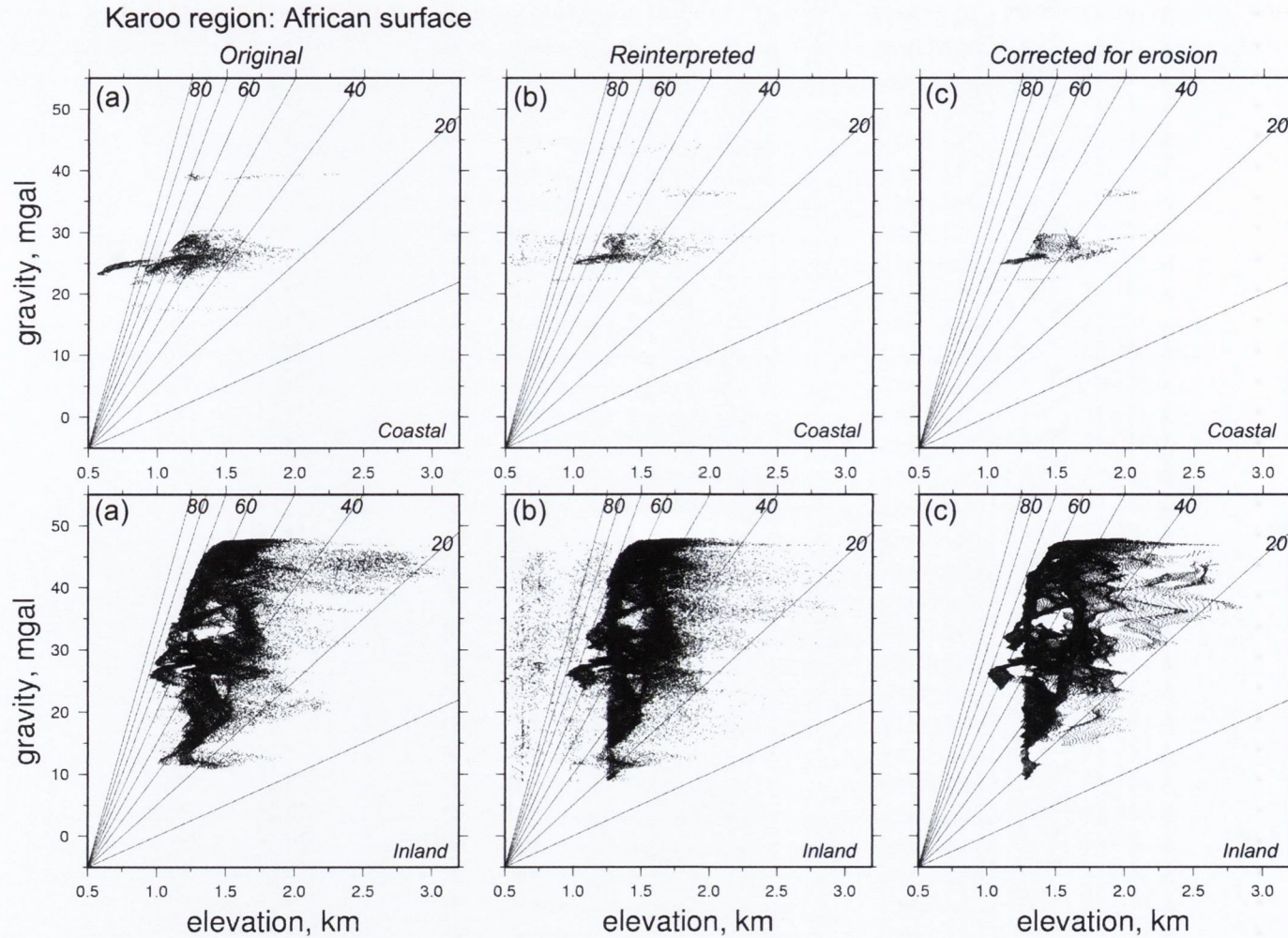


Fig. 3.20: a. The topography of the African surface digitised from King, 1962 b. The topography of the reinterpreted African surface c. The enveloped topography of the reinterpreted African surface plotted against long wavelength free-air gravity in the Karoo region. Regions inland of the escarpment are plotted on the bottom, regions on the coastal side of the escarpment are plotted on the top row. Lines on the graph represent admittance slopes in intervals of 10 mgals km^{-1} .

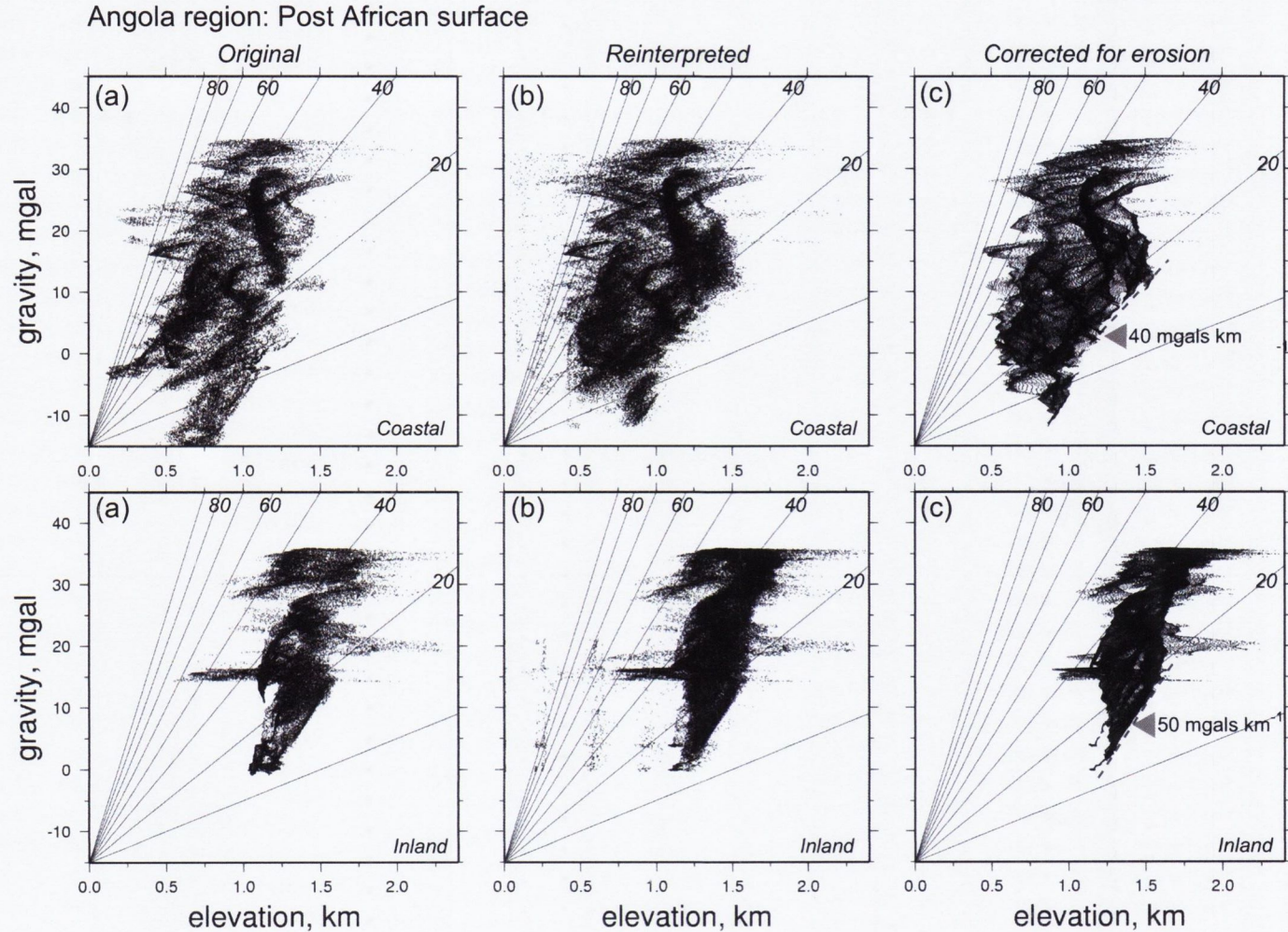


Fig. 3.21: a. The topography of the Post African surface digitised from King, 1962 b. The topography of the reinterpreted Post African surface c. The enveloped topography of the reinterpreted Post African surface plotted against long wavelength free-air gravity in the Angolan region. Regions inland of the escarpment are plotted on the bottom, regions on the coastal side of the escarpment are plotted on the top row. Lines on the graph represent admittance slopes in intervals of 10 mgals km^{-1} .

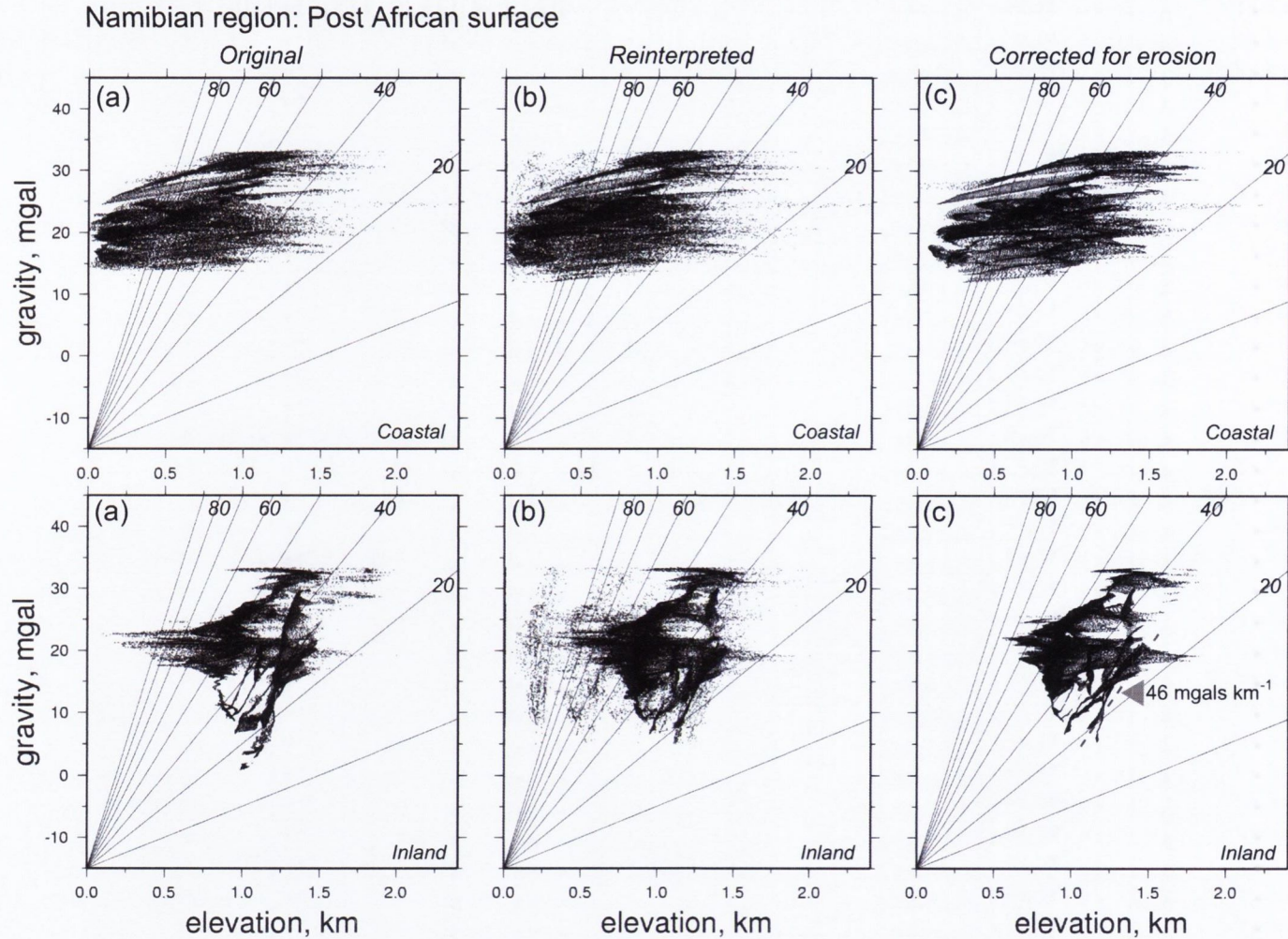


Fig. 3.22: a. The topography of the Post African surface digitised from King, 1962 b. The topography of the reinterpreted Post African surface c. The enveloped topography of the reinterpreted Post African surface plotted against long wavelength free-air gravity in the Namibian region. Regions inland of the escarpment are plotted on the bottom, regions on the coastal side of the escarpment are plotted on the top row. Lines on the graph represent admittance slopes in intervals of 10 mgals km^{-1} .

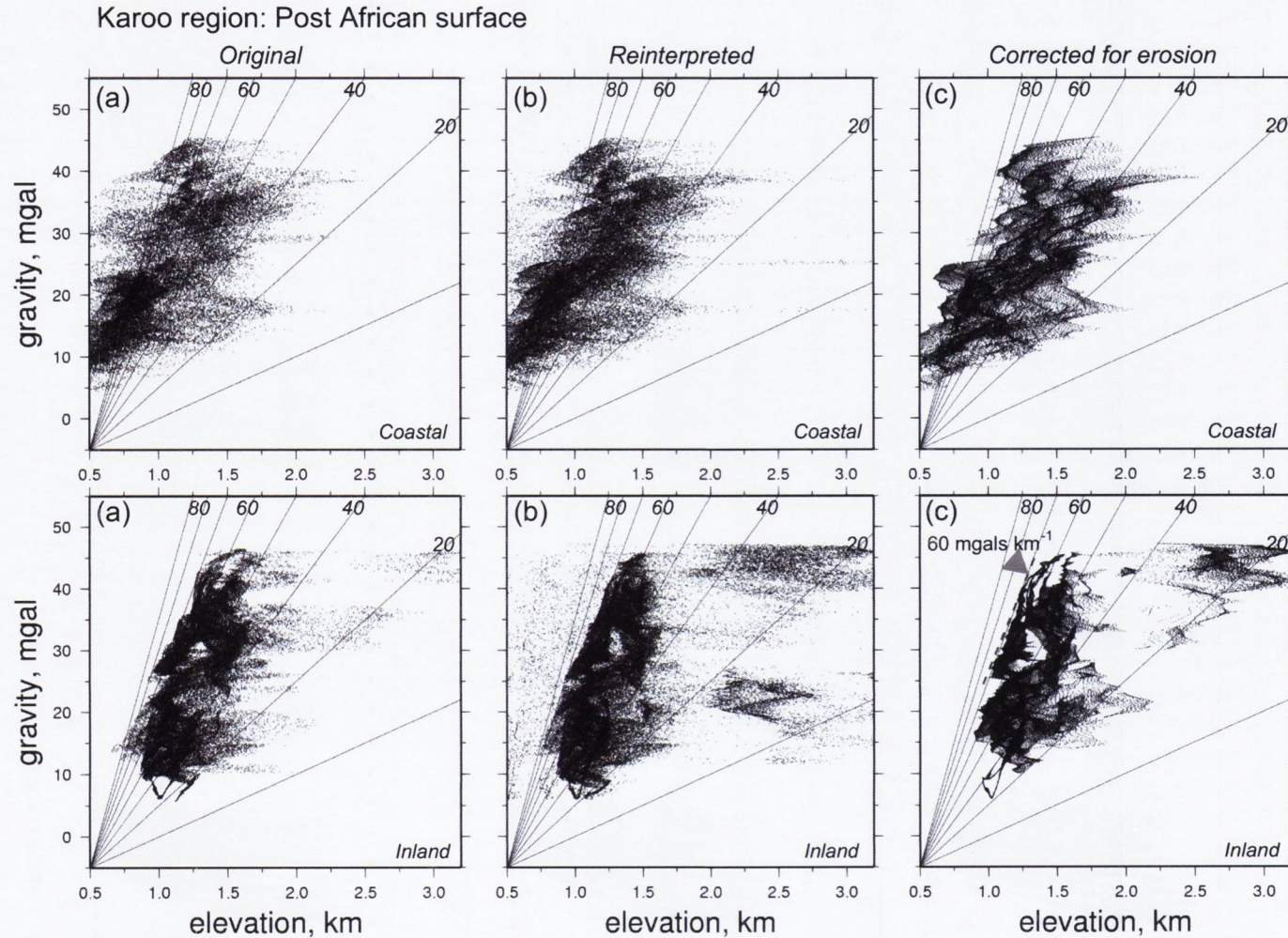


Fig. 3.23: a. The topography of the Post African surface digitised from King, 1962 b. The topography of the reinterpreted Post African surface c. The enveloped topography of the reinterpreted Post African surface plotted against long wavelength free-air gravity in the Karoo region. Regions inland of the escarpment are plotted on the bottom, regions on the coastal side of the escarpment are plotted on the top row. Lines on the graph represent admittance slopes in intervals of 10 mgals km^{-1} .

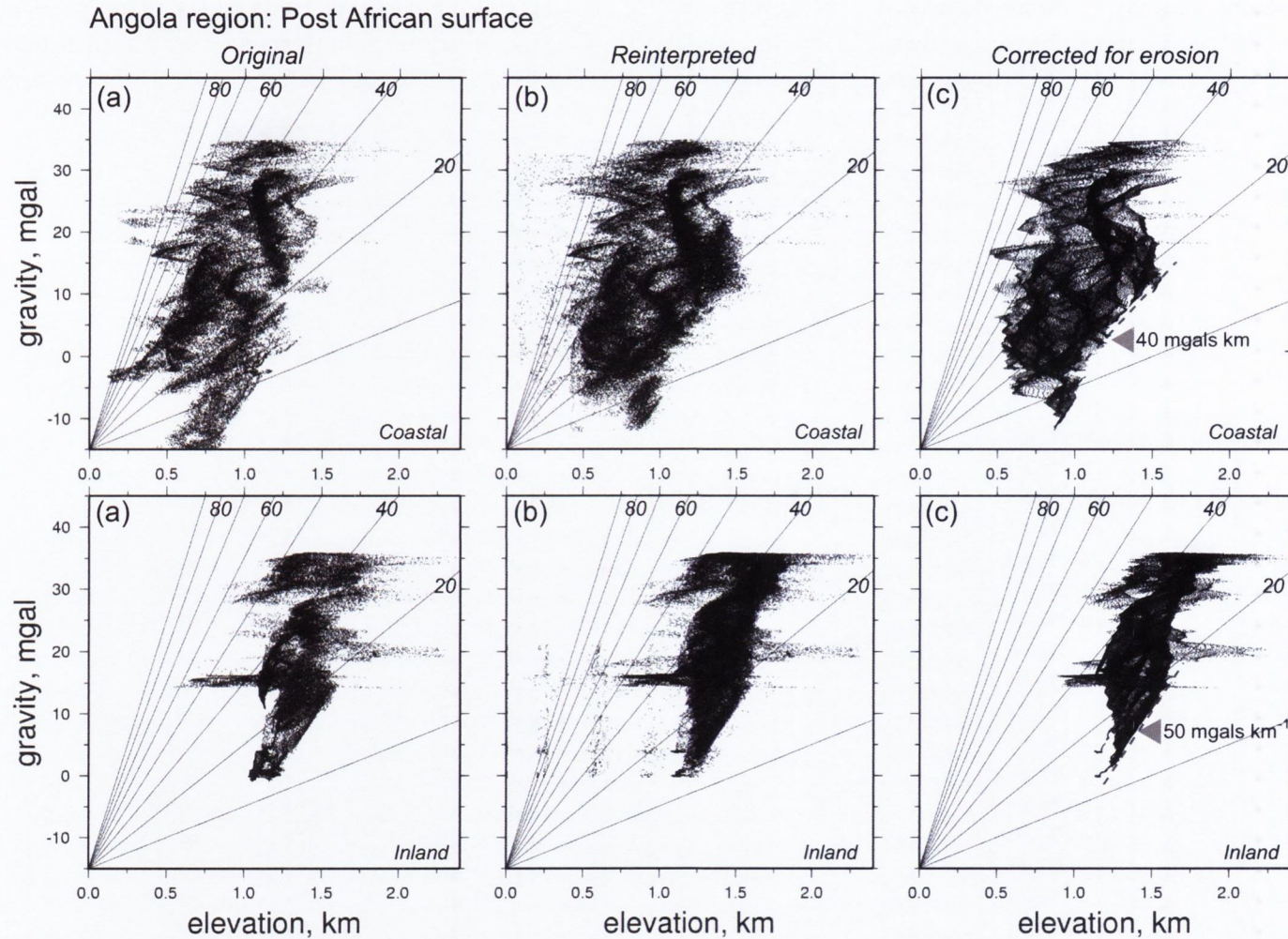


Fig. 3.24: a. The topography of the Post African aggradational surface digitised from King, 1962 b. The topography of the reinterpreted Post African aggradational surface c. The enveloped topography of the reinterpreted Post African aggradational surface plotted against long wavelength free-air gravity in the Angolan region. Regions inland of the escarpment are plotted on the bottom, regions on the coastal side of the escarpment are plotted on the top row. Lines on the graph represent admittance slopes in intervals of 10 mgals km^{-1} .

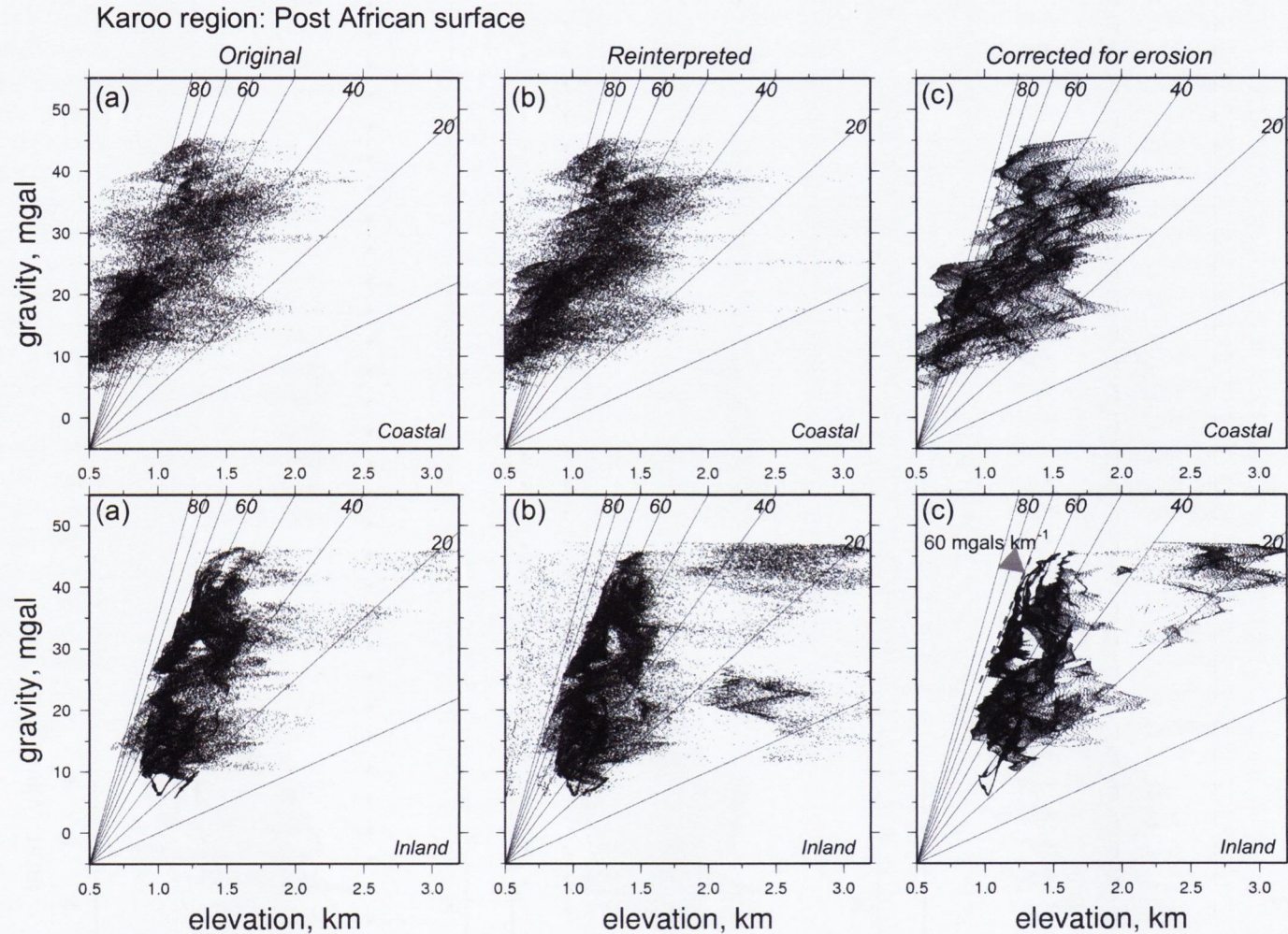


Fig. 3.25: a. The topography of the Post African aggradational surface digitised from King, 1962 b. The topography of the reinterpreted Post African aggradational surface c. The enveloped topography of the reinterpreted Post African aggradational surface plotted against long wavelength free-air gravity in the Karoo region. Regions inland of the escarpment are plotted on the bottom, regions on the coastal side of the escarpment are plotted on the top row. Lines on the graph represent admittance slopes in intervals of 10 mgals km^{-1} .

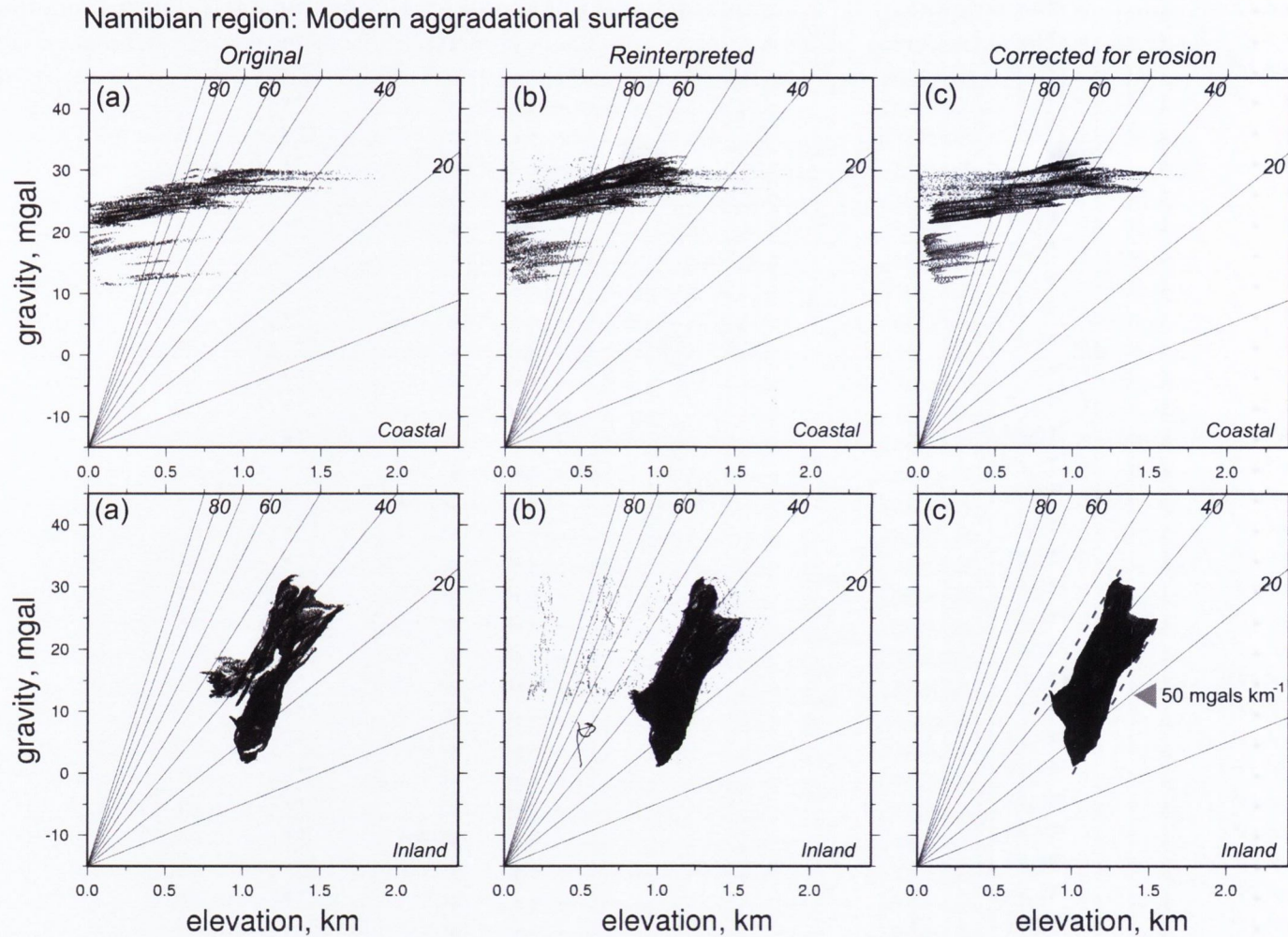


Fig. 3.26: a. The topography of the Modern aggradational surface digitised from King, 1962 b. The topography of the reinterpreted Modern aggradational surface c. The enveloped topography of the reinterpreted Modern aggradational surface plotted against long wavelength free-air gravity in the Namibian region. Regions inland of the escarpment are plotted on the bottom, regions on the coastal side of the escarpment are plotted on the top row. Lines on the graph represent admittance slopes in intervals of 10 mgals km^{-1} .

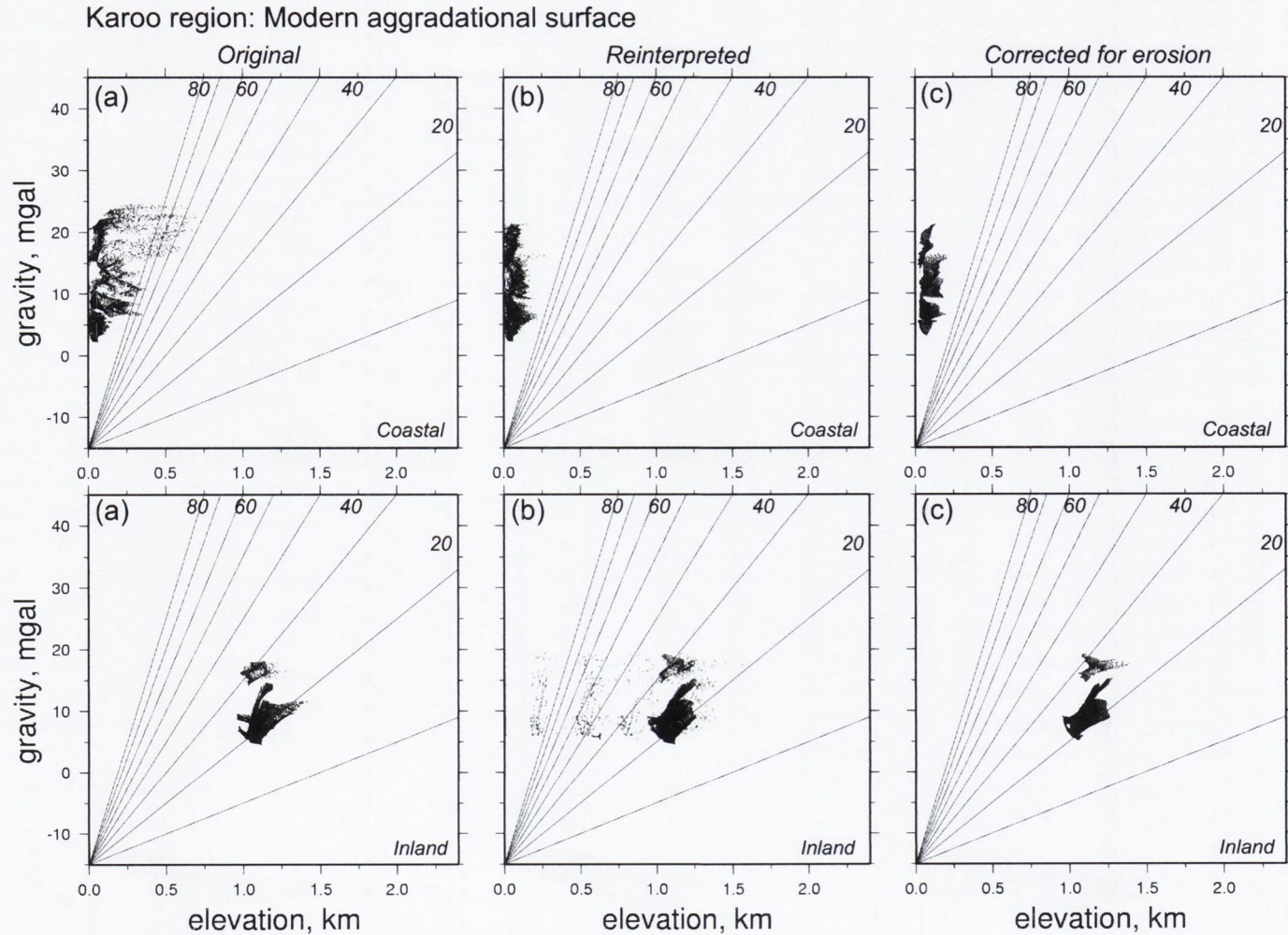


Fig. 3.27: a. The topography of the Modern aggradational surface digitised from King, 1962 b. The topography of the reinterpreted Modern aggradational surface c. The enveloped topography of the reinterpreted Modern aggradational surface plotted against long wavelength free-air gravity in the Namibian region. Regions inland of the escarpment are plotted on the bottom, regions on the coastal side of the escarpment are plotted on the top row. Lines on the graph represent admittance slopes in intervals of 10 mgals km^{-1} .

3.5 Results and interpretation

The elevation of the surfaces was plotted against long wavelength free-air gravity for the different surfaces in the three regions. Recent thermal modelling of AFTA data suggest high amounts of denudation during the Late Cretaceous along the coastal plains below the escarpment of southern Africa (Gallagher et al., 1999; Brown et al., 2002). It is interpreted that the unloading of the coastal plain due to denudation can cause flexural isostatic upwarp that effects the region inland of the coastal plain. In areas of low values of T_e , upwarping associated with denudation is most pronounced at the lip of the escarpment and updoming of the coastal plain (Bishop, 2007). Modeling of escarpment retreat in southern Africa suggests a low T_e value of 10 km to explain denudation patterns and the geological structure of the region (van der Beek et al., 2002). Therefore most of the deformation of the topography due to flexural upwarping should occur near of below the Escarpment. In addition, sediment accumulation at deltas may cause flexural upwarp of the coast (Lucazeau et al., 2003). To test if any of the surfaces were effected by flexural warping, the plots were divided into areas above and below the Great Escarpment to analyse the difference between dated surfaces of the same age. As most of the denudation occurred during the Cretaceous, we would expect to see minimal modification of the younger surfaces due to flexure. The coordinates for the Great Escarpment were obtained from a map produced by Partridge (1998).

Three topography-gravity plots were constructed for each of the surfaces defined by King; one using the surface that was originally digitised from the map, a second using the reinterpreted surface and the third using an enveloped topography of the reinterpreted surface was plotted. Observations for the relationship between the enveloped topography of the reinterpreted surface and long wavelength free-air gravity is summarised in Tables 1.2 and 1.3. Since no reinterpretation was required of the digitised

surface boundaries defined by Partridge and Maud only two topographic-gravity plots were produced; the surface that was originally digitised from the map and the enveloped topography of that surface. Long wavelength free-air gravity was obtained from the Grace gravity field data and low-pass filtered at 800 km as used in previous chapters.

3.5.1 Topography-Gravity relationship for King's surfaces

Gondwana and Post-Gondwana surface

Overall the Gondwana/Post-Gondwana surface is characterised by individual clusters of data with strong horizontal trends (Figure 3.15, 3.16 and 3.17). The horizontal spread of this data may have been caused by deep valleys and scarps that formed during Post-Gondwana dissection of the Gondwana Planation surface as referred to by King, 1962. This is especially true for the Angola and Namibian region where little of the Gondwana surface is preserved (King, 1962). The best preserved areas of Gondwana surface survive between 3050 and 3350 m (King, 1962) and plot as a very small region of maximum elevation on the graph and therefore most of the points plot inland of the Great Escarpment. In general, the maximum elevation of individual clusters coincided with an increase in gravity, suggesting there maybe a relationship between summit height and positive long wavelength free-air gravity anomalies (Figure 3.16).

African Surface

Most of the data points from the African surface plot inland of the Great Escarpment. There is a strong positive correlation between the elevation and long wavelength free-air gravity in the Angolan region but the relationship between the elevation of the African surface and long wavelength free-air gravity was less clear in the Namibian and Karoo regions (Figure 3.18, 3.19 and 3.20). A high concentration of points upper limit of the surface elevation in both the Angolan and Namibian region with slopes of approximately 70 mgals km^{-1} and 40 mgals km^{-1} , respectively. All of the plots show horizontal trends within the data cloud, possibly due to the inclusion of steep near-vertical topography, such as scarps within the surface area.

Post-African Surface

Above the escarpment the Post-African surface in all three regions there is a positive correlation between the elevation and long wavelength free-air gravity (Figure 3.21, 3.22 and 3.23). The upper limit of the Post-African surface's elevation defines a slope of approximately 40 mgals km^{-1} in the Angolan region and 46 mgals km^{-1} within the Namibian region. In the Karoo region, concentrations of points near the lower limit of elevation define slopes of approximately 60 mgals km^{-1} . In much the same way as the African surface plots is affected by horizontal trends within the data. Below the escarpment there is a greater spread of data. In the Namibian region there is strong horizontal trends in a region of positive long wavelength free-air gravity. On the upper limit of the surface's between 0 and 0.75 km defines a slope of just over 10 mgals km^{-1} is visible, for elevations about this the trend becomes near horizontal. This is typical of a hypothesised Surface 2 (Figure 3.7) where an already sloping surface with a steeper scarp further inland is further gently tilted by inland uplift.

Aggradational Surfaces

The Post-African aggradational surface in Angola shows a very strong positive linear correlation both above and below the escarpment (Figure 3.24). The upper limit of the surface elevation defines slopes of approximately 40 and 45 mgals km⁻¹. The modern sediments above the escarpment in the Namibian region show a very strong positive linear correlation. On upper and lower limit of the surface elevation on the plot defines a slope of approximately 50 mgals km⁻¹ indicating a near horizontal aggradational surface tilted much like hypothesised Surface 5 (Figure 3.7). The modern sediment in the Namibian region below the escarpment shows similar horizontal trends as the Post-African surface it covers (Figure 3.27). Therefore the trend is probably representative of the basement and a thin covering of Aeolian sands. With the exception of the modern sediment in the Namibian region below the escarpment there are no horizontal trends in the data comparable to those seen in the data from denudational surfaces. This suggests the the horizontal trends are erosional features.

Trends within the surface plots

On a number of of elevation-gravity plots a high density of points limited to a small region of the graph. The number of data points per pixel were colour coded on the graph to accentuate trends and details in the data cloud that otherwise may have gone unnoticed. The plots reveal complex trends within most of data clouds (Figure 3.28). The upper elevation limit of the Post African surface between gravity values of 5 to 25 mgals reveals a strong linear trends on the plots.

Gondwana, Post-Gondwana

figure	Region	<i>Above Escarpment</i>	<i>Below Escarpment</i>
3.15	Angola	Two clusters of data with horizontal spread, points limited to the upper right hand quadrant, ranges from 1.5 km to 2.5 km and 18 mgals to 35mgals, no clear positive correlation	No points
3.16	Namibia	Multiple clusters of data with horizontal spread, weak linear positive correlation, ranges from 0.75 km to 2.5 km and 20 mgals to 35 mgals	No points
3.17	Karoo	Two large clusters of points with horizontal spread, weak linear positive correlation, both clusters have horizontal trends, ranges from 1.1 km to 3.2 km and 10 mgals to 35 mgals	limited number of points

African

figure	Region	<i>Above Escarpment</i>	<i>Below Escarpment</i>
3.18	Angola	Positive linear correlation, ranges from 1.3 km to 2.4 km and 15 mgals to 35 mgals, high concentration of points on the upper limit of the surface elevation defines a slope of approximately 70 mgals km^{-1} , upper limit of gravity shows a horizontal trend in points	Two clusters of data, show very weak positive correlation, ranges from 0.7 km to 1.7 km and 10 mgals to 30 mgals
3.19	Namibia	Weak positive linear correlation, ranges from 0.6 km to 2 km and 12 mgals to 34 mgals, high concentration of points on the upper limit of the surface elevation between 20 and 30 mgals defines a slope of approximately 40 mgals km^{-1} , between 17 to 22 mgals there is a large range of 1.2 km in elevation	strong horizontal trend in data, ranges from 0.5 km to 1.5 km and 17 mgals to 30 mgals
3.20	Karoo	No clear linear correlation, for data points at elevation 1.25 km show a large range of gravity values from 10 to 40 mgals, data ranges from 1 km to 2.8 km and 10 mgals to 47 mgals	horizontal trend in data, ranges from 1.1 km to 2.1 km and 22 mgals to 37 mgals

Table 3.2: Summary of results for Gondwana and African surfaces defined by King, 1962

<i>Post-African</i>			
figure	Region	<i>Above Escarpment</i>	<i>Below Escarpment</i>
3.21	Angola	Positive linear correlation, ranges from 0.8 km to 2.25 km and 0 mgals to 35 mgals, upper limit of the surface elevation between 0 and 15 mgals defines a slope of approximately 50 mgals km^{-1} , between 15 to 22 mgals and at upper limit of gravity there is strong horizontal trend in data	Weak positive linear correlation, ranges from 0.4 km to 1.8 km and -11mgals to 35 mgals, upper limit of the surface elevation between -11 and 11 mgals defines a slope of approximately 40 mgals km^{-1}
3.22	Namibia	Weak positive linear correlation, ranges from 0.6 km to 1.75 km and 5 mgals to 34 mgals, concentrations of points near upper limit of elevation between 5 and 2.2 mgals define slopes of of approximately 46 mgals km^{-1} , between 17 to 22 mgals strong horizontal trend in data	No positive linear correlation, ranges from 0.1km to 2.1 km and 12 mgals to 34 mgals, strong horizontal trends in data
3.23	Karoo	Positive linear correlation, ranges from 0.8 km to 2.25 km and 5 mgals to 45 mgals, concentrations of points near lower limit of elevation define slopes of of approximately 60 mgals km^{-1} , between 15 to 25 mgals strong horizontal trend in data	Weak positive linear correlation, ranges from 0.4 km to 2.25 km and 5 mgals to 45 mgals, horizontal trends in data

Post-African Aggradational

figure	Region	<i>Above Escarpment</i>	<i>Below Escarpment</i>
3.24	Angola	Strong positive linear correlation, ranges from 0.75 km to 1.5 km and -14 mgals to 19 mgals, upper limit of the surface elevation between -14 and 5 mgals and between 0 and 12 mgals defines a slope of approximately 40 mgals km^{-1}	Strong positive linear correlation, ranges from 1.25 km to 1.6 km and 0 mgals to 14 mgals, trend of data defines a slope of approximately 45 mgals km^{-1}

Modern Aggradational

figure	Region	<i>Above Escarpment</i>	<i>Below Escarpment</i>
3.27	Namibia	Strong positive linear correlation, ranges from 0.8 km to 1.5 km and 0 mgals to 31 mgals, upper and lower limit of the surface elevation defines a slope of approximately 50 mgals km^{-1}	No positive linear correlation, ranges from 0 km to 1.7 km and 11 mgals to 32 mgals, strong horizontal trends in data
??	Karoo	Two small clusters of data, ranges from 0.95 km to 1.4 km and 5 mgals to 20 mgals	No positive linear correlation, cluster of data points showing vertical trend, ranges from 0 km to 0.25 km and 2 mgals to 22 mgals

Table 3.3: Summary of results for Post African and Aggradational Surfaces defined by King, 1962

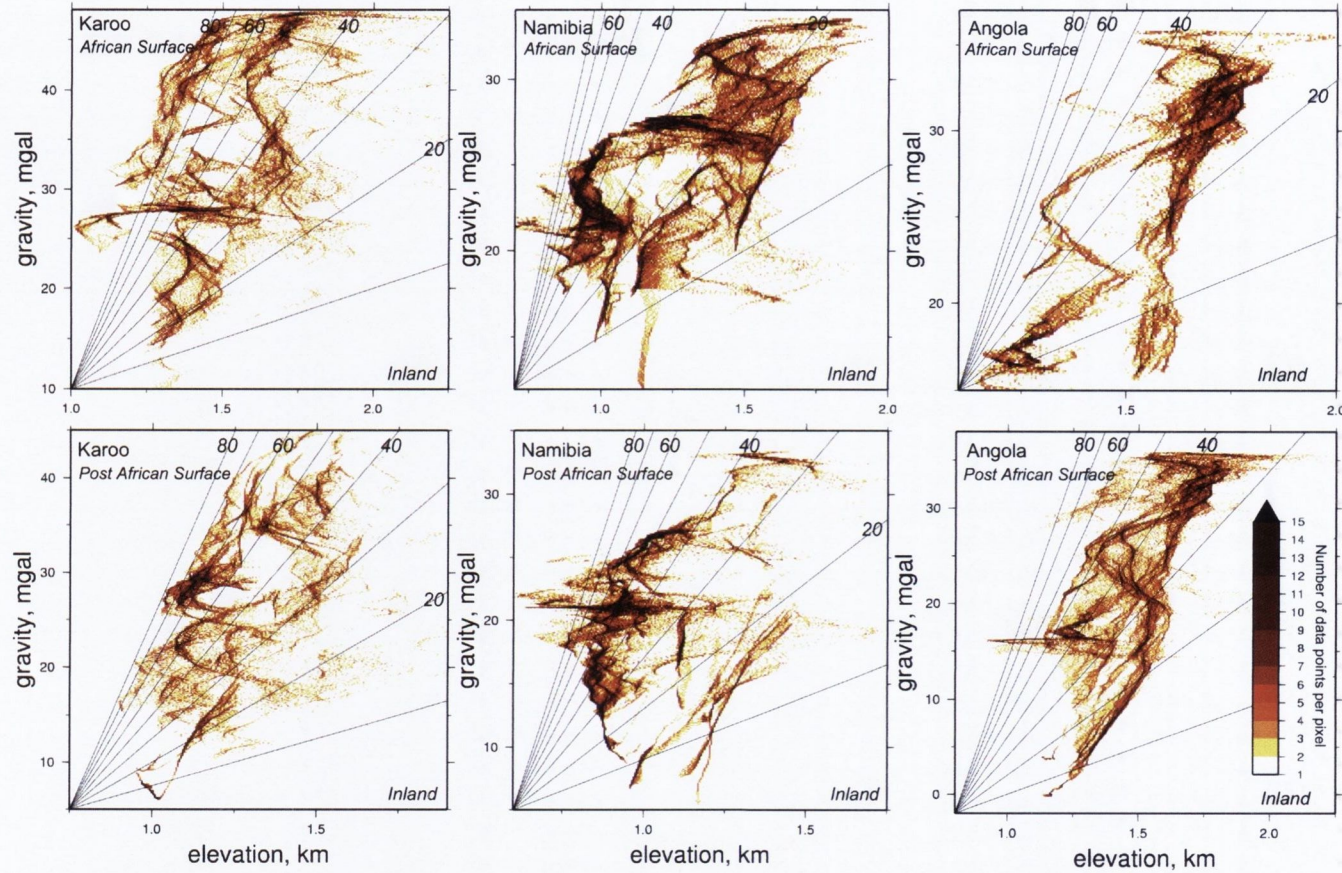


Fig. 3.28: Elevation-gravity plots of King's surfaces that displayed high density of points in one area of the graph. A colour chart illustrates how many data points are displayed in each pixel. The ranges of the plots vary as they are determined by the extent of the datasets. The graphs highlight internal trends within the dense data clouds.

3.5.2 Topographic-Gravity relationships for Partridge and Maud's surfaces

Above the African Surface

The regions that lie above the African surface occur both above and below the escarpment but only are present in areas affected by positive free air gravity anomalies (Figure 3.29 and 3.30). In the Namibia region the surface is characterised by horizontal trends within the data. There is a positive correlation between the topography of the surface and the long wavelength free-air gravity in the Karoo region.

African Surface

The African surface above the escarpment in both the Namibian and Karoo region show a positive linear correlation (Figure 3.31 and 3.32). In addition, the upper limit of the African surface's elevation in Namibia defines a slope of approximately 35 mgals km^{-1} . The overall characteristic of the African surface above the escarpment in both regions is a much steeper slope. Below the escarpment in the Namibian region the data has a strong horizontal trend.

Post-African i Surface

Similar to the African surface, the Post-African surface above the escarpment in both the Namibian and Karoo regions shows a positive linear correlation (Figure 3.33 and 3.34). In the Namibian region the upper limit the surface's elevation of defines a slope of approximately 60 mgals km^{-1} , while in the Karoo region both the upper and lower

limit of the surface elevation defines a slope of approximately 70 mgals km^{-1} .

Post African ii Surface

The Post African surface ii only occurs in the Karoo region below the escarpment at elevations lower than 750 m (Figure 3.35). It has a near vertical trend and the relationship between the topography of the surface and long wavelength free-air gravity is typical of what would be expected from a near horizontal erosional feature that formed after mantle upwelling deformed the region.

Aggradational Surfaces

The Kalahari aggradational surface in the Namibian region shows a very strong positive linear correlation (Figure 3.36). The upper and lower limit of the surface elevation defines a slope of between 40 and 50 mgals km^{-1} . The upper limit probably represents the interfluvial surfaces as seen in the low relief Congo surface (Figure 3.13). The relationship between the topography of the surface and long wavelength free-air gravity is typical of a hypothesised Surface 5 (Figure 3.7), where a near horizontal smooth aggradational surface has been warped by uplift due to mantle convection. The Namibian Aggradational surface (Namib Sand Sea) which is mainly composed of Aeolian sands shows similar horizontal trends as the Post-African surface it covers (Figure 3.36). The initial shape of the aggradational surface is therefore probably controlled by the basement it formed on.

Comparison of Surfaces

What is clear from these observations is that there are often similarities in the plots of different surfaces in the same region. A good example of this is the Above African, African, Post-African i and Namibian aggradational surfaces below the escarpment in the Namibian region that all show strong horizontal trends and all range from 0 km to 1.75 km and 12 mgals to 33 mgals. Elevation-gravity plots of the surface using colour coding of data points per pixel reveal trends within the data clouds (Figure 3.37).

3.6 Discussion

High resolution DEMs can be used to identify low relief plains and surfaces that are common on Africa's surface topography. Profiles across the topography of the low relief surfaces reveal that they often have a long wavelength topography. Previous research has tried to date the formation of the surfaces using a number of techniques but the antiquity of palaeosurfaces in Africa needs further temporal constraints from thermochronology and cosmogenic techniques.

3.6.1 Constraints on the antiquity of surfaces in Africa

Section 3.2.3 discusses the age and form of the different palaeosurfaces as outlined by King (1963) and Partridge and Maud (2000). The antiquity of the Gondwana landscape, the oldest surface as defined by King (1962), has been called into question by a number of researchers. Although there appears to be no direct AFTA and cosmogenic analysis of the Gondwana surface, given the average denudation rates in southern Africa

Above African

figure	Region	<i>Above Escarpment</i>	<i>Below Escarpment</i>
3.29	Namibia	several clusters of data, ranges from 0.7 km to 2 km and 16 mgals to 34 mgals	Strong horizontal trend in data, ranges from 0.25 km to 1.7 km and 15 mgals to 28 mgals
3.30	Karoo	Positive linear correlation, ranges from 1.3 km to 2.4 km and 15 mgals to 35 mgals	Horizontal trend in data, ranges from 0.1 km to 2.5 km and 1 mgals to 45 mgals, majority of points lie within the left lower quartile

African

figure	Region	<i>Above Escarpment</i>	<i>Below Escarpment</i>
3.31	Namibia	Positive linear correlation, ranges from 0.75 km to 2.2 km and 13 mgals to 35 mgals, upper limit of the surface elevation between -14 and 5 mgals defines a slope of approximately 35 mgals km ⁻¹ and at upper limit of gravity there is strong horizontal trend in data	Strong horizontal trend in data, ranges from 0.1 km to 1.6 km and 12 mgals to 26 mgals
3.32	Karoo	Strong positive linear correlation, ranges from 1.2 km to 2.1 km and 11 mgals to 32 mgals	Three clusters of data, weak linear positive correlation, ranges from 0.1 km to 1.8 km and 0 mgals to 38 mgals

Post African i

figure	Region	<i>Above Escarpment</i>	<i>Below Escarpment</i>
3.33	Namibia	Positive linear correlation, ranges from 0.75 km to 1.6 km and 17 mgals to 30 mgals, two clusters of data, the upper limit of the surface elevation of high concentration of points defines a slope of approximately 60 mgals km ⁻¹ , some horizontal trends can also be identified, the slope of the trend of the smaller cluster is approximately 65 mgals km ⁻¹	Strong horizontal trend in data, ranges from 0.1 km to 1.6 km and 12 mgals to 26 mgals
3.34	Karoo	Strong positive linear correlation, ranges from 0.8 km to 1.75 km and 8 mgals to 45 mgals, the upper and lower limit of the surface elevation of high concentration of points defines a slope of approximately 70 mgals km ⁻¹	No positive linear correlation, ranges from 0.2 km to 1.5 km and 5 mgals to 34 mgals

Table 3.4: Summary of results for Above African, African, Post African i

Post African ii

figure	Region	<i>Above Escarpment</i>	<i>Below Escarpment</i>
3.35	Karoo	No positive linear relationship, apparently vertical trend, ranges from 0.05 km to 0.75 km and 1 mgals to 25 mgals	No points

Kalahari Aggradational

figure	Region	<i>Above Escarpment</i>	<i>Below Escarpment</i>
3.36	Namibia	Strong positive linear correlation, ranges from 0.8 km to 1.6 km and 1 mgals to 37 mgals, the upper and lower limit of the surface elevation defines a slope of between 40 and 50 mgals km ⁻¹	No points

Namibia Aggradational

figure	Region	<i>Above Escarpment</i>	<i>Below Escarpment</i>
3.36	Namibia	No points	No positive linear correlation, ranges from 0 km to 1.75 km and 26 mgals to 33 mgals, strong horizontal trends in data

Table 3.5: Summary of results for Above African, African, Post African ii, Kalahari surface, Namibian surface.

measured by AFTA and cosmogenic analysis many researchers believe that the survival of a surface since the Jurassic is unlikely.

The formation of the African surface is considered a result of widespread planation event due to deep and intense weathering during humid conditions in Africa during the Early Cretaceous. By the middle Cretaceous, AFTA suggests that 1 to 3 km has been eroded from the African topography. Partridge (1998) suggested that the African planation surface, cut at two levels above and below the Great Escarpment respectively, was created during a period high denudation rate in the Cretaceous as measure by AFTA. By the early Miocene, most of southern Africa was dominated by the African planation surface which lay at elevations of 500 to 600 m above sea-level inland of the escarpment (Partridge and Maud 1987; 2000). However some researchers maintain that the topography of Africa was reduced to a minimum during the African cycle (King, 1962; Burke, 1996).

Both King (1963) and Partridge and Maud (2000) described the Post-African surface as an imperfectly planed surface. There are a very few locations that provide a direct comparison between cosmogenic isotope dating and the Post African Surface. For example, AFTA and cosmogenic isotope analysis suggests that the Namib pediment between 22° and 24° S, which roughly corresponds to the Post-African surface has experienced very low denudation and has changed little since the onset of the Benguela current during the mid-Miocene. Cosmogenic isotope analysis reveal denudation rates as little as 0.1 m Ma⁻¹. This evidence seems to give support age to a late Pliocene the Post-African surface for this region (Partridge and Maud, 1987) and Partridge (1998). The Post-African surface has been used to infer that there has been as much as 900 m of uplift in southern Africa during the Pliocene (Figure 3.4).

3.6.2 King's surface elevation-gravity plots

In general the elevation of the denudational surfaces as defined by King (1963) show a positive but weak relationship with long wavelength free-air gravity above the escarpment. The correlation shows some improvement after the surfaces was reinterpreted on DEMs and corrected for modern drainage. The oldest surface, the Gondwana surface, usually plots as clusters elongated along the elevation axis (Figure 3.15, 3.16 and 3.17) and the trend is similar to the hypothetical relationship between gravity and scarp topography (Surface 2) as described in Figure 3.7. Often the maximum elevation of the clusters describe a linear trend with gravity, suggesting there maybe a relationship between summit height and positive long wavelength free-air gravity anomalies. Below the escarpment no simple relationship between gravity and elevation of the surfaces was identified.

The elevation-gravity relationship of the Post African surface in Angola and Namibia displays strong trends defined by concentrations of data points within or at the edge of the data cloud (Figure 3.28). A similar observation can be made in the African surface elevation-gravity plots for Angola and Namibia. These trends yield an admittance of between 40 and 50 mgals km⁻¹, which is consistent with dynamically supported topography. Plotting the location of the data points contained within these trends reveals that the strongest gravity-elevation relationships originate from the flanks of the Bie plateau and Namibian highlands (Figures 3.38 and 3.39). Plots of the surfaces located in the Karoo region show a weak correlation between elevation and gravity.

3.6.3 Partridge and Maud's surface elevation-gravity plots

A weak positive relationship was seen between the elevations of the denudational surfaces defined by Partridge and Maud (2000) and long wavelength free-air gravity above the escarpment. The spread of data points was too great to fit linear regressive line but upper and lower elevation limits of some of the data clouds showed a trend. The admittance value suggested from the upper elevation limit of the African surface in Namibia is approximately 35 mgals km^{-1} , which is consistent with admittance estimates for air-loaded continental plates.

3.6.4 Depositional surface elevation-gravity plots

The extent of the Kalahari surface as defined by Partridge and Maud (2000) roughly correlates with the modern depositional surface in Namibia as defined by King (1963).

Depositional surfaces near the edge of the Kalahari (where it rims the Namibia positive gravity anomaly) display an admittance of close to 40 mgals km^{-1} on the elevation-gravity plots indicating that they are dynamically supported (Figure 3.39). The thickness of the Kalahari sediments along the eastern flanks of the Namibian highlands is estimated as less than 100 m (Haddon and McCarthy, 2005). The admittance estimates in the centre of the Kalahari region, below elevations of 1.25 km, are greater than the admittance at the edges. This difference could be explained by more recent infill of sediments, effectively flattening the dynamic topography. The edges of the Kalahari surface may be comparable to the hypothetical preserved depositional surfaces (Surface 5) as described in Figure 3.7. Supporting evidence for rapid sediment infill of this is the Okavango delta, where there is little topographic expression of the vertical motions that have occurred along the fault system, indicating the depositional rate is faster

than the rate of subsidence in the region. Kalahari sediments, over 300m thick have infilled the Etosha depression over the last 65 Ma effectively levelling of the depression (Hipondoka, 2005).

3.7 Conclusions

- Having reviewed the evidence that Africa's topography is defined by widespread contemporaneous surfaces which can be correlated over the entire continent, it is concluded the evidence is very weak and inconsistent with more recent techniques for quantifying evolution. However evidence does suggest the survival of Cenozoic paleo-surfaces to a limited extent.
- Admittance values of ~ 35 to 50 mgals km^{-1} estimated from elevation-gravity plots and indicate sections of the African surface and Post African surface on the flanks of the Bie plateau and Namibian highlands are dynamically supported.
- A strong linear correlation exists in the flanks of the Namibian highlands between the elevation of the Kalahari depositional surface and long wavelength free-air gravity and yields a admittance of 40 mgals km^{-1} consistent with dynamically supported topography.
- The majority of the gravity-elevation plots did not show significant linear correlation, which is inconsistent with the theory that widespread paleo-surfaces (as defined King and Partridge and Maud) can be used to estimate uplift rates caused by mantle convection. This was particularly evident in the plots of surfaces of

the Karoo region. In some cases, the lack of significant gravity topography correlation could be attributed to deposition or erosion occurring after deformation (e.g. the surface of the central Kalahari Basin).

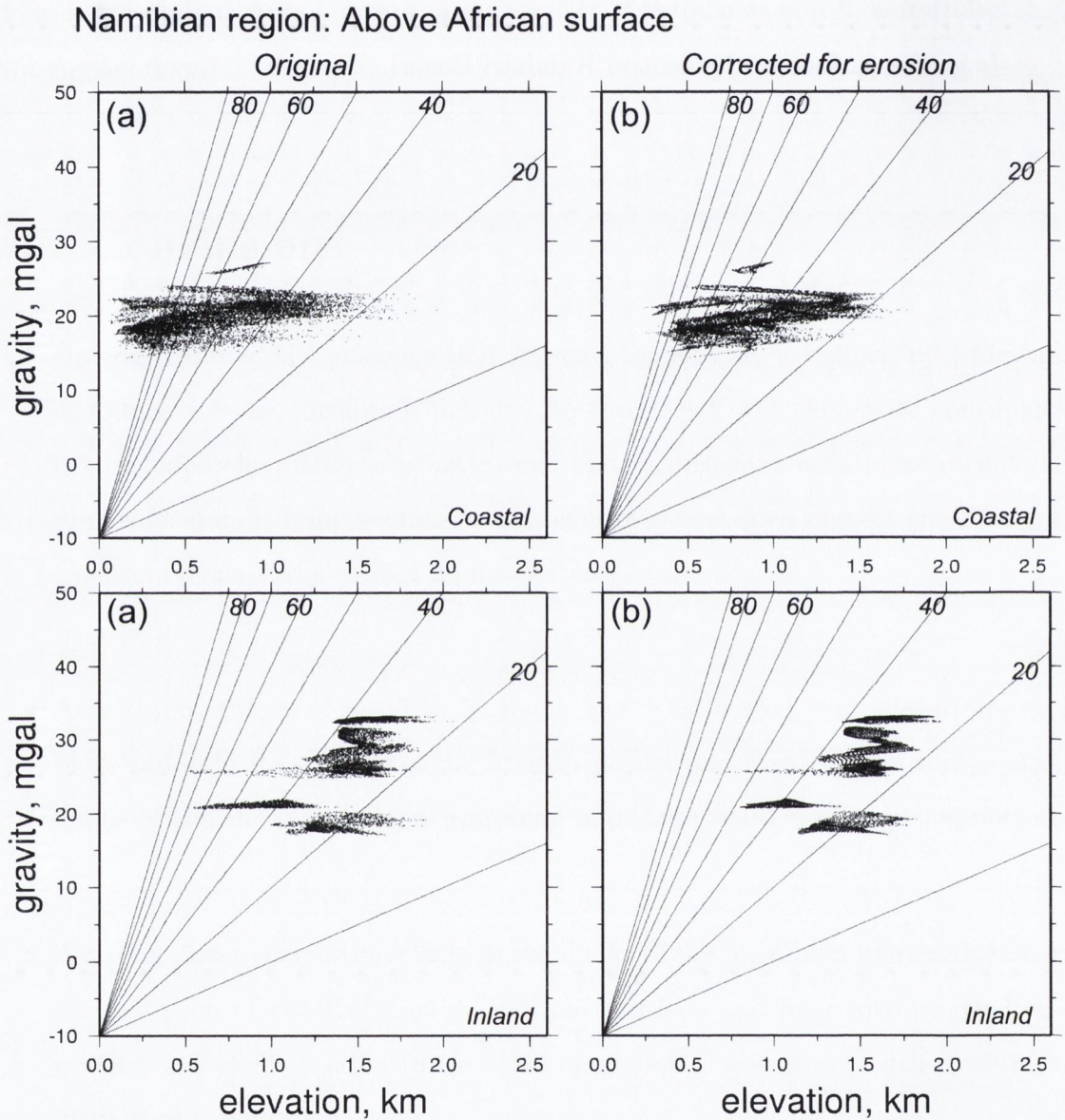


Fig. 3.29: a. The topography of regions above the African surface digitised from the map of Partridge and Maud, 2000 b. The enveloped topography of regions above the African surface plotted against long wavelength free-air gravity in the Namibian region. Regions inland of the escarpment are plotted on the bottom, regions on the coastal side of the escarpment are plotted on the top row. Lines on the graph represent admittance slopes in intervals of 10 mgals km^{-1} .

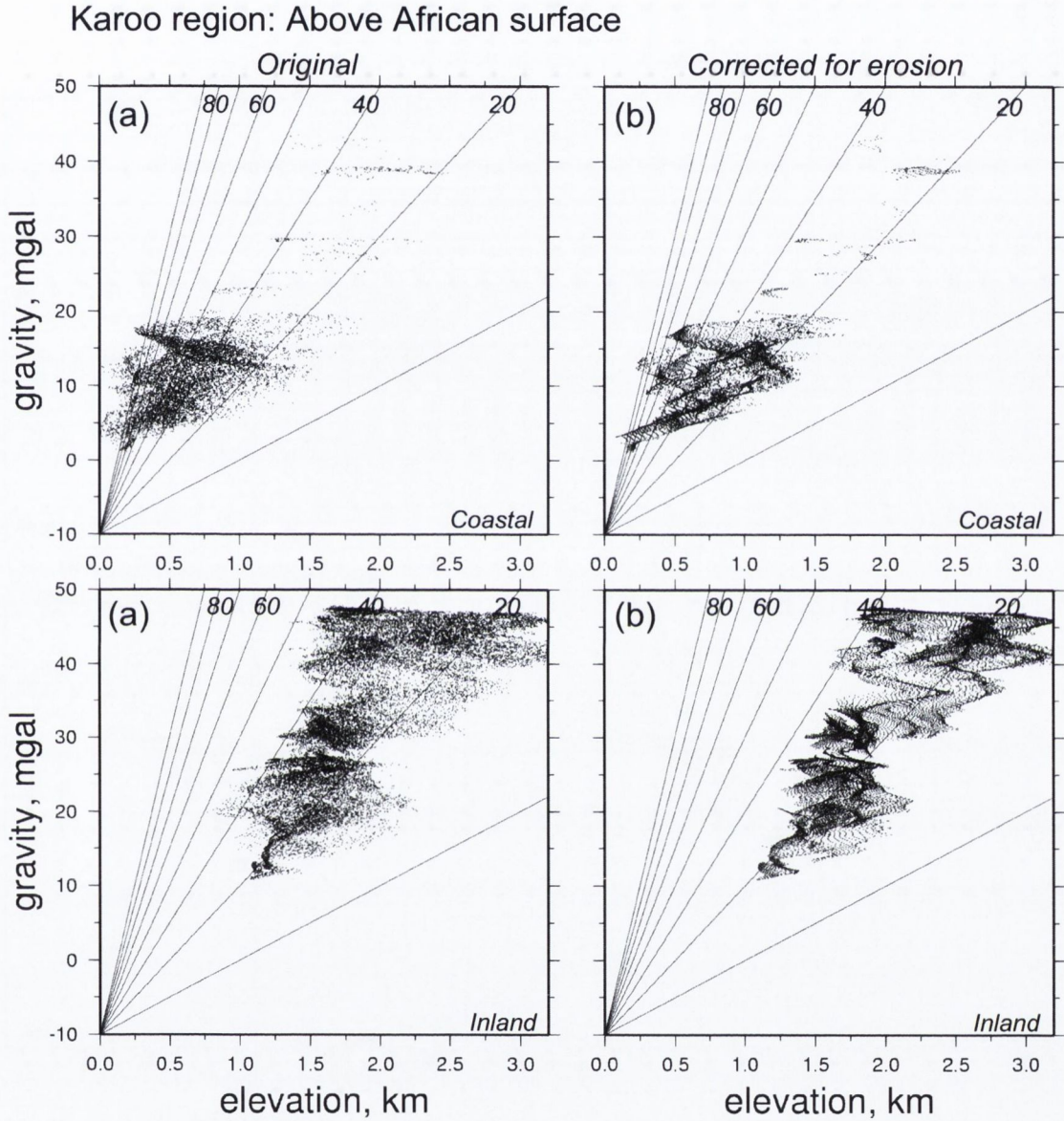


Fig. 3.30: a. The topography of regions above the African surface digitised from the map of Partridge and Maud, 2000 b. The enveloped topography of regions above the African surface plotted against long wavelength free-air gravity in the Karoo region. Regions inland of the escarpment are plotted on the bottom, regions on the coastal side of the escarpment are plotted on the top row. Lines on the graph represent admittance slopes in intervals of 10 mgals km^{-1} .

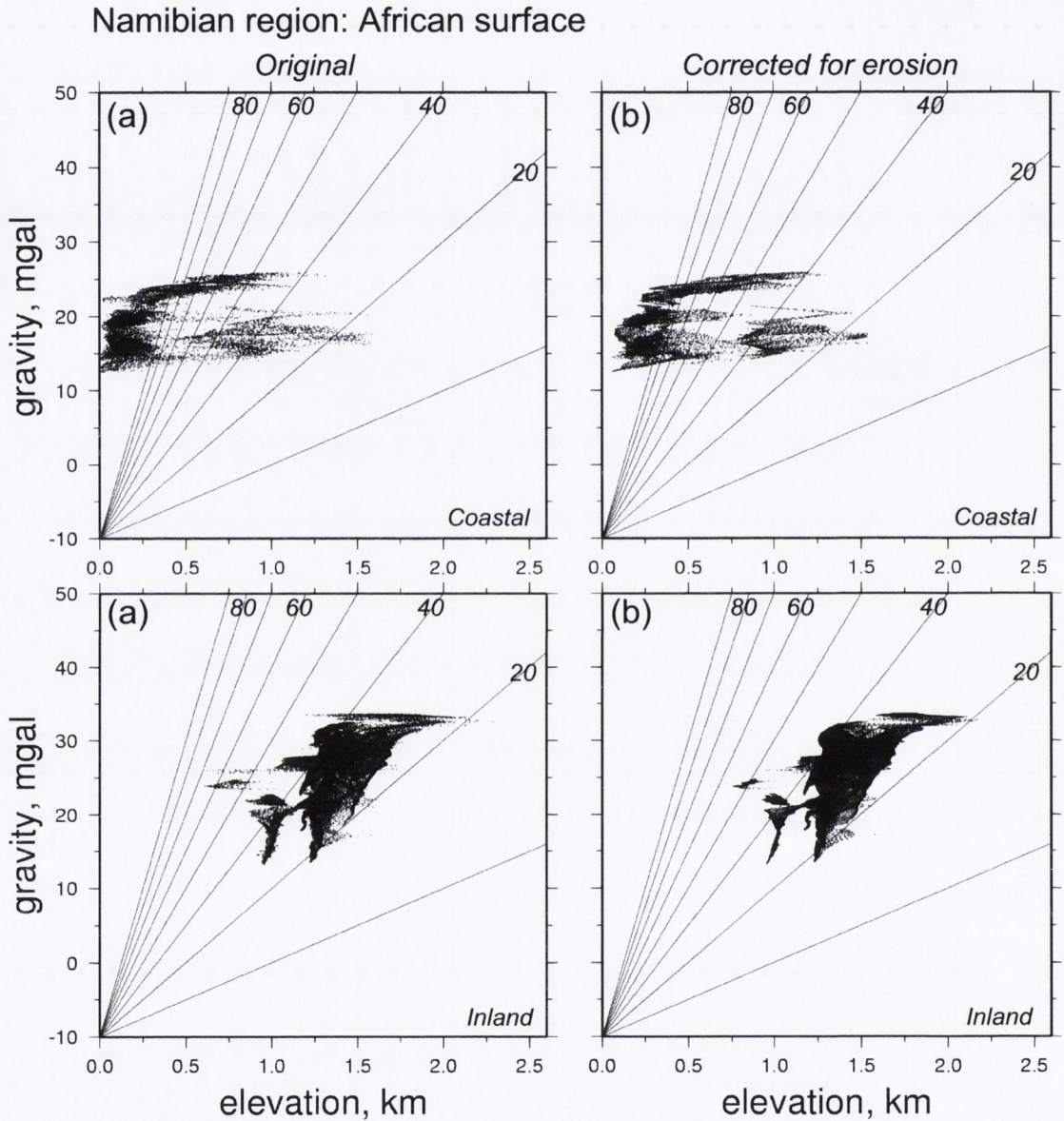


Fig. 3.31: a. The topography of the African surface digitised from the map of Partridge and Maud, 2000 b. The enveloped topography of the African surface plotted against long wavelength free-air gravity in the Namibian region. Regions inland of the escarpment are plotted on the bottom, regions on the coastal side of the escarpment are plotted on the top row. Lines on the graph represent admittance slopes in intervals of 10 mgals km^{-1} .

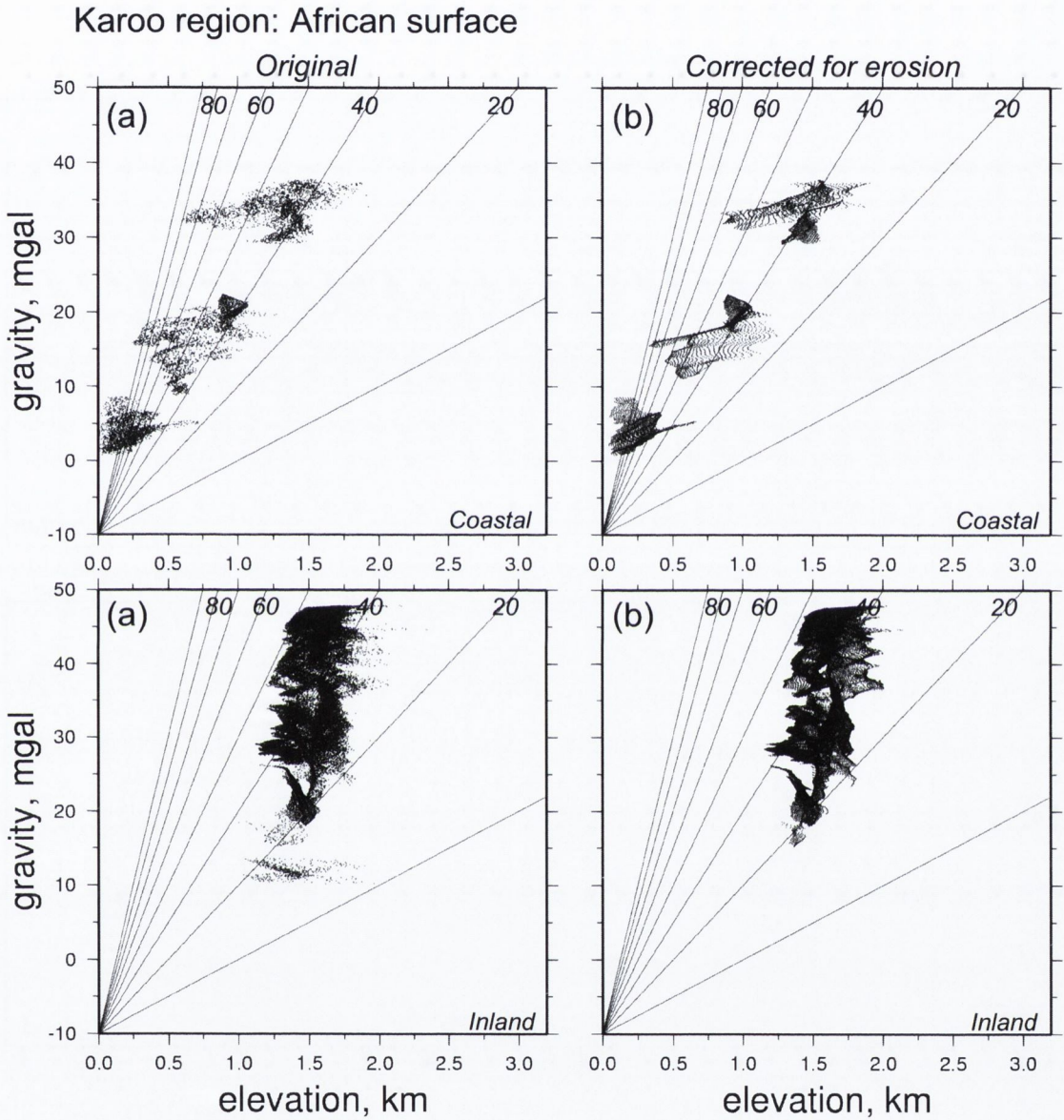


Fig. 3.32: a. The topography of the African surface digitised from the map of Partridge and Maud, 2000 b. The enveloped topography of the African surface plotted against long wavelength free-air gravity in the Karoo region. Regions inland of the escarpment are plotted on the bottom, regions on the coastal side of the escarpment are plotted on the top row. Lines on the graph represent admittance slopes in intervals of 10 mgals km^{-1} .

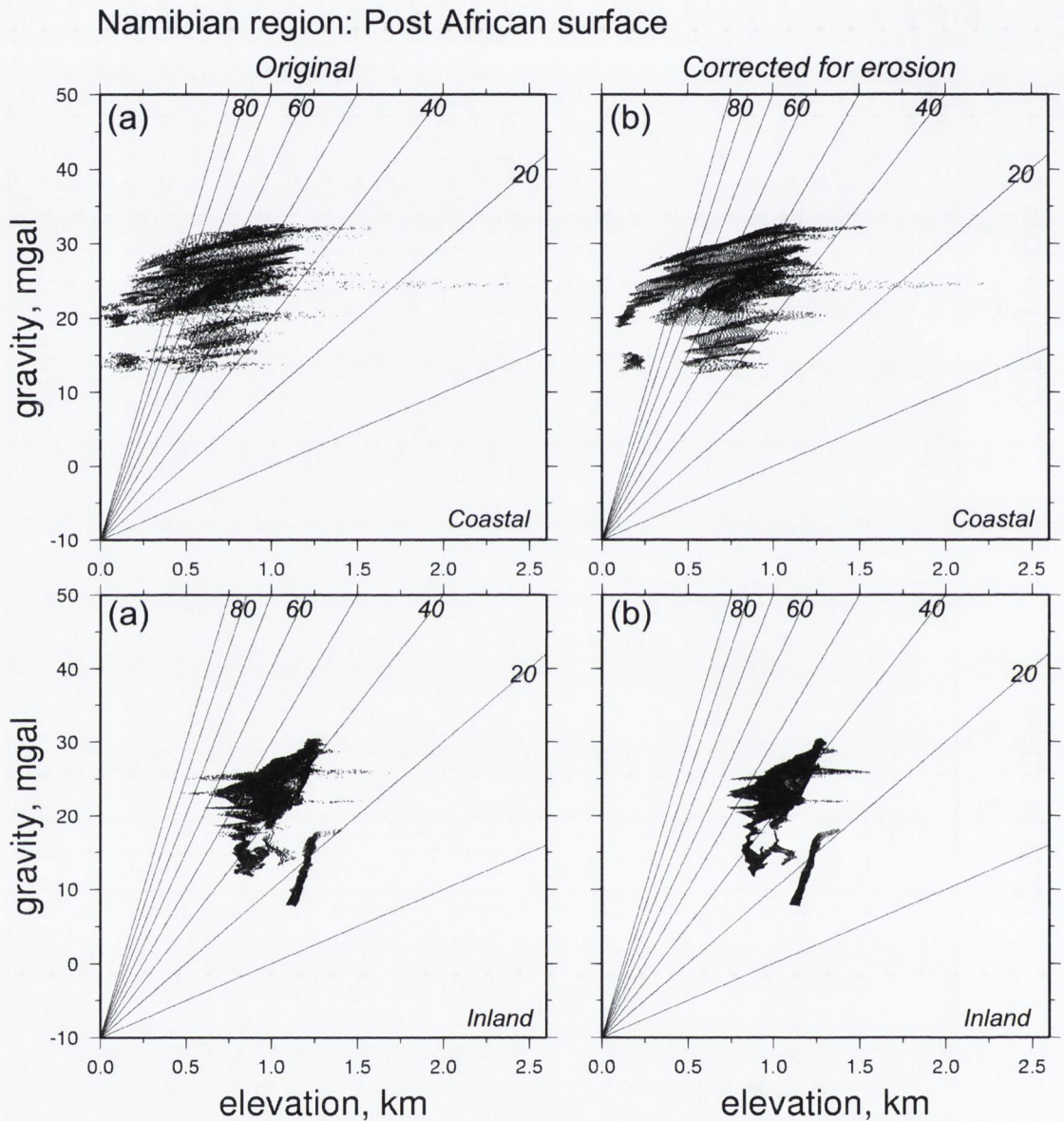


Fig. 3.33: a. The topography of the Post African surface digitised from the map of Partridge and Maud, 2000 b. The enveloped topography of the Post African surface plotted against long wavelength free-air gravity in the Namibian region. Regions inland of the escarpment are plotted on the bottom, regions on the coastal side of the escarpment are plotted on the top row. Lines on the graph represent admittance slopes in intervals of 10 mgals km^{-1} .

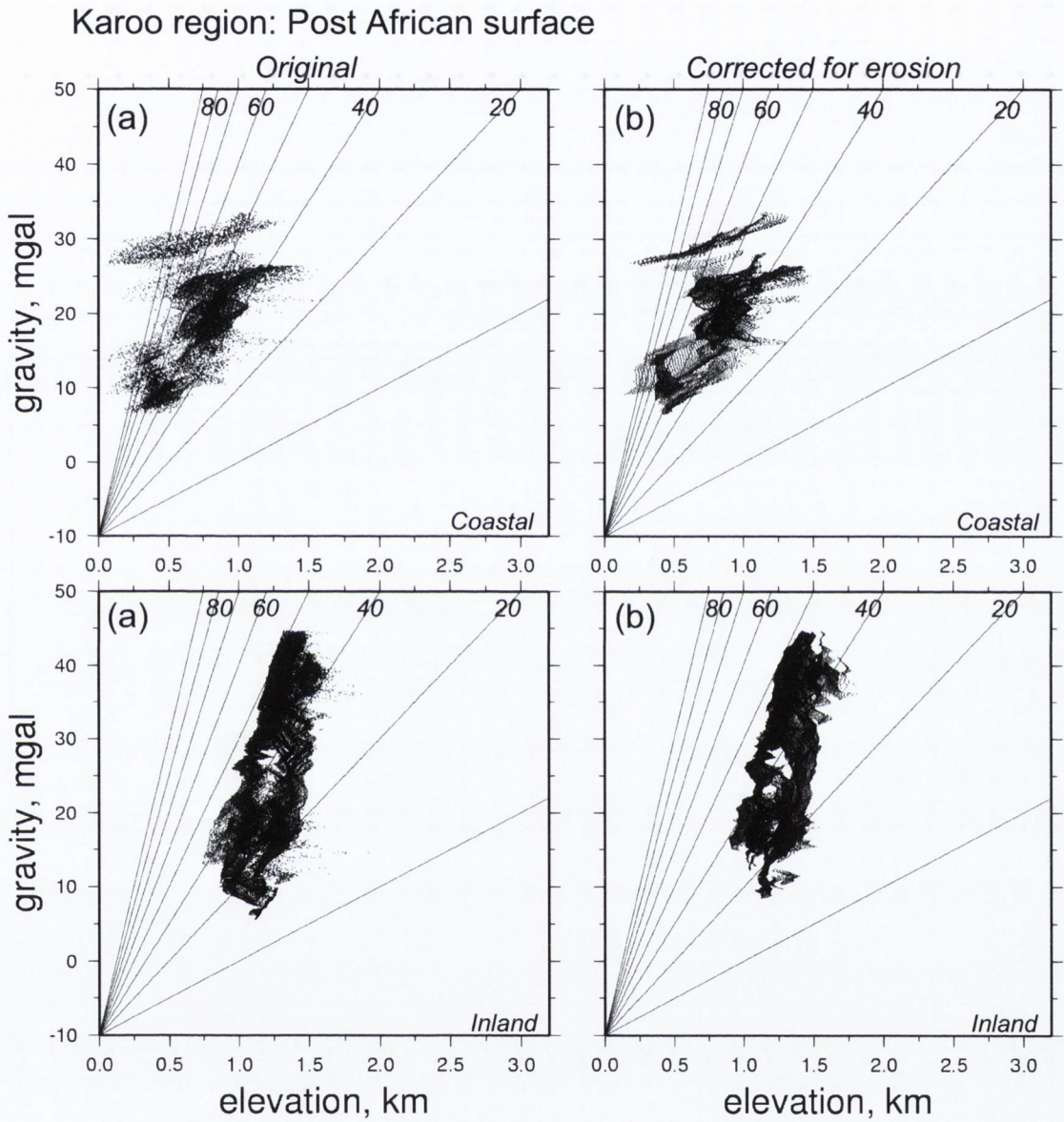


Fig. 3.34: a. The topography of the Post African surface digitised from the map of Partridge and Maud, 2000 b. The enveloped topography of the Post African surface plotted against long wavelength free-air gravity in the Karoo region. Regions inland of the escarpment are plotted on the bottom, regions on the coastal side of the escarpment are plotted on the top row. Lines on the graph represent admittance slopes in intervals of 10 mgals km^{-1} .

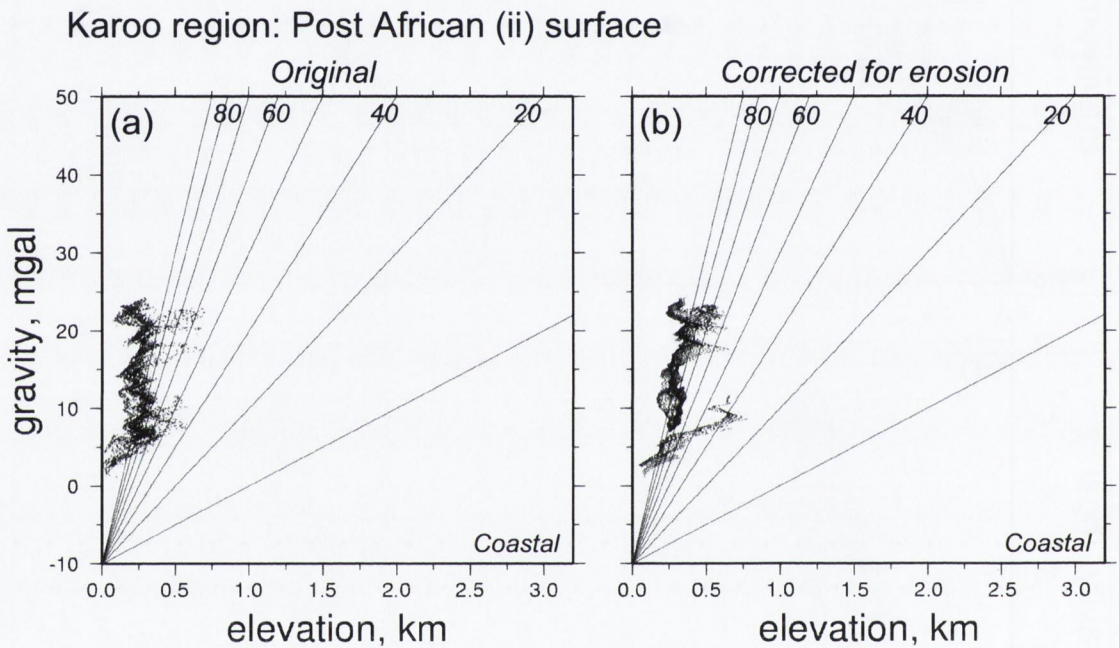


Fig. 3.35: a. The topography of the Post African ii surface digitised from the map of Partridge and Maud, 2000 b. The enveloped topography of the Post African surface plotted against long wavelength free-air gravity in the Namibian region. Regions inland of the escarpment are plotted on the bottom, regions on the coastal side of the escarpment are plotted on the top row. Lines on the graph represent admittance slopes in intervals of 10 mgals km^{-1} .

Namibian region: Aggradational surfaces of the Kalahari desert (bottom) and Namibian desert (top)

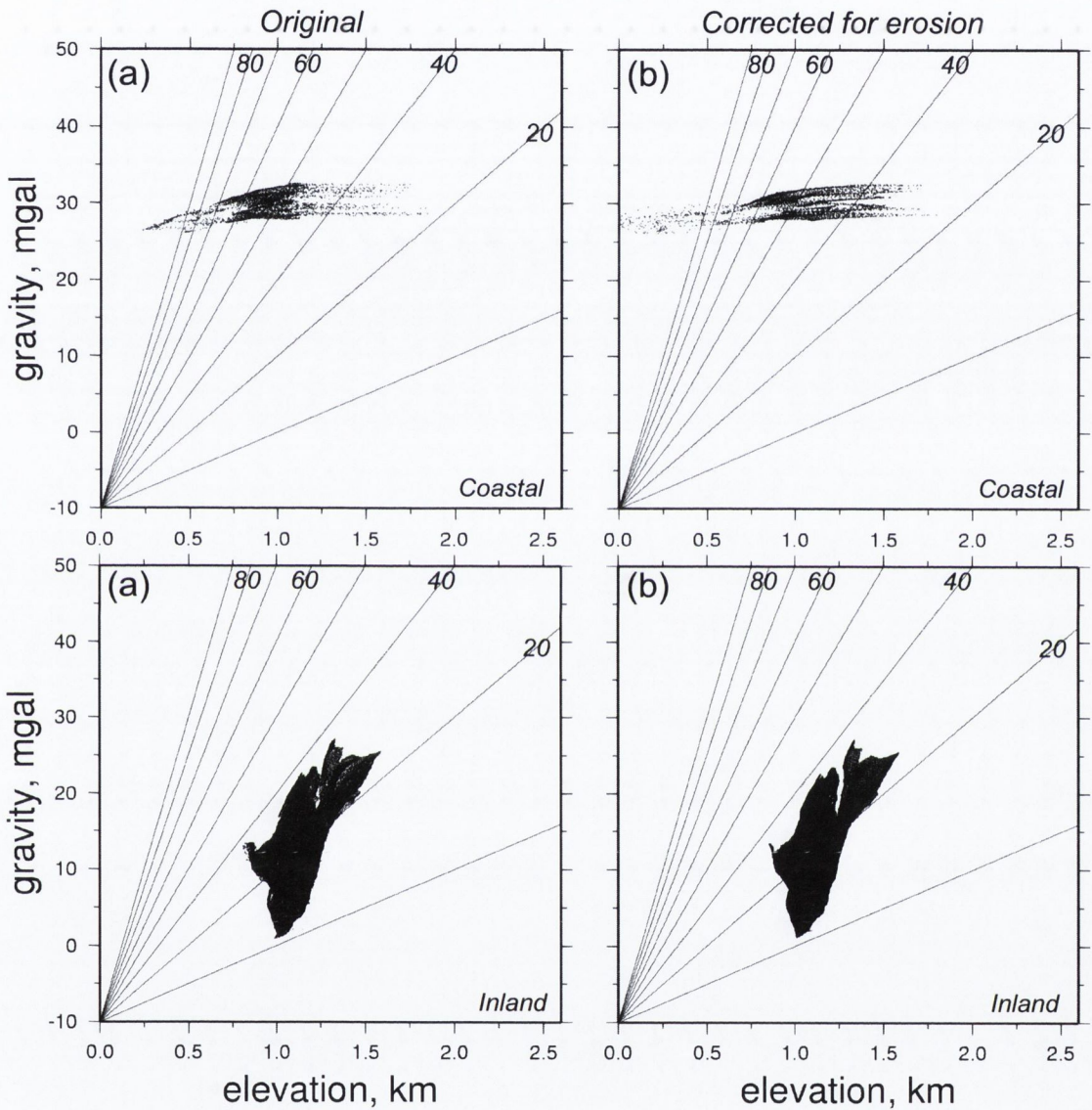


Fig. 3.36: a. The topography of the Kalahari desert aggradational surface (top) and the Namibian desert aggradational surface (bottom) digitised from the map of Partridge and Maud, 2000 b. The enveloped topography of the aggradational surface plotted against long wavelength free-air gravity in the Namibian region. Regions inland of the escarpment are plotted on the bottom, regions on the coastal side of the escarpment are plotted on the top row. Lines on the graph represent admittance slopes in intervals of 10 mgals km⁻¹.

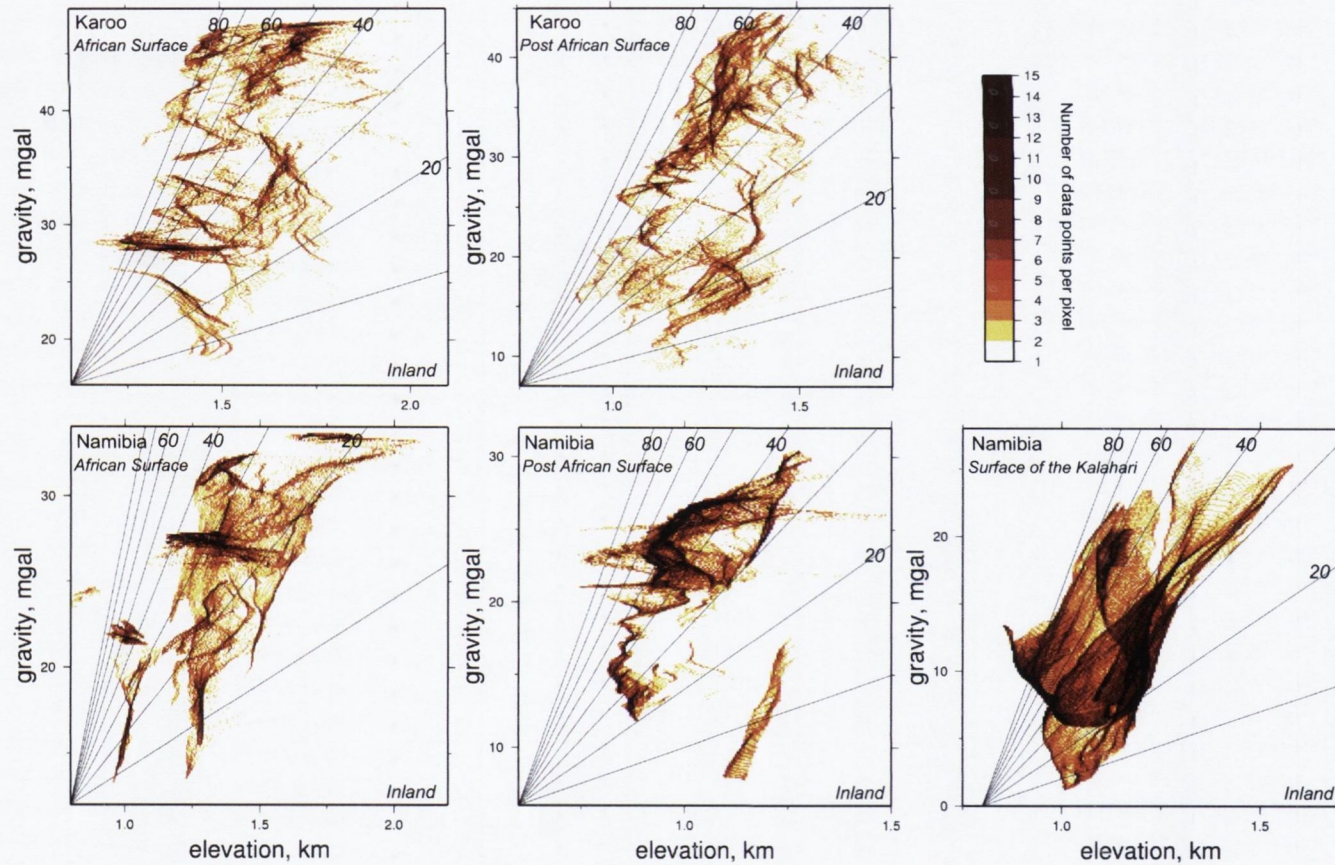


Fig. 3.37: Topography-gravity plots of Partridge and Maud's surfaces that displayed high density of points in one area of the graph. A colour chart illustrates how many data points are displayed in each pixel. The ranges of the plots vary as they are set by the extent of the data points. The graphs highlighting internal trends within dense data clouds.

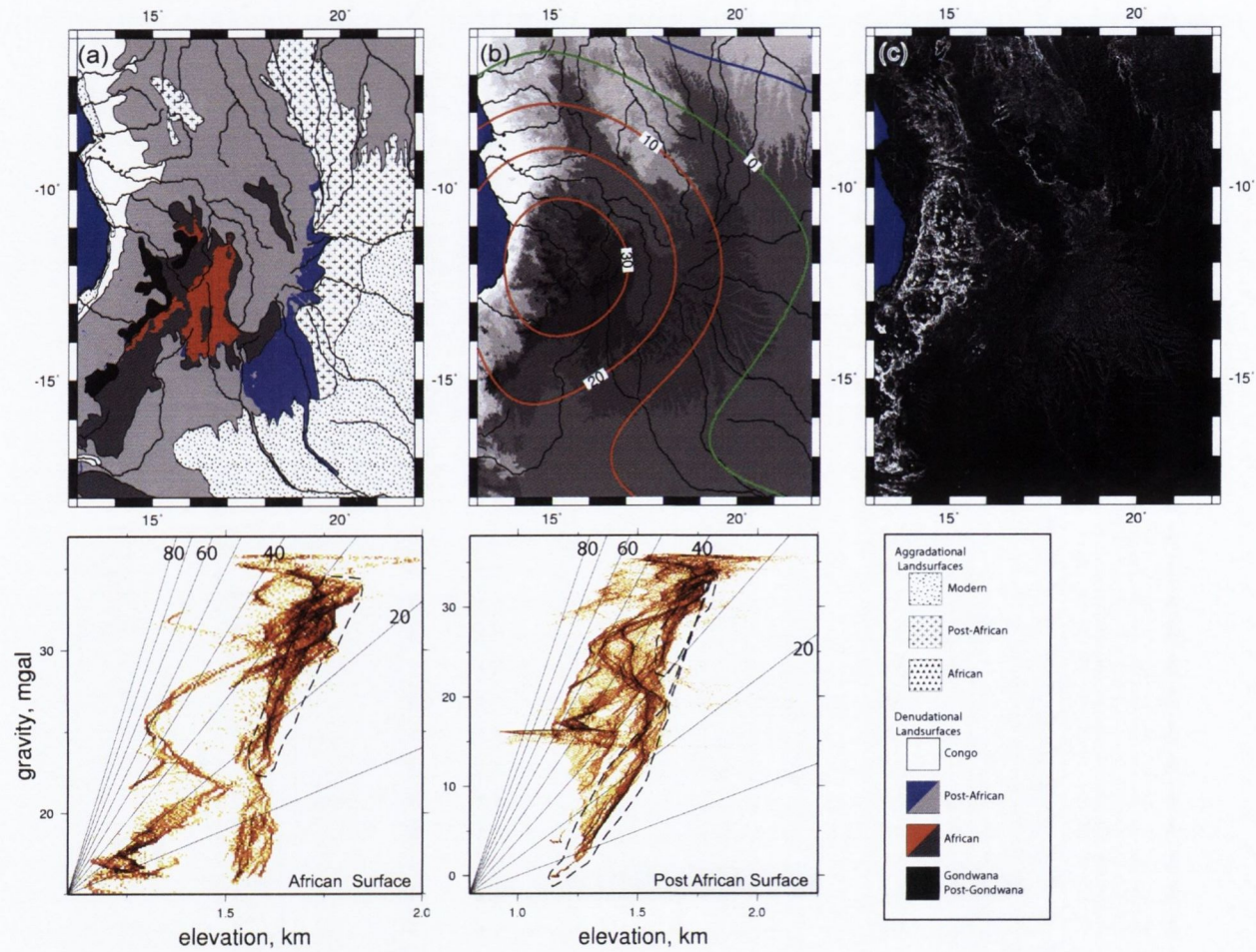


Fig. 3.38: Map of the Angolan region highlighting the location of the data trends in the elevation-gravity plots. The dashed line marks data points selected from the graph. The position of highlighted African surface points are plotted in the map in red. The position of highlighted Post African surface points are plotted in the map in blue.

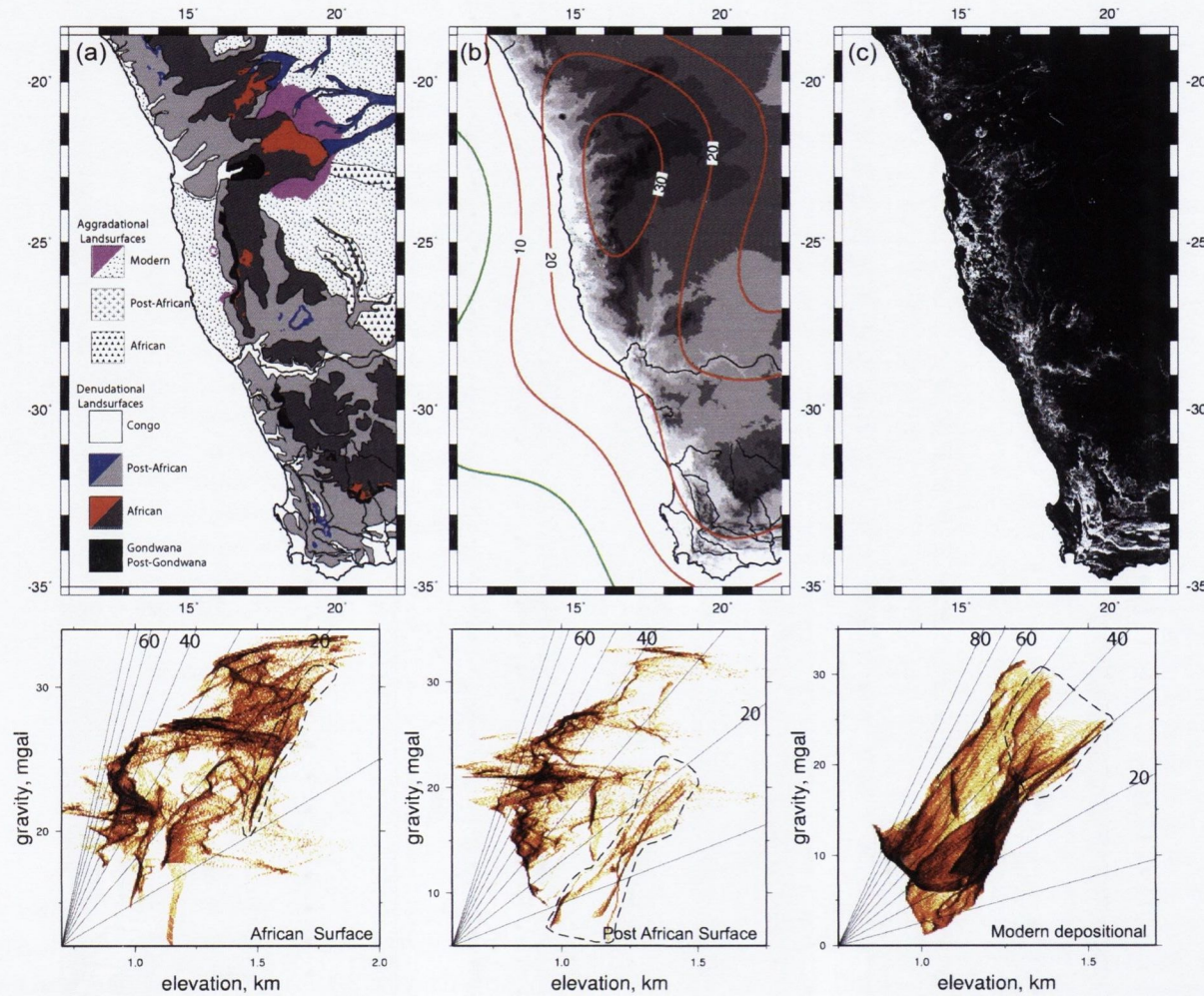


Fig. 3.39: Map of the Namibian region highlighting the location of the data trends in the elevation-gravity plots. The dashed line marks data points selected from the graph. The position of highlighted African surface points are plotted in the map in red. The position of highlighted Post African surface points are plotted in the map in blue. The position of highlighted Modern depositional surface points are plotted in the map in pink.

Chapter 4

Is Africa unique?

4.1 Introduction

Burke (1996) claimed that on 'On Earth, the swell structure of the African Plate is unique' as a result of the African plate being stationary with respect to the hot-spot reference frame. Dynamic topography is thought to be widespread across the Earth's surface but is often masked by tectonic activity, erosional and depositional processes and ice cover.

A basin and swell topography partially supported by mantle convection is pronounced on the African plate. This chapter investigates similar large scale physiographic features other continents that might be linked to mantle convection. Africa has been compared with Venus where mantle upwellings are widespread (Herrick, 1999). In southern Africa, positive long wavelength free-air gravity are associated with regions of high elevation that border the continental margin and suggest that the great escarpment is partly dynamically supported. Marginal swells are a common feature of

many passive continental margins (Ollier and Pain, 2000). Mantle convection near continental margins may be explained by edge-driven convection, which develops in the upper mantle beneath the transition of thick cratonic lithosphere and thin oceanic lithosphere (King and Anderson, 1998; King and Ritesma, 2000).

In addition, the hypsometry of Africa has also been identified as being distinctly different when compared with other continents, possibly as a result of recent uplift (Bond, 1978; Burke, 1996). Mantle convection is predicted to cause uplift in the region of hundreds of meters (Lithgow-Bertelloni and Silver, 1998; Gurnis et al., 2000). The presence of positive dynamic topography on a continent is likely to increase area of continent lying at moderate to high elevations and therefore may be identified in its hypsometry.

This chapter is divided into the following sections:

- This section investigates the association of positive long wavelength free-air gravity anomalies with passive continental margins around the world. The geomorphology and evidence of recent uplift of eight passive margins associated with long wavelength free-air gravity anomalies (southern Africa, West Africa, the east margin of South America, the east margin of Madagascar, the east margin of Australia, Greenland and Norway) are explored. The geological structure of these continental margin is also assessed to see if there is any connection between dynamic topography produced by edge-driven convection and thick cratonic roots as suggested for southern Africa by King and Ritesma (2000).
- The hypsometry of Africa is also thought to be distinctly different when compared with other continents such as South America and this has been used to suggest that Africa has been recently uplifted. This chapter explores reasons for the

hypsometry of Africa and compares it to other continents in the world. It also examines the possible connection between the hypsometry of a region and the last time the crust of that region underwent major tectonic deformation.

4.2 High-elevation passive margins

High-elevation passive margins and their associated major escarpments are a prominent feature of many continents (Figure 4.1). The existence of high topography along passive margins raises two questions. Firstly, why do some passive margin has unusual high elevation considering they have not undergone compressive tectonics in hundreds of millions of years and how has that high topography survived over tens of millions of years of erosion? Secondly, initial uplift of rift margins or shoulders preceding uplift is widely understood to be a result of extensional and rifting tectonics (Buck, 1986). However it is unclear why the high topography of rift shoulders should persist long after the spreading centre has moved away from the margin and the thermal effects associated with rifting have ceased. When the rifting has concluded the region should isostatically correct itself and the region should return to its pre-breakup elevation.

A number of mechanisms have been put forward to explain post-breakup uplift of passive continental margins. Some models for asymmetrically elevated rift margins propose that underplating has occurred, thickening the crust under one side of the rift margin and therefore isostatically supporting the high surface topography (e.g. Matmon et al., 2002). However recent seismological data does not always show evidence of such widespread and massive magmatic underplating under the high regions of the Africa's passive margins (van der Beek et al., 2002). Other workers suggest that the high topography inland of passive margin continents is presently supported by active

upward flow within the mantle. For example, the high topography of the southern African plateau has been attributed to the establishment of the African superswell (Burke, 1996; Partridge, 1998; Brown et al., 2005). Uplift near passive continental margins has been attributed to flexure, caused by sediment loading or unloading due to local denudation. Large off-shore sediment loads may generate onshore flexural uplift. Neogene uplift U.S. Atlantic margin of between 35 and 130m has been attributed to flexure due to pulse of offshore deposition (Pazzaglia and Gardner, 1994). Lucazeau et al., (2003) hypothesised that the migration of depocentres from the Ogooe and Kwanza Rivers to the Congo fan in the Oligocene may have caused a flexural bulge along the coast, created by sediment loading on the continental shelf. Large offshore sediment loads such as deltas may account for flexural uplift on margins in the order of tens to hundreds of metres (Bishop, 2007). Similarly, flexural effects of unloading the crust due to denudation usually along the coastal plains are thought to cause upwarp of adjacent regions (e.g. Gilchrist and Summerfield, 1990; van der Beek et al., 2002).

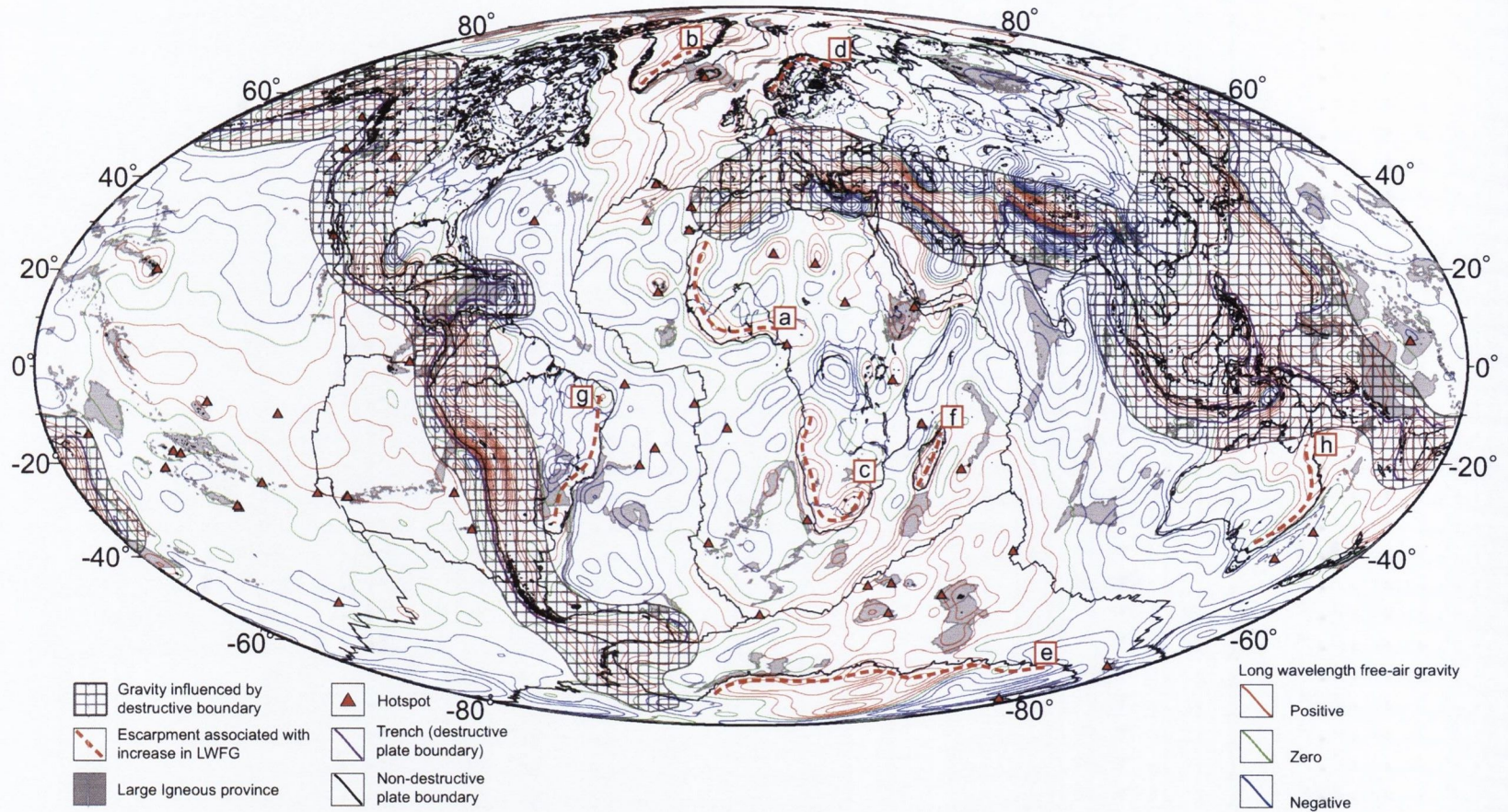


Fig. 4.1: Map of the world, showing escarpments along parallel to passive margins that are associated with long wavelength free-air gravity anomalies. Hotspot, plate-boundary and LIP locations from Coffin et al. (1998).

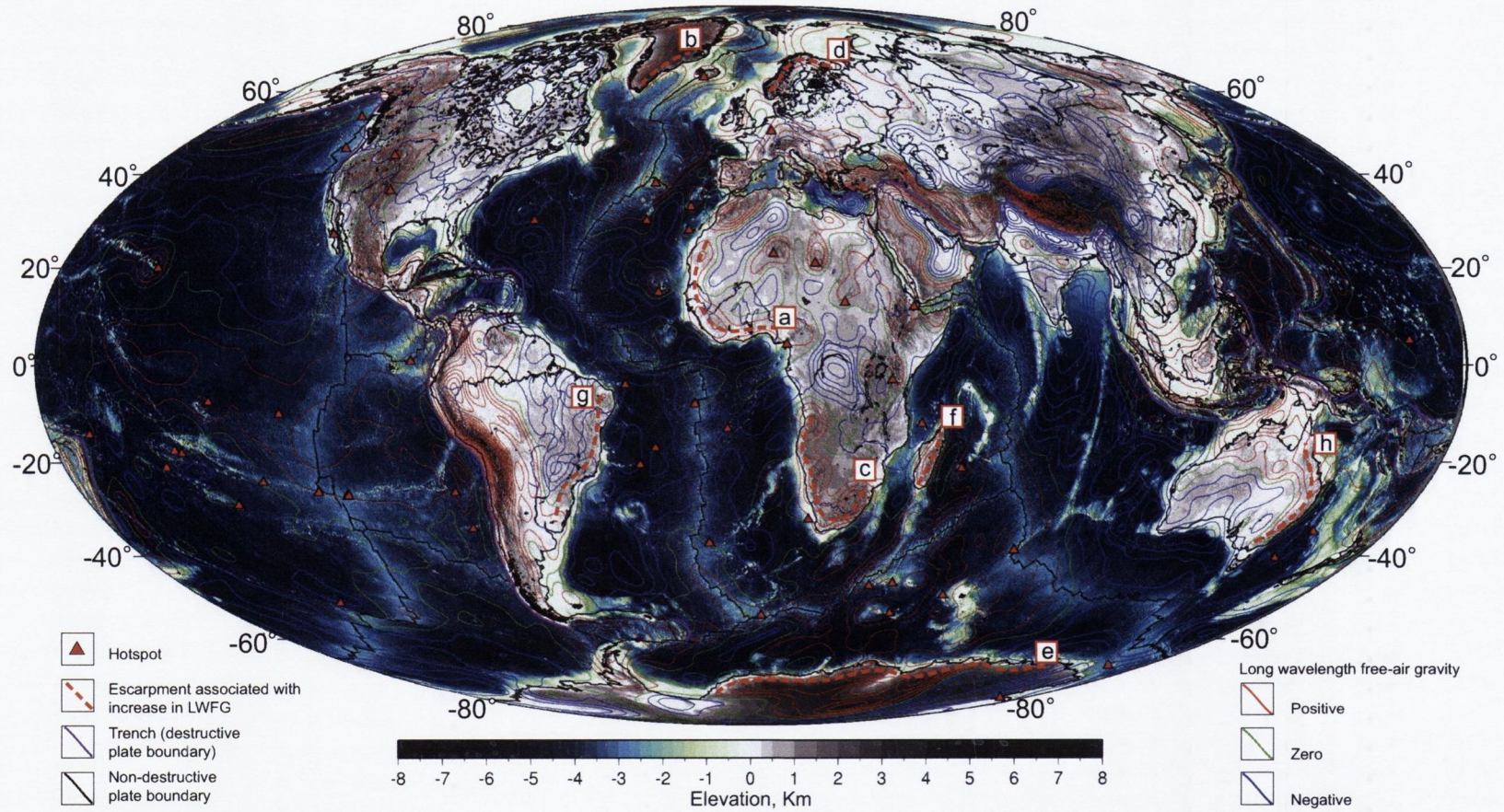


Fig. 4.2: Shaded relief map of the world, showing escarpments along parallel to passive margins that are associated with long wavelength free-air gravity anomalies. Hotspot, plate-boundary and LIP locations from Coffin et al. (1998).

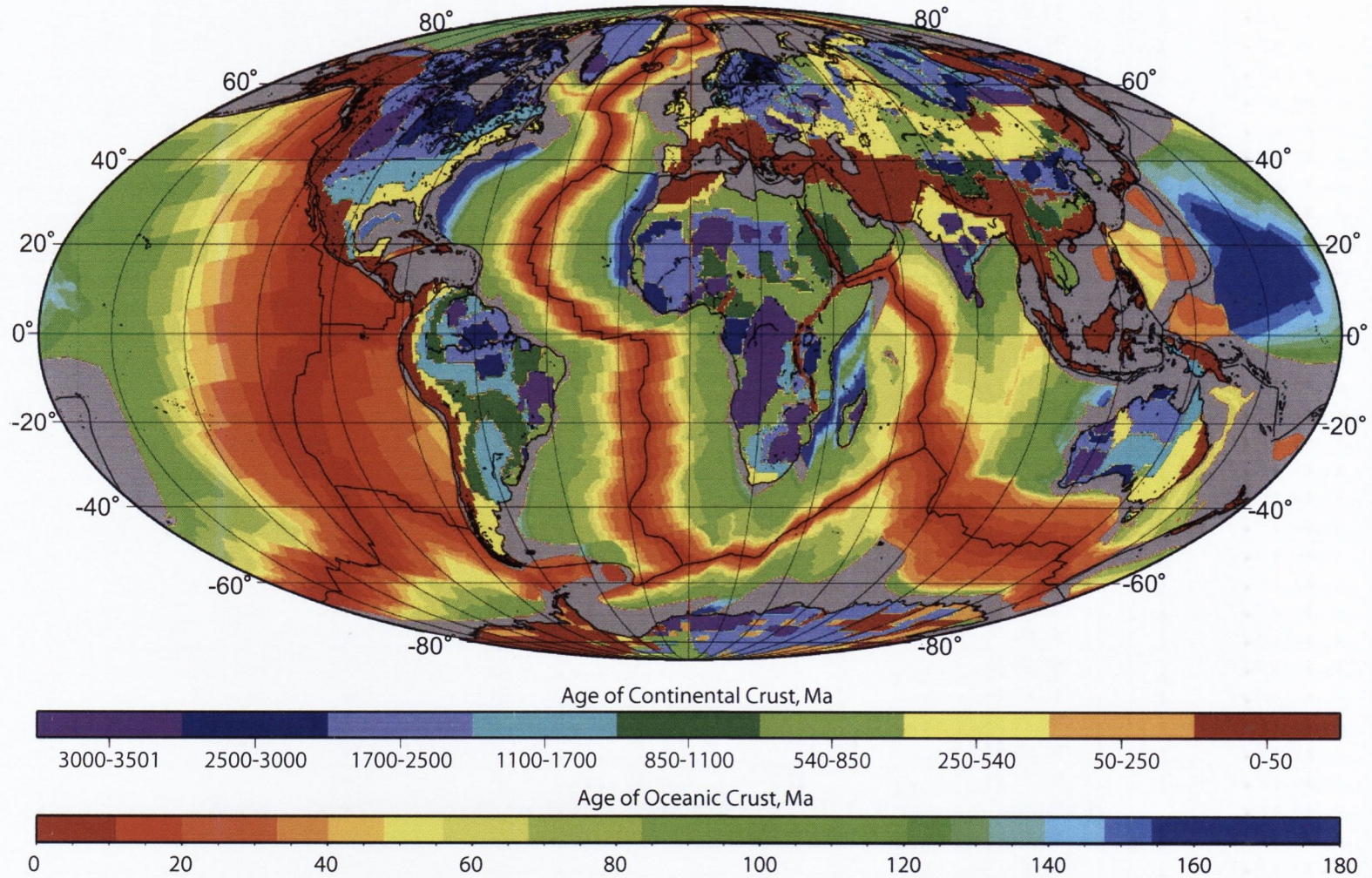


Fig. 4.3: Grid of geological ages of the continental and oceanic crust. Continental data shows the ages of the major orogenic events (Table 4.1), rather than ages of juvenile crust digitised from a $1^\circ \times 1^\circ$ map (after Artemieva, 2006). Oceanic floor ages added using digital age grid of the ocean floor with a grid node interval of 6 arc-minutes (Mueller et al., 1997)

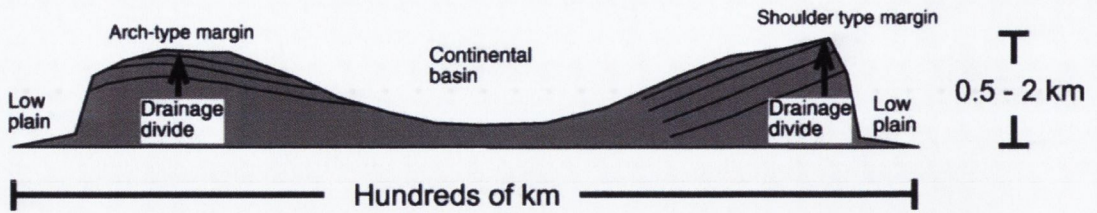


Fig. 4.4: Generalised continental margin geometry after Matmon et al., (2002). Shoulder-type margins are those where the uplift axis is located at edge of the uplifted domain. Along these margins, the drainage divide is coincident with the top of escarpment. Arch-type margins are those where the uplift axis is located inland from edge of the uplifted domain. Along these margins, the drainage divide is separated from top of the escarpment.

Topographic escarpments are a common morphological feature of many high elevation passive continental margins and rift systems (e.g., King, 1955, 1962; Ollier, 1985). The typical morphology of an escarpment is a steep or wall-like scarp running parallel to the coastline or newly developed rift opening. The escarpment forms a boundary between the low elevation coastal plain and the plateau inland of the escarpment lip, which is normally elevated higher than the coastal plain. Commonly the top of the escarpment is referred to as the escarpment lip and is often higher elevation than the surrounding plateau. The classic example of an escarpment is the Great Escarpment in southern African, but escarpments are common feature inland of many passive continental margins (e.g. eastern Australia, eastern Greenland, West Africa, western India and eastern South America). Some passive margins vary substantially in elevation from their conjugate margin. For example the Great Escarpment along the southern Africa margin is elevated much higher than the South American margin.

Three main models have been put forward for the post-breakup evolution of passive continental margins and their associated escarpments; namely the downwarp, scarp retreat and pinned-divide or down-wear models (Figure 4.5). Low-temperature thermochronology and cosmogenic isotope analyses have provided constraints on these

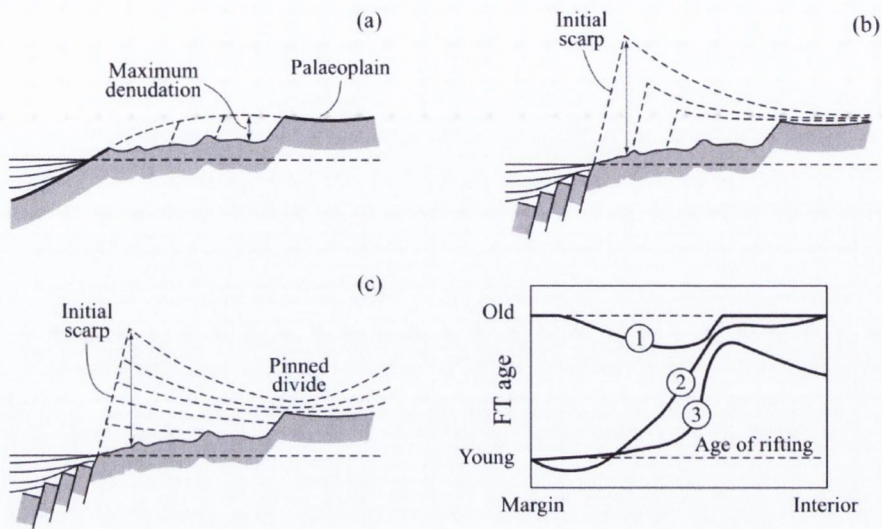


Fig. 4.5: Post-breakup models of the evolution of high-elevation passive continental margins after Gallagher et al., (1999) (a) Model of a high-elevation passive continental margins involving escarpment retreat into a downwarped continental margin. This model does not incorporate flexural rebound due to denudation. The remnants of the downwarped ancient plateau are therefore presumed to be preserved along the outer edge of the coastal plain. (b), (c) Models of a high-elevation passive continental margins involving flexural denudational rebound following (b) escarpment retreat or (c) excavation-in-place of the escarpment. In (b) and (c) the dotted lines represent the total thickness of crust removed as a result of coastal plain formation and denudational rebound. The fourth panel gives a hypothetical spatial distribution of the low-temperature thermochronological ages predicted by the three models (model (a) = 1, model (b) = 2 and model (c) = 3) (from Gallagher et al., 1998)

models. Earlier models for escarpment evolution required that the plateau to be downwarped or downfaulted to form the broad monocline along the margin immediately after continental breakup and the escarpment later retreats inland eroding the downwarped edge of the continent, producing a coastal plain (King, 1962; Ollier and Pain, 1997). Therefore remnants of the ancient paleoplain inland of the escarpment lip should be similar in age to the outer edge of the coastal plain. This model does not allow for the isostatic response to the denudational unloading. Low-temperature thermochronology has highlighted the importance of flexural denudation during escarpment evolution.

For example, Gallagher et al. (1999) showed that large amounts of denudation on the order of kilometres, occurred along the south-west coastal plain of Africa, while substantially less denudation occurred further inland of the escarpment since continental break-up. The apatite fission track data of the south-east coast of Africa show similar results (Brown et al., 2002). Numerical modelling of the denudation predicts upwarp of the region the coast adjacent to coastal plain the due to the flexural rigidity of the lithosphere (e.g. van der Beek et al., 2002).

The scarp retreat model argues that the escarpment originally formed at the edge of the new continental margin by normal faults formed during rifting (Gilchrist and Summerfield, 1990; Gilchrist et al., 1991). The high erosion rate on the surface of the scarp (due to its high relief and slope) cause it to quickly erode inland. The associated denudation due to the retreat of the escarpment may cause flexural upwarp of the margin. The coastal plain is characterised by more moderate denudation rates and the interior region of the continent experiences relatively slow denudation. The apatite fission track age of the region should therefore be oldest in the plateau region inland of the escarpment and youngest at the outer edge of the coastal plain (Gallagher et al., 1999).

The pinned divide model requires the drainage divide to occur inland of the initial steep escarpment that formed during rifting (Kooi and Beaumont 1994; Gilchrist et al., 1991). The large catchment area above the escarpment leads to rapid uniform stream incision of the region seaward of the drainage divide and thus the denudation occurring is downwearing rather than backwearing as seen in the escarpment retreat model. The new escarpment forms and is pinned near the drainage divide. If the base level falls, significant amount of denudation can occur inland of drainage divide and therefore cause the downwearing of the plateau (Gallagher et al., 1999). The apatite fission track age of the region inland of the escarpment should be younger than those

the escarpment retreat model. The main difference between the two models is the timing of the denudation across the coastal plain and the amount of denudation that occurs inland of the escarpment.

Matmon et al. (2002) classified escarpments into 2 types, according to where the drainage divide is positioned relative to the escarpment (Figure 4.4) and suggests that this affects the way the escarpment evolves. The shoulder-type margin are those where the uplift axis is located at the edge of the escarpment and the drainage divide is usually near the top of the escarpment or escarpment lip. The arch-type margins are those where uplift axis is located inland from the escarpment edge and therefore the drainage divide is inland of the escarpment edge. The drainage divide location relative to the escarpment is an important factor in controlling how the escarpment will erode. The limited watersheds of streams flowing down shoulder-type escarpments, mean the stream does not have the power to effectively erode headward even though it is flowing down a steep slope. Streams flowing down arch-type escarpments, in addition to being steep have a large catchment above them and therefore a greater stream power, allowing them to quickly erode back into the escarpment. Matmon et al. (2002) argued that the escarpment and the drainage divide of shoulder-type margin retreated inland at equal rates (similar to the scarp retreat model), while the faster eroding streams along an arch-type margin lead to embayment of the escarpment, as the river valleys erode faster than the interfluves (similar to the pinned divide model). Therefore the sinuosity or degree of embayment of the escarpment should be larger for an arch-type margin (such as Australia) than the shoulder-type (such as southern Africa and South America).

Most escarpment evolution models rely on fluvial erosion as the dominant erosional process and very little research has focused on the evolution of high-elevation passive continental margins in glacial regions. The present-day arid conditions of Antarctica

and parts of Greenland result in low erosion rates and dry-based glacial erosion is probably minimal. However because of repeated glaciation and de-glaciation during the Cenozoic, there would have been high rates of fluvial and wet-based glacial erosion (Behrendt and Cooper, 1991). Nslund (2001) suggested that the escarpment along Dronning Maud Land in East Antarctica was established shortly the break-up of Gondwana due to fluvial erosion. The escarpment retreat due to fluvial erosion continued during the Late Mesozoic to possibly the Middle Cenozoic. Although some erosion due to wet-based glaciation may have occurred during the Middle Cenozoic, the escarpment has largely been preserved by cold based ice sheets.

4.2.1 The Great Escarpment

The southern African escarpment is a very prominent feature of the morphology of Africa (Figure 4.6). Most recent researchers suggest that escarpment was created during the breakup of Africa and South America, 135 Ma (Brown et al., 2000; Partridge and Maud, 1987; Ward and Corbett, 1990) as the result of inherited rift-shoulder uplift (Summerfield, 1990; Kooi and Beaumont, 1994). Previous models suggested the escarpment is a younger feature, the result of base level changes that have quickly retreated parallel to the coast and implies on-going escarpment retreat rate of about a kilometer every million years (King, 1962; Burke, 1996). Low-temperature thermochronology and cosmogenic data indicates that rapid denudation occurred on the coastal plain after continental break-up but subsequent escarpment retreat was slow or negligible (Brown et al., 2002; van der Beek et al., 2002; Cockburn et al., 2000; Gallagher and Brown, 1999; Ward and Corbett, 1990; van der Beek et al., 2002). The Namibian coastal plain experienced a period of accelerated cooling interpreted as an increase of denudation during the late Cretaceous ($\sim 80\text{--}60$ Ma), approximately 40 to 60 Ma after break-up (Gallagher and Brown, 1999). Similarly the coastal plain below

the Drakensberg Escarpment underwent a period of intense denudation between ~91 and 69 Ma (Brown et al., 2002) about approximately 40 to 60 Ma after the Falkland plateau broke away from the region (Reeves and de Wit, 2000). Rates of denudation during this accelerated phase of erosion are estimated to be approximately 100 m Ma^{-1} (Gallagher and Brown, 1999; Brown et al., 2002).

Cosmogenic analysis of samples taken the Drakensberg escarpment (from the cliff face and the summit surface) indicate escarpment retreat rates of 49 and 63 m Ma^{-1} and summit denudation or downwearing rates of about 6 m Ma^{-1} over the past 7 to 10 ka. (Flemming et al., 1999). Low escarpment retreat estimates, of about 10 m Ma^{-1} have been calculated for the Namibian sector of the south-west African margin. Most researchers now agree that escarpments reach their long-term location on the landward edge of the coastal plain soon after breakup either by escarpment retreat (e.g. Partridge and Maud, 1987) or by rapid incision of by rivers seaward of a pre-existing drainage divide located just inland of the present escarpment location (e.g. Brown et al., 2005). Regions with flexible lithosphere i.e. a low values of T_e , have upwarping that is most pronounced at the lip of the escarpment and updoming of the coastal plain (Bishop, 2007). Modeling of escarpment retreat in southern Africa requires a low T_e value of 10km to explain denudation patterns and the geological structure of the region (van der Beek et al., 2002).

Van der Beek et al. (2002) believed that no large-scale Cenozoic tectonic surface uplift event is required to explain the morphology and denudation history of the southeast African margin. However there is strong indirect evidence that suggests regions of the southern African margin have been recently uplifted. At the start of the Neogene period there was a widespread rejuvenation of sediment flux to the major deltas of Africa. Increased sediment supply could have been linked to epeirogenic uplift of Africa during latest Oligocene and Miocene times (Walford, 2003). Seranne and Anka

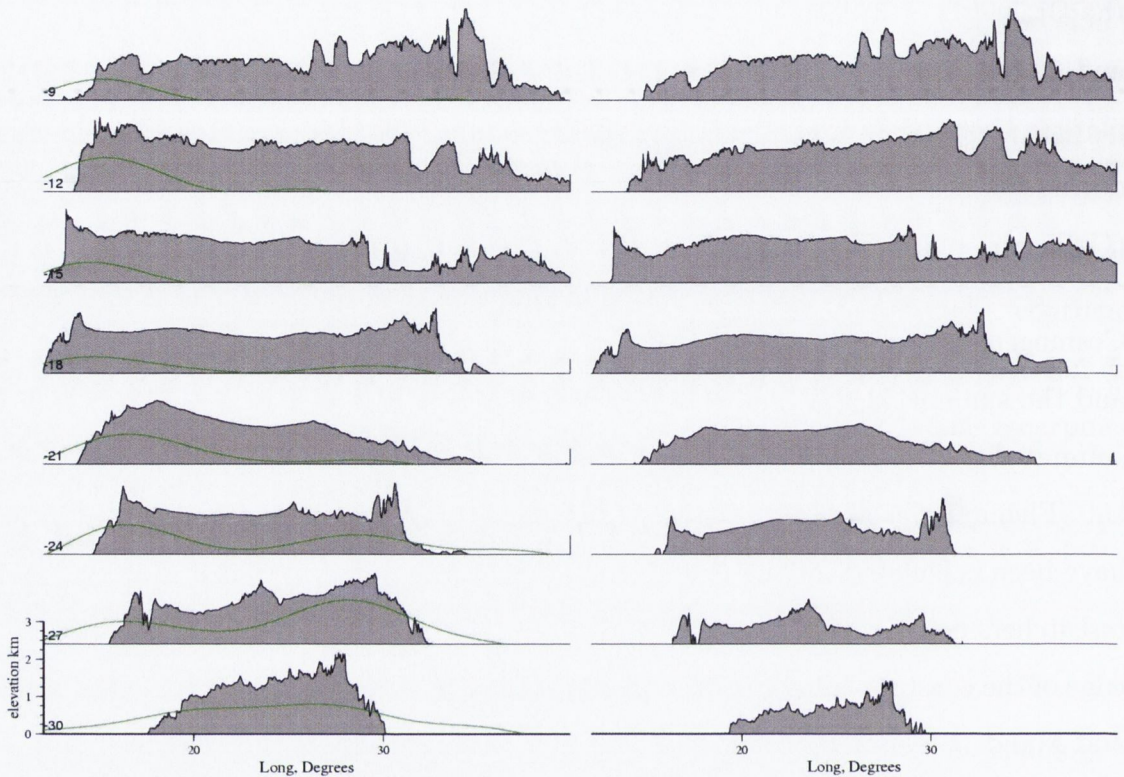


Fig. 4.6: Cross sections through the topography southern Africa parallel to latitude every three degrees (the number on the right hand side denotes degrees of latitude south of the equator). Dynamic topography assuming an admittance of 40 mgals km^{-1} represented as a green line (left) Cross sections through the topography of southern Africa after being corrected for dynamic topography assuming an admittance of 40 mgals km^{-1}

(2005) contend that the south west African coast was uplifted during the Neogene, but accelerated erosion only took place in the Congo catchment due to wetter climatic conditions while the denudation rate of the Namibian region remained low due to arid climate. In addition, they also suggest that Tertiary reactivation of salt tectonics on the equatorial western Africa margin may be explained by tilting caused by uplift along the margin. Fission track data of samples taken from the Angolan coast reveal a thermal event at 10–20 Ma, which supports the theory that uplift of the margin occurred in the Neogene during the exhumation of the Kwanza Basin (Jackson et al.

2005). A large unconformity on the West African shelf and truncation of Late Neogene strata at the seabed observed on seismic reflection profiles implies wholesale uplift of the continental margin in post-Miocene times. Modelling of seismic velocities results in estimates of denudation in the range of 300–800 m (Walford, 2003). The tilting of the African surface in southern Africa also indicates recent uplift of the African margin and the spatially variable uplift rate is estimated in the region of 150–300 m during the Miocene and 100–900 m during the late Miocene (Partridge and Maud, 1987).

4.3 Dynamic topography and mantle edge convection

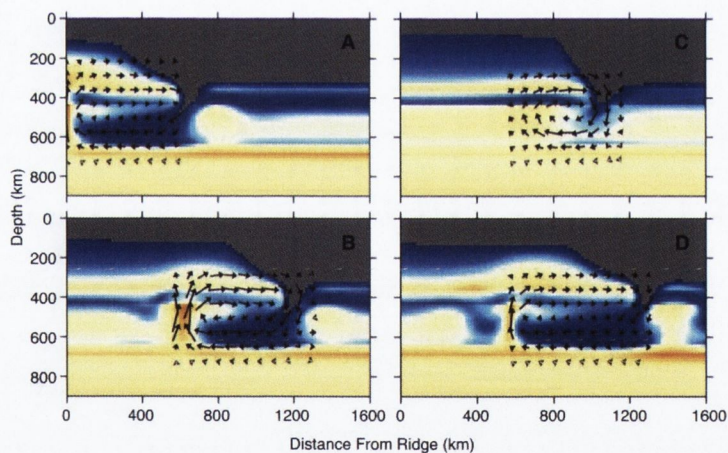


Fig. 4.7: Numerical model of temperature anomalies and velocity fields from calculations with a step change in lithospheric thickness after King and Ritsema (2000). The width of the ocean basin (thin lithosphere) is 600 (A) and 1800 km (B). In each calculation, the width of the ocean basin is fixed throughout time. Both panels are taken 50 Myr after the initial condition. The temporal evolution of the calculation in panel (B) is shown in (C) and (D) at 20 My and 100 My after the initial condition respectively.

Numerical models show that small-scale convection forms in the upper mantle beneath

the boundaries of thick cratonic lithosphere and thin oceanic lithosphere and the resultant convection cells are calculated to be at most 800 to 1000 km wide (Figure 4.7). The models estimate that edge-driven convection reaches a peak velocity of about 30 mm/year about 80 to 100 Myr after the oceanic basin is formed. Cross-sections of the tomography model, S20RTS, across southern Africa and South America appears to support the idea of small-scale, edge-driven convection predicted by numerical models (King and Ritsema, 2000).

One of the distinct features of the southern African continent is the long wavelength free-air gravity positive anomalies that rim its margin (Figure 4.8). Elsewhere in Africa long wavelength free-air gravity positive anomalies are associated with regions that have undergone recent uplift due to mantle up-wellings e.g. the east African rift system and Afar. Modelling of long wavelength free-air gravity can be used to predict dynamic topography. It is possible to view the relief of Africa without the dynamic component of the topography, by assuming an admittance of 40 mgals km^{-1} and subtracting it from the DEM of present day Africa (Figure 4.6). The cross-sections reveal that the prominent escarpment lip is preserved even after dynamic topography is removed (e.g. on the west coast of Africa at 18° and 15° latitude). In most cases, the margin of the continent is elevated below 1 km with escarpment lips often elevated slightly above this height. Short wavelength erosional features are also preserved. In many cases, the asymmetrical topography of the west and east margins are lessened or in some cases removed (e.g. 21° latitude). It is also worth noting that large regions of the Nambian coastline and desert is submerged below sealevel (assuming present day sealevel).

To investigate a possible connection between edge-driven convection in the mantle, surface topography and long wavelength free-air gravity anomalies, cross-sections were plotted through the S20RTS tomography across southern Africa, centred at the equator and then 10° , 20° , 20° below the equator (Figure 4.10 and 4.11). The cross-sections

are 140° long and show the velocity structure of the mantle to a depth of 1000 km.

S20RTS is a global shear velocity model and is derived from free-oscillation splitting, surface-wave dispersion, and body-wave travel time measurements (Ritsema et al., 1999). Seismic surface-wave and body-wave data are most important for resolving the small-scale low shear velocity and constrain the velocity structure roughly in the top third and bottom two-thirds of the mantle, respectively. Vertical resolution of shear velocity heterogeneity in the uppermost 200 km of the mantle is on the order of 30–50 km and therefore structures in the uppermost mantle smaller than 30–50 km cannot be detected. Vertical resolution is greater than 250–300 km in the transition zone between 400–1000 km depth (Ritsema, and Allen, 2003). Overall the resolution should be detailed enough to identify convection cells of over a few hundred kilometres.

Subduction has not occurred under the southern African plate since the Triassic and therefore high velocity structures extending below cratonic regions such as can be interpreted as mantle downwellings (King and Ritsema, 2000). The high velocity structure beneath the Congo is very pronounced and extends to a depth of 700 km. This correlates with the negative long wavelength free-air gravity anomaly of the Congo basin of up to -60 mgals (Figure 4.10A). Similarly, a high velocity structure can be seen beneath the Zimbabwe craton and corresponds to a minor negative long wavelength free-air gravity anomaly of up to -20 mgals (Figure 4.11A). The downwelling in the mantle below the west margin of Africa and the Atlantic lithosphere between 45 and 55 ° from the origin, corresponds to a minor negative long wavelength free-air gravity anomaly of up to -20 mgals (Figure 4.11A).

However the slow velocity structures, which could be interpreted as hot mantle upwellings are more difficult to correlate with long wavelength free-air gravity anomalies. For example the positive long wavelength free-air gravity anomalies of the Angolan cra-

ton (Figure 4.10B) and Kaapvaal craton (Figure 4.11B) do not appear to be associated with mantle upwellings. The East African rift (E.A.R.) system is an exception and the double peaked positive long wavelength free-air gravity anomaly corresponds with a slow velocity structure, which is interpreted as not upwelling mantle beneath the rift system (Figure 4.10A). The mantle below Madagascar, a region of positive free-gravity, is also a zone of slow velocity (Figure 4.11A).

4.4 Swath topographic profiles of passive margins

In this section, topographic swath profiles of passive continental margins and their associated escarpments on southern Africa and seven other margins are studied (Figure 4.8 and 4.9). These margins were selected on the following criteria: they have been tectonically inactive for a long period of time; they are associated with topographic swells or highs near the edge of these margins; they display increases in long wavelength free-air gravity elongated parallel to the margin or escarpment (Figure 4.1 and 4.2). Commonly the evolution of the escarpment associated with the passive margin suggests that high elevation, have been present since continental break-up or soon after (Bishop, 2007). However a number of passive margins show evidence of uplift during the Cenozoic.

Deep young canyons that incise Cenozoic sediments on Madagascar are proof of substantial uplift in the Neogene, perhaps related to the onset of regional plume-induced uplift in East Africa around 30–35 Ma (Burke 1996; de Wit, 2003). Volcanic activity and associated seismic events in central and northern Madagascar spanning the past 10–15 Ma also may imply recent uplift (de Wit, 2003).

Apatite fission track (AFT) thermochronology indicates domal uplift of the south-

ern Norwegian by approximately 1 to 1.5 km during the Neogene (Rohrman et al., 1995). Modeling of gravity and geoid residual shows data evidence that the region is supported by the sub-Moho low-density material (Ebbing and Olesen, 2005; Ebbing, 2007). Tomographic models of the sub-Moho beneath the dome area, estimate low seismic velocity anomalies consistent with low-density mantle (Bannister et al., 1991). The surface uplift has been interpreted as a result of hot asthenosphere upwelling under the cold cratonic lithosphere (Rohrman and van der Beek 1996).

Apatite fission track analysis also suggests Cenozoic uplift and erosion in east Greenland (Hansen and Brooks, 2002; Hansen et al., 2001). Here there is also a clear long wavelength domal shape of the topography, associated with cratonic regions in central Greenland that is thought to have been generated by rapid uplift during the Oligocene–Miocene (Brooks, 1985). The uplift history of East Greenland is complicated by the passing of the Iceland plume under the area at approximately 40 Ma (Rohrman and van der Beek 1996) by the positive long wavelength free-air gravity anomaly would suggest that the long wavelength topography is dynamically supported. Furthermore, the mountainous region west Greenland between 65–71° N is also viewed as a result of Cenozoic phases of uplift and erosion. Uplift and rapid erosion between 36 and 30 Ma led to the formation of a planation surface during the Oligocene and Miocene. The planation surface was then tilted and uplifted to present-day altitudes of up to 2 km in two phases that occurred between 11 and 10 Ma and between 7 and 2 Ma (Japsen et al., 2006).

Uplift data on the East Antarctica is limited. Nslund (2001) suggested that the escarpment along Dronning Maud Land in East Antarctica was established shortly the break-up of Gondwana due to fluvial erosion and implied that the region was elevated during continental breakup. Further uplift and escarpment retreat may have occurred during the Middle Cenozoic, during or prior to the Oligocene (Nslund, 2001). The

Mount Johnston Formation (early Miocene glaciomarine sediments), deposited near the Lambert Glacier basin in East Antarctica have been uplifted at least 1483m during the past 20 Ma (Hambrey and McKelvey, 2000). It is interesting to note the coast of East Antarctica between -20° – 50° longitude shared a boundary with the south east African coast until it began to rift apart at approximately 170 Ma (Reeves, 2000).

4.4.1 Methodology

Swath profiles are taken from coastlines across escarpments in the different regions as outlined on topographic maps in Figures 4.8 and 4.9. The profiles were made by projecting elevation points from a 55 km-wide swath centred on the line of the section. The length of the swath profiles were between 325 and 425 km and therefore should display the escarpment and the region inland of the escarpment. The minimum, maximum and mean elevations of the projected points were then determined along the profile. In most cases the swath profile were generated using SRTM30 plus, with resolution of approximately 1 km. Antarctica and Greenland were first corrected for ice thickness and ice loading as described later in this chapter. The average elevation line map shows the smoothed topography and thus is suitable for recognizing long wavelength geomorphic features. As the profiles are taken perpendicular to the escarpment the minimum elevation should reflect the average depth of fluvial incision of the rivers eroding back into the escarpment and maximum elevation of the swaths should represent the interfluves. Long wavelength free-air gravity was used to calculate the dynamic component of the topography, assuming an admittance of 40 mgals km^{-1} . A profile of varying predicted dynamic topography was taken through the centre of the swath and plotted on the swath. Because most of the gravity anomalies are long wavelength and are usually elongated parallel to the escarpment, dynamic topography did not vary by much over the 55 km-wide swath. Plotting the increase of dynamic

topography allows the assessment of the potential contribution mantle convection may have had on the surface topography but does not predict the total dynamic component of the topography.

According to Matmon et al. (2002) classification, the southern African and the South American margin have shoulder-type escarpments and the Australian margin has an arch type escarpment. Matmon et al. (2002) did not include escarpments in glacial regions such as Antarctica, Greenland or Norway. Evidence suggests that these escarpments may have formed due to fluvial erosion during inter-glacial periods throughout the Cenozoic (Behrendt and Cooper, 1991). As discussed previously, shoulder type escarpment should retreat in a more uniform escarpment profiles, while the arch-type escarpment forms a greater degree of embayment of the escarpment. Higher degrees of embayment should result in the greater differences between minimum elevation and maximum elevation of the swaths should be along the escarpment. Glacial erosion of the passive margins also may create large variation in the topography perpendicular to the swath as glaciers erode U-shaped valleys through the escarpment. Minor variations in the maximum and minimum vertical elevation of the profiles may imply flat or low relief plateaus and plains, with minimal fluvial incision.

4.4.2 Results

Southern Africa

The escarpment in southern Africa as defined by Partridge and Maud (1987) is a steep change in topography occurring at an elevation of approximately 1 km. In the swath profile the escarpment is normally visible on the maximum elevation surface. Swaths along 15° S to 18° S latitude inland of the escarpment show very little variation be-

tween the maximum and minimum elevation reflecting a flat plateau (Figure 4.12). The escarpment and region around it shows high variation in relief. The minimum elevation along the Angolan coastline along 11° S and 12° S latitude indicates knickpoints between 40 and 80 km inland of present day sealevel. The Namibian coastal region between 20° S and 25 ° S displays only minor vertical variation between maximum and minimum elevation (Figure 4.12). The low relief of the region may be as a result of low fluvial erosion rates of the ephemeral rivers in the area. In contrast the Orange river at 29° S and 29° S latitude shows high vertical variation between maximum and minimum elevation and the minimum elevation of the base river valley is under 500 m. The peak of maximum elevation on coastal plain of the swath along 21° S latitude is the Brandberg Mountains. The Brandberg Mountains reach heights of 2.4 km. The Brandberg Intrusion forms a dome-shaped plateau which is visible of the figure.

The high short wavelength topography on the swaths of the coastal plain of the south coast of southern Africa are formed by the remnants of sedimentary strata that were deformed during the Carboniferous to Permian, called the Cape Fold Belt (Figure 4.14 (right)). The fold axis is perpendicular to the line of the profiles. Therefore average elevation line probably represents a cross-section through a topography controlled by synclines and anticlines. The increase in dynamic topography along the south coast of southern Africa correlates closely with the average elevation of the swaths, suggesting the landscape may have been tilted. Substantial variation on the swaths is displayed between maximum and minimum elevations inland of the escarpment. The Drakensberg mountains are a prominent feature on the swath of the east margin of southern Africa along -29° and -30° latitude (Figure 4.14). Inland of the escarpment, the topography varies by up to 1.5 km.

Generally, we see a coastal plain sloping down towards sealevel with a variation between the the maximum and minimum elevations of 0.25 to 1 km. The escarpment is usually

marked on the maximum elevation line as a steep increase in slope. The base of the escarpment is usually situated at altitude of between 0.8 and 1 km. The topography in the vicinity of the escarpment and in particular inland of the escarpment often has a high relief and varies by up to 1.5 km. Further inland of the escarpment the variation between maximum and minimum elevation decreases as the relief becomes smoother. A sudden steepening of the minimum elevation may indicate the top of a drainage divide or a knickpoint in the drainage system. In most cases the break in slope of the minimum elevation occurs either near or inland of the escarpment lip indicating some embayment of the escarpment by river valleys. Increases in dynamic topography suggest the the coastal plain may have been tilted.

Passive Margin	Fig	Age of continental lithosphere (Myr)	Age of oceanic lithosphere (Myr)
southern Africa (west)	4.12 and 4.13	3000 to 3501 in north, 540 to 850 in south	120 to 130
southern Africa (east)	4.14	3000 to 3501	120 to >160
southern Africa (south)	4.14	250 to 540	120 to 125
West Africa (west)	4.15 and 4.16	850 to 3000	155 to 180
West Africa (south)	4.16 and 4.17	1700 to 2500	85 to 120
Madagascar (east)	4.18	2500 to 3500 (on west coast)	85 to 120
Greenland (east)	4.19	1700 to 3500	50 to 55
Norway (west)	4.19	1700 to 2500 (south) 250 to 540 (north)	50 to 55
Australia (east)	4.20	0 to 50 (north) 250 to 540 (south)	45 to 70
Antarctica (east)	4.21 and 4.22	1700 to 3500	145 to 155
South America (east)	4.23 and 4.24	55 to 180	

Table 4.1: Summary of structures associated with high-elevation passive continental margins

West Africa

Much of the topography along the West African margin lies close to sealevel and in some cases the dynamic topography is higher than the maximum elevation on the swath (Figure 4.15 4.16 and 4.17). This would require that large regions of West Africa be under present day sea level prior to the emplacement of dynamic support. The domal shape of long wavelength surface topography in areas appears to correspond to dynamic topography predictions (e.g. Figure 4.15 swath along 24° and 23° latitude and 4.17 along 5° longitude). There appears to be no major escarpment formation in this region and the swath profiles imply that fluvial dissection appears to be minor.

Madagascar

The minimum elevation along the profiles of Madagascar reflect its wedge shaped morphology (Figure 4.18). The morphology of the island is very like an uplifted or tilted normal fault block. The east margin the displays a steep escarpment, while inland of the west side of the island the escarpment is more gently sloping. Increases in predicted dynamic topography do not appear correspond with this wedge-shaped morphology. The minimum and maximum elevation along the swath profiles vary by 0.5 to 1 km in most areas and there does not appear to be many extensive flat plains. Potential river knickpoints migrating inland from east coast of Madagascar may be identified in profiles along -21° -22° -23° and -24° latitude. The escarpment lip reaches 1.5 km in elevation near the centre of the island.

Greenland

The resolution of the topography is poor due to the corrected for ice sheets, however it is still possible to pick out some of the larger scale morphological features of the region from the swath profiles (Figure 4.19). The minimum elevation of the swath profiles decreases steeply to below sealevel with no evidence of a coastal plain. This feature is not seen on the non-glaciated margins and maybe a result of glacial erosion creating fjords. The seaward side of the escarpment shows evidence of embayment on the profile. The escarpment lip reaches 1.8 km in the south and 2.4 km in the north. Inland of the escarpment the low variation in minimum and maximum elevation reflects a low relief plateau.

Norway

The clear domal structure of the topography of south Norway can be identified in the maximum and average elevation of the swath profiles (Figure 4.19). The large divergence between the maximum and minimum elevation of the swath may reflect the high rate of glacial dissection in the region. A positive long wavelength free-air gravity of up to 35 mgals is associated with the southern region of Norway, which would predict a substantial component of dynamic topography (see Figure 4.8). However increases in predicted dynamic topography along the profiles were minimal i.e. the high topography but not the warping can be explained by predicted dynamic topography. In the northern margin of Norway there is even less correlation between the topography and the predicted dynamic topography, with the maximum dynamic topography occurring offshore.

Australia

The escarpment lip reaches elevations of 1 km, as can be seen on the maximum elevation of swath profiles taken across the Australian escarpment (Figure 4.20). In general the drainage divide on the profiles appears to be inland of the escarpment lip. The wedge shape of the minimum elevation of the profile along 30° latitude is remarkably similar to the profiles across Madagascar. Inland of the escarpment a low relief plain can be identified by the low variance in minimum and maximum elevation on the swaths taken along -28° , -29° , -30° and -33° latitude. These plains are elevated below 30 m, much lower than the inland plateaus of Africa. Tilting of up to 200 m is indicated by dynamic topography estimates.

Antarctica

The resolution of the topography is poor across Antarctica (Figure 4.21 and 4.22). The escarpment lip reaches 2.5 km in places. The face of the escarpment along 10° , 5° , and 25° longitude west of the meridian is exceptionally flat when compared with the other escarpment faces. There is a lot of variation in morphology and elevation between the swath profiles taken along the eastern margin. Some swath profiles e.g. 10° 5° and 25° longitude of the margins show similar morphology to the swath profiles taken across south east Africa, with a steep escarpment face and elevated inland plateau. The large variation in morphology of the profiles may be due to dissection of particular regions during phases of wet glaciation as suggested by Naslund (2001).

South America

The topography of the northern regions of South America increase inland from the coast, and in most cases the maximum elevation reaches 1 km (Figure 4.23), however there is recognisable escarpment or extensive low relief plain. Further south, there is a more familiar wedge-shaped escarpment (Figure 4.24). The region inland and near the escarpment displays a large divergence between the maximum and minimum elevation of the swath while the inland region shows a low variation in minimum and maximum elevation reflecting a low relief plateau.

4.4.3 Discussion

Many high-elevation passive margins have associated positive long wavelength free-air gravity anomalies elongated parallel to the margin. Although escarpment evolution models suggest that high topography of the margin may have existed since rifting or a tens of millions of years after continental break-up, there is evidence that many of the margins have experience of uplift during the Cenozoic. Many of the world highest passive margins occur along cratonic belts. There appears to be no clear relationship between margin/escarpment height and the age of the oceanic lithosphere along the associated with the margin. Although escarpments originated from the break-up of continents, mantle convection may have caused swells along the the margin which in turn has contibuted to the topography of the escarpment and caused rejuvenation along the margin.

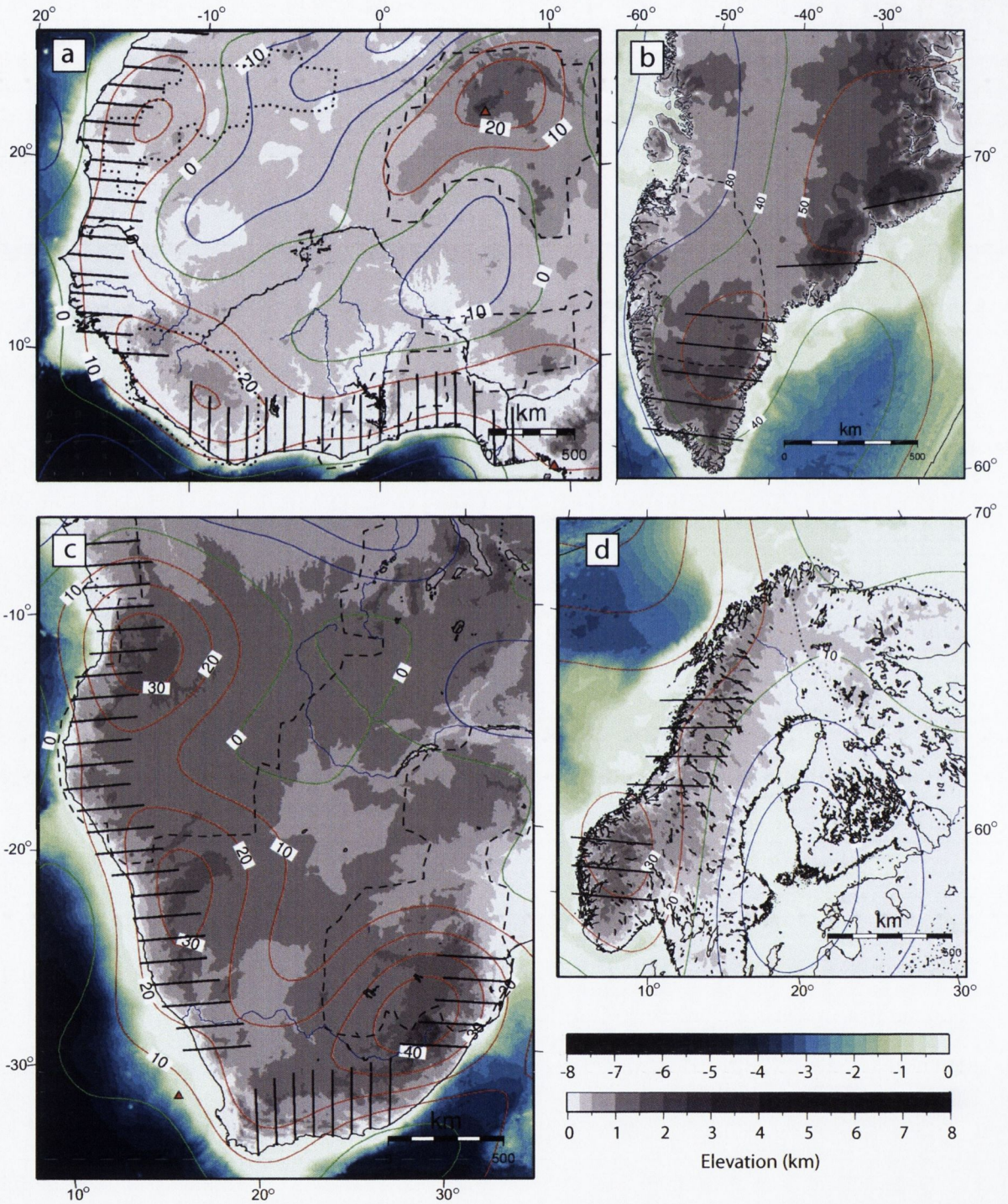


Fig. 4.8: Topographic map of escarpments in (a) West Africa , (b) Greenland , (c) southern Africa , (d) Norway, note that Greenland's elevation has been represents bedrock elevation and has been corrected for loading due to ice. Crust older than 2.5 Ga is outlined by a dashed line. Black lines represent the line the swath profiles were taken along. Contours of long wavelength free-air gravity every 10 mgals are superimposed on topography; Green contours equal average, blue contours equal below average and red contours equal above average, gravity for the region

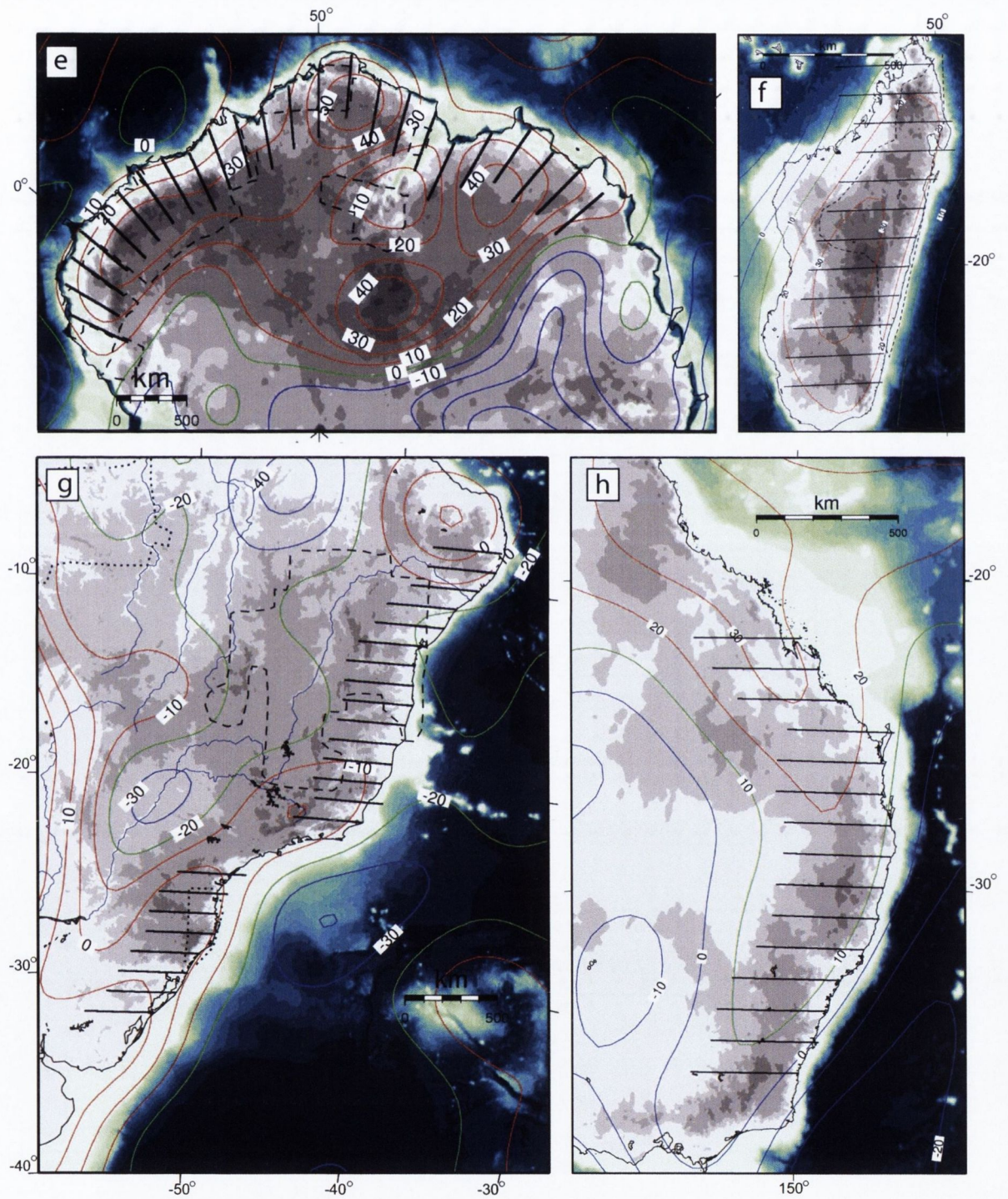


Fig. 4.9: Topographic map of escarpments in (e) Antarctica , (f) Madagascar , (g) South America , (h) East Australia, note that Antarctica's elevation has been represents bedrock elevation and has been corrected for loading due to ice. Black lines represent the line the swath profiles were taken along. Crust older than 2.5 Ga is outlined by a dashed line. Contours of long wavelength free-air gravity every 10 mgals are superimposed on topography; Green contours equal average, blue contours equal below average and red contours equal above average, gravity for the region

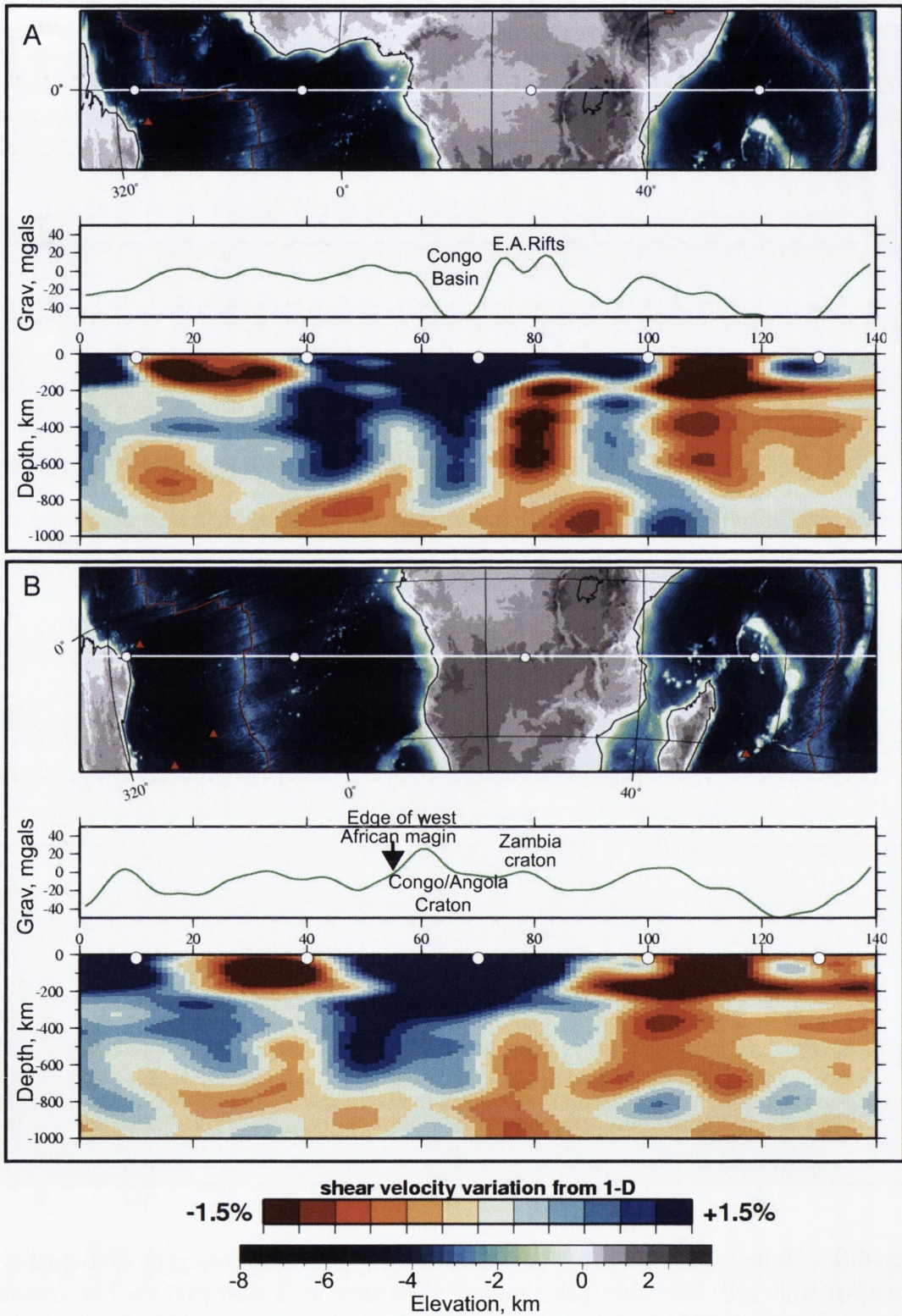


Fig. 4.10: A 140° wide cross section through S20RTS across southern Africa. The location of the cross-section is marked as a white line on the relief map. long wavelength free-air gravity is represented by a green line.

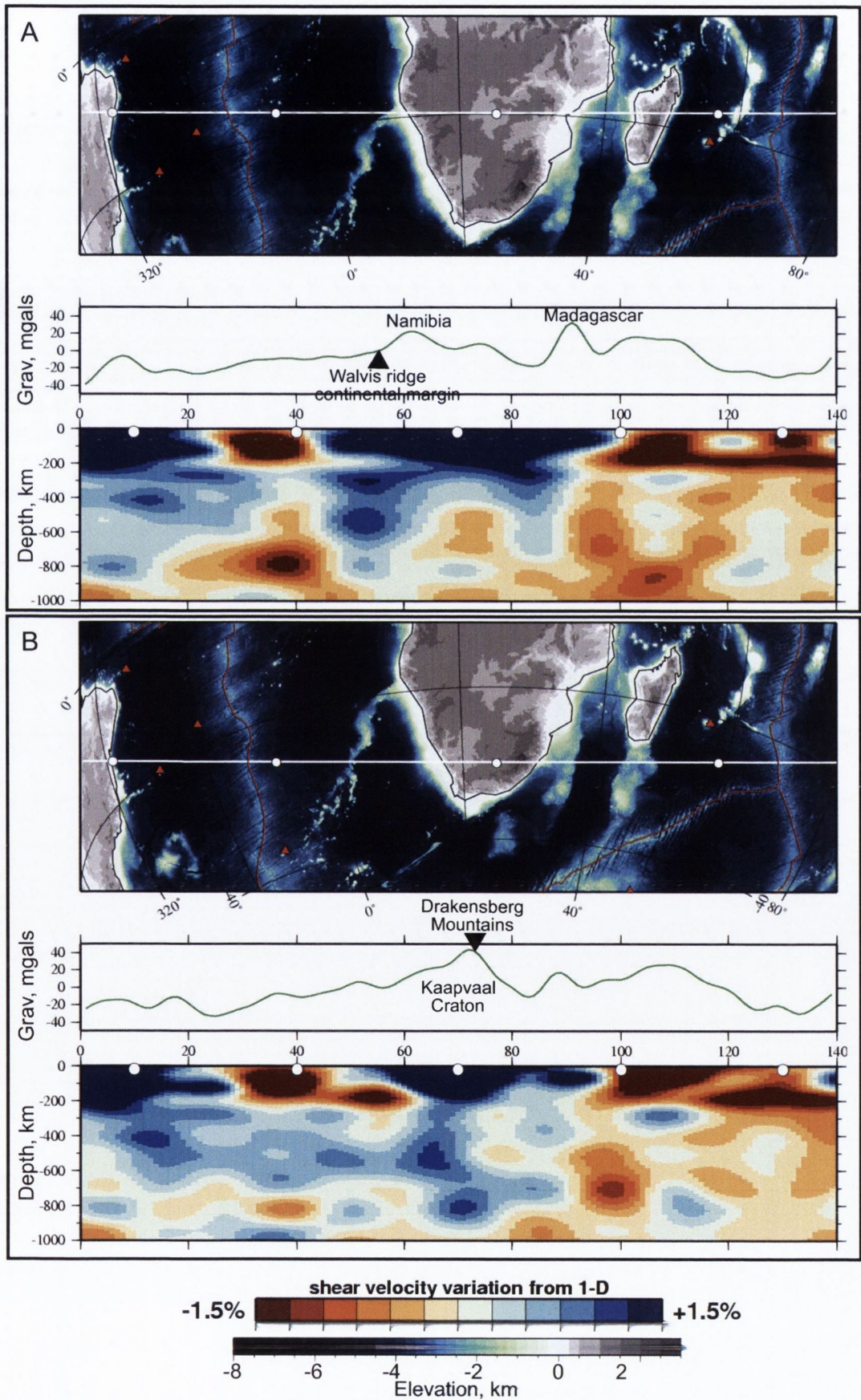


Fig. 4.11: A 140° wide cross section through S20RTS across southern Africa.

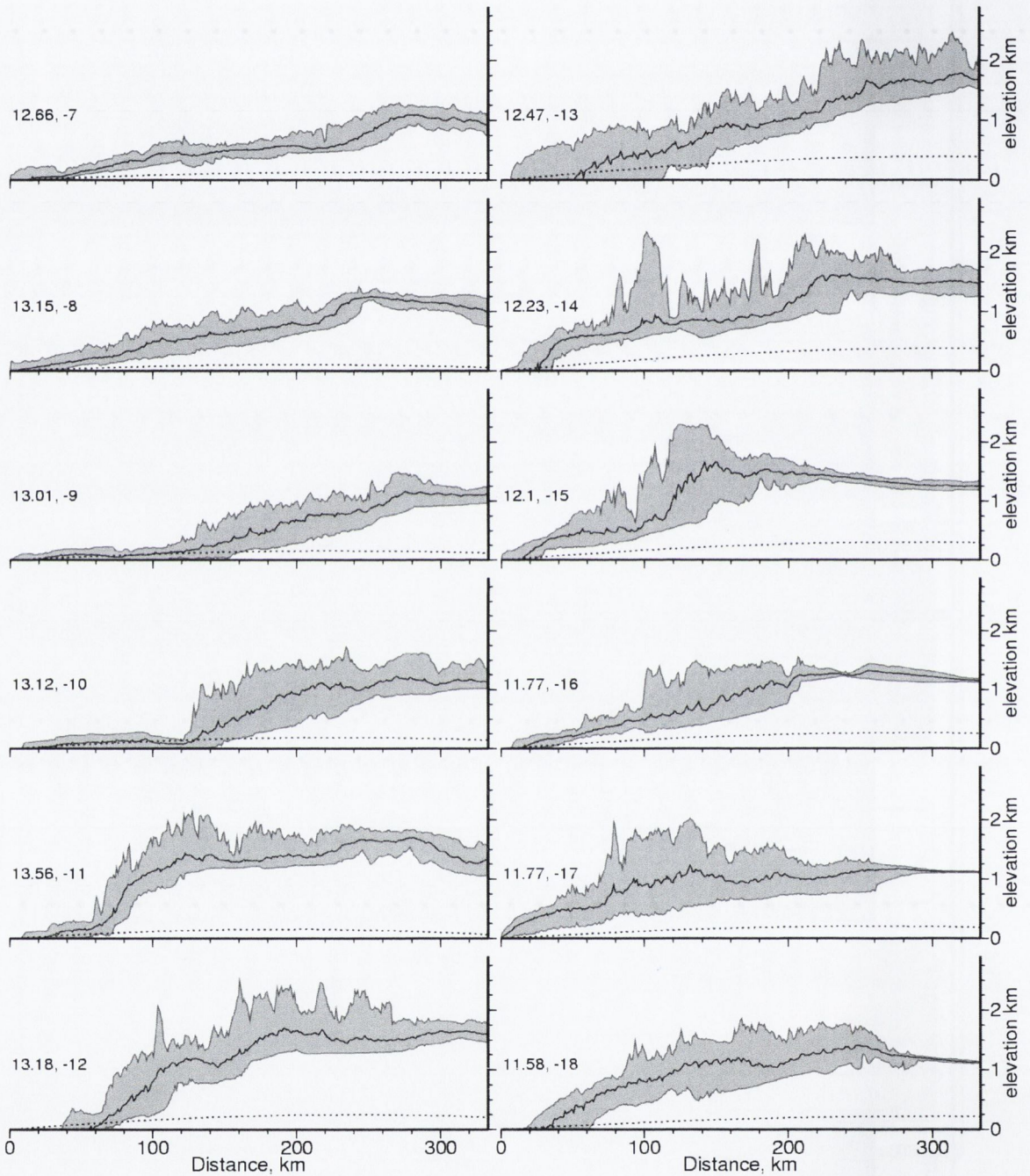


Fig. 4.12: Swaths along the south west coast of Africa. Dashed line shows increase an long wavelength free-air gravity parallel to centre of swath

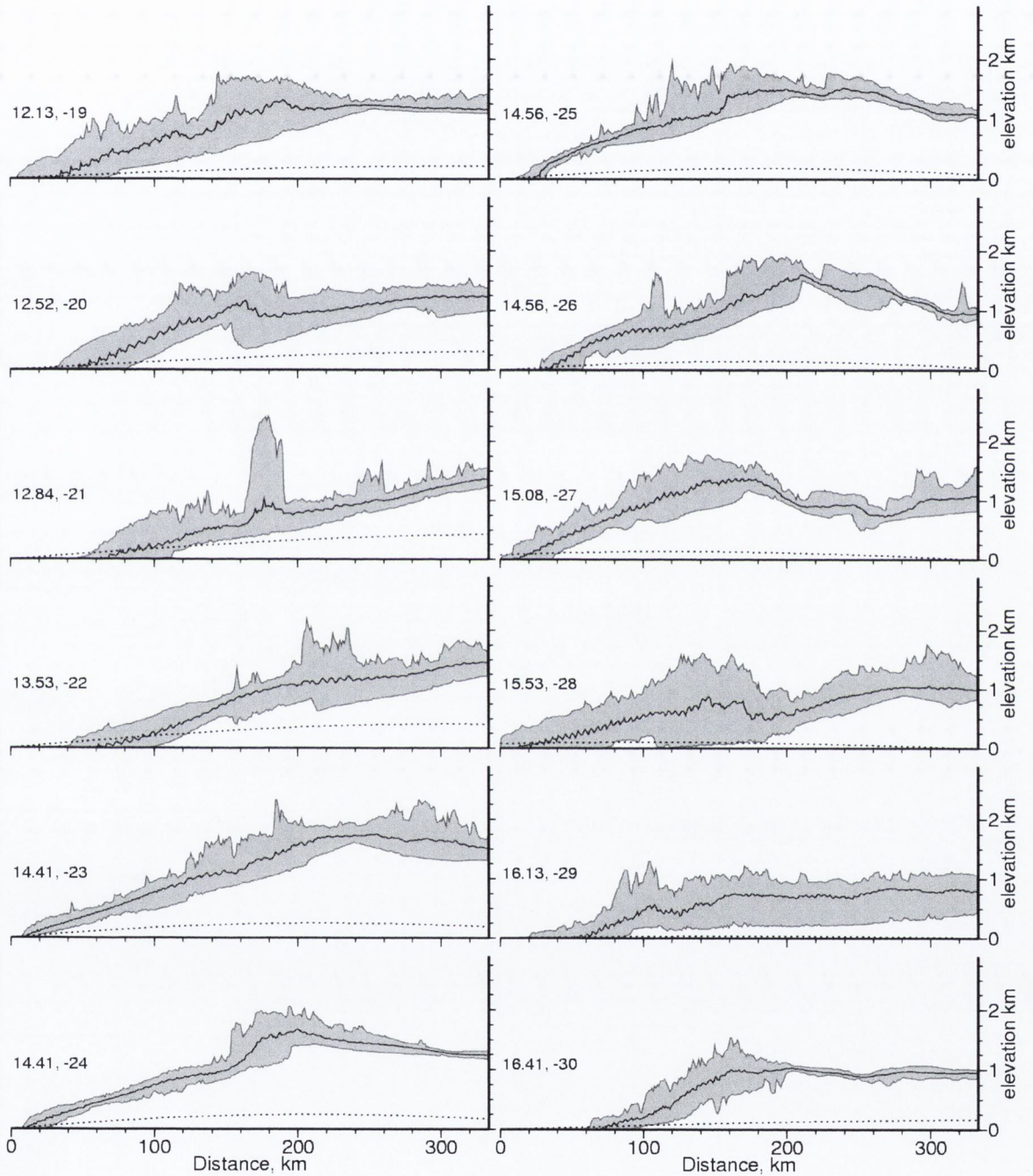


Fig. 4.13: Swaths along the south west coast of Africa. Dashed line shows increase in long wavelength free-air gravity parallel to centre of swath

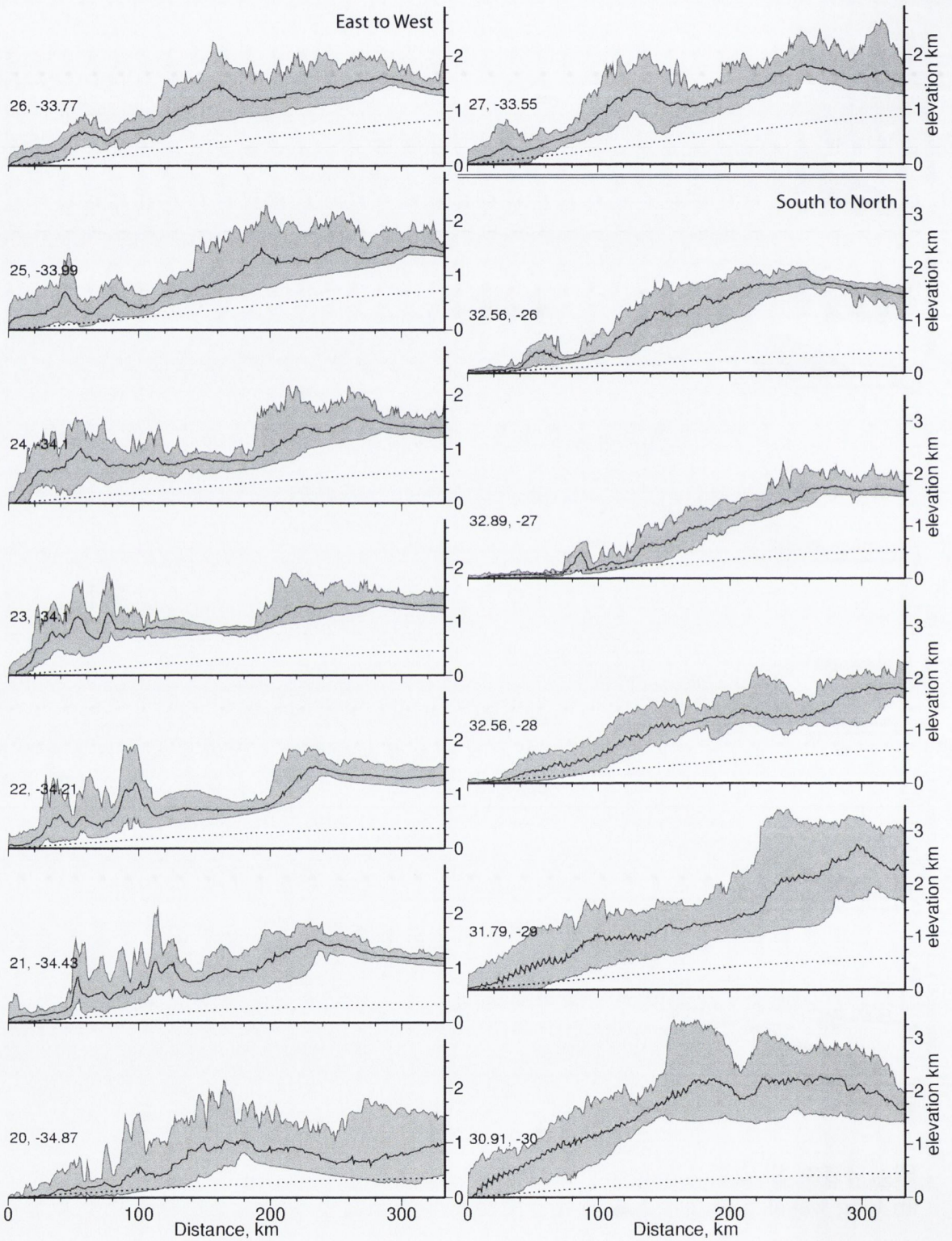


Fig. 4.14: Swaths of southern Africa in a East-West direction (left hand column) and South-North direction (right hand column). Dashed line shows increase in long wavelength free-air gravity parallel to centre of swath

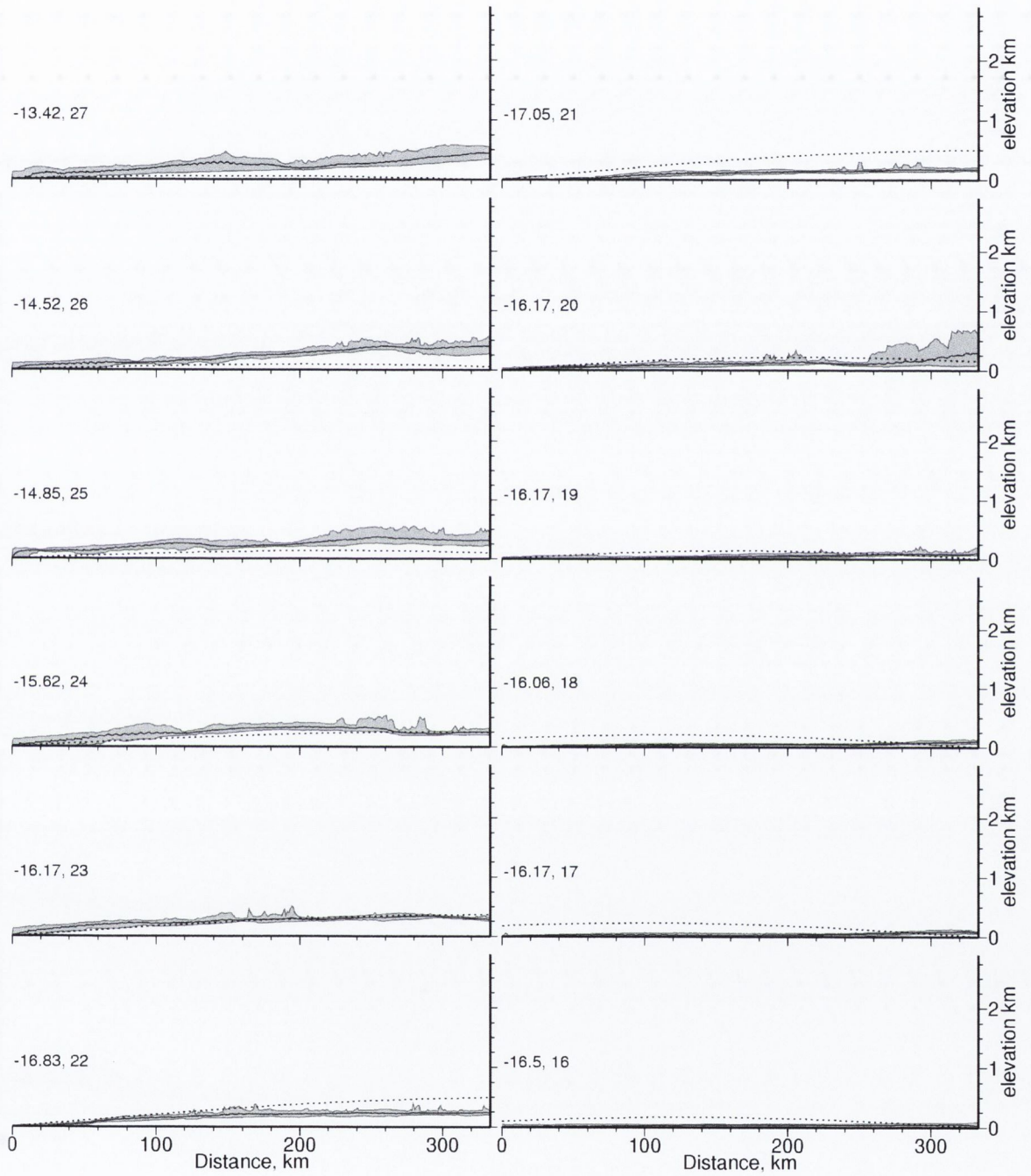


Fig. 4.15: Swaths of West Africa in a West-East direction. Dashed line shows increase in long wavelength free-air gravity parallel to centre of swath

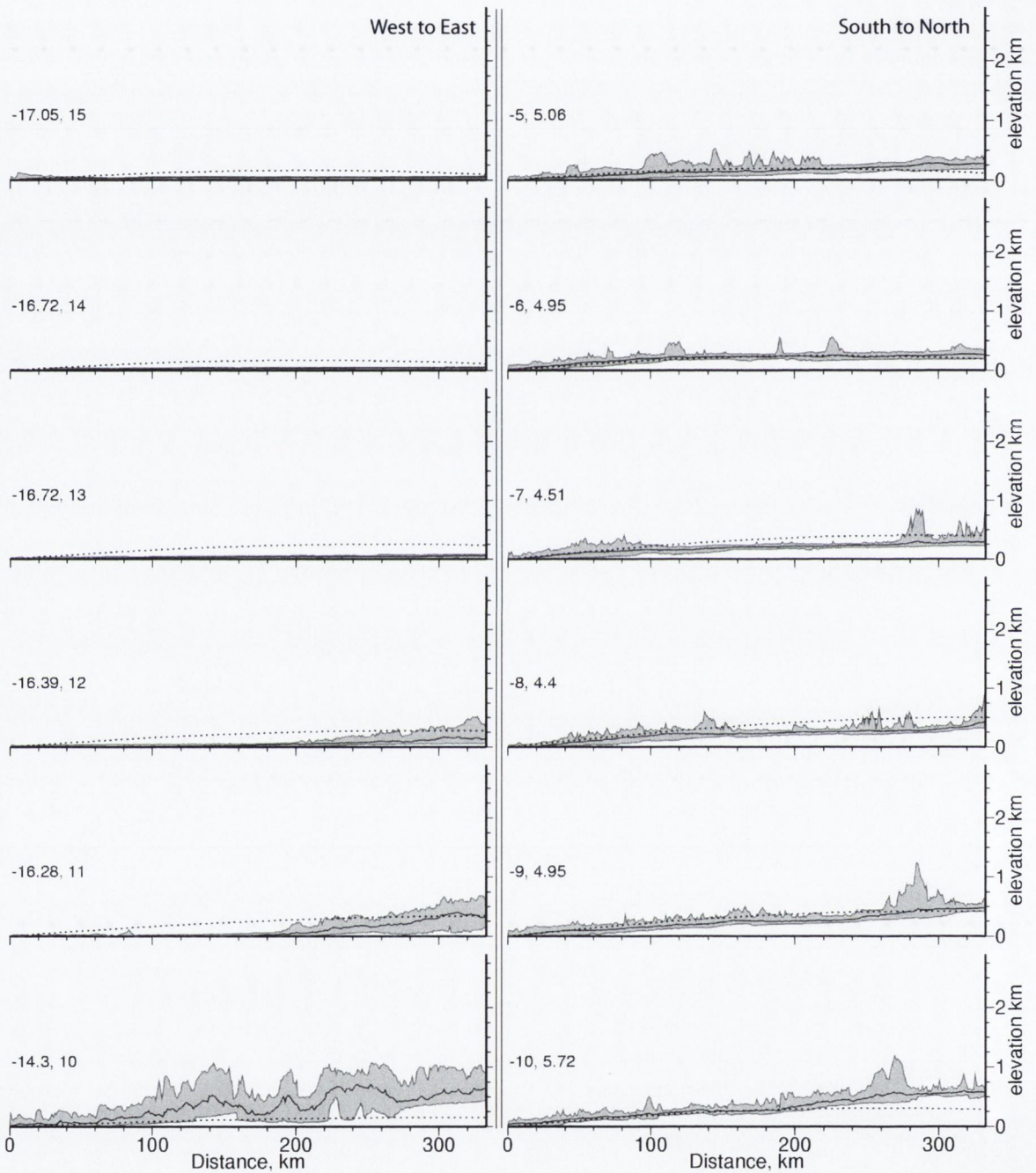


Fig. 4.16: Swaths of West Africa in a West-East direction (left hand column) and in a South-North direction (right hand column). Dashed line shows increase in long wavelength free-air gravity parallel to centre of swath

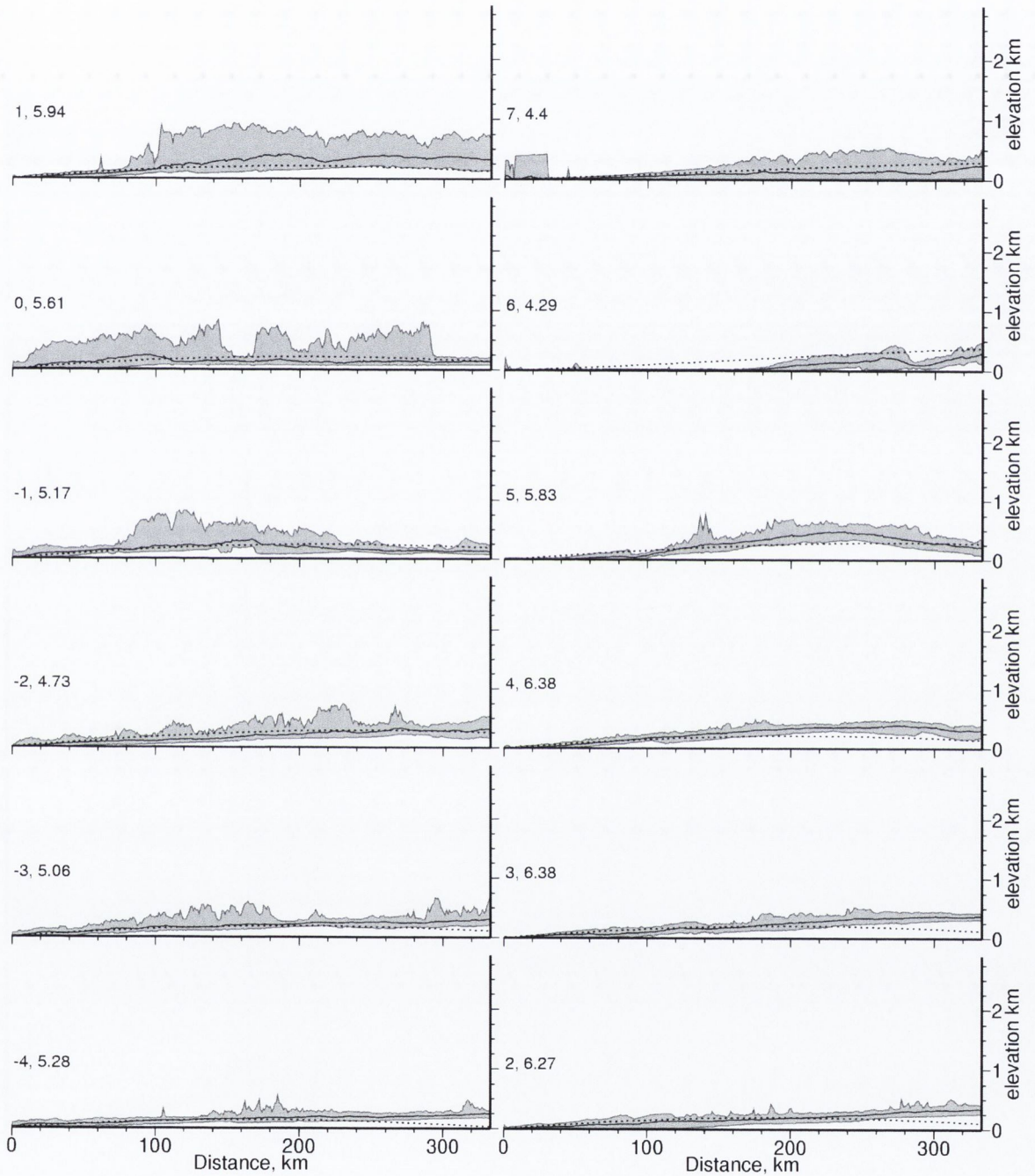


Fig. 4.17: Swaths of West Africa in a South-North direction . Dashed line shows increase an long wavelength free-air gravity parallel to centre of swath

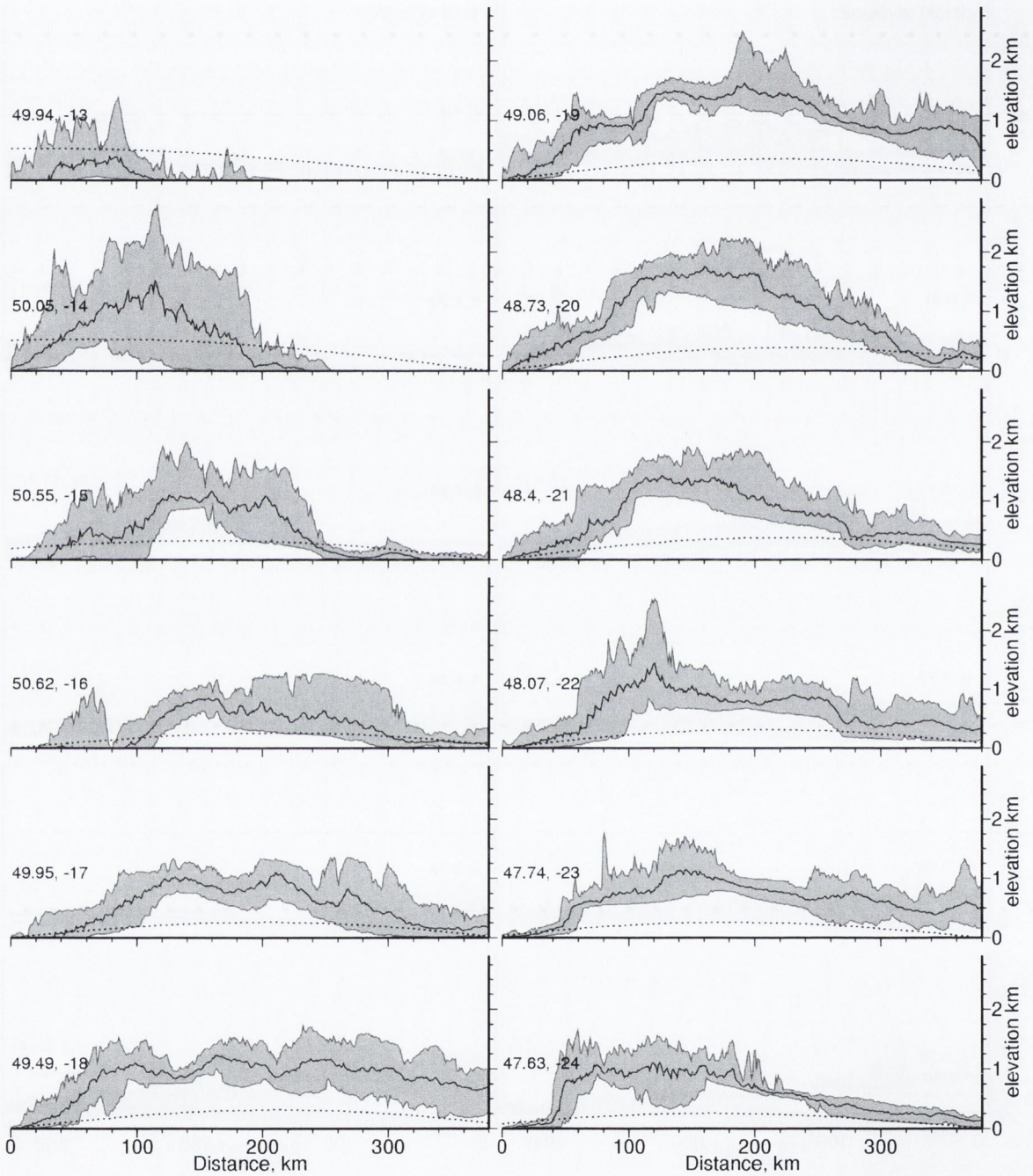


Fig. 4.18: Swaths of Madagascar in a East-West direction. Dashed line shows increase an long wavelength free-air gravity parallel to centre of swath

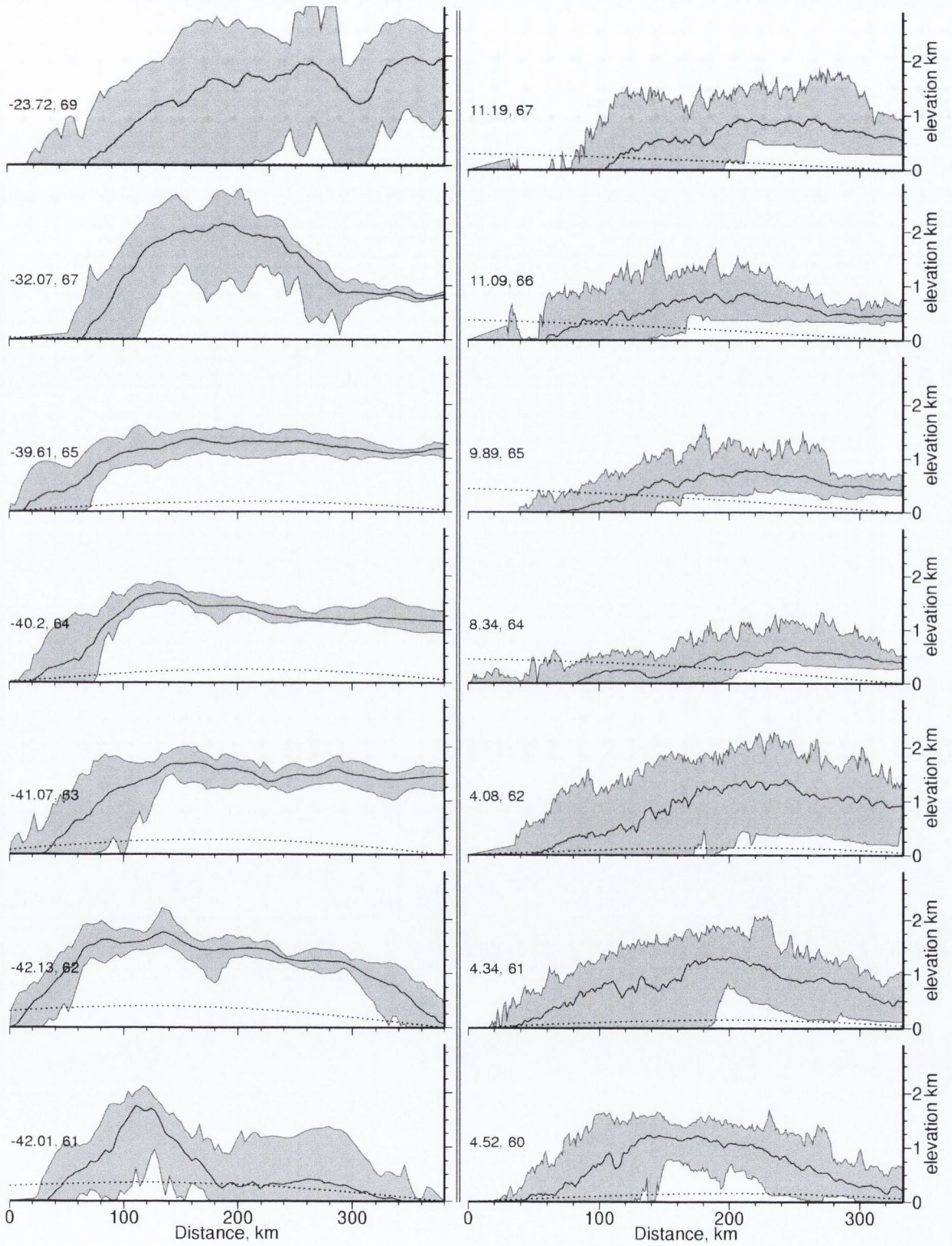


Fig. 4.19: Swaths of Greenland in a East-West direction (left hand column) and of Norway in a West-East direction (right hand column). Dashed line shows increase in long wavelength free-air gravity parallel to centre of swath

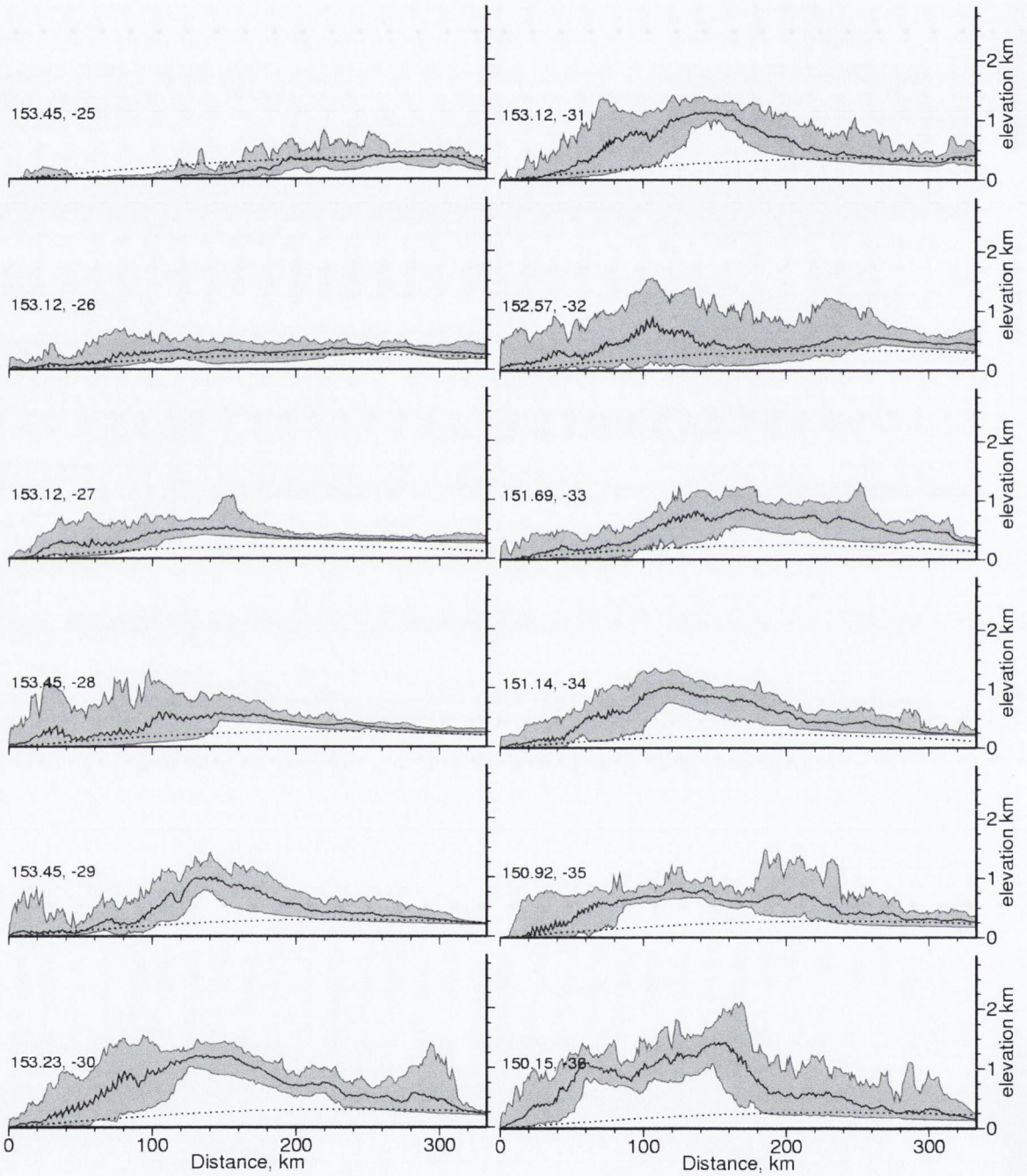


Fig. 4.20: Swaths of Australia in a East-West direction. Dashed line shows increase an long wavelength free-air gravity parallel to centre of swath

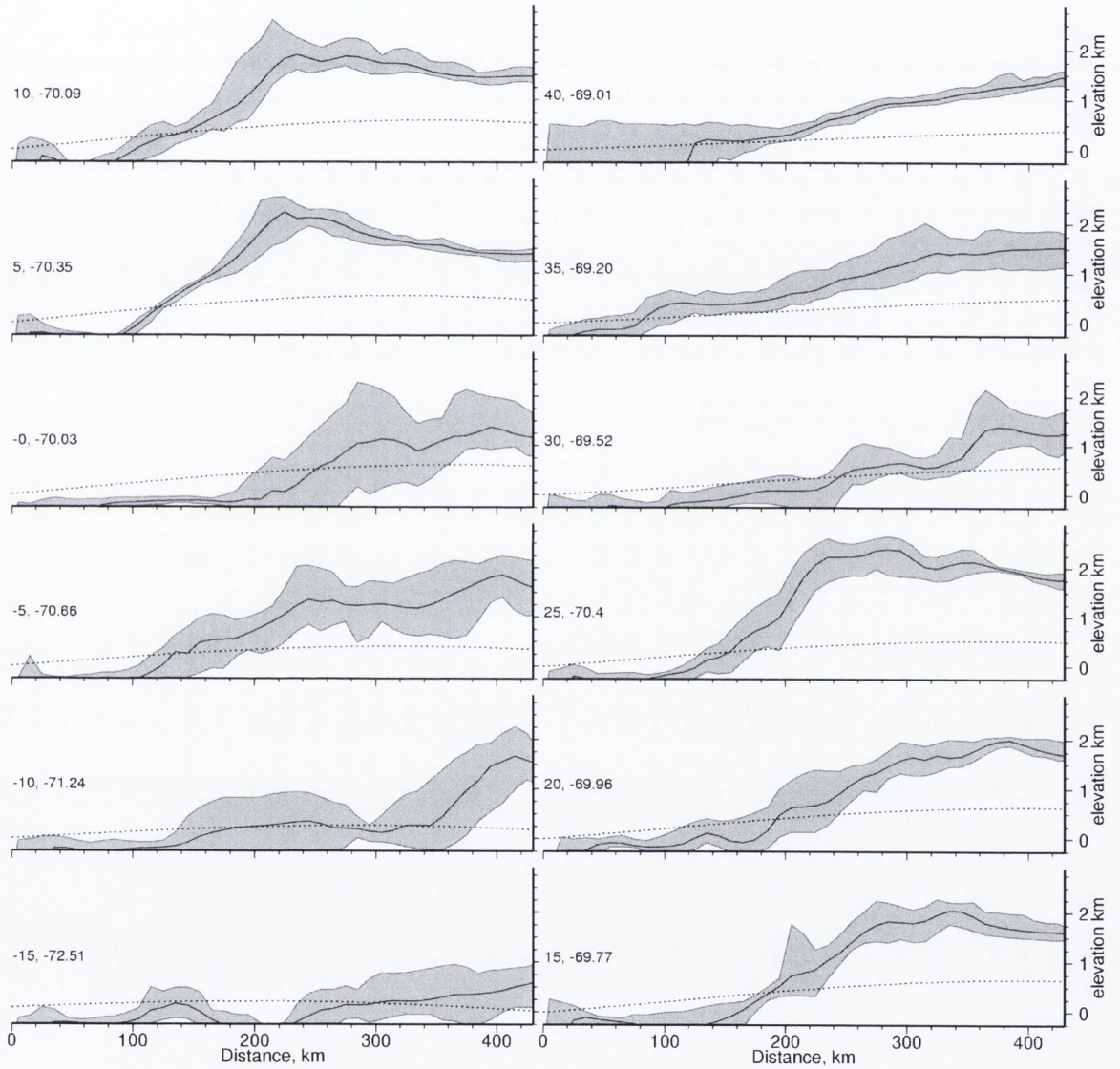


Fig. 4.21: Swaths of Antarctica in a North-South direction. Dashed line shows increase in long wavelength free-air gravity parallel to centre of swath

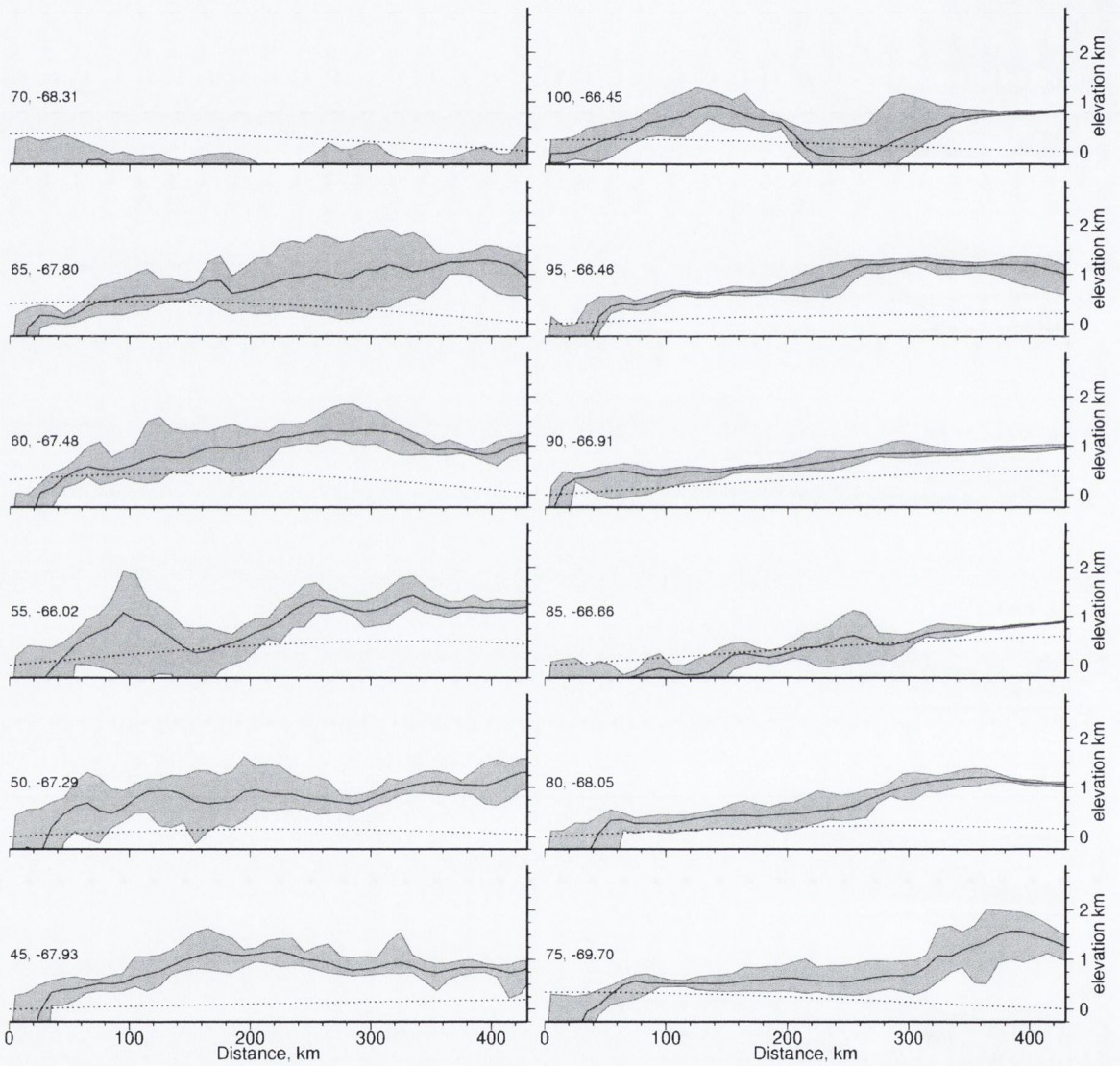


Fig. 4.22: Swaths of Antarctica in a North-South direction. Dashed line shows increase in long wavelength free-air gravity parallel to centre of swath

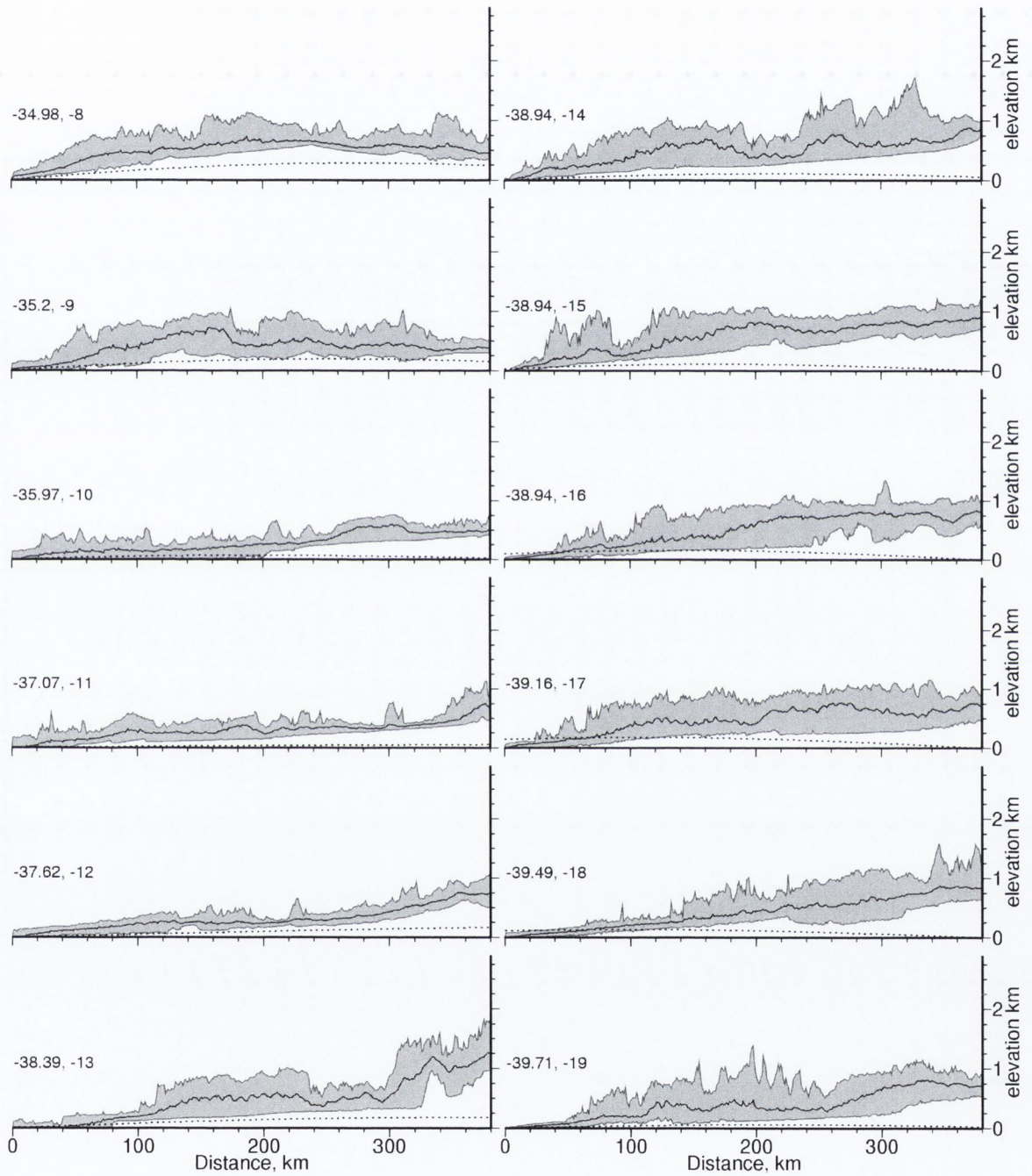


Fig. 4.23: Swaths of South America in a East-West direction. Dashed line shows increase in long wavelength free-air gravity parallel to centre of swath

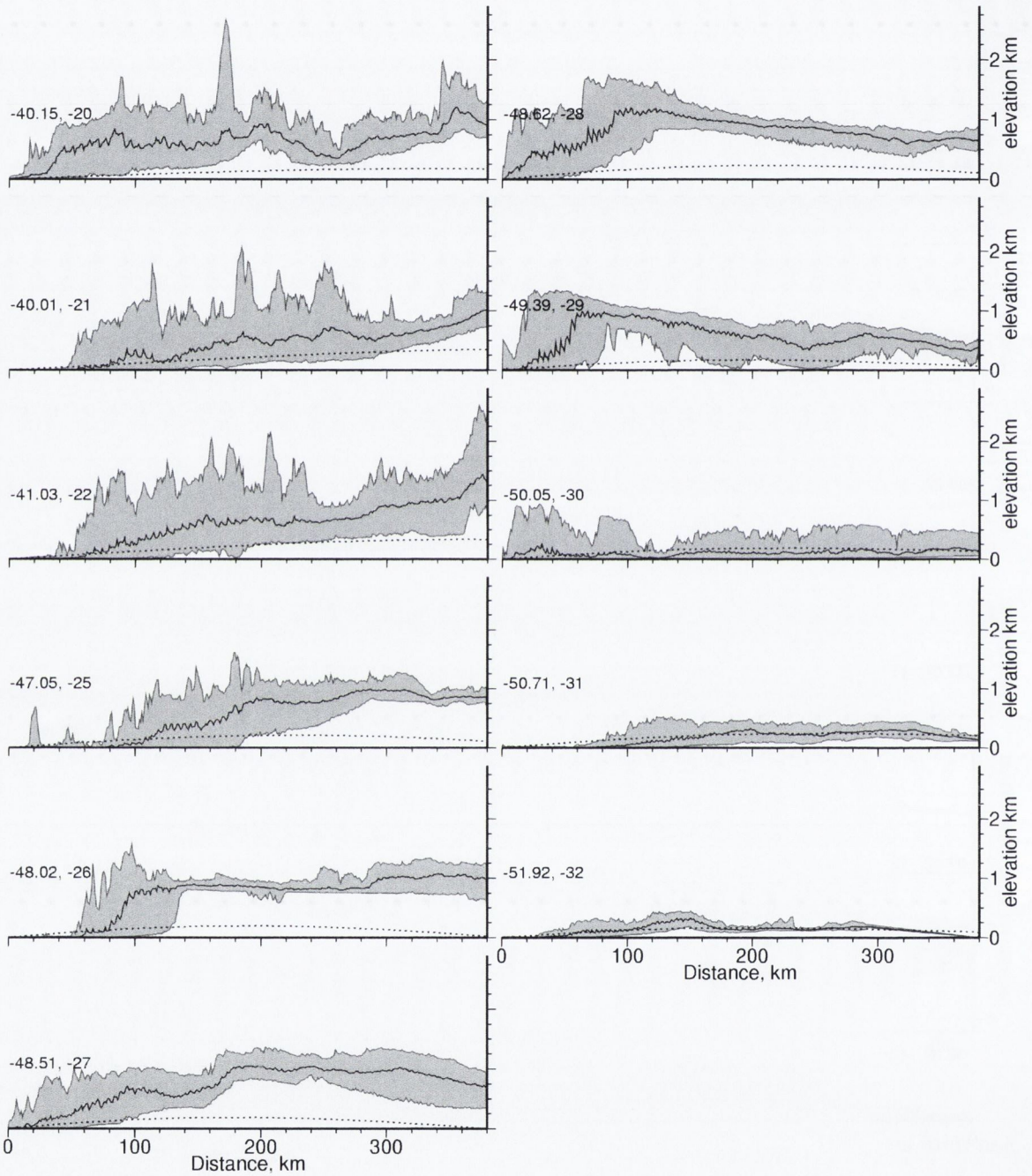


Fig. 4.24: Swaths of South America in a East-West direction. Dashed line shows increase an long wavelength free-air gravity parallel to centre of swath

4.5 Hypsography of the World

4.5.1 Background

Hypsometry illustrates the distribution of elevations within a defined area, usually on the surface of Earth. Hypsometric curves is a plot of the fraction of area in a region that is below a given height, normalised relative to maximum area and elevation. Hypsometric integrals measure the ratio of area beneath the hypsometric curve to the total graph area (Strahler, 1952) and have been used to characterise the hypsometry of regions ranging from individual catchments (e.g. Strahler, 1952) to entire continents (e.g. Harrison et al., 1983). Although by its definition the hypsometric integral can fall anywhere between 0 and 1, it has been noted in fluvial landscapes that the it generally varies between 0.3 and 0.6 (Brocklehurst and Whipple, 2004).

Dynamic topography on the surface of Africa has been documented up to 1,350 m (Lithgow-Bertelloni and Silver, 1998) and the average component of dynamic topography on continents is probably less than 1 km. Landmasses affected by converging plate tectonics have large areas uplifted in excess of 2,500 m with peaks sometimes reaching 6,000 to 8,000 m. Therefore large regions of dynamic topography effecting continent hypothetically cause a larger proportion of a continent to be moderately elevated and cause a bulge in the hypsometric curve. Africa's hypsometric curve resembles that of a high plateau and has been described as distinctly different to all other continents (Bond, 1978). Comparisons between the hypsometric curve of Africa and South America have been used to emphasise the unusually large area that is moderately elevated (Burke, 1996).

Hypsometric curves and integrals can be used to interpret the degree of dissection

of a landscape and the relative landform age. Convex-up curves with high integrals are characteristic for youthful, undissected landscapes while smooth, s-shaped curves are typical of more mature landscapes (Figure 4.25). Concave-up curves typify old and deeply dissected landscapes (Strahler, 1952). Hypsometry of a catchment with differing values have been also interpreted as a result of varying erosion processes. In particular, the differences in hypsometry between fluvial and glacial regions have been highlighted (e.g. Montgomery et al., 2001; Brocklehurst and Whipple, 2004). Montgomery et al., (2001) suggested that the varying hypsometry in catchments was due to the dominant erosional process in the region. The study of the hypsometric curves in different zones across the Andes showed that the primary process acting in a region, either fluvial, glacial or tectonic controls the basin morphology. The Andes were divided into 3 climatically controlled zones the northern, central and southern Andes. In the northern Andes high precipitation rates give rise to normal fluvial erosion rate, maintaining a narrow mountain range and resulted in a concave-up hypsometric curves. In the central Andes region low erosion rates outside major river valleys, allowing tectonic processes to dominate the region and leading to crustal thickening by tectonic wedge propagation. hypsometric curves of catchments in the central region are nearly linear to convex-up. In the southern Andes glaciers selectively erode the higher regions of the mountain range but results in excess area in the region elevated below the glacial limit and created a shoulder in the concave-up hypsometric curve. Brocklehurst and Whipple (2004) found that the position of equilibrium-level altitude (ELA) within the drainage basin is the dominant variable in determining the hypsometry of a basin. The ELA refers to the average elevation at which ablation (removal of snow by evaporation and melting) balances snow accumulation and is often referred to as the snow-line. However once the ELA falls below a critical level, the glaciers deeply scour below the ELA lowering the hypsometric curve and integral (Figure 4.25).

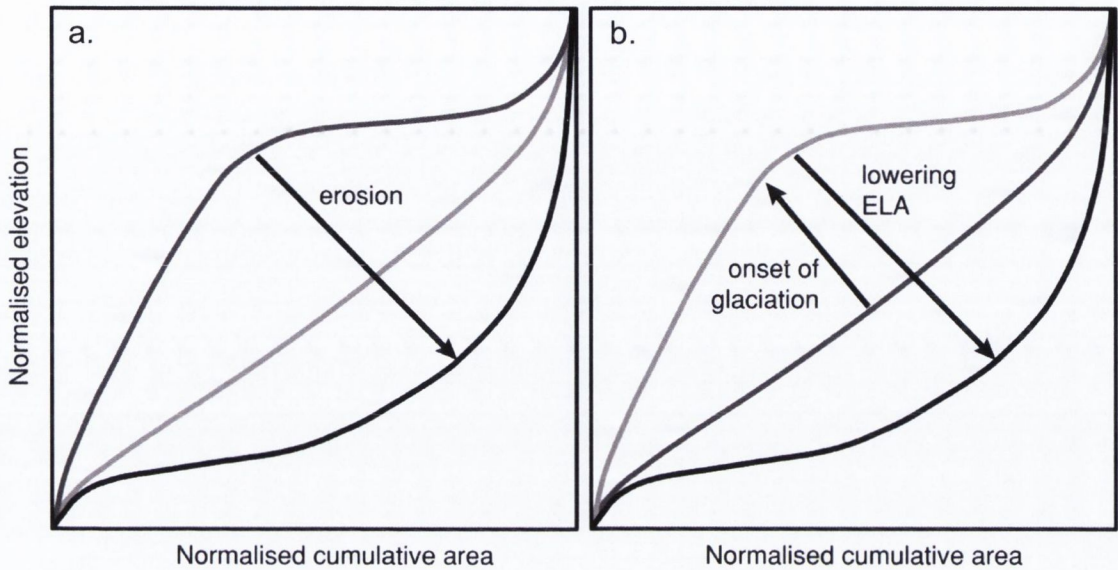


Fig. 4.25: Cartoon to illustrate the progressive evolution of hypsometric curves in glacial and fluvial landscapes redrawn from Brocklehurst and Whipple (2004). (a) Progression of hypsometric curves of a fluvial landscape, after Strahler (1952), from a youthful (dark grey), through a mature equilibrium stage (light grey) to a very mature 'monadnoc' stage (black) (b) Hypsometric curves illustrating the progression as glaciation modifies an initially fluvial landscape (dark grey). Initiation of cirque glaciers associated with a high equilibrium-level altitude (ELA) will raise the hypsometric curve and integral (light grey). Subsequent lowering of the ELA and development of large valley glaciers will lower the hypsometric curve back through its original position, to a significantly lower position (black).

4.5.2 Methodology

Hypsometric curves were calculated for the different continents on earth for 100 m elevation intervals using a 5 minute resolution DEM (Figure 4.26). SRTM-plus 30 second data was sampled to create a 5 minute global resolution DEM. In general, for the purposes of this study we divided the globe into regions with a landmass greater in area than Madagascar that was separated from other landmasses by a large expanse of water (Figure 4.26) and/or a tectonic plate boundary. For example, Greenland although not considered a continent in its own right, was considered separately to North America

because it was a large landmass (nearly four times the area of Madagascar) that is separated from North America by a substantial body of water, Baffin Bay. Greenland was also considered a passive margin continent as the region contains no destructive boundaries. The Australian landmass was considered separately to the the Island of New Guinea (Papua is a province of Indonesia and Papua New Guinea) and the North Island in New Zealand both areas of subduction that are separated from Australia by bodies of water. The islands of Indonesia were also regarded as an independent landmass. The hypsometric curves for the landmass as outlined above can be compared with the hypsometric curves of the regions above sea level of the various tectonic plates in Figure 4.26.

Most of Greenland and Antarctica are covered with thick sheets of ice, which smoothes out morphological features and adds up to 3 km of elevation to the original elevation of the bedrock. Therefore correcting the topography for ice thickness and ice loading in Greenland and Antarctica is important for any morphological analysis. This was done using two datasets for the different regions. The ice thickness grid for Greenland was generated using data with a 5 km resolution based on approximately 700,000 data points collected in the 1990s from a University of Kansas airborne ice penetrating radar (Bamber et al., 2001). The ice thickness grid for Antarctica was generated using data compiled by the BEDMAP project using terrestrial methods of measurement, primarily radar and seismic sounding to produce a model of the thickness of the Antarctic Ice Sheet (Lythe et al., 2000). The ice thickness data has resolution of 5km but resolution is only justified by the original data density only over a few parts of the ice sheet and therefore the overall resolution of the dataset is less.

Ice thickness datasets were sampled at a resolution of 5 minutes, for the purpose of measuring the hypsometry of Greenland and Antarctica. To obtain the current bedrock elevation, the ice thickness is taken away from the surface elevation of the

region. Isostatic depression, caused by long-term changes in the ice mass loading of the Earth's crust, is adjusted to restore the bedrock elevations in the absence of the ice sheet. Assuming a mean densities of 3370 kg m^{-3} and 910 kg m^{-3} for the mantle and ice respectively, the amount of adjustment needed is $910/3370$ times the ice thickness or just under a third of the thickness of the ice.

Strahler (1952) suggested there was a connection between the hypsometry of a basin and the stage of evolution the basin had reached, and that the hypsometric integral decreased as the landscape matured after a period of orogeny. The regions of the continents were divided according to the age that the continental crust underwent a major crust-forming events (Figure 4.3). The hypsometric curves of each of the crustal ages for each continent were plotted out to establish if there is a relationship between the hypsometry and the last major tectonic event of the region (Figure 4.27). In addition, the hypsometric integral was calculated for each of the curves (Figure 4.30). Pike and Wilson (1971) proved mathematically that the hypsometric integral (HI) equated the elevation-relief ratio, E, so that:

$$HI = \frac{H_{mean} - H_{min}}{H_{max} - H_{min}} \quad (4.1)$$

where H_{mean} , H_{max} and H_{min} are the mean, maximum and minimum elevations of the basins, respectively. The elevation-relief ratio has the advantage of being easier to numerically obtain than the hypsometric integral and therefore this equation was used to calculate the HI of the hypsometric curves for this study.

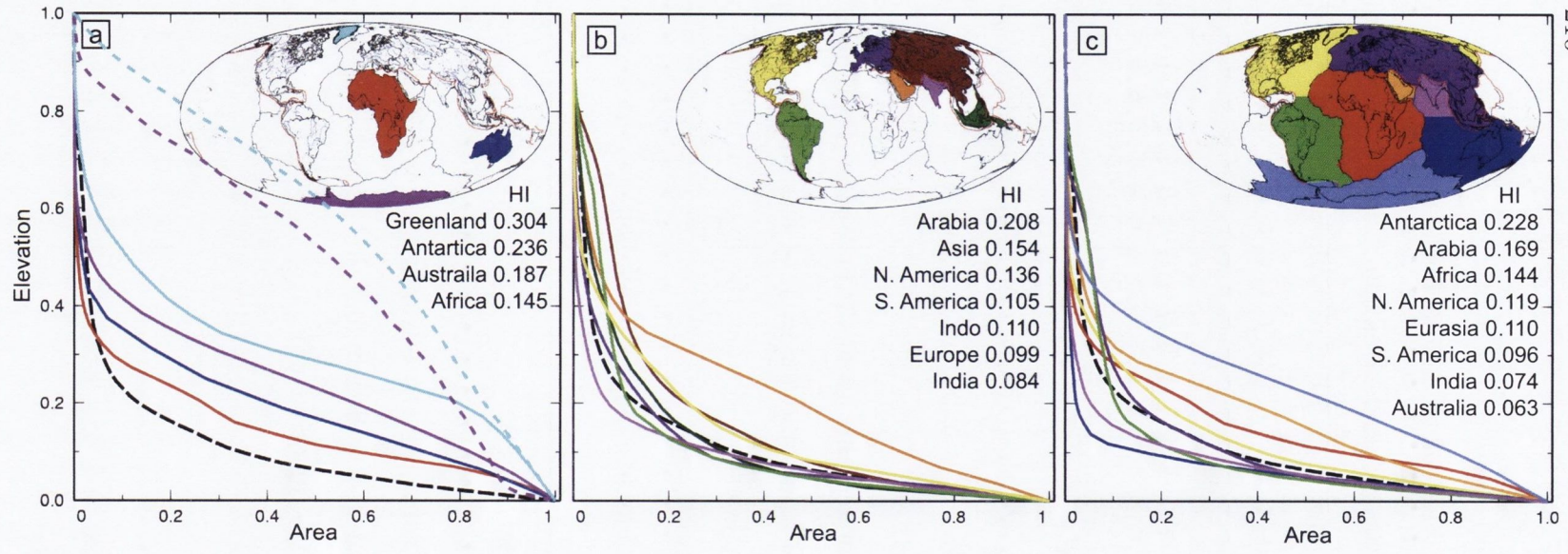


Fig. 4.26: Hypsometric curves of landmasses that contain (a) no destructive plate boundaries (b) destructive plate boundaries. (c) hypsometric curves of tectonic plates. Dashed black curve represents the global hypsometric curve. The colours of the hypsometric curves relate to the regions on global map filled in with the same colour. Topography has been corrected for ice thickness and loading in Greenland and Antarctica. The dashed coloured hypsometric curves represent Greenland and Antarctica before they were corrected for ice cover. The hypsometric integrals, HI, for each of the curves are listed on the right-hand side of each graph.

4.5.3 Results

Hypsometric curves of regions affected by positive gravity anomalies have a higher proportion of area with elevations of between 0.75 and 1.5 km when compared with other continental regions of the world (Figure 4.28). Similarly, there is a positive linear correlation between increasing long wavelength free-air gravity and the hypsometric integral for the region (Figure 4.29). At high long wavelength free-air gravity values an inflection point at ~ 1 km is identified between the concave upward curve of higher elevations and the convex upward curve at lower elevations.

There appears to be no strong relationship between the HI of a region and the last major tectonic event that has affected the crust (Figure 4.30). In general cratons of over 3000 Ma seem to have some of the highest HI values and vary between 0.15 and 0.65, while the HI of crust that has recently been deformed in the past 50 Ma usually falls between 0.12 and 0.35. HI values regardless of the crustal age tend to be higher for landmasses with no destructive boundaries, than landmasses that have tectonically active boundaries.

The hypsometric curve of all landmasses on the surface of the earth plots as a concave-up shape, with a gentle slope at low elevations, which steepens rapidly at higher elevations. The majority of landmasses on earth with large subduction zones such as South America, North America and Indonesia share similar hypsometric curves and vary little from the global hypsometric curve (Figure 4.26b). This similarity may be a result of large regions of land elevated at moderate and low elevations, and narrow ranges of mountains created by subduction processes having high elevation.

The south west edge of the Arabian plate, along the Red Sea, forms a divergent boundary with the African Plate. Much of the south west region of the Arabian landmass

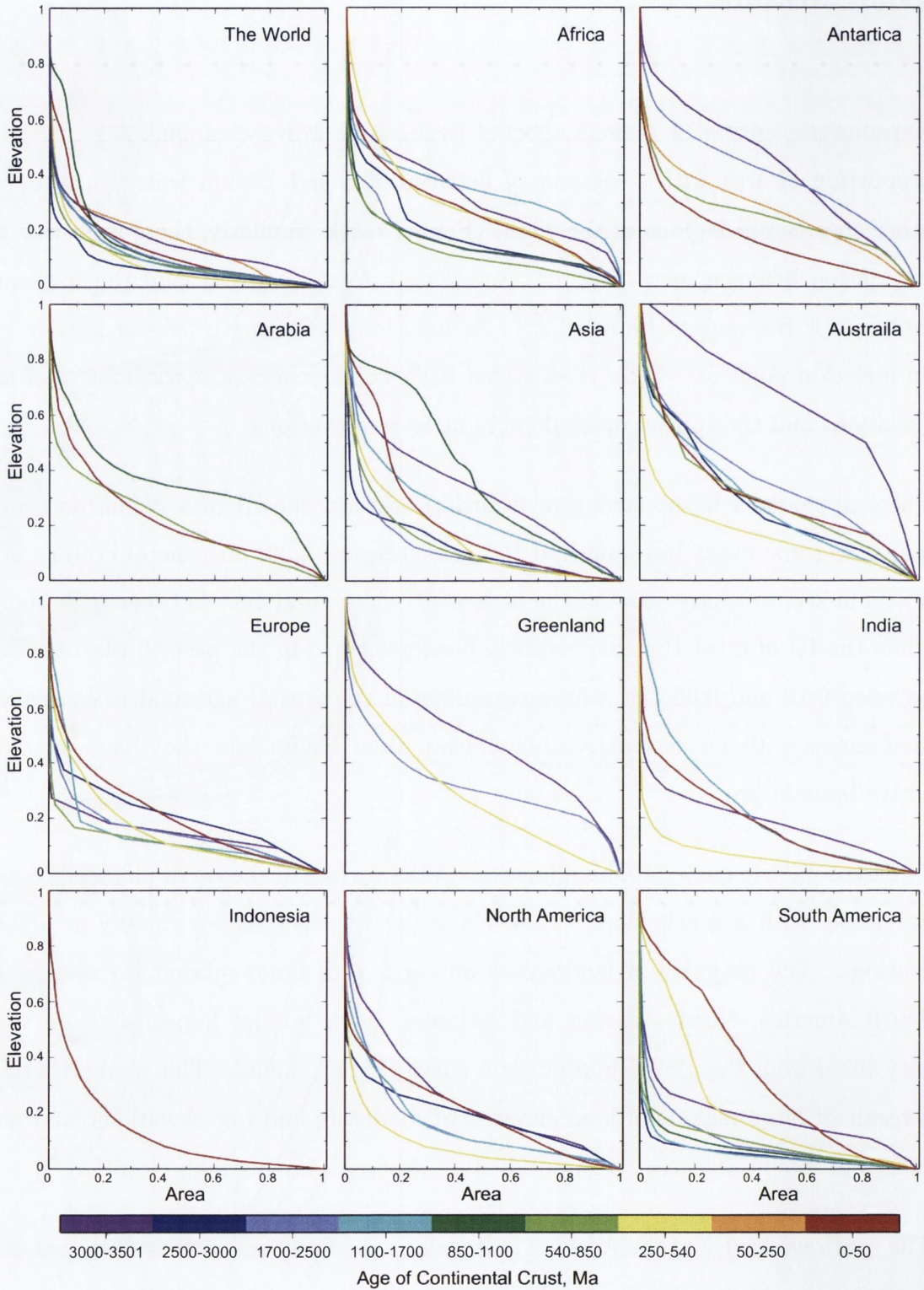


Fig. 4.27: Hypsometric curves of regions with different crustal ages for each of the landmasses

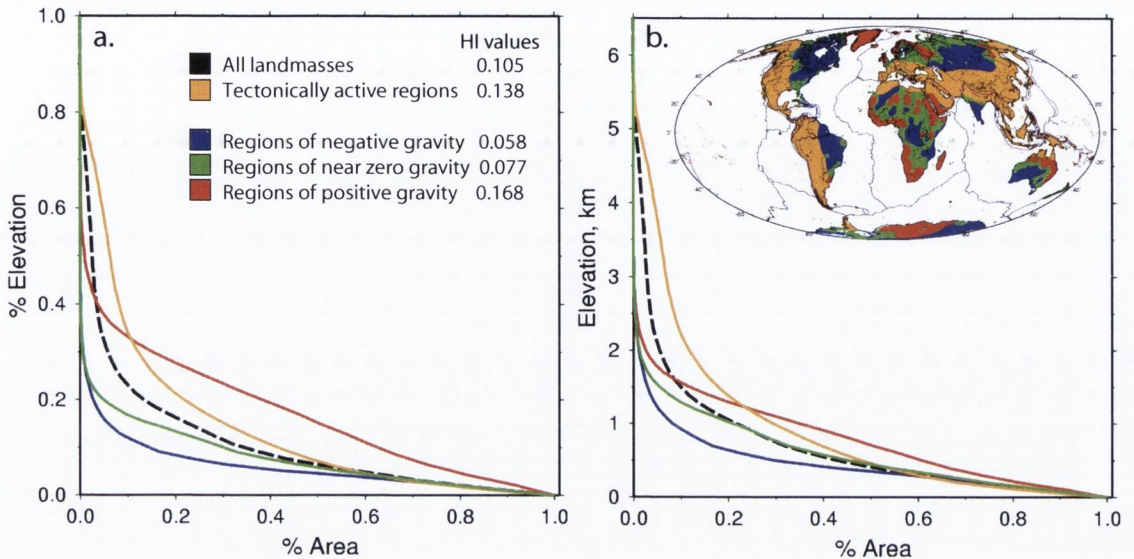


Fig. 4.28: Hypsometric curves and integrals comparing regions associated with different long wavelength free-air gravity anomalies. Areas that are effected by present day tectonic processes are separated. Plot (a) uses elevation as a percentage of the maximum elevation; Plot (b) uses absolute elevation in km.

reaches elevations of over 1,000 m and, this region of high topography extends into the plate interior. Seismic tomography and anisotropy of the mantle below the Red Sea suggests topography dynamically supported by large-scale viscous flow in the mantle which is responsible for the dramatic tilting of the Arabian platform (Daradich et al., 2003; Hansen et al., 2006). The uplifted south west region is dominated by the Arabian Shield, which is dated as between between 850 and 1,100 Ma (Figure 4.3). This hypsometric curve that relates to the 850–1,100 Ma interval in the Arabian land-mass has an inflection point, convex up at lower elevations and concave down at higher elevations (Figure 4.26) and a relatively high hypsometric integral of 0.36, when compared to the hypsometric integrals of the younger crust in the Arabian land-mass (Figure 4.26).

Broad regions of tectonically uplifted areas due to continental collision such as the portion of the Asian landmass in the Himalayas contribute to an increase in the area of the continent at greater elevation (Figure 4.26b). The hypsometry of the Arabian land-

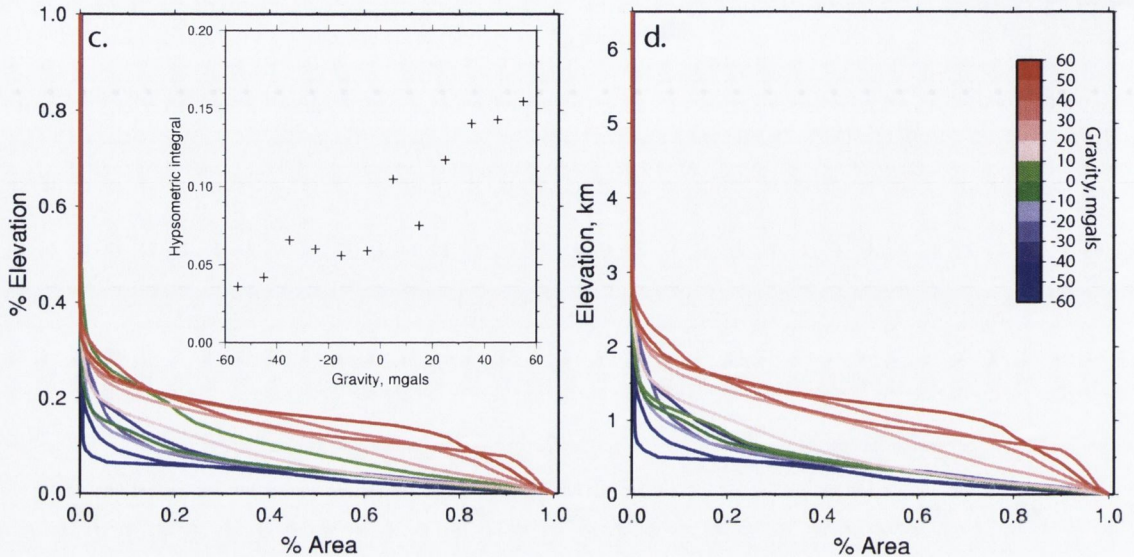


Fig. 4.29: Hypsometric integrals compare regions of the earth with similar long wavelength free-air gravity anomaly. Regions are divided into intervals of 10 mgals, from a minimum of -60 mgals to a maximum 60 mgals. Plot (a) uses elevation as a percentage of the maximum elevation; Plot (b) uses absolute elevation in km.

mass deviates from the typical hypsometric curves of tectonically active landmasses and a larger than average area is elevated at medium and lower elevations. The Zagros fold belt, formed by a complex convergent boundary of the Eurasian Plate and Arabian plate, creates a narrow mountain belt along the north-eastern border of the Arabian landmass. The Zagros mountains in the north-east of the Arabian landmass are elevated above 500 m, with peaks of 3,000 m.

The hypsometry of landmasses with no convergent boundaries vary from the hypsometry of the global average (Figure 4.26a). In general landmasses surrounded by passive margins appear to have a large area at low to medium elevations and high HI values when compared with most other landmasses with convergent boundaries and the hypsometry of the global average. The African and Australian landmasses follows this trend with a larger area at low and medium elevations and a higher HI than the global average. When we compare the hypsometric curve of the Australian landmass with

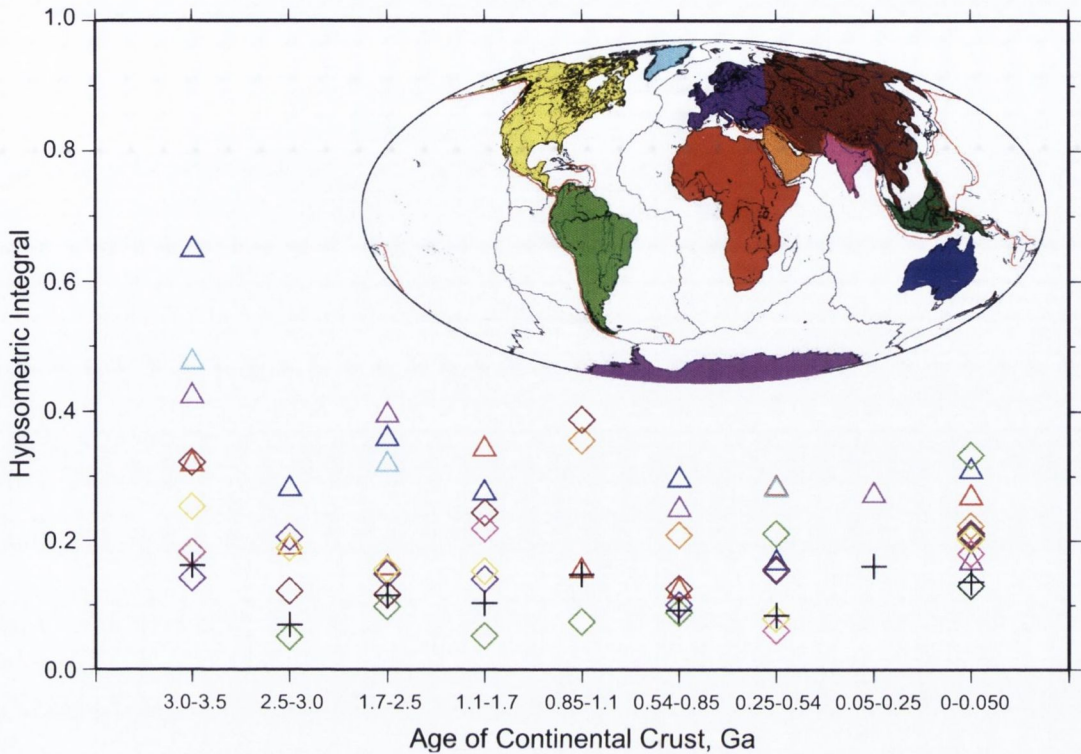


Fig. 4.30: Hypsometric integrals of regions with different crustal ages for each of the landmasses. Black crosses represent the HI for the world, triangles represent landmasses with destructive plate boundaries, diamonds represent landmasses that contain no destructive plate boundaries. The colour of the symbols relate to the regions filled in with the same colour

the Indo-Australian Plate, they are substantially different (Figure 4.26). The north-eastern margins of the Indo-Australian Plate has destructive plate boundary with the Pacific Plate, which resulted in the active uplift of the Island of New Guinea and the North Island of New Zealand. The central east-west mountain range of the Island of New Guinea over 1600 km in total length rising up to 4,884 m high, and is formed as a result of a collision between the northern margin of Australia with an island chain during the last 37 myrs (Audley-Charles, 1991). Mount Ruapehu is an active strato-volcano at the southern end of the Taupo Volcanic Zone in North Island, New Zealand with peaks reaching 2,797 m. In contrast, the Australian mainland is the lowest and flattest continental landmass on Earth. Its highest peak is Mount Kosciuszko reaching

2,228 m. The elevation of these tectonically active regions may be what is causing the differences of the hypsometric curves between the Indo-Australian Plate and the Australian continent and illustrates that the shape of hypsometric curves are probably sensitive to small areas of high elevation.

The Antarctic continent, and in particular East Antarctica has an unusually high topography, even after it is adjusted for ice cover and isostatic effects caused by the mass of the ice. The modal height of East Antarctica is 700 m higher than that of the global ensemble of continents (Cogley, 1984). In addition, the hypsometric curve of Antarctica has a pronounced convex-up shape and the hypsometric integral is unusually high (Figure 4.26). This unusual hypsometry and high topography of Antarctica has been attributed to recent hotspot epeirogeny (Cogley, 1984) or low erosion rates during the time it has been covered in ice (Hay and Southam, 1977). The hypsometric curve of Greenland plots with two inflection points and is convex-up at lower elevations and concave-up at higher elevations. The Greenland landmass also has the highest hypsometric integral of all the landmasses.

4.5.4 Discussion

4.5.5 High elevation margins

Many high-elevation passive margins have associated positive long wavelength free-air gravity anomalies elongated parallel to the margin. Although escarpment evolution models suggest that high topography of the margin may have existed since rifting or shortly after continental break-up, there is evidence that many of the margins have experienced uplift during the Cenozoic (Table 4.1). Many of the world highest passive margins occur along cratonic belts (Figure 4.3). The transition beneath thick cratonic

lithosphere and thin oceanic lithosphere is thought to drive edge-driven convection in the upper mantle (King and Anderson, 1998; King and Ritesma, 2000). Edge-driven convection may partially support the elevations of passive margins along cratonic belts. There appears to be no clear relationship between margin/escarpment height and the age of the oceanic lithosphere along the associated margin (Table 4.1).

Topographic swaths and predicted dynamic topography of margins suggest mantle convection may have caused tilting and/or uplift of the margins resulting in recent rejuvenation along the margin (Figure 4.12 to 4.24).

4.5.6 Hypsometry of the continents

There is a positive linear correlation between average long wavelength free-air gravity and the hypsometric integral for continents (Figure 4.29). Hypsometric curves of regions with positive gravity anomalies have a higher proportion of area with elevations of between 0.75 and 1.5 km when compared with other continental regions of the world (Figure 4.28). This is consistent with the hypothesis that positive dynamic topography would be reflected in the hypsometry of continents by increasing the proportion of the area of higher elevations in the region of hundreds of meters.

There appears to be no strong relationship between the HI of a region and the last major tectonic event to affect the crust (Figure 4.30). However this may be due to the simplification of the map used, which assigns the age of large regions of the continents according to the last major tectonic event to take place in that region.

In general, landmasses with no regions that have been deformed by plate tectonics tend to have higher than average HI and larger areas at medium to low elevations. Montgomery et al. (2001) and Brocklehurst and Whipple (2004) outlined the importance

that erosional process might play in the hypsometry of a catchment and therefore we cannot rule out that the effects that glaciation has on an entire landmass as a whole may be responsible for the unusually high hypsometric integrals of Greenland and Antarctica. Greenland, Antarctica, Arabia, Australia and Africa all have high HI values (Figure 4.26).

4.6 Conclusions

- Many high-elevation passive margins have associated positive long wavelength free-air gravity anomalies elongated parallel to the margin indicating that the high-elevation passive margins may be partially supported by mantle convection. There is geological evidence in published literature for recent rejuvenation along many of the margins studied in this section.
- Many of the world highest passive margins occur along cratonic belts. However there appears to be no clear relationship between maximum margin height and the age of the oceanic lithosphere along the associated with the margin.
- There appears to be a positive linear relationship between increasing hypsometry integrals and long wavelength free-air gravity. It is likely that dynamic topography can be identified in the hypsometry of a continent.
- The high HI values and hypsometric curves of the Greenland, Antarctica, Arabia, Australia and Africa landmasses indicates the presence of positive dynamic topography.

Chapter 5

Discussion and Conclusions

5.1 Introduction

Careful examination of geomorphology reveals that it is possible to identify the effects of mantle convection in the topography of Africa. This study has concentrated on (1) geomorphic analysis of detailed topographic models and (2) the relationship between topography and free-air gravity at long-wavelengths. The analysis would not have been made possible without the availability of recently released satellite topography and gravity data. In south-west Central Africa, rates of dynamically supported vertical motions can be estimated, and compared with rates predicted from seismic tomographic data and numerical convection models.

In response to the main aims of this study as outlined in section 1.2, the conclusions are as follows:

- The geomorphology of the south-west region of Central Africa indicates it has

recently experienced uplift of up to 800 m. Measured uplift rates centred on the Bie Plateau are $\sim 40 \text{ m Myr}^{-1}$, slightly higher than those estimated by published dynamic topographic models.

- A strong linear correlation exists between sections of palaeosurfaces in Namibia and Angola, revealing an admittance of 40 mgals km^{-1} , consistent with dynamically supported topography. The elevation of main palaeosurfaces in southern Africa did not show significant linear correlation with free-air gravity. This does not preclude that the south African topography is affected by mantle convection. Pronounced topography prior to deformation and/or deposition or erosion occurring after deformation may have masked the relationship between topography and gravity.
- Dynamic topography is particularly well developed on the African plate but is probably present on many continents on Earth. High continental passive margins are common feature on Earth. The evolution of escarpments suggest that high inland topography is formed soon after continental break up. However, convective currents in the upper mantle below the edge of continental plates may contribute to the topography of passive margins. The linear relationship between HI values and long wavelength free-air gravity indicate that that dynamic support is significant worldwide, and not just in Africa (Figure 4.29).

5.2 Implications of findings on wider issues

This study looked at direct observations of dynamic support rather than just theoretical calculations. In contrast, the calculated dynamic support models based on tomography (Section 1.3.3) or Slab models (Section 1.3.4) contain many assumptions.

The main assumption is the mantle radial viscosity structure. Small changes in the viscosity structure will make big differences in the predicted dynamic support. The spatial extent of the predicted uplift pattern largely depends on what part of the mantle the model uses to control dynamic topography. For example Gurnis et al. (2000) concluded the the lower mantle was controlling dynamic topography. The resolution of the seismic images may also effect the dynamic topography prediction although the resolution of more recent models is much improved. Results from this study therefore provide a useful constraint for numerically predicted dynamic topography.

Predicting vertical motions through geomorphological analysis of river profiles and palaeosurfaces also provides spatial resolution. This spatial resolution of vertical motion due to the convecting mantle has been achieve in the oceans before, but has been more difficult to obtain on continents. Most admittance calculations were done in the spectral domain, which gives a single value for the analysis region. For example admittance calculated in Central Africa in the spectral domain is consistent with dynamic support of the topography in that region. However it provides no information as to which features are providing this signal (Figure 1.4).

Since it was possible to date specific geomorphological features caused by dynamic support it was possible to provide estimates for changes in dynamic support. Tomography models only provide a snap shot of the velocity structure of the present day mantle. The measured rates of change of dynamic topography could be used to constrain rates of mantle convection.

5.3 Implications for southern Africa

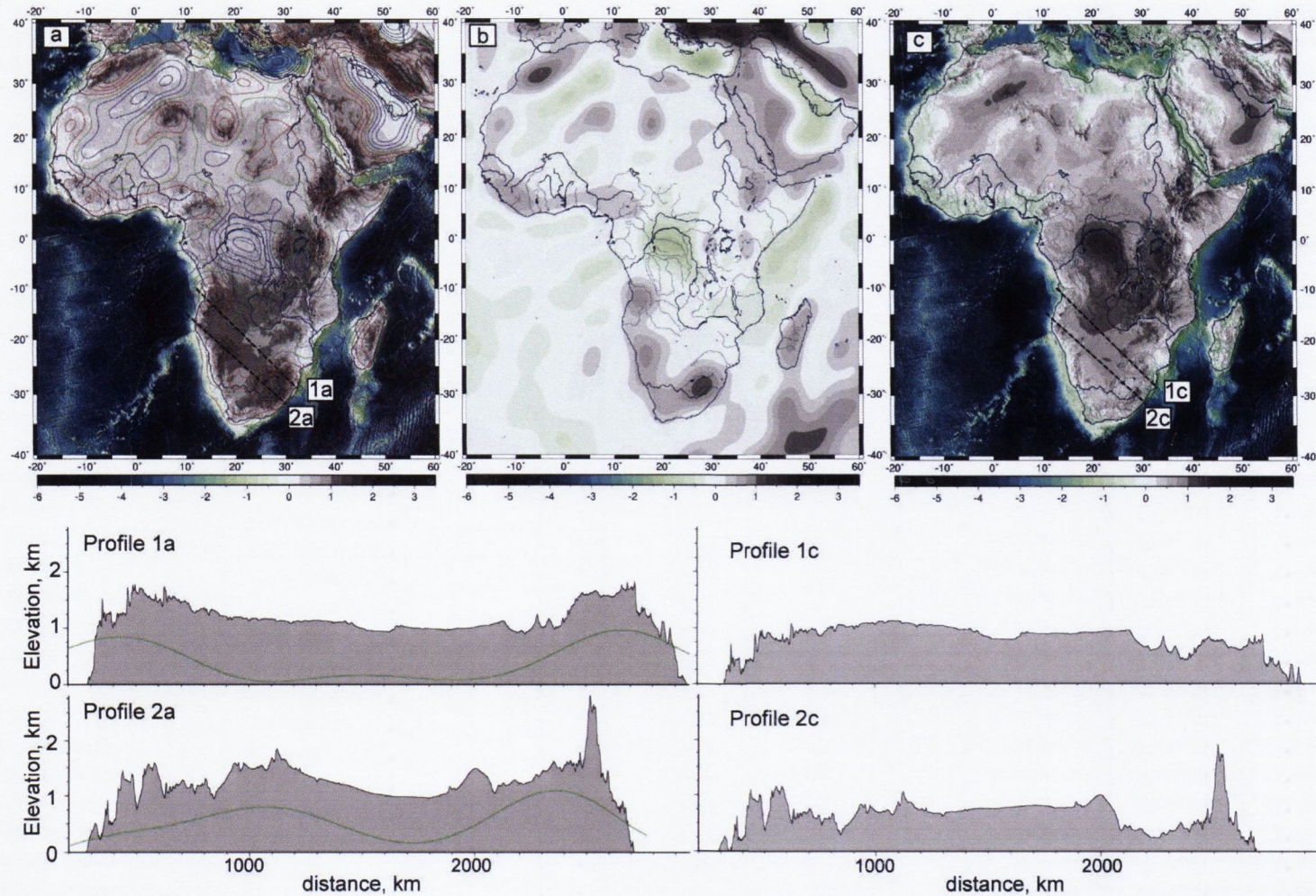


Fig. 5.1: (a) Present day topography of Africa, (b) Dynamic topography of Africa as predicted by long wavelength free-air gravity using an admittance of 40 mgals km^{-1} (c) Dynamic topography subtracted from present day topography. 1a and 2a: Cross-sections of the topography of Africa. Green lines represent the dynamic component of the topography as estimated in map (c). 1c and 2c: Cross-sections of the topography of Africa with the dynamic component removed.

Southern Africa remains highly elevated even after removing the dynamic component of the African topography as predicted by long wavelength topography (Figure 5.1). Profiles through the residual topography reveal shorter wavelength topographic features such as the escarpment would survive, however the topography inland of the escarpment is almost level at 1 km. Partridge and Maud (2000) described the Miocene landscape as dominated by the African planation surface which lay at elevations of 500 to 600 m above sea-level inland of the escarpment, similar to what is seen in the cross-sections 1c and 2c in Figure 5.1. Large sedimentary basins such as the Kalahari Basin and the Congo Basin stand out as positive features, which may be explained partially by recent deposits infilling the depressions. The Congo Basin is elevated at up to 1.5 km after dynamic topography is removed. Mesozoic–Recent sediments account for ~ 1 km occupying the present-day Congo Basin (Hartley and Allen, 1994; Giresse, 2005). Dynamic topography associated with the Congo Basin may therefore be long lived.

5.4 Problems

The spatial extent of the predicted uplift is not consistent with dynamic topography predicted from tomographic models (Figure 1.5 and 1.7). Conrad and Gurnis (2003) predict uplift began southern Africa at ~ 30 Ma. However they estimate an uplift pattern with the higher rates highest occurring in the centre of the Kalahari. Section 5.2 outlines some of the issues that may impact on the spatial resolution of dynamic topography predicted from tomographic models.

The Post-African depositional surface the southern Congo River catchment shows a strong linear correlation on a gravity elevation plot (Figure 2.16). However, most other gravity-elevation plots of other palaeosurfaces display weak correlation. In some

cases lack of a significant gravity topography correlation can be attributed to deposition or erosion occurring after deformation (e.g. the surface of the central Kalahari Basin). Surfaces such as the Gondwana and African surface are likely to have had a pronounced topography prior to deformation, which affected the trends on that data plots. However, in general using the elevation of palaeosurfaces correlated over large regions did not yield clear results between topography and gravity. Adjusting for residuals of topography within the surface and more careful corrections for the incision of modern drainage in a smaller area such as the regions identified in Namibia and Angola may improve results (Figure 3.38 and 3.39).

5.5 Further work

Further to the conclusions drawn from in this dissertation, there is significant potential for further research arising from this study.

- Quantification of sediment flux for the rivers draining into the Gulf of Guinea and Tanzania and rift grabens in East Africa. Sediment flux estimates for the the rivers draining into the Gulf of Guinea were estimated using very few seismic lines (e.g. Leturmy et al., 2002; Walford et al., 2003) and more accurate measurement would improve the understanding of how the central African drainage system evolved. In addition, sediment flux in Tanzania and rift grabens in East Africa could be used to estimate the response of the sediment flux to uplift of the East African Rift.
- The age of the Sable Ogres is not carefully constrained because of lack of fossiliferous evidence. A cosmogenic isotopes study of the Post-African surface in Angola

be used to estimate the age of the surface. The timing of uplift events affecting the Bie Plateau may benefit from an AFTA analysis of the Kwanza river valley.

- Recent research has improved structural models of the continental plates (e.g. Artemieva et al., 2006; Priestley et al., 2006). These models could be used to assess the impact of crust and lithospheric thickness on free-air gravity anomalies in Africa.

References

- Anderson, R. N., McKenzie, D. P. and Sclater, J.G. 1973. Gravity, bathymetry and convection within the Earth. *Earth Planet. Sci. Lett.*, **18**, 391–407.
- Artemieva, I.M, 2006. Global 1° x 1° thermal model TC1 for the continental lithosphere: Implications for lithosphere secular evolution. *Tectonophysics*, **416**, 245–277
- Audley-Charles, M. G. 1991. Tectonics of the New Guinea Area *Annual Review of Earth and Planetary Sciences* **19**, 17–41.
- Bamber J., S. Ekholm, and W. B. Krabill, 2001. A new, high-resolution digital elevation model of Greenland fully validated with airborne laser altimeter data. *J. Geophys. Res.*, **106**, 33773–33780.
- Bannister, S. C., Ruud, B. O., and Husebye, E. S. 1991. Tomographic estimates of sub-Moho seismic velocities in Fennoscandia and structural implications. *Tectonophysics*, **189**, 37–53.
- Behrendt, J. C. and Cooper, A. K. 1991. Evidence of rapid Cenozoic uplift of the shoulder escarpment of the West Antarctic rift system and a speculation on possible climate forcing. *Geology*, **19(4)**, 315–319.

- Bierman, P.R. and Caffee, M. 2001. Slow rates of surface erosion and sediment production across the Namib desert and escarpment, southern Africa. *Am. J. Sci.*, **301**, 326–358.
- Bishop P. 2007. Long-term landscape evolution: linking tectonics and surface processes
Long-term landscape evolution. *Earth Surf. Process. Landforms*, **32**, 329–365
- Bond, G. 1978. Evidence for Late Tertiary uplift of Africa relative to North America, South America, Australia and Europe. *Journal of Geology*, **86**, 47–65.
- Brocklehurst, S. H. and Whipple, K. X. 2004. Hypsometry of glaciated landscapes. *Earth Surf. Proc. Landf.*, **29**, 907–926.
- Brooks, C.K. 1985. Vertical crustal movements in the Tertiary of central East Greenland: a continental margin at a hot spot. *Z. Geomorph. N.F.*, **54**, 101–117.
- Brown, R. W., Gallagher, K. and Duane, M. J. 1994. A quantitative assessment of the effects of magmatism on the thermal history of the Karoo sedimentary sequence, *African Journal of Earth Science*, **18**, 227–243.
- Brown R. W., Gallagher K., Gleadow A. J. W. and Summerfield M. A. 2000. Morpho-tectonic evolution of the South Atlantic margins of Africa and South America. *In: Summerfield M. A. (ed) Geomorphology and global tectonics*, Wiley 255–281
- Brown, R., Gallagher, K., Raab, M., Summerfield, M. 2005. Raising southern Africa: quantifying the erosional response of the African superswell. *Geophysical Research Abstracts*, **7**,
- Brown R. W., Rust D.J., Summerfield M. A., Gleadow A. J. W. and DeWit M. C. 1990. An early Cretaceous phase of accelerated erosion on the south-western margin of Africa: evidence from apatite fission track analysis and the offshore sedimentary record. *Nuclear Tracks and Radiation Measurements*, **17**, 339–350.

- Brown R. W., Summerfield, M. A. and Gleadow, A. J. W., 1994. Apatite fission-track analysis: its potential for the estimation of denudation rates and implications for models of long-term landscape development. *In: Kirkby M. J. (eds) Process Models and Theoretical Geomorphology*, Wiley, New York. 24–53.
- Brown R. W., Summerfield, M. A. and Gleadow, A. J. W., 2002 Denudational history along a transect across the Drakensberg Escarpment of southern Africa derived from apatite fission track thermochronology. *J. Geophys. Res.*, **107**, B12
- Buck, W.R. 1986. Small scale convection induced by passive rifting: the cause for uplift of rift shoulders. *Earth Planet. Sci. Lett.*, **77**, 362–372.
- Burke, K., and Wilson, J. T. 1972. Is the African plate stationary? *Nature* **239**, 387–390.
- Burke, K. 1996. The African Plate. *S. Afr. J. Geol.*, **99**, 341–409.
- Cahen, L., Lepersonne, J. 1952. Equivalence entre le Systeme du Kalahari du Congo belge et les Kalahari beds d’Afrique australe. *Mem. Soc. Belge Geol., Pal., Hydrol., Series 8* **4**, 63.
- Campbell, I. H., and Griffiths, R. W., 1990, Implications of mantle plume structure for the evolution of flood basalts *Earth and Planetary Science Letters*, **99**, 79–93.
- Cockburn, H. A. P., Summerfield, M. A. and Seidl M.A., 1999. Quantifying denudation rates on inselbergs in the central Namib Desert using in situ-produced cosmogenic ^{10}Be and ^{26}Al . *Geology* **27**399–402.
- Cockburn, H. A. P., Brown, R. W., Summerfield, M. A., and Seidl, M. A. 2000. Quantifying passive margin denudation and landscape development using a combined fission-track thermochronology and cosmogenic isotope analysis approach. *Earth Planet. Sci. Lett.*, **179**, 429–435.

- Coffin, M.F., Lawver, L.A., and Gahagan, L.M., 1998. Atlas of Paleogeographic Reconstructions, *Plates Progress Report No. 215-0798, University of Texas*
- Cogley, J. G. 1984. Deglacial hypsometry of Antarctica. *Earth Planet. Sci. Lett.*, **67**, 284–96.
- Cogley, J. G. 1985. Hypsometry of the continents. *Zeitschrift für Geomorphologie, supplementband*, **53**.
- Conrad, C. P. and Gurnis M. 2003. Mantle flow, seismic tomography and the breakup of Gondwanaland: Integrating mantle convection backwards in time. *Geochemistry, Geophysics, Geosystems*, **4**, 1031.
- Cox, K. G. 1989. The role of mantle plumes in the development of continental drainage patterns. *Nature*, **342**, 873–877.
- Crosby, A. 2006. *Aspects of the relationship between topography and gravity on the Earth and Moon*. Unpublished Ph.D. dissertation, University of Cambridge.
- Crosby, A., McKenzie, D. P., Slater, J. G. 2006. The relationship between depth, age and gravity in the oceans. *Geophysical Journal International*, **166**, 553–573.
- Crough, S. T., Morgan, W. J., and Hargraves, R. B. 1980 Kimberlites: their relation to mantle hotspots, *Earth and Planet. Sci. Letters*, **50**, 260–274.
- D'Agostino, N., Jackson, J.A., Dramis F. and Funiciello R., 2001 Interactions between mantle upwelling, drainage evolution and active normal faulting: an example from the central Apennines (Italy), *Geophys. J. Int.* **147**, 475–497.
- Daly, M. C., Lawrence, S.R., Diemu-Tshiband, K. and Matouana, B. 1992. Tectonic evolution of Cuvette Centrale, Zaire. *J. Geol. Soc. London*, **149**, 539–546.

- Daradich, A., Mitrovica, J. X., Pysklywec, R. N., Willet, S. D. and Fortre, A. M. 2003. Mantle flow, dynamic topography, and rift-flank uplift of Arabia. *Geology*, **31**, 901-904.
- Davis, W. M. 1899. The geographical cycle. *Geographical Journal*, **14**, 481-504.
- De Ploey, J., Lepersonne, J. and Stopps, G. 1988 Sedimentologie et origine des sables de la Serie des sables ocres et de la Serie des Gros polymorphes (Systeme du Kalahari) au Congo occidental. *Mus. Roy. Afrique Centr., Tervuren, Belgique*, **61**, 72.
- De Wit, M.J., 2003. Madagascar, heads it's a continent, tails its an island. *Annual Review of Earth and Planetary Sciences*, **31**, 213-248.
- Dixey F. 1942. Erosion cycles in central and southern Africa. *Trans. Geol. Soc. S. Afr*, **45**, 151-167.
- Dollar, E.S.J., 1998. Palaeofluvial geomorphology in southern Africa: a review. *Prog. Phys. Geogr.*, **22**, 325-349.
- Doornkamp, J.C., Temple, P.H., 1966. Surface, drainage and tectonic instability in part of southern Uganda. *Geogr. J.* **132**, 238-252.
- Doucoure , C.M. and de Wit, M.J. 2003. Old inherited origin for the present near-bimodal topography of Africa. *Journal of African Earth Sciences*, **36(4)**, 371-388.
- Duncan, R.A., Hooper, P.R., Rehacek, J., Marsh, J.S. and Duncan, A.R., 1997. The timing and duration of the Karoo igneous event, southern Gondwana. *Journal of Geophysical Research*, **102**, 18,127-18,138.

- Dunlevey, J.N., Ramluckan, V.R. and Mitchell, A.A. 1993. Secondary mineral zonation in the Drakensberg Basalt Formation, South Africa. *South African Journal of Geology*, **96**, 216–220.
- Dziewonski, A.M. 1984. Mapping the lower mantle: determination of lateral heterogeneity in P velocity up to degree and order. *J. Geophys. Res.* **89**, 5929–5952.
- Ebbing, J. 2007. Isostatic density modelling and Neogene reveals the "missing" root of the Scandes. *Norwegian Journal of Geology*, **87**, 13–20
- Ebbing, J. and Olesen, O., 2005. The Northern and Southern Scandes structural differences revealed by an analysis of gravity anomalies, the geoid and regional isostasy. *Tectonophysics*, **411**, 73–87.
- Fairhead, J. D. and Reeves, C. V., 1977. Teleseismic delay times, Bouguer anomalies and the inferred thickness of the African plate. *Earth planet. Sci. Lett.*, **36**, 63–76
- Fitton, J. G. 1987. The Cameroon line, West Africa: a comparison between oceanic and continental alkaline volcanism *In: Fitton J.G. and Upton B.G.J., (eds) Alkaline Igneous Rocks* Geol. Soc. London, Spec. Publ., **30**, 273–291.
- Fleming, A., Summerfield, M.A., Stone, J.O., Fifield, L.K. and Cresswell, R.G., 1999 Denudation rates for the southern Drakensberg escarpment, SE Africa, derived from in-situ-produced cosmogenic ³⁶Cl: initial results. *Journal of the Geological Society of London*, **156**, 209–212
- Forsyth, D.W., 1985. Subsurface loading and estimates of the flexural rigidity of the continental lithosphere. *Journal Geophysical Research*, **90**, 12623–12632.
- Gallagher K. and Brown R., 2009 Denudation and uplift at passive margins: the record on the Atlantic Margin of southern Africa, *Philos. Trans. R. Soc. Lond.*, **357**,

835–859.

- Gallagher, K., Brown, R. and Johnson, C. 1998. Fission track analysis and its applications to geological problems. *Ann. Rev. Earth Planet. Sci.*, **26**, 519–572.
- George, R., Rogers, N. and Kelly, S. 1998. Earliest magmatism in Ethiopia: Evidence for two mantle plumes in one flood basalt province. *Geology*, **26**, 923–36
- Gilchrist, A.R. and Summerfield, M.A. 1990. Differential denudation and flexural isostasy in formation of rift-margin upwarps. *Nature*, **346**, 739–742.
- Giresse, P. 2005 Mesozoic–Cenozoic history of the Congo Basin. *Journal of African Earth Sciences*, **43**, Issues 1-3, 301–315.
- Goldrick G, Bishop P. 1995. Differentiating the roles of lithology and uplift in the steepening of bedrock river long profiles: an example from southeastern Australia. *Journal of Geology* **103**, 227–221.
- Goudie, A.S. 1995. *The Changing Earth: Rates of geomorphological processes*. Blackwell.
- Grand, S.P., Van der Hilst, R.D., and Widiyantoro, S., 1997. Global seismic tomography: A snapshot of convection in the Earth *GSA Today* **7**, no.4, 1–7.
- Grekoff, N., 1958. Ostracodes du Bassin du Congo. III: Tertiaire. *Ann. Mus. Roy. Congo belgium*, **22**, 36.
- Gripp, A.E. and Gordon, R.G. 1990. Current plate velocities relative to the hotspots incorporating the NUVEL-1 global plate motion model. *Geophys. Res. Lett.*, **17**, 1,109–1,112.

- Guiraud, R. and Bosworth, W. 1997. Senonian basin inversion and rejuvenation of rifting in Africa and Arabia: Synthesis and implications to plate-scale tectonics, *Tectonophysics*, **282**, 39–82.
- Gunnell Y. 1998. The interaction between geological structure and global tectonics in multistoreyed landscape development: a denudation chronology of the South Indian shield. *Basin Research*, **10**, 281–310.
- Gurnis, M., Mitrovica, J.X., Ritsema, J., and van Heijst, H.J., 2000, Constraining mantle density structure using geological evidence of surface uplift rates: The case of the African Superplume. *Geochemistry, Geophysics, Geosystems*, **1**, 1525–2027.
- Hack J.T. 1957. Studies of longitudinal stream profiles in Virginia and Maryland. *United States Geological Survey Professional Paper*, **294-B**, 45–97.
- Hack J.T. 1973. Stream-profile analysis and stream gradient index. *Journal of Research of the US Geological Survey*, **1**, 421–429.
- Haddon, I.G. and McCarthy T.S. 2005. The Mesozoic-Cenozoic interior sag basins of Central Africa: Late Cretaceous-Cenozoic Kalahari and Okavango basins. *Journal of African Earth Sciences*, **43**, 316–333.
- Hambrey, M. and McKelvey, B. 2000. Major Neogene fluctuations of the East Antarctic ice sheet: stratigraphic evidence from the Lambert Glacier region. *Geology*, **28** 887–890.
- Hansen, K., Bergman, S.C. and Henk, B. 2001. The Jameson Land basin (east Greenland): a fission track study of the tectonic and thermal evolution of the Cenozoic North Atlantic spreading regime, *Tectonophysics* **331**, 307–339.

- Hansen S., Schwartz S., Al-Amri A., and Rodgers A. 2006. Combined plate motion and density-driven flow in the asthenosphere beneath Saudi Arabia; evidence from shear-wave splitting and seismic anisotropy. *Geology* **34**, 869–872.
- Harrison, C. G. A., Miskell, K. J. Brass, G. W. Saltzman, E. S. and Sloan, J. L. 1983. Continental hypsography. *Tectonics*, **2**, 357–377.
- Hartley, R.W. and Allen, P.A., 1994. Interior cratonic basins of Africa: relation to continental break-up and role of mantle convection. *Basin Res.* **6**, 95–113.
- Hartley, R., Watts, A. B. and Fairhead J. D. 1996. Isostasy of Africa. *Earth Planet. Sci. Lett.* **137**, 1–18,
- Hay, W. W., and Southam, J. R. 1977. Modulation of marine sedimentation by the continental shelves. *In: Andersen N.R. and Malahoff A., (eds) The Role of Fossil Fuel CO₂ in the Oceans.* Plenum Press, New York, 569–605.
- Herrick, R.R. 1999. Small mantle upwellings are pervasive on Venus and Earth. *Geophys. Res. Lett.* **26**, 803–806.
- Hills, E.S. 1975. *Physiography of Victoria.* Whitcombe and Tombs, Melbourne.
- Hipondoka, M.H.T., 2005. *The development and evolution of Etosha Pan, Namibia.* Unpublished Ph.D. dissertation, Bayerische Julius-Maximilians-Universitt Wrzburg, Wrzburg.
- Hipondoka, M.H.T., Jousse, H., Kempf J. and Busche D. 2006. Fossil evidence for perennial lake conditions during the Holocene at Etosha Pan, Namibia. *South African Journal of Science*, **102**, 93–95.
- Hofmann, C., Courtillot, V., Feraud, G., RocP., Yirgu, G., Ketefo, E., and Pik, R. 1997. Timing of the Ethiopian flood basalt event and implications for plume birth and global change. *Nature*, **389**, 838–841.

- Holmes, A. 1944 *Principles of Physical Geology*. Nelson, London and Edinburgh.
- Howard, A.D., and Kerby, G., 1983. Channel changes in badlands. *Geological Society of America Bulletin*, **94**, 739–752.
- Howard, A.D., Dietrich, W.E., and Seidl, M.A. 1994. Modeling fluvial erosion on regional to continental scales. *Journal of Geophysical Research*, **99**, 13971–13986.
- Hovius, N. 1998. Controls on sediment supply by large rivers, Relative Role of Eustasy, Climate and Tectonism in Continental Rocks, *SEPM Special Publication*, **59**, 3–16.
- Husson, L. 2006 Dynamic topography above retreating subduction zones, *Geology*, **34**, 741–744
- Ishii, M. and Tromp, J., 2004. Constraining large-scale mantle heterogeneity using mantle and inner-core sensitive normal modes, *Phys. Earth planet. Int.*, **146**, 113–124.
- Japsen, P., Bonow, J.M., Green, P.F., Chalmers, J.A. and Lidmar-Bergstrom, K. 2006 Elevated, passive continental margins: Long-term highs or Neogene uplifts. New evidence from West Greenland. *Earth Planet. Sci. Lett.*, **248**, 315–324.
- Jessen, O. 1936. *Reisen und Forschungen in Angola*. Reimer, Berlin, Germany, 397.
- Jolivet M., Ritz J-F., Vassallo R., Larroque C., Braucher R., Todbileg M., Chauvet A., Sue C., Arnaud N., De Vicente R., Arzhanikova A., Arzhanikov S. 2007. The Mongolian summits : An uplifted, flat, old but still preserved erosion surface. *Geology*, **35** 871–874.
- Jones S.M. and White N., 2003. Shape and size of the starting Iceland plume swell, *Earth Planet. Sci. Lett.* **216**, 271–282.

- Jackson, M.P.A., Hudec, M.R. and Hegarty, K.A. 2005. The great West African Tertiary coastal uplift: fact or fiction? A perspective from the Angolan divergent margin. *Tectonics*, **24**.
- King, L.C. 1942. *South African Scenery*. Oliver and Boyd, Edinburgh, U.K., 308.
- King, L.C. 1944. Geomorphology of the Natal Drakensberg. *Trans. of the Geol. Soc. of South Africa*, **47**, 255–282.
- King, L.C. 1953. Canons of landscape evolution. *Bull. Geol. Soc. Am.*, **64**, 721–752.
- King, L.C. 1955. Pedeplanation and isostasy: an example from South Africa. *Quarterly Journal of the Geological Society*, **111**, 353–359.
- King, L.C. 1957. *The uniformitarian nature of hillslopes*. *Trans. R. Soc. Edin.*, 17, 81–102.
- King, L.C. 1962. *Morphology of the Earth* Oliver and Boyd, Edinburgh, U.K., 699 pp.
- King, L.C. 1972. *The Natal monocline: explaining the origin and scenery of Natal, South Africa*. Geology Department, University of Natal, South Africa.
- King S. D. and Anderson, D.L. 1998. Edge-Driven Convection, *Earth Planet. Sci. Lett.*, **160**, 289–296.
- King S. D. and Ritsema J., 2000 African hotspot volcanism: small-scale convection in the upper mantle beneath cratons. *Science*, **290**, 1137–1140.
- Kirby, E., and Whipple, K., 2001. Quantifying differential rock-uplift rates via stream profile analysis. *Geology*, **29** 415–418.
- Kooi, H. and Beaumont G. 1994. Escarpment evolution on high-elevation rifted margins: insights derived from a surface process model that combines diffusion, advection and reaction. *Journal of Geophysical Research*, **99**, 12191–12209.

- Larsen, T.B. and Yuen, D.A. 1997. Ultrafast upwelling bursting through the upper mantle. *Earth Planet. Sci. Lett.*, **146**, 393–399.
- Laske, G. and Masters, G., 1997. A global digital map of sediment thickness. *EOS Trans. AGU*, **78**, F483.
- Leturmy P., Lucazeau F., Brigaud F. 2003 Dynamic interactions between the gulf of Guinea passive margin and the Congo river drainage basin: 1. Morphology and mass balance. *J. Geophys. Res.*, **108**, (B8) 2383.
- Lithgow-Bertelloni, C. and Silver P.G. 1998. Dynamic topography, plate driving forces, and the African superswell. *Nature* **395**, 269–72
- Lucazeau F., Brigaud F. and Leturmy, P. 2003. Dynamic interactions between the gulf of Guinea passive margin and the Congo river drainage basin: 2. Isostasy and uplift. *J. Geophys. Res.*, **108** (B8), 2384
- Lythe, M.B., Vaughan, D.G. and the BEDMAP Consortium. 2000. *BEDMAP - bed topography of the Antarctic. 1:10,000,000 scale map. BAS (Misc) 9*. Cambridge, British Antarctic Survey.
- Matmon, A., Bierman, P. and Enzel Y. 2002. Pattern and tempo of great escarpment erosion. *Geology*, **30**, 1135–1138
- McCarthy, T.S., Moon, B.P. and Levin, M. 1985. *Geomorphology of the western Bushmanland Plateau, Namaqualand, South Africa*. South African Geographic Journal, 67, 67–178.
- McKenzie, D. 1994. The Relationship between Topography and Gravity on Earth and Venus. *Icarus*, **112**, 55–88.
- McKenzie, D. 2003. Estimating T_e in the presence of internal loads. *J. Geophys. Res.*, **108**, 2438.

- McKenzie, D. and Fairhead, D. 1997. Estimates of the effective elastic thickness of the continental lithosphere from Bouguer and free air gravity anomalies. *J. Geophys. Res.*, **102**, 27,523–27,552.
- McKenzie, D.P. and Weiss, N. 1975. Speculations on the thermal and tectonic history of the earth. *Geophys. J. Roy. Astr. Soc.*, **42**, 131–174.
- Milliman, J.D. and Syvitski, J.P.M. 1992. Geomorphic/Tectonic Control of Sediment Discharge to the Ocean: The Importance of Small Mountainous Rivers. *J. Geol.*, **100**, 525–544.
- Montgomery, D.R., Balco, G., and Willet, S.D. 2001. Climate, tectonics, and the morphology of the Andes *Geology*, **29** 579–582.
- Moore, A.E and Larkin, P.A. 2001. Drainage evolution in south-central Africa since the break-up of Gondwana. *South African Journal of Geology*, **104**, 47–68.
- Mueller, R.D., Roest, W.R., Royer, J.Y., Gahagan, L.M. and Sclater, J.G., 1997. Digital isochrons of the world's ocean floor, *J. geophys. Res.*, **102**, 3211–3214.
- Nslund, J. 2001. Landscape development in western and central Dronning Maud Land, East Antarctica. *Antarctic Science*, **13**, 302–311.
- Ni, S., Ding, X., Helmberger, D.V. and Gurnis, M. 1999 Low-velocity structure beneath Africa from forward modeling, *Earth Planet. Sci. Lett.* **170**, 497 – 507.
- Ni, S., Tan, E., Gurnis, M., Helmberger, D.V. 2002. Sharp sides to the African superplume. *Science*, **296**, 1850–1853.
- Ni, S. and Helmberger, D.V. 2003. Further constraints on the Africa superplume structure. *Physics of the Earth and Planetary Interiors* **140**, 243–251.

- Nicholson S. E., 2000 The nature of rainfall variability over Africa on time scales of decades to millenia. *Global and Planetary Change* **26**, Issues 1-3, 137–158.
- Nyblade, A. A. and Robinson, S. W. 1994. The African Superswell. *Geophysical Research Letters*, **21**, 765-768.
- Ollier, C.D. and Pain, C.F. 1997 Equating the basal unconformity with the palaeoplain: a model for passive margins. *Geomorphology*, **19**, 1–15.
- Ollier, C. D. and Pain, C. F. 2000 *The Origin of Mountains*, Routledge, London.
- Parsons, B. and Daly, S. 1983. The Relationship Between Surface Topography, Gravity Anomalies, and Temperature Structure of Convection. *J. Geophys. Res.*, **88**, 1,129–1,144.
- Partridge, T.C. 1998. Of diamonds, dinosaurs and diastrophism: 150 million years of landscape evolution in southern Africa. *25th Alex du Toit Memorial Lecture. South African Journal of Geology*, **101**, 165–184.
- Partridge, T.C. and Maud, R.R. 1987. Geomorphic evolution of southern Africa since the Mesozoic. *South African Journal of Geology*, **90**, 179–208.
- Partridge, T.C. and Maud, R.R. 2000 *Cenozoic of Southern Africa*. Oxford Monographs on Geology and Geophysics No. 40. Oxford University Press
- Pazzaglia F.J. and Gardner, T.W. 1994. Late Cenozoic flexural deformation of the middle U.S. passive margin. *Journal of Geophysical Research*, **99**, 143–12.
- Phillips, J.D. 2002. Erosion, isostatic response, and the missing peneplains. *Geomorphology*, **45**, 225–241.
- Pickford, M., Senut, B. and Dauphin, Y. 1995a. Biostratigraphy of the Tsondab Sandstone Namibia based on gigantic avian egg shells. *Geobios*, **28**, 85–98.

- Pickford, M., Senut, B., Mein, P., Morales, J., Soria, D., Neito, M., Ward, J. and Bamford, M. 1995b. The discovery of Lower and middle Miocene vertebrates at Auchas, southern Namibia. *C. R. Acad. Sci., Paris, SerIIa*, **322**, 901–906.
- R.J. Pike and S.E. Wilson, 1971. Elevation–relief ratio, hypsometric integral, and geomorphic area–altitude analysis. *Geological Soc. America Bulletin* **82**, 1079–1083.
- Priestley, K., McKenzie, D. and Debayle, E., 2006. The state of the upper mantle beneath southern Africa, *Tectonophysics*, **416**, 101–112.
- Reeves, C. V. and de Wit, M.J., 2000. Making ends meet in Gondwana: retracing the transforms of the Indian Ocean and reconnecting continental shear zones. *Terra Nova* **12**, No.6, 272–282.
- Reeves, C.V., 2000. The geophysical mapping of Mesozoic dyke swarms in southern Africa and their origin in the disruption of Gondwana. *Journal of African Earth Sciences*, **30**, 499–513.
- Ricard, Y., Richard, M., Lithgow-Bertelloni, C. and Le Stunff, Y., 1993. A geodynamic model of mantle density heterogeneity, *J. geophys. Res.*, **98**, B, 21 895–909.
- Richards, M. A., Duncan, R. A., and Courtillot, V. E., 1989. Flood basalts and hotspot tracks: Plume heads and tails. *Science*, **246**, 103–108.
- Ritsema, J., and Allen, R.M., 2003. The elusive mantle plume. *Earth and Planetary Science Letters*, **207**, 1–12.
- Ritsema, J., van Heijst, H.J. and Woodhouse, J.H. 1999. Complex shear velocity structure beneath Africa and Iceland. *Science*, **286**, 1925–1928.
- Rohrman, M. and van der Beek, P. 1996 Cenozoic postrift domal uplift of North Atlantic margins: An asthenospheric diapirism model. *Geology*, **24**, 901–904.

- Rohrman, M., van der Beek, P. A., Andriessen, P. A. M. and Cloetingh, S. 1995. Mesozoic morphotectonic evolution of Southern Norway: Neogene domal uplift inferred from apatite fission track thermochronology *Tectonics*, **14**, 704–718.
- Sahagian, D. 1988. Epeirogenic motions of Africa as inferred from Cretaceous shoreline deposits. *Tectonics* **7**, 125–138.
- Seranne, M. and Anka, Z. 2005. South Atlantic continental margins of Africa: A comparison of the tectonic vs climate interplay on the evolution of equatorial west Africa and SW Africa margins. *J. African Earth Sciences* **43**, special issues 1-3: Phanerozoic evolution of Africa, 283–300.
- Sklar, L.S. and Dietrich, W.E., 2001. Sediment and rock strength controls on river incision into bedrock. *Geology*, **29**, 1087-1090.
- Stankiewicz, J. and de Wit, M. J. 2006 A proposed drainage evolution model for Central Africa: Did the Congo flow east? *Journal of African Earth Sciences* **44**, Issue 1, 75–84.
- Steinberger, B., Schmeling, H. Marquart, G., 2001. Large-scale lithospheric stress field and topography induced by global mantle circulation, *Earth planet. Sci. Lett.*, **186**, 75–91.
- Stewart, K., Turner, S., Kelley, S., Hawkesworth, C., Kirstein, L. and Mantovani, M., 1996. 3-D ^{40}Ar – ^{39}Ar geochronology in the Paran continental flood basalt province. *Earth and Planetary Science Letters*, **143**, 95–109.
- Stock, J.D., and Montgomery, D.R., 1999. Geologic constraints on bedrock river incision using the stream power law *Journal of Geophysical Research*. **104**, 4983–4993.

- Tackley, P. J., Stevenson, D. J., Glatamaier, G. A. and Schubert, G. 1994. Effects of multiple phase transitions in a three-dimensional spherical model of convection in Earth's mantle. *J. Geophys. Res.*, **99**, 15,877–15,901.
- Tapley, B.D., Bettadpur, S., Watkins, M.M. and Reigber, C.H., 2004. The Gravity Recovery and Climate Experiment: mission overview and early results, *Geophys. Res. Lett.*, **31**, L09607, doi:10.1029/2004GL019920.
- Tiley, R., McKenzie, D. and White, N. 2003 The elastic thickness of the British Isles. *Journal of the Geological Society of London*, **160**, 499–502.
- Tinker J.H., de Wit M.J. and R. Brown, 2008. Mesozoic exhumation of the southern Cape, South Africa, quantified using apatite fission track thermochronology. *Tectonophysics*, **455** 77–93.
- Thomas, D.S.G. and Shaw, P.A., 1988. Late Cainozoic drainage evolution in the Zambezi Basin: geomorphological evidence from the Kalahari Rim. *Journal of African Earth Sciences*, **7**, (4), 611–618.
- Thomas, D. S. G. and Shaw, P. A. 1990. The deposition and development of the Kalahari Group sediments, Central Southern Africa. *J. Afr. Earth Sci.*, **10**, 187–197.
- Twidale, C.R. 2002. The two-stage concept of landform and landscape development involving etching: Origin, development and implications of an idea. *Earth-Science Reviews*, **57**, 37–74.
- Twidale, C.R. 2003 a. 'Canons' revisited and reviewed: Lester King's views of landscape evolution considered 50 years later *GSA Bulletin* **115**, 1155–1172.
- Twidale, C.R. 2003 b The enigma of survival: problems posed by very old paleosurfaces. *Physical Geography* **24**, 26–60

- van der Beek, P. and Braun, J. 1999. Controls on post mid-Cretaceous landscape evolution in the southeastern highlands of Australia: Insights from numerical surface process models. *Journal of Geophysical Research*, **104**, 4945–4966.
- Van der Beek, P., Summerfield, M.A., Braun, J., Brown, R. W. and Fleming, A. 2002. Modelling post breakup landscape development and denudational history across the southeastern African (Drakensberg Escarpment) margin. *Journal of Geophysical Research*, **107**,B12 DOI 10.1029/2001JB000744.
- van der Beek, P and Bishop, P. 2003. Cenozoic river profile development in the upper Lachlan catchment (SE Australia) as a test of quantitative fluvial incision models. *J. Geophys. Res.* **108**, 2309.
- Van der Wateren, F.M., and Dunai, T.J., 2001, Late Neogene passive margin denudation history – Cosmogenic isotope measurements from the central Namib Desert. *Global and Planetary Change*, **30**, 271–307.
- Visser, J. N. 1995. Post-glacial Permian stratigraphy and geography of southern and central Africa: boundary conditions for climatic modelling. *Palaeo. Palaeoclim. Palaeoeco.* **118**, 213–243.
- Walford, H. L. 2003. *Spatial and Temporal Variation of African Epeirogeny*. Unpublished Ph.D. dissertation, University of Cambridge.
- Walford, H.L., White, N.J. and Sydow J.C., 2005. Solid sediment load history of the Zambezi Delta. *Earth Planet. Sci. Lett.* **238**, 49–63.
- Ward, J. D. and Corbett, I. 1990. Towards an age for the Namib *In*: Seely, M.K., (eds) *Namib ecology: 25 years of Namib research* Transvaal Museum Monograph **7**, Pretoria, 17–26

- Watts, A.B. 2001 Isostasy and flexure of the lithosphere. *Cambridge University Press, Cambridge.* 458
- Watts, A.B. and Daly, S.F. 1981. Long wavelength gravity and topography anomalies. *Ann. Rev. Earth Planet. Sci.*, **9**, 415–448.
- Wellington, J. H. 1938. The Kunene River and the Etosha Plain. *South African Geographical Journal.* **20**, 21–33.
- Whipple, K.X. 2004. Bedrock rivers and the geomorphology of active orogens. *Annu. Rev. Earth Planet. Sci.* **32**, 151–185.
- Whipple, K.X., and Tucker, G.E. 1999. Dynamics of the stream-power river incision model: Implications for height limits of mountain ranges, landscape response timescales, and research needs. *Journal of Geophysical Research* **104** 17661–17674.
- White, N. and Lovell, B. 1997. Measuring the pulse of a plume with the sedimentary record. *Nature*, **387**, 888–891.
- White, R. S. and McKenzie, D. P. 1995. Mantle plumes and flood basalts. *J. Geophys. Res.*, **100**, 17,543–17,585.
- Zhao, D. 2001. Seismic structure and origin of hotspots and mantle plumes. *Earth and Planetary Science Letters*, **192**, 251–265.